Rational Engineering of Polyfluorene based Conjugated Polymers for Sensing and Antibacterial Applications

A thesis submitted by

Moirangthem Anita Chanu

Roll No. 186122048

to

Indian Institute of Technology Guwahati

for the award of the degree of

Doctor of Philosophy

Department of Chemistry

Indian Institute of Technology Guwahati

Guwahati-781039

June 2024

Dedicated To My Family

INDIAN INSTITUTE OF TECHNOLOGY GUWAHATI
Department of Chemistry

STATEMENT

I do hereby declare that the work contained in the thesis entitled **"Rational Engineering of Polyfluorene based Conjugated Polymers for Sensing and Antibacterial Applications"** is the result of investigations carried out by me in the Department of Chemistry, Indian Institute of Technology Guwahati, Guwahati, Assam India under the supervision of Prof. Parameswar Krishnan Iyer, Professor, Department of Chemistry, Indian Institute of Technology Guwahati, Guwahati, Assam, India. This work has not been submitted elsewhere for the award of any degree.

June, 2024 **Moirangthem Anita Chanu**

IIT Guwahati

INDIAN INSTITUTE OF TECHNOLOGY GUWAHATI
Department of Chemistry

CERTIFICATE

This is to certify that the work contained in the thesis entitled **"Rational Engineering of Polyfluorene based Conjugated Polymers for Sensing and Antibacterial Applications"** by **Moirangthem Anita Chanu**, a Ph.D. student of Department of Chemistry, Indian Institute of Technology Guwahati, for the award of degree of Doctor of Philosophy has been carried out under my supervision and this work has not been submitted elsewhere for any degree.

June, 2024
Guwahati

Prof. Parameswar Krishnan Iyer
Thesis Supervisor
Department of Chemistry
Indian Institute of Technology Guwahati
Guwahati – 781039
Assam, India.

Acknowledgements

As I am reaching the end of an intense and incredibly memorable journey that has led me to this stage in my academic career, I would like to thank everyone who has helped to make this thesis possible. It is really hard to list all who sincerely helped me, and I would like to thank all of them. Without their direction and guidance, this thesis would not have been able to be prepared or completed.

I am incredibly grateful to my thesis supervisor, Prof. Parameswar Krishnan Iyer for his expert guidance, freedom to work, scholarly inputs, and prudent suggestions during my research work. His approach to transforming serendipitous observations into new possibilities has always encouraged me to keep pursuing my research interest and has always served as a beacon for me in the future. I earnestly thank him for his expert supervision, consistent encouragement, and inspiration in this academic journey and life in general

I offer my sincere gratitude to my doctoral committee members, Prof. Abu Taleb Khan, Prof. G. Krishnamoorthy, and Prof. A.S. Achalkumar, for periodically evaluating my work and providing insightful suggestions and comments that incited me a lot to improve my research work.

I express my sincere thanks to Prof. Vibin Ramakrishnan for providing an opportunity to work in an interdisciplinary area through collaboration and strong support along with lab facilities.

The completion of this thesis was made possible with the invaluable assistance of my collaborator, Kalpana Kumari. Her timely support and insightful suggestions motivated me to broaden my research perspectives.

I extend my heartfelt gratitude to my senior labmates, Dr. Laxmi Raman Adil, Dr. Nehal Zahra, Dr. Subrata Mondal, and Dr. Arvin Sain Tanwar, for generously sharing their vast knowledge, continuous encouragement, valuable advice, and support throughout my thesis work. I also express my sincere regards to Retwik Bhaiya for his unwavering assistance and moral support. I am fortunate to have such wonderful people who always stepped up to assist when needed.

I am grateful to all faculty members of the Department of Chemistry, IIT Guwahati for their help and encouragement and also the non-teaching staff of the Department for their

technical support. I am thankful to the Central Instruments Facility (CIF), Centre for Nanotechnology (CNT), IIT Guwahati for various characterization facilities.

I gratefully acknowledge all my teachers, especially Prof Homendra Naorem, Dr. Francis A. S. Chipem, Prof. Nongmaithem Rajmuhon Singh, for their excellent teachings, proper guidance, and treasurable advices, which undoubtedly greatly influence my decision to pursue doctoral research.

It is a pleasure to convey my heartfelt thanks to all my dear labmates Arvin Bhaiya, Raman Bhaiya, Niranjan Bhaiya, Che Binota, Adil Bhaiya, Subrata Bhaiya, Nehal Di, Debasish Bhaiya, Ramesh Bhaiya, Indrani Di, Maimur Bhaiya, Rabindra Bhaiya, Ritesh Bhaiya, Retwik Bhaiya, Nasima Di, Kavita, Debika, Rajdikshit, Priyam, Tapashi, Mayur, Sushant, Da Geetmani, Tamal, Soumalaya, Hirak, Sayantani, Anwesha Di, Paromita Di, Himangshu, Ramkrishna, Deepak, Manab, Srinivas, Dheeraj, Mrinalini, Antim, Mizanur, Ananta Jupitara Di for providing a friendly environment in the lab and making the journey memorable. I always found discussions and suggestions with them to be insightful.

I take this opportunity to express my gratitude to my friends (but not limited to) Mongoli, Anjali, Sinchini, Gloria, Sophia, Debika, Da Somorjit, Da Kisan, Che Gaitri, Premeshwori, Gyani, Sonia, Anju, Ila Di, Sumitra, Anisha, Anjela for their timely suggestion, inspiration, help and moral support.

Finally, my PhD endeavour could not be completed without the everlasting love, unconditional support, and blessings of my family. I would like to express my sincere gratitude with great honour to my family members who gave me lots of love, strength, kind support and blessings which made me to complete this journey.

Thank you everyone for your endless support and encouragement

Moirangthem Anita Chanu

Synopsis

The content of this synopsis report entitled **"Rational Engineering of Polyfluorene based Conjugated Polymers for Sensing and Antibacterial Applications"** is divided into five chapters. *Chapter1* give brief introduction about the respective research area where the scope and significance of the subsequent chapters are discussed. *Chapter 2* discussed the development of benzimidazole functionalised polyfluorene homopolymer (PFBZ) and its specific detection of bilirubin (jaundice biomarker) in the real serum samples as well as the preparation of fluorescence paper-based test kits for onsite bilirubin detection. *Chapter 3* discussed the synthesis of polyfluorene based copolymers PFP and PF2CN with the monomer M2CN playing a key role in tuning the emission wavelength as well as AIEE activity. Further, these polymers were utilized for the detection of pendimethalin (mutagenic and carcinogenic herbicide) in real vegetables and natural water samples and also a smartphone integrated point of care testing device was developed for rapid onsite detection in a very straightforward manner. *Chapter 4* discussed the development of a series of copolymers P1, P2 and P3 by incorporation of M4 monomer and their structure property relationship in the molecular and aggregated level. Further the AIEE active P3 polymer is modified into PFAN polymer by functionalizing with methyl imidazole which act as a receptor for HSA/BSA (predominant protein in human and animals' sera) in the aqueous medium. The PFAN detection of HSA/BSA shows significant color change which is beneficial for the construction of smartphone integrated point of care testing device for rapid onsite detection. *Chapter 5* discuss the development of conjugated polyelectrolytes PFTMI and PFTPyMI and their antibacterial application.

Chapter 1: Introduction

Conjugated polymers (CPs) are categorized as a unique type of organic macromolecules formed by alternate σ (single) bond and highly delocalized π (multiple) bond along its backbone. The research on CPs began in the late 1970's and has gained a tremendous attention since the discovery of polyacetylene's electrical properties after halogen doping. After 23 years of progress, such an initial step of switching plastic insulator like polyacetylene into an electrically conductive metal was honored in 2000 with Nobel Prize in Chemistry jointly to the three pioneered Scientist Alan J. Heeger (University of California), Alan G. MacDiarmid (University of Pennsylvania), and Hideki Shirakawa (University of Tsukuba). Since then, there

have been massive advancement in the interdisciplinary research of material science, biological science and optoelectronic devices.

Conjugated polymers (CPs) are gaining popularity as a promising material for sensing and biological application due its high absorption coefficient, intense emission, super sensitivity, low detection limits, ease of solution process ability etc. Such a superior property of CPs as compared to small molecule is because of its highly delocalized π electrons allowing efficient exciton migration along the backbone as a whole. The different parts of CPs along with some common backbone chain such as poly (p-phenylene ethylene) (PPE), polyfluorene (PF), poly (p-phenylene) (PPP), poly (p-phenylene vinylene) (PPV), poly (p-pyrrole) (PPy), polythiophene (PT) etc. are shown in Figure 1(a), (b). Further, the integration of ionic functional groups upon CPs (conjugated polyelectrolytes) not only improved the solubility in aqueous solution but also serve as a binding site for various charge species like protein, DNA, surfactants etc.

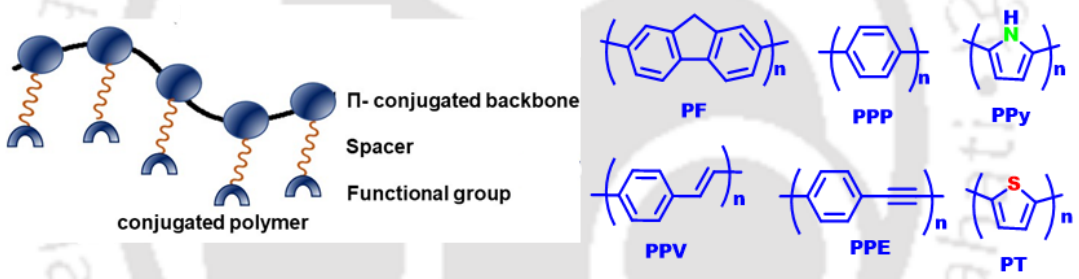

Figure 1: (a) Pictorial representation of conjugated polymer (b) Structures of some well-known conjugated polymer system.

CP as Amplified Signal Transducer:

CPs could be employed as an amplified transducer to translate a biological or chemical recognition signal into a measurable signal by simply modifying the hydrophobic backbone or side chain or both. The photophysical signal is determined by the effective conjugation length, chemical nature, intermolecular and intramolecular packing arrangements that provides suitable mechanism for sensing. In the process excitons are transfer into an acceptor in solution or interchain polymer in aggregate or in solid state thereby generating amplified change in fluorescence signal. Such an amplify signal is more appealing in CPs based sensor than the small molecule based sensor where Swager and co-workers first demonstrated this amplified property known as "Molecular Wire Effect," in 1995. According to this, the fluorescence response in CPs are due to the collective response of the backbone as the whole chain, which

ultimately results in signal amplification when compared to small molecule-based sensors where the change in fluorescence signal usually occurred due to a single chromophore after binding events as shown in Figure 2. This property makes CPs highly demanding in sensing and biomedical applications allowing the use of very dilute probe concentration.

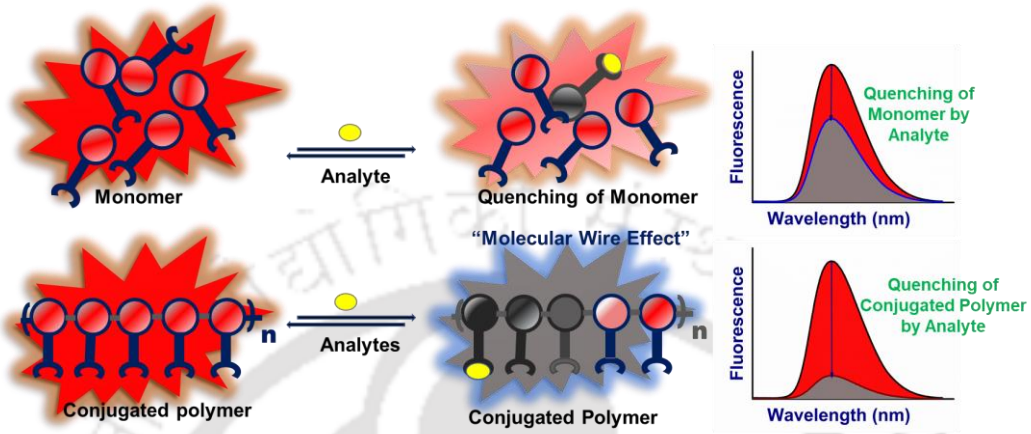

Figure 2: Pictorial representation of fluorescence quenching in monomer and polymer by analyte molecules.

Engineering CPs for Sensing and Antibacterial Applications:

Over the past few years, CPs with varied backbone and side chain functionalities have been designed for sensing of chemical and biological species such as explosives, toxic chemicals, protein, biomarkers, pathogens etc (Figure 3). The inherent signal amplification property of the CP-based sensor results in a low detection limit (ppb to ppt level) and hence more biocompatible. Homopolymer having various receptors is extensively used in sensing and antibacterial application because of its easy synthetic pathway. Continuous effort has been made by the researcher worldwide for the development of donor- acceptor (D-A) based conjugated polymers to tuned the color of luminescence as well to obtain the ratiometric response in sensing, to achieve naked eye detection and quantification of various analytes for practical applications. In recent years, considerable attention has been given to obtain AIE/AIEE (aggregation induced emission/aggregation induced enhanced emission) polymer due to their diverse applications covering the field of optoelectronic devices, bio/chemo sensor, phototheranostic, anti-counterfeiting and many more.

Moreover, bacterial infection and the rising problem of multi-drug resistance pathogens demands new efficient antibacterial materials. Conjugated polyelectrolytes are regarded as good antibacterial materials due to their high antibacterial activity, biocompatibility, and good photo and thermal stability.

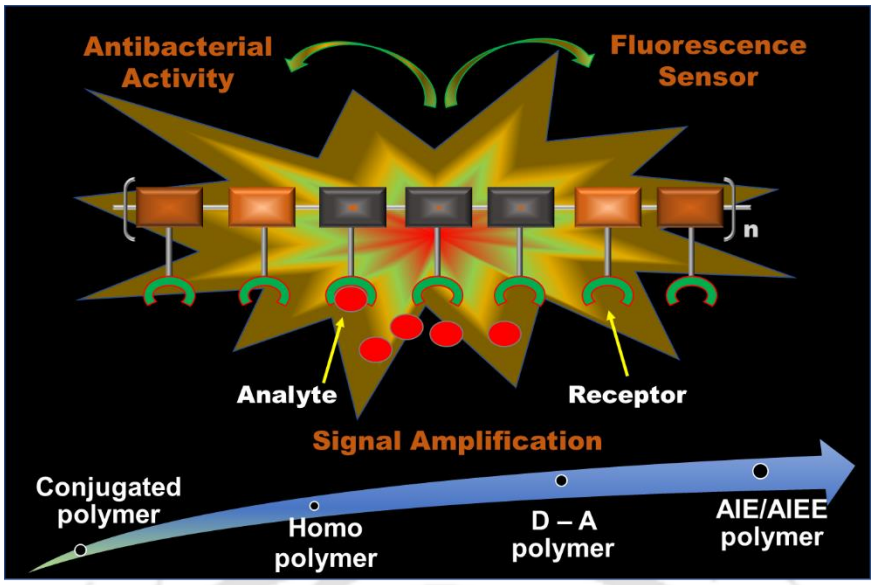

Figure 3: Schematic diagram illustrating the signal amplification properties of several CPs (homopolymer, D-A polymer, and AIE/AIEE polymer) for utilization as a fluorescence sensors or/and antibacterial agents.

Among the conjugated polymers, polyfluorene is as effective blue emissive materials with high photoluminescence efficiency and high thermal stability for practical application. The polyfluorene blue emission can be tuned to desired colors by designing donor-acceptor (D-A) strategy in the backbone. The incorporation of AIE unit into the D-A polymer will improve the sensing performance allowing solid state detection with tunable color.

Chapter 2: Conjugated Polymer Nanoparticles as a Fluorescence Probe for Amplified Detection of Human Serum Bilirubin

In this Chapter 2, a conjugated homopolymer, poly1,1'-((2,7-dimethyl-9H-fluorene-9,9-diyl) bis(hexane-6,1-diyl)) bis(1H-benzo[d]imidazole) (PFBZ) was synthesized incorporating with a specific receptor benzimidazole for bilirubin detection using a low-cost and straightforward oxidative coupling polymerization. The PFBZ polymer spontaneously forms nanoparticles in aqueous medium and unveils excellent sensitivity and selectivity towards bilirubin in an aqueous PBS medium with LOD 6.9 pM, which is far less than the clinically relevant range. The sensing mechanism is based on probe-analyte interaction chemistry and FRET, which were confirmed from both experimental and theoretical studies. This method is successfully utilized for the quantitative determination of BR in real serum samples. Also, a portable florescent test kit was fabricated for onsite detection (Figure 4).

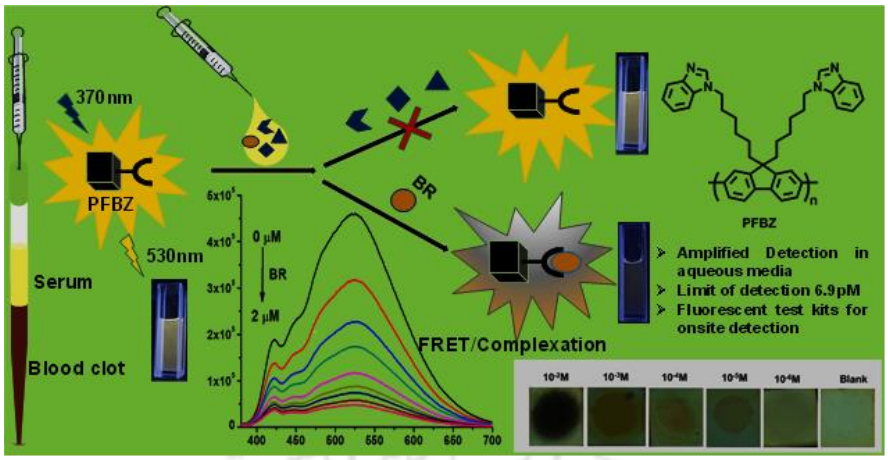

Figure 4: Schematic representation of bilirubin detection by PFBZ polymer

Chapter 3: Receptor Free AIEE Conjugated Polymer Nanoparticle based PoC device for Amplified Detection of Pendimethalin

In this chapter 3, the concept of Aggregation induced enhanced emission (AIEE) property combined with polymer science as an innovative approached of designing sensory material allowing solution and solid-state detection with signal amplification, biocompatibility and portability. Polyfluorene based polymers PFP and PF2CN polymers were developed (Figure 5) and highlighted the importance of M2CN monomer for AIEE, red shifted emission and sensing of Pendimethalin as compared to PFP. The PF2CN-CPNs shows ultra-sensitivity towards PDM with LOD 2.8 nM. The simultaneous occurrence of PET and FRET serve as "Receptor Free" selective sensor for pendimethalin (PDM). Further, the sensing platform provides a practical approach for designing a portable smartphone-based Point of care (PoC) device for onsite detection offering an easy and quick response that could be beneficial in preventing PDM residues from being consumed through food samples and natural water sources (Figure 6).

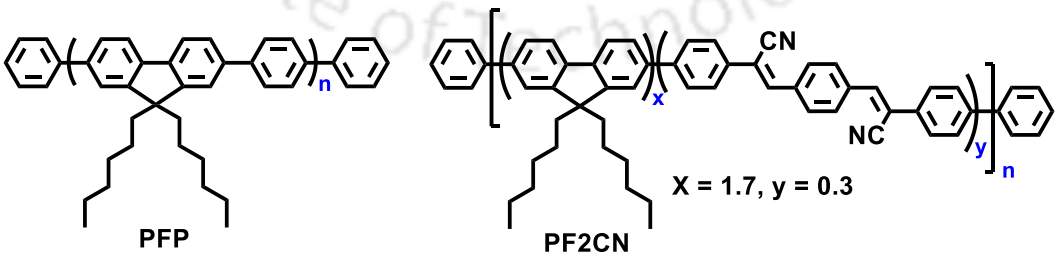

Figure 5: Structure of PFP and PF2CN polymers

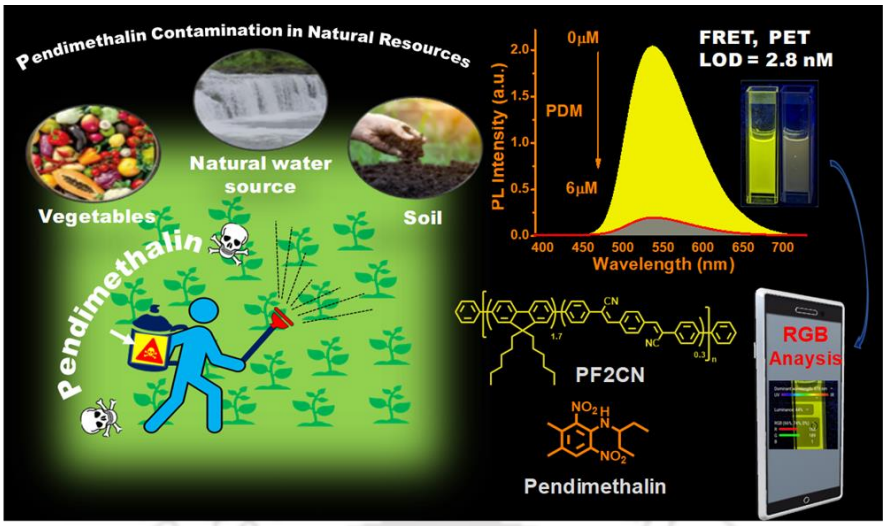

Figure 6: Schematic representation of Pendimethalin detection using PF2CN polymer

Chapter 4: Ratiometric Turn-On Detection of HSA using Aggregation Induced Enhanced Emission Conjugated Polyelectrolyte and Prototype Smartphone based Sensor

In this chapter 4, a series of Conjugated polymer (CPs) P1, P2 and P3 were developed (Figure 7) by taking consideration of molecular movements, a key features of matter playing crucial roles in their structures and behaviours. Different mole fraction of AIE monomer were incorporated into the polyfluorene backbone in order to unravel the correlation between photophysical property and their structure-property relationships at the molecular and aggregate levels which is quite challenging due to diversity and complexity of structures and behaviours. In the process, the photophysical properties of the resulting copolymers are highly tuned which could be beneficial for various types of application. Further, the AIE-P3 polymer is functionalised with methyl imidazole to obtain a conjugated polyelectrolyte (PFAN) and utilized for the light up detection of human serum albumin (HSA). Computational and experimental studies were performed to understand the binding energy and mechanism for interaction and are in good agreement. The method of detection is direct and involves substantial color change that motivates us to make a smartphone integrated point of care decvce (PoC) for onsite detection (Figure 8). Though small molecules based AIEgens are widely used, the exploration of new AIE active conjugated polymers (CPs) will be a promising research in the near future.

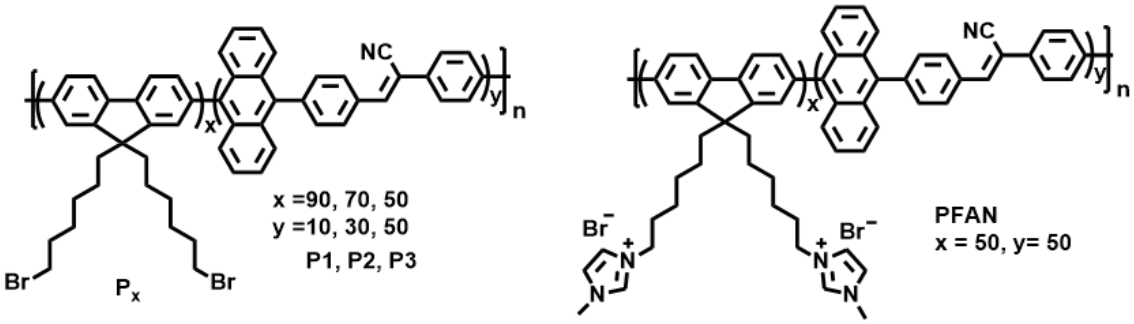

Figure 7: Structure P1, P2, P3 and PFAN polymers

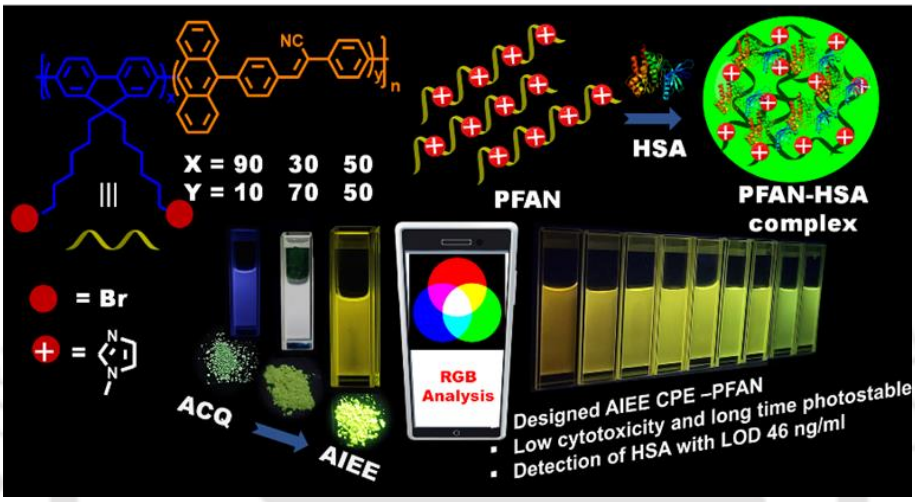

Figure 8: Schematic representation for polyfluorene backbone tuning in solution and solid state and the HSA detection by PFAN polyelectrolyte.

Chapter 5: Switching from Cationic Side Chain into Cationic Backbone in Polyfluorene Polyelectrolytes to Effectively Combat Antibiotic Resistance and Biocompatible Antibacterial Coating

In this chapter 5, two conjugated polyelectrolytes (CPEs) PFTMI and PFTPyMI were designed (Figure 9) in order to address the rising global problem of bacterial infection, which threatens human health and civilization. PFTMI-CPE has pendant methyl imidazole groups and PFTPyMI CPE has pendant methyl imidazole and pyridinium ion in its backbone chain where both of them shows colour change upon anchoring with bacterial membrane allowing easy detection. PFTPyMI-CPE shows better antibacterial activity via membrane disruption, with the more positive charge density aiding more electrostatic and hydrophobic interactions as revealed from FESEM study (Figure 10). Further both the CPEs are low cytotoxic to normal HEK 293 cell lines and toxic to HeLa cell which open up a new avenue for exploration in real-time biomedical applications. Further CPEs are employed as an anti-coating agent over a cotton pad, and the results are quite promising and far better than the commercially available antibiotic Kanamycin.

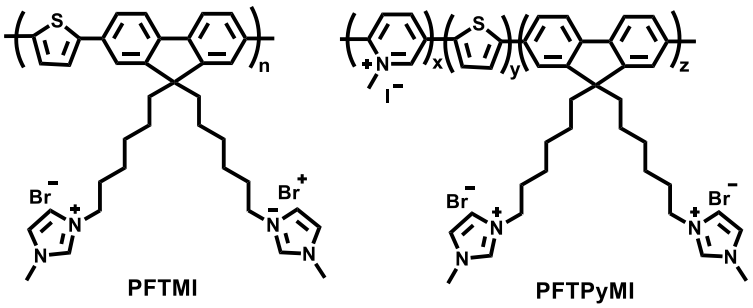

Figure 9: Structure of PFTMI and PFTPyMI polyelectrolytes.

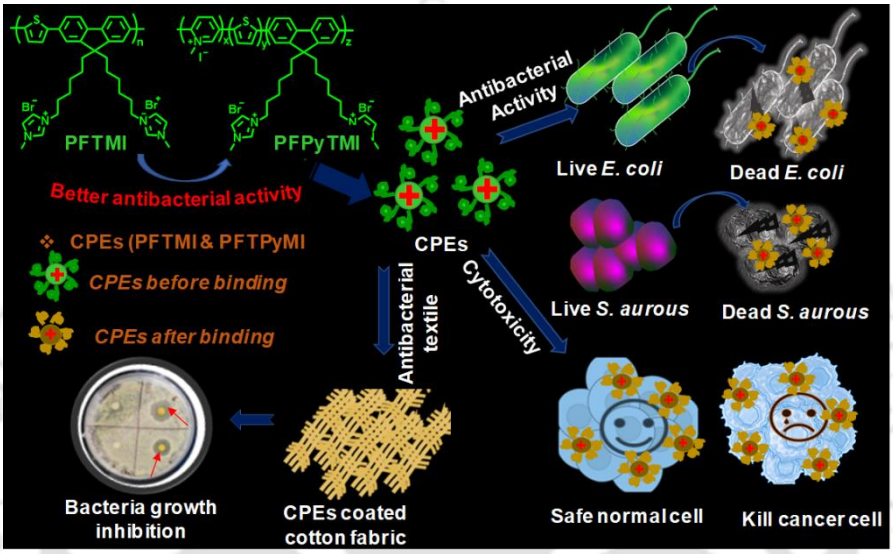

Figure 10: Schematic representation of bacterial membrane anchoring by cationic polyelectrolytes leading to membrane disruption

Conclusion

In conclusion, various novel conjugated polymers were developed by modifying the pendant side chains and planar backbone of polyfluorene. Oxidative coupling polymerization, Suzuki and Stille cross coupling polymerization reaction were used to obtain the CPs in good yield. The incorporation of non-planar monomer having accepting tendency into the planar backbone of polyfluorene results in highly tuned photophysical properties that are applicable for detection of several chemical and biological analytes such as bilirubin, a jaundice biomarker; pendimethalin, a mutagenic and carcinogenic herbicide; HSA/BSA, a predominate protein of human and animal sera and bacteria.

Furthermore, using the aforesaid strategy, there is still scope for developing novel conjugated polymers with multifunctional properties for a wide range of applications to serve mankind.

Contents

CHAPTER 1

Introduction

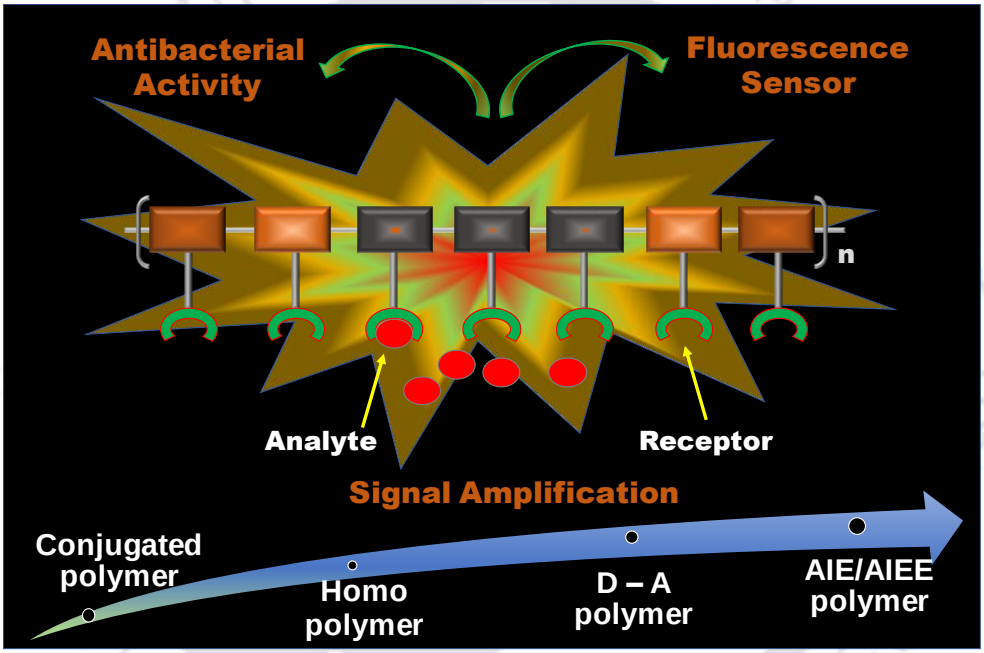

1.1 Conjugated Polymers (CPs):

Conjugated polymers (CPs) are categorized as a unique type of organic macromolecule with a structural framework consisting of alternate σ and π bonds. These π electrons are highly delocalized, leading to excellent optoelectronic properties such as absorption, emission, and charge mobility.[1] The research on CPs began in the late 1970s and has gained tremendous attention since the discovery of polyacetylene's electrical properties after halogen doping.[2, 3] After 23 years of progress, such an initial step of switching plastic insulators like polyacetylene into an electrically conductive metal was honored in 2000 with the Nobel Prize in Chemistry jointly to the three pioneer Scientists i.e., Alan J. Heeger (University of California), Alan G. MacDiarmid (University of Pennsylvania), and Hideki Shirakawa (University of Tsukuba). Since then, CPs have become a preferred functional material in the realms of interdisciplinary research such as material science, biological science and optoelectronic devices.[4-6] Moreover, CPs are being explored as a unique and smart sensory material because of their remarkable optical and electrical properties, facile processability, good photo/thermal stability, and signal amplification properties.[7, 8]

The different parts of CP along with some well-known backbone such as poly(p-phenylene ethylene) (PPE), polyfluorene (PF), poly(p-phenylene) (PPP), poly(p-phenylene vinylene) (PPV), poly(p-pyrrole) (PPy), polythiophene (PT) etc. are shown in Figure 1.1(a), 1.1(b). Based on the requirement, this π-conjugated backbone can be modified into a copolymer consisting of more than one monomeric units or by incorporating pendant side chain with or without functional groups.[5, 9] The integration of ionic functional groups upon CPs (conjugated polyelectrolytes) not only improved the solubility in aqueous solution but also served as a binding site for various charge species like protein, DNA, surfactants, metal ions and anions etc.[10-13]

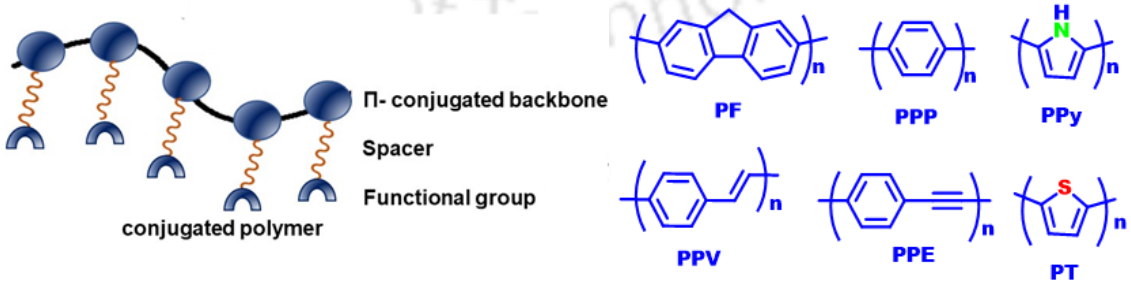

Figure 1.1: (a) Pictorial representation of conjugated polymer, (b) Structures of some well-known conjugated polymer systems.

1.2 Design and Development of Different Types of CPs:

The conjugated backbone of CPs is the basis for excellent optoelectronic properties. This backbone can be engineered in various ways to tune their physical or electronic properties. For instance, copolymerizing an electron-rich backbone with varied amounts of electron-deficient monomer is a general approach to reduce the band gap due to the formation of hybridized molecular orbital.[14] Further, a solid-state emissive polymer can be designed by suppressing the intramolecular motion or intermolecular interaction, which is highly demanded in organic light-emitting diodes (OLEDs),[6] solid-state laser,[15] polymer light-emitting transistor,[16] luminescence-based sensing bio-imaging, etc. Broadly conjugated polymers can be studied into (1) homopolymer (2) D-A acceptor polymer, and (3) AIE or AIEE polymer based on their designed strategies. The following Figure 1.2 shows examples of homopolymers (CP1, CP2, CP3), D-A polymers (CP4, CP5, CP6), and AIE/AIEE polymers (CP7, CP8, CP9).

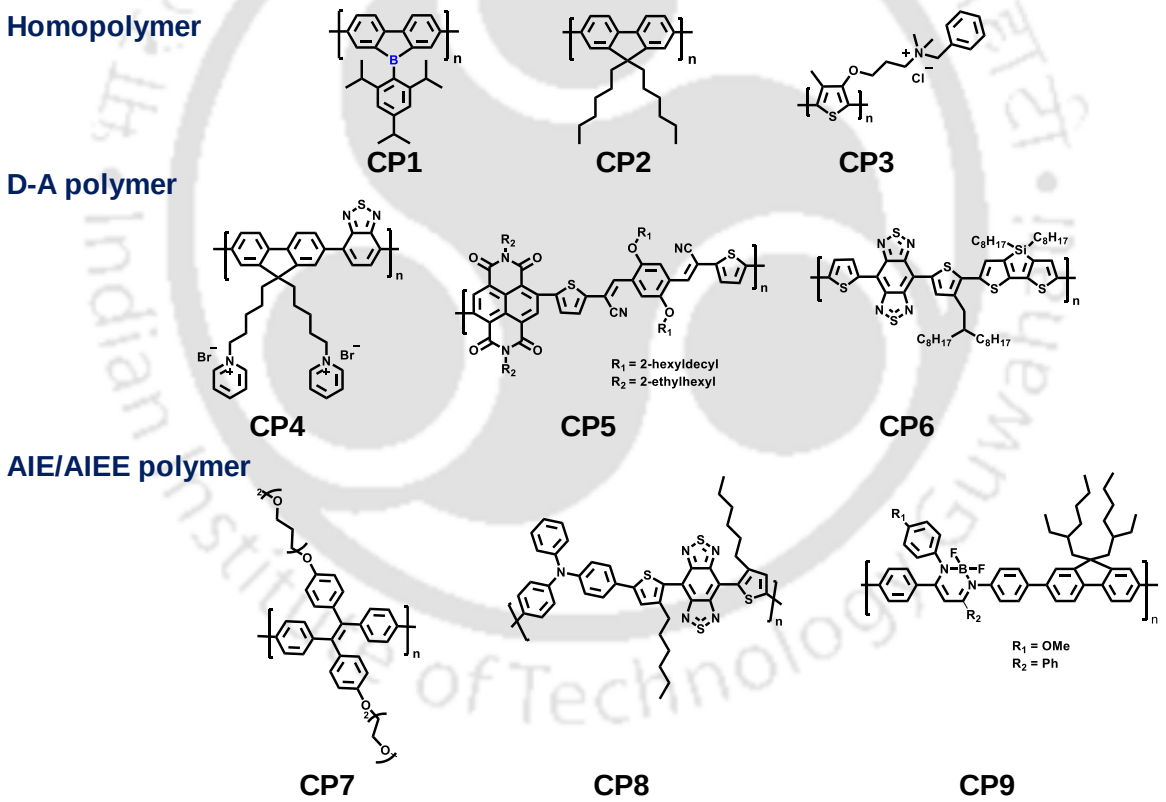

Figure 1.2: Structures of some conjugated homopolymers (CP1, CP2, CP3), D-A polymers (CP4, CP5, CP6) and AIE/AIEE polymers (CP7, CP8, CP9).

1.2.1 Homopolymer

The CP designed by only one type of monomeric unit (repeating unit) is called a homopolymer. Polyacetylene is a simple conjugated homopolymer, and halogen doping on it resulted in the

discovery of conducting polymers.[3] Synthetic chemists became interested in developing novel conducting polymers with desirable characteristics in the 1980s.[17] The low optical band gap 'boron' substituted poly(9-borafluorene) (Figure 1.2 CP1) homopolymer ($E_{g,opt}$ = 2.28 eV) was developed whose band gap is significantly reduced from alkyl substituted polyfluorene and polycarbazole based homopolymer ($E_{g,opt}$ ~3 eV).[18] Moreover, the conformations and stability of polyfluorene are found to be affected by the length of alkyl substituents, with even carbon atoms being more rigid than odd carbon atoms.[17] This conformation plays a key role in controlling the charge carrier mobility, efficiency and stability of photoelectric devices.[20, 21] Several new backbones of homopolymers have also been developed for various purposes, such as sensing and theranostics.[18, 22] Interestingly, the dual state (both solution and condensed states) emission feature of polyfluorene decorating with a specific receptor for target analyte of interest are employed for sensing, bioimaging, and cancer theranostics.[23-25]

1.2.2 D-A polymer

To adjust the optical and electrical band gaps, donor-acceptor (D-A) polymers are developed with an architecture in which the polymer's backbone comprises of electron-rich (donor) and electron-deficient units, resulting in a gradient in electron density within the backbone. The dihedral angle of adjacent monomeric units along the conjugated backbone regulates the intramolecular charge transport dynamics. For instance, the coplanarity of adjacent units maximizes the π-orbital overlap, resulting in efficient electron or hole transport. Torsion, on the other hand, diminishes π-orbital overlap, creating conformational traps, which in turn hamper the charge transport process.[26] Similarly, considerable π-orbital overlap improves intermolecular charge transport through π-π stacking and interchain interactions.[27, 28] Thus, the development of high-performance, generally low band gap polymer requires effective intra/inter-molecular charge transfer at the segmental level. This has sparked interest in identifying structure-property relationships. In the last few years, several D-A-based polymer backbones have been developed depending on needs such as band gap or optical characteristics for various applications such as sensing,[29] OFET devices,[30] bioimaging and photo theranostics,[9,] etc.

1.2.3 AIE/AIEE polymer

CPs with high solid-state emission are essential for the development of modern optoelectronic devices, sensing and therapeutic applications, and so on.[5, 31, 32] However, conventional luminophores suffer from aggregation-caused quenching (ACQ) phenomena, wherein they are

highly emissive in the solution state but non-emissive or less emissive in the solid state or aggregated state, which limits their practical utility. The main reason for the ACQ nature is the planarity of the molecular structure (e.g., perylene) leading to the formation of non-emissive aggregate through π–π stacking [Figure 1.3(a)].[33] To address the above issue, the concept of aggregation induced emission (AIE) or aggregation induced enhanced emission (AIEE) were developed, as initially reported by the Tang group in 2001.[34] Here the π–π stacking of planar ACQ molecule is restricted by a twisted propeller or butterfly-like molecular design, e.g., tetraphenylethylene (TPE), 10,10′,11,11′-tetrahydro-5,5′-bidibenzo [a, d] [7]-annulenylidene (THBA). In the solution state, such propeller-like structures have a high degree of freedom for intramolecular rotation, and this motion utilizes excited state energy, resulting in the formation of a non-emissive (AIE) or less-emissive (AIEE) state. However, in the aggregated (condensed) state, restriction of such intramolecular motions (RIM), such as restriction of intramolecular rotation (RIR) in TPE and restriction of intramolecular vibration (RIV) in THBA, allows maximal utilization of excited energy for emergence (AIE) or enhancement (AIEE) of emission [Figure 1.3(b)].[35] The fundamental distinction between AIE and AIEE is their emissive properties. In AIE, the molecule emits nothing in its solution state but becomes emissive in the aggregated (condensed) state. In AIEE, the molecule emits in the solution state, and its emission is enhanced in the aggregated (condensed) state.

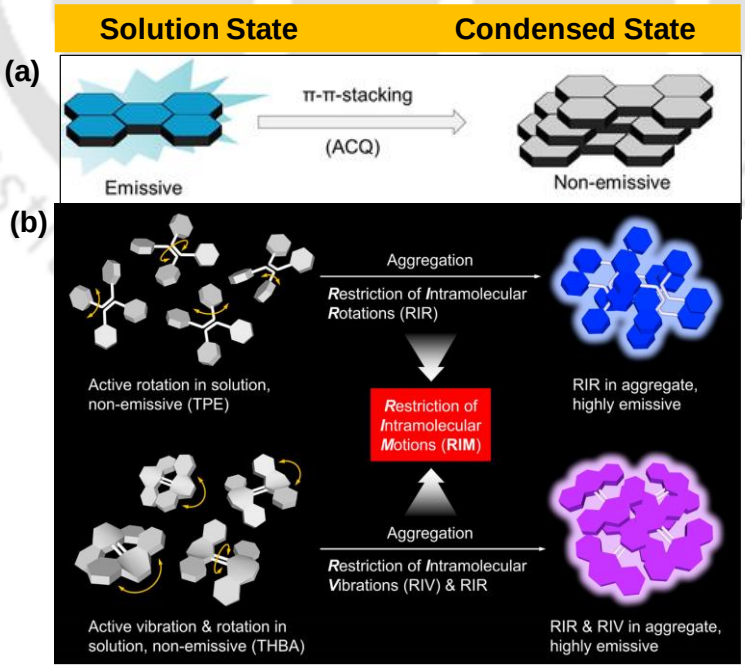

Figure 1.3: (a) ACQ in Perylene due to π–π stacking, (b) Mechanism of AIE/AIEE: RIR in TPE and RIV in THBA (RIM = RIR + RIV).

In recent years, considerable attention has been devoted to designing smart AIE/AIEE polymers with diverse structures and configurations for various advanced applications.[5, 31, 36] Figure 1.4 provides various strategies for designing AIE/AIEE polymers such as (A) direct polymerization of AIE monomer; (B) copolymerization of AIE monomer with other monomers; (C) use of AIE inactive precursor generates AIE polymer after reaction; (D), (E) attachment of AIE active moiety in the side chain of polymerizable monomer undergoing homo/copolymerization reaction and (F) used of AIE-active initiator which results in the linear polymerization with AIE active monomer at the terminal of polymer.[37]

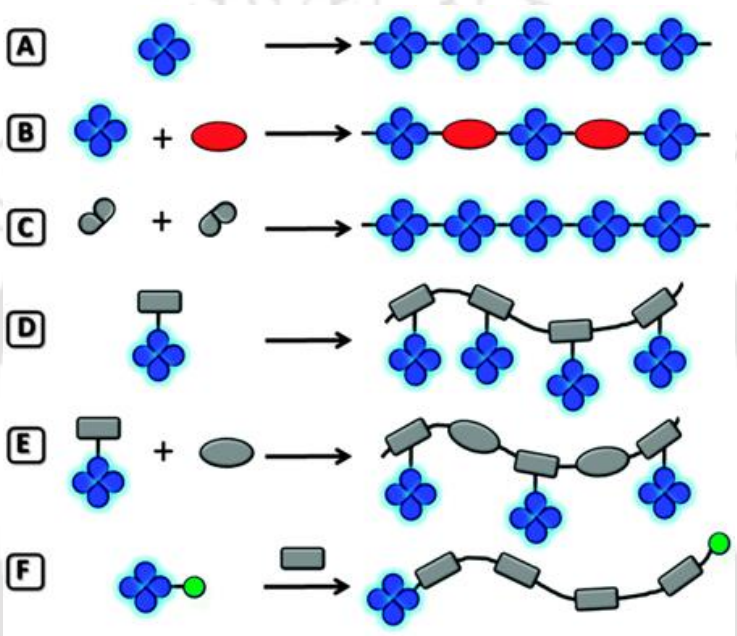

Figure 1.4: Various design strategies for AIE/AIEE polymers. Reproduced with permission from Ref. 37. Copyright 2014 Royal Society of Chemistry.

1.3 Fluorescent Sensor

A fluorescence sensor is an analytical tool that converts physical, biological, or chemical recognition into a measurable optical signal. A typical fluorescent sensor contains two basic components: a recognition unit (i.e., receptor) and a signaling unit [Figure 1.5(a)]. The receptor senses or responds to external stimuli through either chemical or physical interaction, whereas the signaling unit translates these chemical or physical events into a meaningful output optical signal. Depending on the output optical signal, fluorescent sensors can be studied into turn-off, turn-on, ratiometric, and chemodosimeters [Figure 1.5(b)]. Turn-off, turn-on, and ratiometric sensors are types of optical signals formed when an analyte physically interacts with the probe, resulting in the quenching, enhancement, and shifting of the probe's fluorescence, respectively. These changes could be induced by numerous non-covalent interactions between the probe and

the analyte, either in the ground or excited state, or both, and the process is usually reversible. A fluorescent chemodosimeter, on the other hand, is typically based on a specific reaction involving the irreversible translation of a fluorescent signal caused by the analyte of interest.[38]

Sensors with efficient sensitivity and selectivity are in constant demand in a wide range of arena cybersecurity. Fluorescent sensors have been widely explored as biosensors and chemo sensors due to their cost-effectiveness, excellent sensitivity, quick response time, and simplicity and portability. Various functional materials such as metal-organic framework (MOF), carbon nanoparticles, metal oxides, organic small molecules, and polymers are being developed and explored for the specific detection of several biomarkers and environmental toxic contaminants. CPs, on the other hand, are a potential sensing material due to their excellent photo physical characteristics, good chemical and thermal stabilities, biocompatibility, and signal amplification capability.

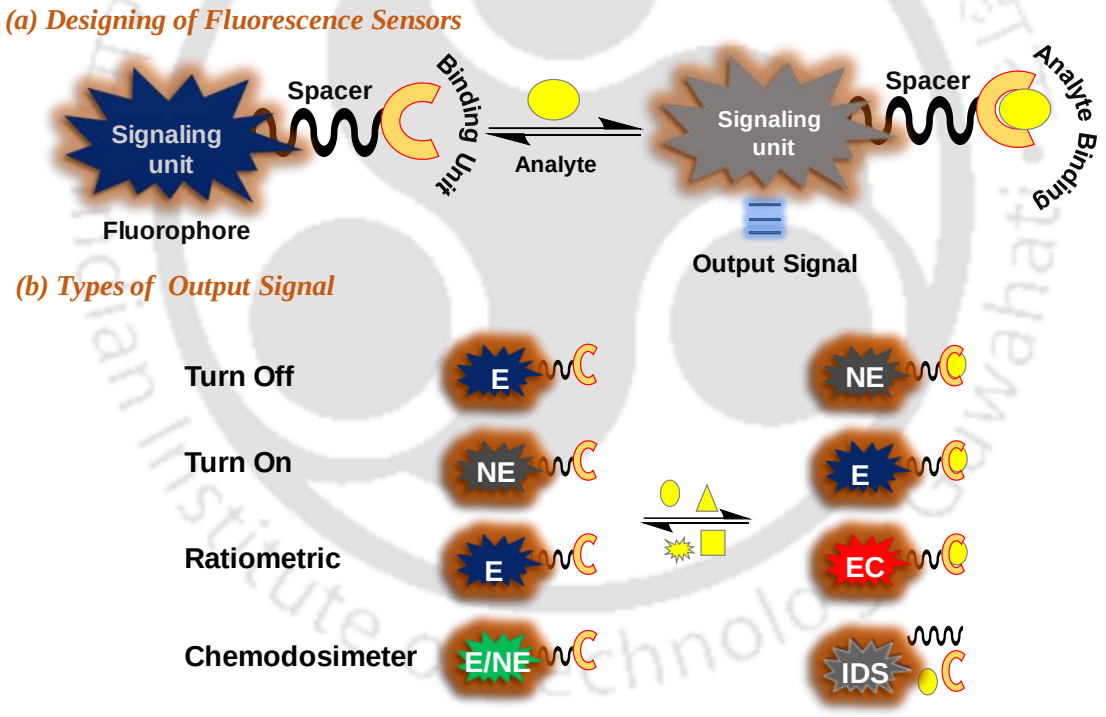

Figure 1.5: (a) Basic components for designing a fluorescence sensor, (b) Various types of sensors based on the output signal.

The primary design approach for CP-based chemo/biosensors is to integrate the receptor (recognition unit) and the signaling unit (conjugated backbone), allowing these two components to communicate with one another. During the binding event, the analyte causes variation in the physical properties of CPs, which is assessed as an amplified signal response.

Thus, functionalizing a conjugated backbone with a specific receptor not only adjusts the desired physical characteristics but also boosts the sensitivity and selectivity of CPs towards the target analyte of interest.[39, 40]

1.4 Mechanisms of Sensing

Fluorescence signals after probe-analyte binding are governed by various detection mechanisms. The detection mechanism can be broadly classified into (a) non-covalent interaction mechanism (NCIM), (b) interaction-free mechanism (IFM), and (c) reaction-based mechanism (RBM).

1.4.1 Non-Covalent Interaction Mechanism (NCIM)

The fluorophore and target analytes interact non-covalently, resulting in changes in fluorescence signals. Some of the non-covalent interaction mechanisms are discussed below

1.4.1.1 Ground-state complex (GSC): Most of the fluorophores have opposite charge with respect to the target analyte, allowing fluorophore-analyte selective interaction. These interactions result in the formation of GSC, which exhibits unique photo physical characteristics such as an absorption spectrum entirely different from that of the fluorophore and can undergo non-radiative decay, leading to a change in fluorescence signal.[41, 42] The resultant fluorescence intensity for the GSC is dependent on the quencher (analyte) concentration, which can be simply determined from the association constant (K_s) as:

$$K_s = [F\text{-}Q]/[F][Q]$$

Where the symbols [F-Q] = GSC concentration, [F] = uncomplex fluorophore concentration and [Q] = quencher (analyte) concentration.

1.4.1.2 Photo-induced electron transfer (PET): In the PET mechanism, photoexcitation of fluorophore (donor) generates excited state electron donors (D*), where D* donates an electron to electron accepting species (A), generating a complex $[D^{+}\cdot A^{-}]$ * [Figure 1.6]. This charge transfer (CT) complex relaxes to the ground state through a non-radiative decay process; however, exciplex emission may occur in some situations. The excess electron on the acceptor may eventually return to the electron donor. The PET mechanism generally gives turn off response.[42]

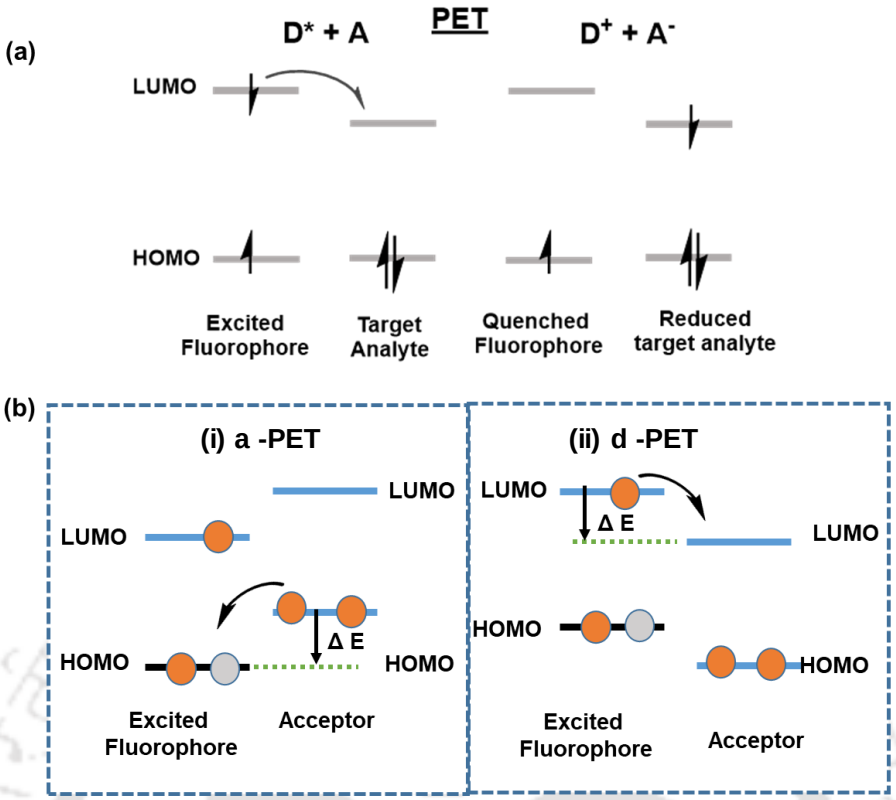

Figure 1.6: Schematic representation of the frontier molecular orbital (FMO) for (a) PET mechanism and [(b) (i)] a- PET mechanism, [(b) (ii)] d- PET mechanism.

Further, the depth insight of PET mechanism can be studied into (i) a-PeT and (ii) d-PeT processes with proper diagrams for better mechanistic insight of PET mechanism.

(i) a-PET: characterized by transfer of electron from the HOMO of acceptor towards the empty HOMO of the excited state fluorophore. Here, the HOMO level of acceptor should lie above the HOMO of the excited state fluorophore. Figure [(b)(i)]

(ii) d-PET: characterized by transfer of electron from the LUMO of excited state fluorophore towards LUMO of the electron deficient acceptor. Here the LUMO level of acceptor should lie below the LUMO of the excited state fluorophore. Figure [(b)(ii)]

1.4.1.3 Förster Resonance Energy Transfer (FRET): In the FRET mechanism, the photo excited D* (fluorophore) undergoes relaxation to the ground state by releasing excited energy that is absorbed by A (analyte or absorber) and is used for the excitation to a higher-level energy state (A*) [Figure 1.7(a)]. The energy transfer rate is determined by three factors: (1) The relative dipole orientation of D and A, (2) the degree of spectral overlap between the absorption spectrum of A and the emission spectrum of D [Figure 1.7(b)] and (3) the Förster distance, i.e.

distance between the D and the A.[43] FRET occurs due to long-range dipolar interactions between D* and A, and hence it is not affected by steric influences.[42]

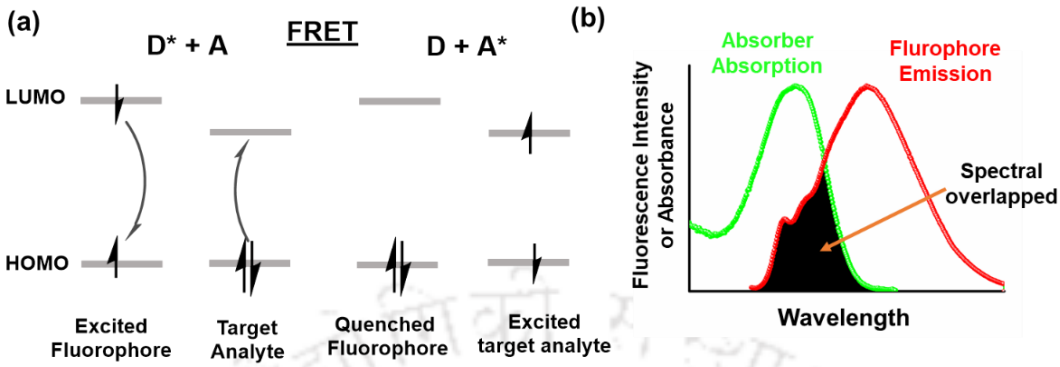

Figure 1.7: (a) Schematic representation of the frontier molecular orbital (FMO) for the FRET mechanism. (b) Spectral overlapped between the absorption spectrum of the absorber and the emission spectrum of the fluorophore.

1.4.1.4 Intramolecular/Intermolecular Charge Transfer (CT). In the intramolecular CT process, the fluorophore typically comprises both electron-rich and electron-deficient sites and electron/charge transfer occurs from an electron-rich donor (D) unit to an electron-deficient acceptor (A) moiety within the same molecule, i.e., through bond electron/charge transfer. The process primarily occurs in the excited state of a molecule, in which photoexcitation enables the transfer of an electron from one fragment of a molecule/ion to its other counterpart in the excited state, resulting in a charge distribution that differs from that of the ground state. The

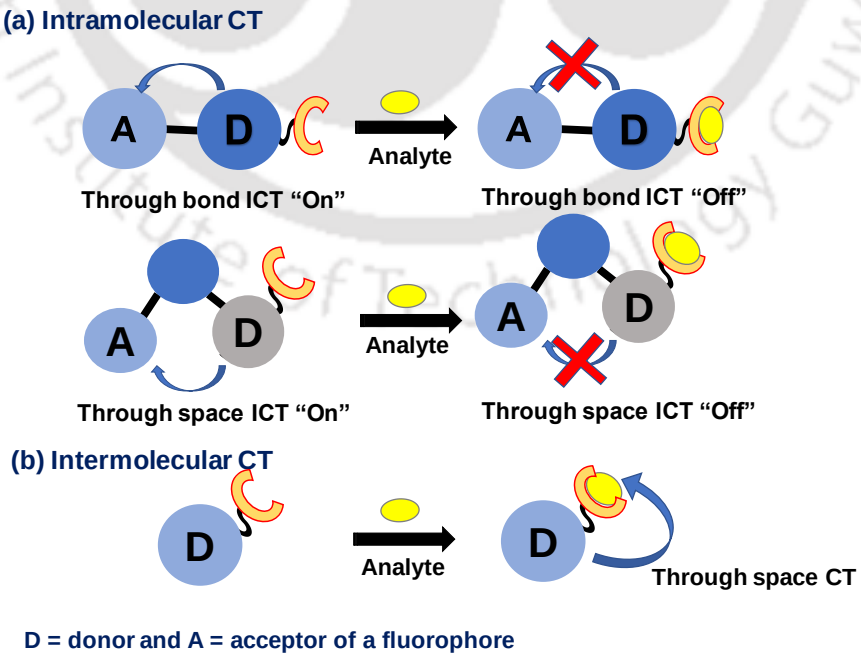

Figure 1.8: Schematic representation of (a) Intramolecular through bond and through space charge transfer; (b)Intermolecular through space charge transfer.

addition of an analyte during this state may undergo ICT On-Off, modifying the fluorescence signal.[44] However, in addition to through bond electron/charge transfer, there is also intramolecular and intermolecular through-space charge/electron transfer, in which the donor and acceptor groups are in proper configuration [Figure 1.8].[45, 46]

1.4.1.5 Twisted Intramolecular Charge Transfer (TICT). It is a type of intramolecular charge transfer that occurs in a fluorophore with a twisted donor-acceptor (D-A) architecture. According to it, a twisted fluorophore has two local minima in the first excited state (S1) potential energy surface (PES). Upon photoexcitation, the fluorophore will initially enter a locally excited (LE) state with planar geometry and then twist in a perpendicular direction to enter the TICT state. With the twist, the extent of ICT progressively increases until an electron is transferred from the "D" to the "A" group which leads to the complete charge separation between them [Figure 1.9]. Such a TICT state is generally less/non-emissive, but an intense fluorescence can be noticed when chemical reactions or physical interaction inhibit TICT rotations (giving LE/ICT state). The TICT process creates significant changes in fluorescence intensities/lifetimes, giving a great opportunity to design a fluorescent probe.[47]

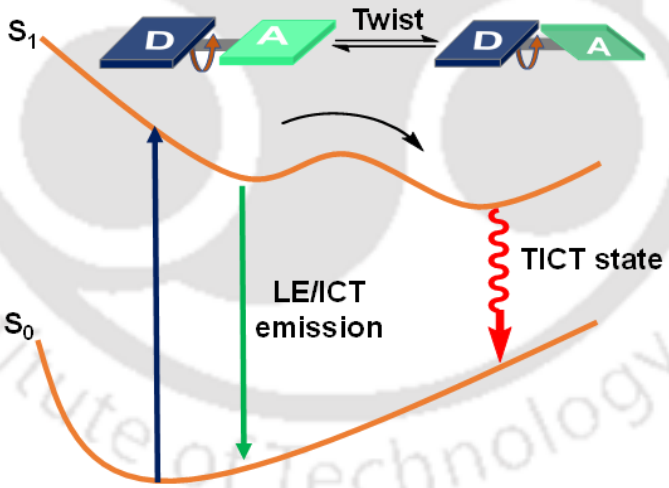

Figure 1.9: Schematic representation of LE/ICT emission and TICT state.

1.4.2 Interaction-Free Mechanism (IFM)

The fluorophore and analyte do not interact directly in this case, but the matching of structural, electronic, or photo physical properties causes fluorescence changes. Some interaction-free sensing mechanisms are discussed below

1.4.2.1. Inner filter effect (IFE): The IFE was first thought to be a fluorescence measurement error, but in recent years it has been investigated as a sensing mechanism.[41, 48] In this case, the

analyte (absorber) reabsorbs the excitation or emission energy of the fluorophore, resulting in an exponential quenching of the fluorophore emission. The IFE can be classified as primary IFE (pIFE) if the analyte absorbs excitation energy or secondary IFE (sIFE) if the analyte absorbs the emission energy of the fluorophore. IFE-based sensing mechanisms operate on simple principles that do not require any interaction between the fluorophore and the analyte. However, it requires the perfect spectral overlap of the absorption spectrum of the analyte (e.g., NACs) with the excitation and/or emission spectra of the fluorophore [49] [Figure 1.10].

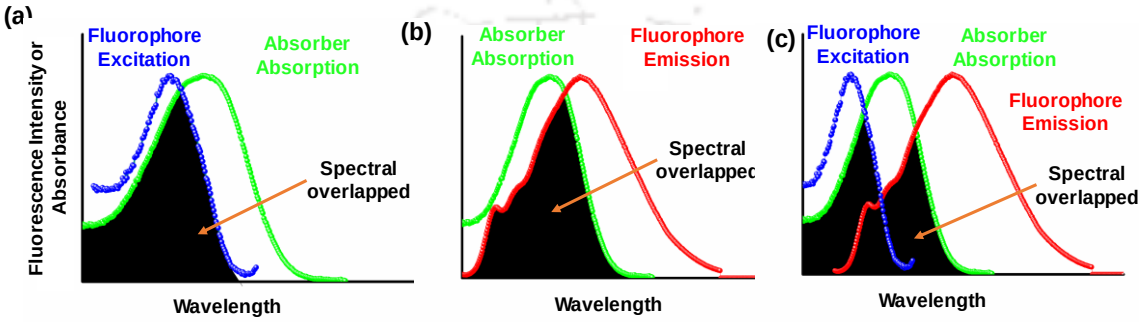

Figure 1.10: IFE spectral overlapped condition of absorber (analyte) with (a) the fluorophore excitation, (b) fluorophore emission, and (c) both excitation and emission of fluorophore

1.4.2.2. Indicator displacement assay (IDA): IDA is another interaction-free sensing mechanism based on host/guest chemistry in which a host molecule (macromolecules or small molecules) with a cavitand structure holds an appropriate guest. Typically, the guest is a dye (indicator molecule) preferentially displaced by an analyte due to its greater affinity for the host[42, 50] [Figure 1.11].

Figure 1.11: Schematic representation of IDA-based host-guest mechanism. Reproduced with permission from Ref. 50. Copyright 2020 Royal Society of Chemistry

1.5.3 Reaction Based Mechanism (RBM)

If the host-guest interaction chemistry is based on an irreversible chemical reaction with a change in fluorescence signal, then the indicator is called a chemodosimeter. The designed strategy of chemodosimeter required two basic functional units i.e. reaction site and a spectroscopic signaling unit. The reaction site of the host reacts with the target analyte, which

is then translated into a measurable optical signal by the signaling unit. Figure 1.12 demonstrates two primary ways to design luminescence chemodosimeters; (a) the analyte serves as a reactant, chemically binding to the chemodosimeter to produce a new product. And (b) the analyte catalyzes a chemical reaction, resulting in the modification of the chemodosimeter and a corresponding change in its optical properties.[51]

Figure 1.12: Reaction-based mechanism leading to the formation of new product or modification of chemodosimeter. Reproduced with permission from Ref. 51. Copyright 2013 American Chemical Society.

1.5 Signal Amplification in CPs

CPs could be employed as an amplified transducer to translate a biological or chemical recognition signal into a measurable signal by simply modifying the hydrophobic backbone or side chain or both.[52] The photo physical signal is determined by the effective conjugation length, chemical nature, intermolecular and intramolecular packing arrangements that provide a suitable mechanism for sensing. In the process, excitons from a donor are transferred into an acceptor in solution or an interchain polymer in aggregate or in a solid state, thereby generating amplified change in the fluorescence signal.[53] Such an amplified signal is more appealing in CPs based sensor than the small molecule-based sensor, where Swager and co-workers first demonstrated in 1995 in poly(phenylene ethynylene) functionalized with cyclophane (PPE CP) for the sensing of paraquat, and this amplified property is known as the "Molecular Wire Effect." Paraquat is an electron-deficient analyte that reversibly interacts with PPE-CP and forms rotaxane complexes, resulting in remarkable fluorescence quenching of PPE-CP. An equivalent small molecular probe containing cyclophane was synthesized to verify the signal amplification mechanism, and the movement of exciton and its role were explored within a single isolated polymeric chain. This investigation shows that polymers exhibit 65-fold higher quenching than model small molecular probes.[54] As a result, CPs in solution behave like a one-

dimensional wire, and the fluorescence response of a single CPs-analyte binding event is due to the collective response of the backbone as the whole chain due to efficient migration of exciton or charge carriers, which ultimately results in signal amplification when compared to small molecule-based sensors, where the change in fluorescence signal is usually occurred by a single chromophore after binding events as shown in Figure 1.13. This property makes CPs highly demanding in sensing and biomedical applications, allowing the use of very dilute probe concentrations

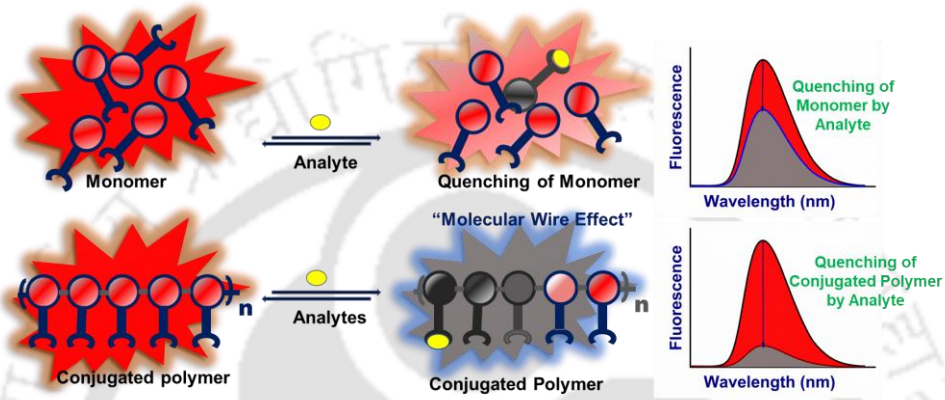

Figure 1.13: Pictorial representation of fluorescence quenching in monomer and polymer by analyte molecules.

1.6. Stern Volmer Theory for Fluorescence Quenching

In the quenching process, the quencher (the target analyte) -fluorophore (probe) interaction led to a decrease in the intensity of fluorescence of the donor and its lifetime. The quenching process is divided into two types, viz. static quenching and dynamic quenching, depending on the mode of molecular interactions between the fluorophore and the quencher.

Static or ground state complexation

$$X + Q \overset{K_a}{\rightleftharpoons} [X,Q] \xrightarrow{h\nu} [X^*,Q] \longrightarrow X + Q \qquad 1$$

Dynamic or collisional quenching

$$X^* + Q \xrightarrow{K_q} X + Q \qquad 2$$

Here, X and X* represent the fluorophore in the ground state and excited state, Q is the quencher, K_a denotes the association constant for the ground state complex [X, Q] quenching constant, and K_q is the bimolecular quenching rate constant.

Both static and dynamic;

$$I_0/I = 1 + K_{sv}[Q] \qquad 3$$

Where I_0 and I are the fluorescence intensity of the fluorophore before and after the addition of an analyte, $K_{sv,}$ and Q represent the Stern Volmer constant and the concentration of the quencher, respectively.

Static quenching occurs due to the formation of a non-fluorescent fluorophore-quencher complex before the photoexcitation process (equation 1). In contrast, dynamic quenching occurs due to a collision between the fluorophore and the quencher at the excited state, leading to the nonradiative decay of the fluorophore[41] (equation 2). There are several parameters to distinguish between these two quenching processes. In the case of static quenching, the fluorescence intensity of the fluorophore decreases without affecting the excited-state lifetime of the fluorophore-quencher complex, as this complex formed at the ground state that is independent of quencher concentration. However, the lifetime of dynamic quenching decreases with the concentration of quencher as the addition of quencher results in non-radiative decay of the fluorophore to the ground state.

It is also feasible that both of these processes exist simultaneously in the system. Therefore, to define fluorescence quenching by these two limiting mechanisms, the Stern-Volmer equation is used (equation 3).

When quenching is solely a dynamic process, $K_{sv} = K_q\tau_0$, where 'Kq' and 'τ_0' represent the bimolecular quenching constant and excited state fluorescence lifetime of fluorophore X*, respectively. Accordingly, the Stern-Volmer equation can be modified as equation 3.1

$$\tau_0/\tau = I_0/I = 1 + K_q\tau_0[Q] \qquad 3.1$$

And if quenching is solely a static mechanism, $K_{sv} = K_a$, where 'Ka' signifies the dissociation constant for the ground state complex.[55] In this scenario, the Stern-Volmer can be expressed as equation 3.2

$$I_0/I = 1 + K_D[Q] \qquad 3.2$$

Hence, the S-V curve should be linear if a static or dynamic process dominates the quenching mechanism.

In the case of dynamic quenching, the fluorophore lifetime should vary linearly with the concentration of the quencher, but the fluorescence lifetime remains unchanged in static quenching [Figure 1.14]. However, in several systems, the S-V plot displayed nonlinearity,

indicating the presence of multiple mechanisms such as fluorophore aggregation, reabsorption, mixed dynamic and static mechanisms, etc.[42]

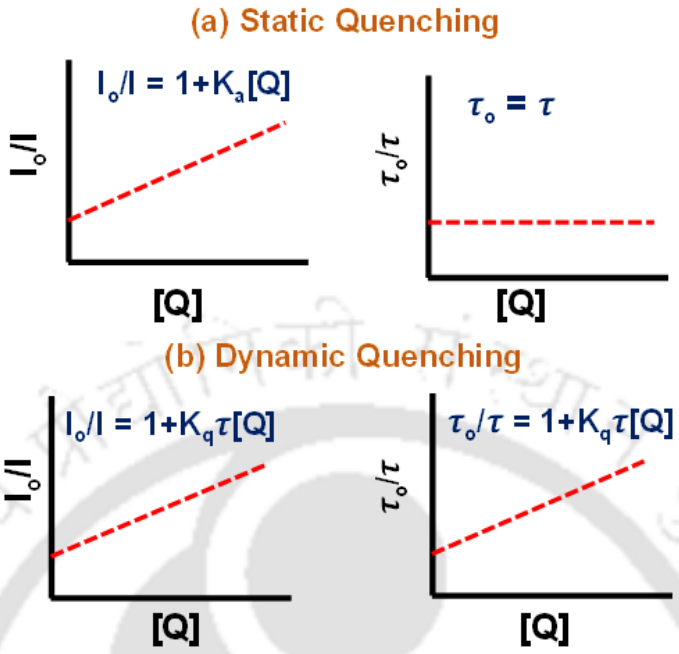

Figure 1.14: Fluorescence intensity (I) and decay lifetime (τ) vs quencher concentration [Q] plots in static and dynamic quenching.

1.7 Application of CP as a Bio/Chemo Sensor

CP's unique properties, which include a high absorption coefficient, a high photoluminescence quantum yield (PLQY), super sensitivity, biocompatibility, good thin-film forming ability, resistance to photo bleaching and high thermal stability, make it an ideal sensory material for the detection of various biomarkers and environmental toxic contaminants, pathogens, etc.

1.7.1 Selected Examples for CP as Bio/Chemo Sensor

In 2020, Zhiyi Yao et al. designed a water-soluble polythiophene-based cationic polyelectrolyte (PMT-1) via $FeCl_3$ oxidative coupling polymerization [Figure 1.15].[56] The polymer (PMT-1) self-assembles into a nanoaggregate upon supramolecular interaction with Flavin mononucleotide (FMN) due to a synergistic effect of noncovalent interactions involving electrostatic, hydrophobic, and π-π interactions. Moreover, the PMT-1-based FMN sensor generates a ratiometric signal (yellow-purple), allowing visual detection of FMN in aqueous and practical samples. The sensor offers a broad detection range, a rapid reaction time, and excellent selectivity and sensitivity, with a limit of detection (LOD) of 1.1 nM in the buffer and 32 nM in the actual real sample.

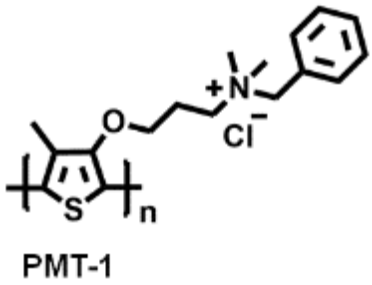

Figure 1.15: Structure of PMT conjugated polymer.

In 2022, Hoon Choi et al. developed a set of novel CPs (BDTBT-NI, BDTBT-NDI, and BDTBT-PDI) with a donor (D)-σ-acceptor (A) dyad architecture incorporated with NI, NDI, or PDI as acceptors in their side chains and BDTBT as donor backbones of CPs [Figure 1.16].[57] Among them, BDTBT-PDI has been found to have more efficient intramolecular PET energy transfer (EnT) due to the stronger accepting tendency of PDI. Further, BDTBT-PDI selectively complexes with $Fe^{2+,}$ giving a "Turn On" response, and this BDTBT-PDI: Fe^{2+} complex was demonstrated as an excellent sensor for spermine in urine samples. Finally, a portable fluorescent paper-based test kit was made for the detection of spermine vapor from fermented food. Moreover, the "On-Off" fluorescence response due to dual sensing of Fe^{2+} and spermine by BDTBT-PDI offers to create a molecular logic gate. The detection limit (LOD) of BDTBT-PDI for Fe^{2+} was reported as 43.6 pM, while BDTBT-PDI: Fe^{2+} for spermine detection was found to be 0.16 nM.

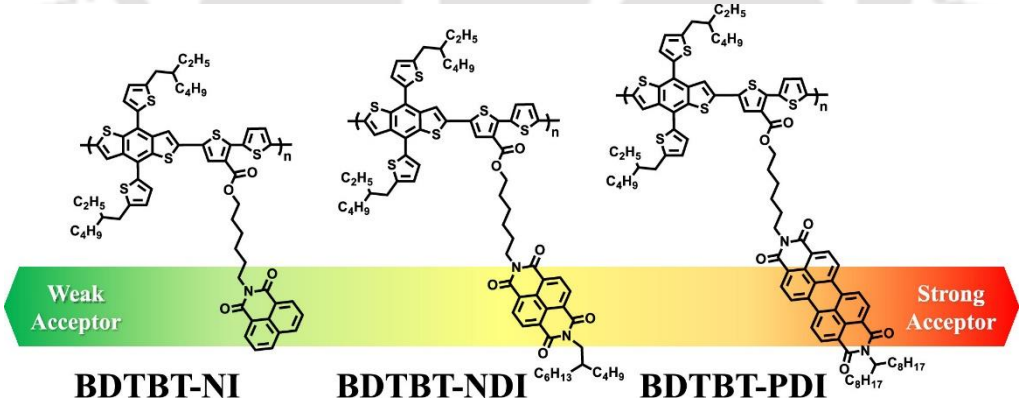

Figure 1.16: Structure of BDTBT-NI, BDTBT-NDI and BDTBT-PDI conjugated polymers. Reproduced with permission from Ref. 57. Copyright 2022 American Chemical Society.

In last few years, the most successful application of CP-based sensors is the detection of electron-deficient nitro compounds. Both polymers have electron-rich carbazole backbones and an AIE active moiety, tetraphenylethylene (TPE), on the side chains [Figure 1.17].[58] The polymers show an amplified fluorescence sensing response towards TNB with a quenching constant of 2.14 x 10^5 M^{-1}. The reason behind the amplified response is the polymer's

architecture. The polymer takes on a twisted 3D structure in a nanoaggregate state, which forms a twisted 3D structure in a nanoaggregate state. Such an architecture facilitates the fast inter-chain exciton diffusion as well as excited state charge transfer.

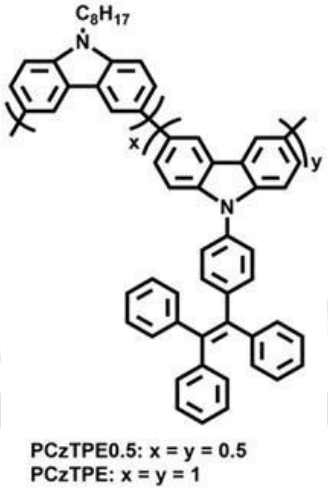

Figure 1.17: Structure of PCzTPE0.5 and PCzTPE conjugated polymers.

Similarly, Iyer et al. also synthesized a novel "receptor-free" AIEE polymer (PFTPBZ) by incorporating an AIE unit (TPBZ) into the conjugated backbone via Suzuki polymerization reaction [Figure 1.18].[59] This polymer detected PA and TNT differently by simply altering the THF: Water fractions (f_w), where TNT is sensed in the aggregated state (95 % f_w and 40 % f_w) and PA in both aggregated state (95 % f_w and 40 % f_w) and solution state (THF). The limit of detection (LOD) for TNT was respectively 53.74×10^{-6} M and 14.26×10^{-7} M at in 95 % f_w, 40 % f_w. Whereas for PA, it was respectively 28.16×10^{-7} M, 10.47×10^{-6} M, and 47.39×10^{-8} M in THF, 95 % f_w and 40 % f_w. The mechanisms for both PA and TNT selective detection were FRET and PET. Finally, cost-effective PFTPBZ-coated yellow fluorescent paper strips were made for visual, quantitative detection of these nitro explosives based on the intensity of dark color.

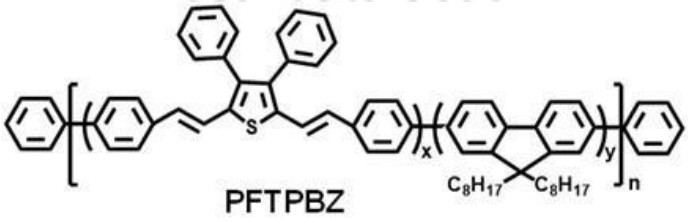

Figure 1.18: Structure of PFTBZ conjugated polymer.

Tang et al. synthesized a multifunctional conjugated polyelectrolyte (PBFBT-NP) to detect nitroreductase (NTR) enzyme, which was overexpressed in hypoxic tumors [Figure 1.19].[60]

The sensory material incorporates a p-nitrophenyl group on the pendent chain, which undergoes an intramolecular PET process, giving rise to very low emissions. The addition of NTR results in a 110-fold increase in fluorescence due to PET inhibition, which converts the p-nitrophenyl group to the p-aminophenyl group via a chemical process. As a result, an in vitro selective NTR sensing technique has been developed with a limit of detection (LOD) of 2.9 ng/ml. Furthermore, the probe was successfully used to image hypoxic tumors and NTR-expressed pathogens like bacteria (*E. coli*), and it demonstrated exceptional antibacterial properties against E. coli when exposed to white light.

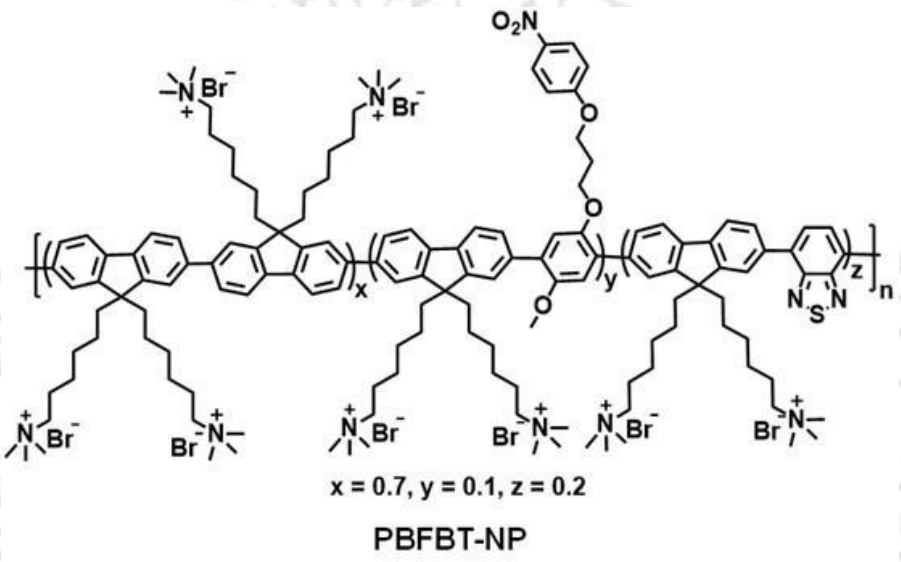

Figure 1.19: Structure of PBFBT-NP conjugated polyelectrolyte.

Huang et al. combine supramolecular chemistry with polymer science by developing a novel supramolecular cross-linked CP network based on host-guest interactions between the pendent DB24C8 units of a CP and the DBA unit of a bis-ammonium cross-linker (SC-CP) [Figure 1.20].[61] Because of CP inter/intra chain aggregation, this supramolecular network showed less fluorescence than pristine CP. Due to the multi-responsive nature of these host-guest interactions, the supramolecular structural network can be disrupted by several external signals, resulting in an increase in fluorescence. As a result, the network can act as multifunctional fluorescence sensors for pH and temperature variation, gas, cation (K^+), and anion (Cl^-). Moreover, this supramolecular CP cross-link network can be used to fabricate a film that enhances fluorescence when exposed to ammonia by disrupting the network's structure via protonation.

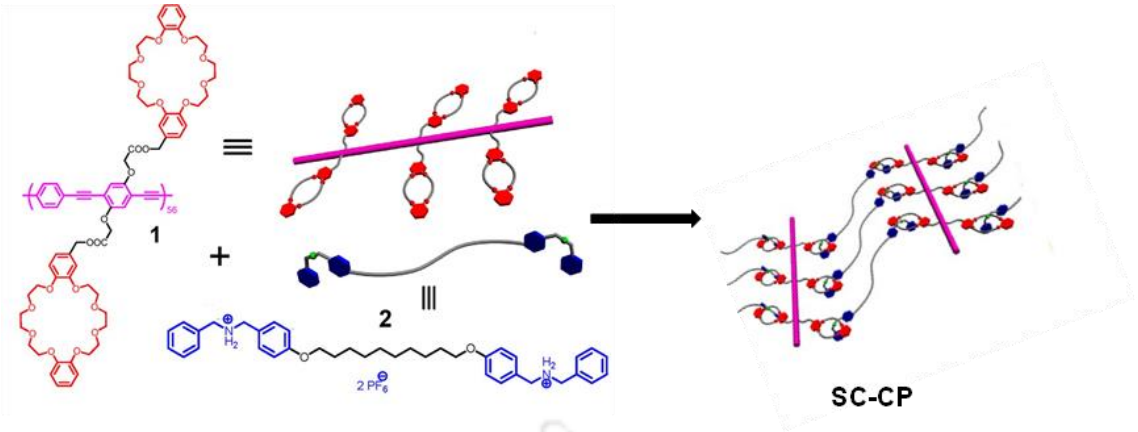

Figure 1.20: Structure of supramolecular crosslinked conjugated polymer (SC-CP). Adapted with permission from Ref. 61. Copyright 2013 American Chemical Society.

1.8 Application of CP as an Antibacterial Material

Bacterial infection is one of the most serious global threats to health and society. Besides, the rising problem of multi-drug resistance bacterial species demands new efficient antibacterial materials.[62] Polymers are regarded as good antibacterial materials due to their high efficacy, biocompatibility, and good photo and thermal stability.[63]

1.8.1 Selected Examples for CP as Antibacterial Materials

Shu Wang et al. synthesized a novel cationic polymer (PPV-NMe^{3+}) that can successfully discriminate between a fungus (C. albicans), Gram-positive bacteria (B. subtilis), and Gram-negative bacteria (E. coli).[64] PPV-NMe^{3+} can differentially bind to microbial cell walls with distinct components, where a unique fluorescent microscopic imaging trend was observed after staining with the polymer in the PBS solution of varied ionic strengths [Figure 1.21]. The isothermal titration shows that electrostatic interactions dominate PPV-NMe^{3+} binding to C. albicans and E. coli, whereas hydrophobic interactions dominate PPV-NMe^{3+} binding to B. subtilis. The approach for detecting pathogenic microorganisms is very simple and can be done within 3 hours.

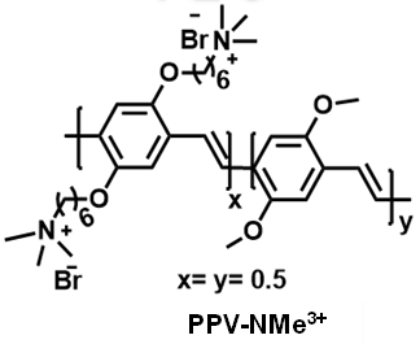

Figure 1.21: Structure of PPV-NMe^{3+} conjugated polymer.

Yanli Tang et al. developed a multifunctional fluorescent co-assembly made of neutral PFVBT polymer and cationic surfactant CTAB to kill bacteria in an efficient and economical manner by disrupting the bacterial membrane without the need for light energy or chemical reactions [Figure 1.22].[65] By reprecipitation method, CTAB was enclosed around the conjugated polymer PPVBT via hydrophobic interaction, resulting in a positively charged shell layer. Here, CTAB could make the co-assembly more hydrophilic and produce positive charges. The 30-minute incubation of PFVBT-CTAB co-assembly at 0.80 μg/mL killed over 91 % of *Escherichia coli* bacteria, while incubation with 1.0 μg/mL led to the death of over 96 % of *Staphylococcus aureus*.

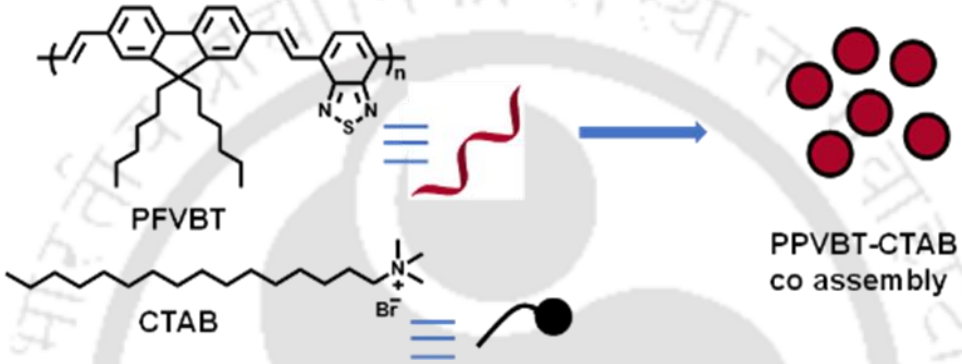

Figure 1.22: Structure of PPVBT-CTAB co-assembly conjugated polymer nanoparticle. Adapted with permission, Ref.65. copyright 2018 American Chemical Society.

Considering the role of positive charge for antibacterial activity, Shu Wang et al. synthesized a cationic CPs (PFPhim) that comprises cationic imidazolium at the backbone in addition to quaternary ammonium at the side chains[66] [Figure 1.23]. Evidence has shown that the cationic backbone increases interactions with negatively charged bacterial membranes, resulting in increased antibacterial activity under both dark and light irradiations.

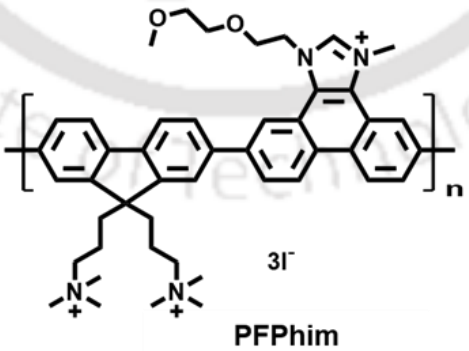

Figure 1.23: Structure of PFPhim conjugated polymer.

1.9 Objectives and Conclusion of the Thesis Work

The primary emphasis of the current thesis work was to design and develop various types of CP and utilize them as fluorescent sensors for various biologically and environmentally

important analytes, with the main purpose of overcoming the problems and obstacles associated with existing sensing systems. Various CPs, such as homopolymer, AIEE polymer, and conjugated polyelectrolytes, are rationally designed and successfully utilized as rapid, sensitive, and on-site monitoring portable testing devices for disease biomarkers, pesticides, and bacteria. The basic goal and conclusion for each work are provided below:

- Bilirubin (BR) is a biomarker of jaundice and liver malfunction. The human serum contains <25 μM (<1.2 mg/dL) of BR is considered as good health which increases up to 50 μM during the jaundice condition. Such a medical condition is fatal as it can accumulate in body organs; thereby, its toxicity leads to mental disorders, hepatitis, Gilbert syndrome, brain damage, anemia, and even death in neonates due to the inhibition of mitochondrial functions. Chapter 2 discussed the design and development of a conjugated homopolymer incorporated with a specific receptor, benzimidazole and the implementation of it as a selective sensor for BR from the real human serum. Further fluorescence paper-based test kits were made for onsite detection.
- Pendimethalin (PDM) is a chemically synthesized herbicide primarily employed to control broadleaf weeds and woody plants. It enters our environment from production industries and by human activity in farming. PDM residues in edible food and water sources is a serious worldwide problem linked to various health issues. Chapter 3 discussed the design and development of a "receptor free" AIEE conjugated polymer for the detection of pendimethalin. As a preventive measure for preventing its consumption of edible food stuffs, a portable smartphone PoC device was constructed based on fluorescent response of newly synthesized AIEE CP.
- Chapter 4 explored structure-motion-property relationship of a conjugated molecular, emphasizing the importance of controlling molecular motion and charge transfer of an organic luminogen, which is the key to giving various photo physical properties. For these 3 sets of CPs were developed, and their photo physical properties were studied in solution and condensed state. Finally, an AIEE CPE was developed for the detection of a biologically important protein, i.e., serum albumin whose abnormal concentration is linked to various health issues. The ratiometric response of the polymer towards serum albumin is beneficial for the construction of real-time visual detecting devices based on smartphones.
- The emergence of antibiotic-resistant pathogen infections has become a public health concern, putting pressure on global healthcare systems. According to Center for Disease Control and Prevention (CDCP) research, the number of individuals afflicted by multidrug-

resistant bacterial infections is approximately two lakhs every year, with an average death rate of 10 million by 2050. As a result, there is an urgent demand for the development of new antimicrobial materials with high efficacy and biocompatibility. Chapter 5 discussed the development of cationic CPEs and the detection of bacteria ratiometrically. The antibacterial properties of the developed CPEs are superior to those of commercially available antibiotics. Moreover, the CPEs are less cytotoxic towards mammalian cells but show efficient killing towards cancerous cells, suggesting a good material for healthcare applications.

References:

1. Heeger, A. J., Semiconducting polymers: The Third Generation. *Chem. Soc. Rev.* **2010,** *39* (7), 2354-2371.

2. Shirakawa, H., The Discovery of Polyacetylene Film: The Dawning of an Era of Conducting Polymers (Nobel Lecture). *Angew. Chem. Int. Ed.* **2001,** *40* (14), 2574-2580.

3. Shirakawa, H.; Louis, E. J.; MacDiarmid, A. G.; Chiang, C. K.; Heeger, A. J., Synthesis of electrically conducting organic polymers: halogen derivatives of polyacetylene, (CH). *J. Chem. Soc., Chem. Commun.***1977,** (16), 578-580.

4. Pecher, J.; Mecking, S., Nanoparticles of Conjugated Polymers. *Chem. Rev.* **2010,** *110* (10), 6260-6279.

5. Hu, R.; Yang, X.; Qin, A.; Tang, B. Z., AIE polymers in sensing, imaging and theranostic applications. *Mater. Chem. Front.* **2021,** *5* (11), 4073-4088.

6. Gather, M. C.; Köhnen, A.; Meerholz, K., White Organic Light-Emitting Diodes. *Adv. Mater.* **2011,** *23* (2), 233-248.

7. Thomas, S. W.; Joly, G. D.; Swager, T. M., Chemical Sensors Based on Amplifying Fluorescent Conjugated Polymers. *Chem. Rev.* **2007,** *107* (4), 1339-1386.

8. Lin, P.; Yan, F., Organic Thin-Film Transistors for Chemical and Biological Sensing. *Adv. Mater.* **2012,** *24* (1), 34-51.

9. Wei, Z.; Xin, F.; Zhang, J.; Wu, M.; Qiu, T.; Lan, Y.; Qiao, S.; Liu, X.; Liu, J., Donor–acceptor conjugated polymer-based nanoparticles for highly effective photoacoustic imaging and photothermal therapy in the NIR-II window. *Chem. Commun.* **2020,** *56* (7), 1093-1096.

10. You, J.; Park, T.; Kim, J.; Heo, J. S.; Kim, H.-S.; Kim, H. O.; Kim, E., Highly Fluorescent Conjugated Polyelectrolyte for Protein Sensing and Cell-Compatible Chemosensing Applications. *ACS Appl. Mater. Interfaces* **2014,** *6* (5), 3305-3311.

11. Liang, J.; Li, K.; Liu, B., Visual sensing with conjugated polyelectrolytes. *Chem. Sci.* **2013,** *4* (4), 1377-1394.

12. Li, Z.; Lou, X.; Yu, H.; Li, Z.; Qin, J. An Imidazole-Functionalized Polyfluorene Derivative as Sensitive Fluorescent Probe for Metal Ions and Cyanide. *Macromolecules* **2008**, *41* (20), 7433-7439.

13. Dong, S.; Ou, D.; Qin, J.; Li, Z. New Imidazole-functionalized Polyfluorene Derivatives: Convenient Postfunctional Syntheses, Sensitive Probes for Metal Ions and Cyanide, and Adjustable Output Signals with Diversified Fluorescence Color. *J. Polym. Sci. A Polym. Chem.* **2011**, *49* (15), 3314-3327.

14. Creamer, A.; Wood, C. S.; Howes, P. D.; Casey, A.; Cong, S.; Marsh, A. V.; Godin, R.; Panidi, J.; Anthopoulos, T. D.; Burgess, C. H.; Wu, T.; Fei, Z.; Hamilton, I.; McLachlan, M. A.; Stevens, M. M.; Heeney, M., Post-polymerisation functionalisation of conjugated polymer backbones and its application in multi-functional emissive nanoparticles. *Nat. Commun.* **2018,** *9* (1), 3237.

15. McGehee, M. D.; Heeger, A. J., Semiconducting (Conjugated) Polymers as Materials for Solid-State Lasers. *Adv. Mater.* **2000,** *12* (22), 1655-1668.

16. Chaudhry, M. U.; Panidi, J.; Nam, S.; Smith, A.; Lim, J.; Tetzner, K.; Patsalas, P. A.; Vourlias, G.; Sit, W.-Y.; Firdaus, Y.; Heeney, M.; Bradley, D. D. C.; Anthopoulos, T. D., Polymer Light-Emitting Transistors with Charge-Carrier Mobilities Exceeding 1 cm2 V−1 s−1. *Adv. Electron. Mater.* **2020,** *6* (1), 1901132.

17. Heeger, A. J., Semiconducting and Metallic Polymers: The Fourth Generation of Polymeric Materials. *J. Phys. Chem. B* **2001,** *105* (36), 8475-8491.

18. Adams, I. A.; Rupar, P. A., A Poly(9-Borafluorene) Homopolymer: An Electron-Deficient Polyfluorene with "Turn-On" Fluorescence Sensing of NH3 Vapor. *Macromol. Rapid Commun.* **2015,** *36* (14), 1336-40.

19. Dias, F. B.; Morgado, J.; Maçanita, A. L.; da Costa, F. P.; Burrows, H. D.; Monkman, A. P., Kinetics and Thermodynamics of Poly(9,9-dioctylfluorene) β-Phase Formation in Dilute Solution. *Macromolecules* **2006,** *39* (17), 5854-5864.

20. Prins, P.; Grozema, F. C.; Nehls, B. S.; Farrell, T.; Scherf, U.; Siebbeles, L. D. A., Enhanced charge-carrier mobility in β-phase polyfluorene. *Phys. Rev. B* **2006,** *74* (11), 113203.

21. Zhang, X.; Hu, Q.; Lin, J.; Lei, Z.; Guo, X.; Xie, L.; Lai, W.; Huang, W., Efficient and stable deep blue polymer light-emitting devices based on β-phase poly (9, 9-dioctylfluorene). *Appl. Phys. Lett.* **2013,** *103* (15).

22. Song, J.; Kang, X.; Wang, L.; Ding, D.; Kong, D.; Li, W.; Qi, J., Near-infrared-II photoacoustic imaging and photo-triggered synergistic treatment of thrombosis via fibrin-specific homopolymer nanoparticles. *Nat. Commun.* **2023,** *14* (1), 6881.

23. Muthuraj, B.; Mukherjee, S.; Patra, C. R.; Iyer, P. K., Amplified Fluorescence from Polyfluorene Nanoparticles with Dual State Emission and Aggregation Caused Red Shifted Emission for Live Cell Imaging and Cancer Theranostics. *ACS Appl. Mater. Interfaces* **2016,** *8* (47), 32220-32229.

24. Chanu, M. A.; Mondal, S.; Zehra, N.; Tanwar, A. S.; Iyer, P. K., Conjugated Polymer Nanoparticles as a Fluorescence Probe for Amplified Detection of Human Serum Bilirubin. *Appl. Phys. Lett.* **2022,** *4* (5), 3491-3497.

25. Tanwar, A. S.; Adil, L. R.; Afroz, M. A.; Iyer, P. K., Inner Filter Effect and Resonance Energy Transfer Based Attogram Level Detection of Nitroexplosive Picric Acid Using Dual Emitting Cationic Conjugated Polyfluorene. *ACS Sens.* **2018,** *3* (8), 1451-1461.

26. Lemaur, V.; Cornil, J.; Lazzaroni, R.; Sirringhaus, H.; Beljonne, D.; Olivier, Y., Resilience to Conformational Fluctuations Controls Energetic Disorder in Conjugated Polymer Materials: Insights from Atomistic Simulations. *Chem. Mater.* **2019,** *31* (17), 6889-6899.

27. Liu, C.; Hu, W.; Jiang, H.; Liu, G.; Han, C. C.; Sirringhaus, H.; Boué, F. o.; Wang, D., Chain conformation and aggregation structure formation of a high charge mobility DPP-based donor–acceptor conjugated polymer. *Macromolecules* **2020,** *53* (19), 8255-8266.

28. Cendra, C.; Balhorn, L.; Zhang, W.; O'Hara, K.; Bruening, K.; Tassone, C. J.; Steinrück, H.-G.; Liang, M.; Toney, M. F.; McCulloch, I., Unraveling the unconventional order of a high-mobility indacenodithiophene–benzothiadiazole copolymer. *ACS Macro Lett.* **2021,** *10* (10), 1306-1314.

29. Tanwar, A. S.; Chanu, M. A.; Parui, R.; Barman, D.; Im, Y.-H.; Krishnan Iyer, P., Dynamic quenching mechanism based optical detection of carcinogenic Cr(vi) in water and on economical paper test strips via a conjugated polymer. *RSC Appl. Polym.* **2024**.

30. Ryu, H. S.; Kim, M. J.; Kang, M. S.; Cho, J. H.; Woo, H. Y., Dicyanodistyrylbenzene-Based Copolymers for Ambipolar Organic Field-Effect Transistors with Well-Balanced Hole and Electron Mobilities. *Macromolecules* **2018,** *51* (20), 8258-8267.

31. Lu, L.; Wang, K.; Wu, H.; Qin, A.; Tang, B. Z., Simultaneously achieving high capacity storage and multilevel anti-counterfeiting using electrochromic and electrofluorochromic dual-functional AIE polymers. *Chem. Sci.* **2021,** *12* (20), 7058-7065.

32. Hu, R.; Qin, A.; Tang, B. Z., AIE polymers: Synthesis and applications. *Prog. Polym. Sci.* **2020,** *100*, 101176.

33. Wang, Y.; Nie, J.; Fang, W.; Yang, L.; Hu, Q.; Wang, Z.; Sun, J. Z.; Tang, B. Z., Sugar-Based Aggregation-Induced Emission Luminogens: Design, Structures, and Applications. *Chem. Rev.* **2020,** *120* (10), 4534-4577.

34. Luo, J.; Xie, Z.; Lam, J. W. Y.; Cheng, L.; Chen, H.; Qiu, C.; Kwok, H. S.; Zhan, X.; Liu, Y.; Zhu, D.; Tang, B. Z., Aggregation-induced emission of 1-methyl-1,2,3,4,5-pentaphenylsilole. *Chem. Commun.* **2001,** (18), 1740-1741.

35. Chua, M. H.; Zhou, H.; Zhu, Q.; Tang, B. Z.; Xu, J. W., Recent advances in cation sensing using aggregation-induced emission. *Mater. Chem. Front.* **2021,** *5* (2), 659-708.

36. Hu, R.; Kang, Y.; Tang, B. Z., Recent advances in AIE polymers. *Polym. J.* **2016,** *48* (4), 359-370.

37. Hu, R.; Leung, N. L. C.; Tang, B. Z., AIE macromolecules: syntheses, structures and functionalities. *Chem. Soc. Rev.* **2014,** *43* (13), 4494-4562.

38. Sahoo, S. K.; Sharma, D.; Bera, R. K.; Crisponi, G.; Callan, J. F., Iron(iii) selective molecular and supramolecular fluorescent probes. *Chem. Soc. Rev.* **2012,** *41* (21), 7195-7227.

39. Zhu, C.; Liu, L.; Yang, Q.; Lv, F.; Wang, S., Water-Soluble Conjugated Polymers for Imaging, Diagnosis, and Therapy. *Chem. Rev.* **2012,** *112* (8), 4687-4735.

40. Anantha-Iyengar, G.; Shanmugasundaram, K.; Nallal, M.; Lee, K.-P.; Whitcombe, M. J.; Lakshmi, D.; Sai-Anand, G., Functionalized conjugated polymers for sensing and molecular imprinting applications. *Prog. Polym. Sci.* **2019,** *88*, 1-129.

41. Lakowicz, J. R., In Principles of Fluorescence Spectroscopy. Springer, US: Boston, MA: 2006.

42. Tanwar, A. S.; Meher, N.; Adil, L. R.; Iyer, P. K., Stepwise elucidation of fluorescence based sensing mechanisms considering picric acid as a model analyte. *Analyst* **2020,** *145* (14), 4753-4767.

43. Sun, X.; Wang, Y.; Lei, Y., Fluorescence based explosive detection: from mechanisms to sensory materials. *Chem. Soc. Rev.* **2015,** *44* (22), 8019-8061.

44. Xu, Y.; Li, B.; Li, W.; Zhao, J.; Sun, S.; Pang, Y., "ICT-not-quenching" near infrared ratiometric fluorescent detection of picric acid in aqueous media. *Chem. Commun.* **2013,** *49* (42), 4764-4766.

45. Xi, H.; Liu, Y.; Yuan, C.-X.; Li, Y.-X.; Wang, L.; Tao, X.-T.; Ma, X.-H.; Zhang, C.-F.; Hao, Y., Through space charge-transfer emission in lambda (Λ)-shaped triarylboranes and the use in fluorescent sensing for fluoride and cyanide ions. *RSC Adv.* **2015,** *5* (57), 45668-45678.

46. Gromov, S. P.; Ushakov, E. N.; Vedernikov, A. I.; Lobova, N. A.; Alfimov, M. V.; Strelenko, Y. A.; Whitesell, J. K.; Fox, M. A., A Novel Optical Sensor for Metal Ions Based on Ground-State Intermolecular Charge-Transfer Complexation. *Org. Lett.* **1999,** *1* (11), 1697-1699.

47. Liu, S.; Ou, H.; Li, Y.; Zhang, H.; Liu, J.; Lu, X.; Kwok, R. T. K.; Lam, J. W. Y.; Ding, D.; Tang, B. Z., Planar and Twisted Molecular Structure Leads to the High Brightness of Semiconducting Polymer Nanoparticles for NIR-IIa Fluorescence Imaging. *J. Am. Chem. Soc.* **2020,** *142* (35), 15146-15156.

48. Tanwar, A. S.; Hussain, S.; Malik, A. H.; Afroz, M. A.; Iyer, P. K., Inner Filter Effect Based Selective Detection of Nitroexplosive-Picric Acid in Aqueous Solution and Solid Support Using Conjugated Polymer. *ACS Sens.* **2016,** *1* (8), 1070-1077.

49. Chen, S.; Yu, Y.-L.; Wang, J.-H., Inner filter effect-based fluorescent sensing systems: A review. *Anal. Chim. Acta* **2018,** *999*, 13-26.

50. Ghale, G.; Nau, W. M., Dynamically Analyte-Responsive Macrocyclic Host–Fluorophore Systems. *Acc. Chem. Res.* **2014,** *47* (7), 2150-2159.

51. Yang, Y.; Zhao, Q.; Feng, W.; Li, F., Luminescent Chemodosimeters for Bioimaging. *Chem. Rev.* **2013,** *113* (1), 192-270.

52. Feng, X.; Liu, L.; Wang, S.; Zhu, D. J. C. S. R., Water-soluble fluorescent conjugated polymers and their interactions with biomacromolecules for sensitive biosensors. *Chem. Soc. Rev.* **2010,** *39* (7), 2411-2419.

53. Rochat, S.; Swager, T. M., Conjugated Amplifying Polymers for Optical Sensing Applications. *ACS Appl. Mater. Interfaces* **2013,** *5* (11), 4488-4502.

54. Swager, T. M., The Molecular Wire Approach to Sensory Signal Amplification. *Acc. Chem. Res.* **1998,** *31* (5), 201-207.

55. Tan, C.; Atas, E.; Müller, J. G.; Pinto, M. R.; Kleiman, V. D.; Schanze, K. S., Amplified Quenching of a Conjugated Polyelectrolyte by Cyanine Dyes. *J. Am. Chem. Soc.* **2004,** *126* (42), 13685-13694.

56. Zhang, L.; Li, S.; Sun, Y.; Xiao, K.; Song, G.; Lu, P.; Yin, S.; Huang, K.; Yao, Z., Self-assembly of flavin mononucleotide and a cationic polythiophene in aqueous media: spectroscopic studies and sensing applications. *Polym. Chem.* **2020,** *11* (22), 3762-3767.

57. Kwon, N. Y.; Kim, Y.; Kataria, M.; Park, S. H.; Cho, S.; Harit, A. K.; Woo, H. Y.; Cho, M. J.; Park, S.; Choi, D. H., Donor-σ-Acceptor Dyad-Based Polymers for Portable Sensors: Controlling Photoinduced Electron Transfer via Tuning the Frontier Molecular Orbital Energies of Acceptors. *Macromolecules* **2022,** *55* (5), 1609-1619.

58. Dong, W.; Fei, T.; Palma-Cando, A.; Scherf, U., Aggregation induced emission and amplified explosive detection of tetraphenylethylene-substituted polycarbazoles. *Polym. Chem.* **2014,** *5* (13), 4048-4053.

59. Adil, L. R.; Gopikrishna, P.; Krishnan Iyer, P., Receptor-Free Detection of Picric Acid: A New Structural Approach for Designing Aggregation-Induced Emission Probes. *ACS Appl. Mater. Interfaces* **2018,** *10* (32), 27260-27268.

60. Zhang, X.; Zhao, Q.; Li, Y.; Duan, X.; Tang, Y., Multifunctional Probe Based on Cationic Conjugated Polymers for Nitroreductase-Related Analysis: Sensing, Hypoxia Diagnosis, and Imaging. *Anal. Chem.* **2017,** *89* (10), 5503-5510.

61. Ji, X.; Yao, Y.; Li, J.; Yan, X.; Huang, F., A Supramolecular Cross-Linked Conjugated Polymer Network for Multiple Fluorescent Sensing. *J. Am. Chem. Soc.* **2013,** *135* (1), 74-77.

62. Mahira, S.; Jain, A.; Khan, W.; Domb, A. J., Antimicrobial Materials—An Overview. In *Antimicrobial Materials for Biomedical Applications*, Domb, A. J.; Kunduru, K. R.; Farah, S., Eds. *RSC*: **2019**; 1-13.

63. Jain, A.; Duvvuri, L. S.; Farah, S.; Beyth, N.; Domb, A. J.; Khan, W., Antimicrobial polymers. *Adv. Healthcare Mater.* **2014,** *3* (12), 1969-1985.

64. Yuan, H.; Liu, Z.; Liu, L.; Lv, F.; Wang, Y.; Wang, S., Cationic Conjugated Polymers for Discrimination of Microbial Pathogens. *Adv. Mater.* **2014,** *26* (25), 4333-4338.

65. Wang, L.; Zhao, Q.; Zhang, Z.; Lu, Z.; Zhao, Y.; Tang, Y., Fluorescent Conjugated Polymer/Quarternary Ammonium Salt Co-Assembly Nanoparticles: Applications in Highly Effective Antibacteria and Bioimaging. *ACS Appl. Bio Mater.* **2018,** *1* (5), 1478-1486.

66. Xu, Q.; He, P.; Wang, J.; Chen, H.; Lv, F.; Liu, L.; Wang, S.; Yoon, J., Antimicrobial activity of a conjugated polymer with cationic backbone. *Dyes Pigm.* **2019,** *160*, 519-523.

CHAPTER 2

Conjugated Polymer Nanoparticles as a Fluorescence Probe for Amplified Detection of Human Serum Bilirubin

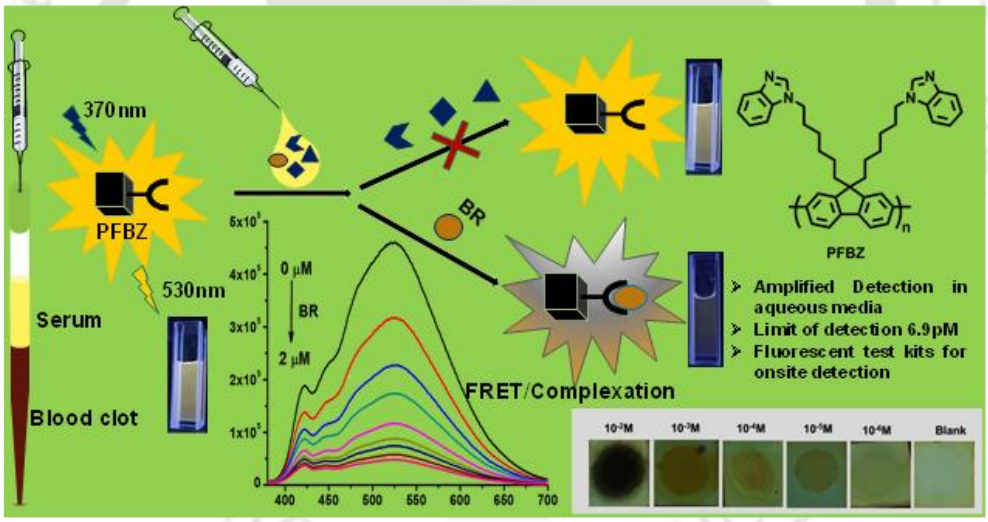

Chanu, M. A.; Mondal, S.; Zehra, N.; Tanwar, A. S.; Iyer, P. K *ACS Appl. Polym. Mater.* **2022**, *4* (5), 3491-3497.

Abstract

Bilirubin (BR) is a potent biomarker for jaundice and liver malfunction. However, its quantitative determination remains a bottleneck due to the interference of numerous biomolecules present in the blood serum. To overcome this, a conjugated polyfluorene derivative, poly1,1'-((2,7-dimethyl-9H-fluorene-9,9-diyl) bis(hexane-6,1-diyl)) bis(1H-benzo[d]imidazole) (PFBZ), was synthesized by incorporating it with a specific receptor benzimidazole for BR detection using a low-cost and straightforward oxidative coupling polymerization. The PFBZ polymer spontaneously forms nanoparticles in an aqueous medium and unveils excellent sensitivity towards BR in an aqueous PBS medium with LOD 6.9 pM, which is far less than the clinically relevant range. The sensing mechanism is based on probe-analyte interaction chemistry and FRET, which were confirmed from both experimental and theoretical studies. This platform offers excellent sensitivity and selectivity, which motivated us to successfully explore the quantitative determination of BR in real serum samples. This sensing method is straightforward, noninvasive, and can be used as a biomedical sensor to diagnose the onset of jaundice and liver malfunction.

Keywords: conjugated polymer nanoparticles; fluorescence; bilirubin; jaundice; FRET; IFE; complexation

2.1 Introduction

Bilirubin (BR) is a neurotoxic, yellow-orange degradation product of heme catabolism whose turnover is greatly associated with jaundice.[1, 2] Under a typical physiological state, BR is enzymatically converted to mono and di-glucuronide conjugates in the liver and gets rid of the body along with the body fluids.[3] The human serum contains <25 μM (<1.2 mg/dL) of BR, which increases up to 50 μM during the jaundice condition.[4, 5] Such a medical condition is fatal as it can accumulate in body organs; thereby, its toxicity leads to mental disorders, hepatitis, Gilbert syndrome, brain damage, anemia, and even death in neonates due to the inhibition of mitochondrial function.[6-11] Several reports have found that a low serum BR level is also connected with several diseases like coronary artery disease (CAD) and atherosclerosis.[12, 13] Thus, monitoring the abnormal concentration of BR, a key biomarker for various physiological processes in our body, precisely and early in low concentration is of immense importance to ensure early treatment.

Clinically, the BR level is tested either by the diazo method or the peroxidase method based on the color change of the serum.[14, 15] The major disadvantage is that the diazo reaction sometimes leads to a false positive response as it detects an amine group. Moreover, it is pH^-dependent; the sample needs pretreatment to precipitate out protein, which often co-precipitates with BR.[16] Besides, the final product decomposes if excess diazo reagents are not eliminated from the reaction mixture quickly. Currently, the peroxidase- method is widely used as a routine clinical testing method, but the method is indirect and requires multiple measurements with a relatively long response time.[17] Several enzyme-based methods have also been reported, but they are prone to having less stability and using expensive enzymes. Moreover, enzyme catalytic and electro catalytic reactions are greatly affected by slight changes in temperature, pH, and chemical compounds surrounding them.[18, 19] As such, there is an immediate requirement for finding a quick, simple, and economical method for the precise analysis of BR levels in blood serum. Recently, the demand for fluorescence probes in biosensing and bioimaging has grown increasingly due to their noninvasive nature, cost-effectiveness, fast response, and easy detection of various biomarkers with excellent sensitivity and selectivity. Although various fluorescence probes such as quantum dots,[20] small organic molecules,[21] MOF,[2] nanosheet[22] and conjugated polymers (CPs)[23, 24] have been reported to detect BR in the complex biosystem, they need improvements in terms of sensitivity and selectivity for real-time practical applications. Moreover, conjugated polymer nanoparticles (CPN) have emerged as a versatile

nanomaterial, promising great potential in the field of biosensing, bioimaging, and nanomedicines. The inherent properties of CPN, such as outstanding fluorescence brightness, high photo stability, tunable optoelectronic property, and excellent biocompatibility, make them highly attractive in the field of material science.[25-27] The applicability of CPNs as biosensing platforms for molecular diagnosis of human diseases is an active area of research in view of their facile functionalization and tunable surface chemistry with excellent light-harvesting properties. The active exciton migration in the CPNs facilitates amplified energy transfer, which can be utilized for the development of ultrasensitive biosensor.[28, 29]

In recent years, few CPs have been reported for the detection of BR. However, no CPN-based probe has been explored for BR detection. Additionally, most of the sensing mechanisms focus only on the spectral overlap between the probe and the analyte, such as resonance energy transfer (RET), electron transfer processes, or/and the inner filter effect (IFE) mechanism. Meanwhile, less attention has been paid to probe-analyte interaction chemistry, resulting in a lack of the required selectivity from competitive biomolecules. An ideal probe should have high sensitivity as well as selectivity, which again depends on the choice of the receptor. However, choosing a new receptor to explore specific sensing of a target analyte is quite challenging.[30-32]

Herein, we have designed a novel conjugated polymer nanoparticle PFBZ [poly1,1'-((2,7-dimethyl-9H-fluorene-9,9-diyl)bis(hexane-6,1-diyl))bis(1H -benzo[d]imidazole] with a specific receptor for the selective detection of BR. The pendant benzimidazole moiety strapped to the side chains of the PFBZ polymer nanoparticle imparts solubility in polar organic solvents and spontaneously forms nanoparticles in aqueous media.[33] The polymer nanoparticle exhibits ultra-sensitivity towards BR with a detection limit in the picomolar range due to the combined effect of a huge spectral overlap of polymer emission with BR absorption and ground state complexation. Low-cost, portable paper strips were fabricated to demonstrate the ability of PFBZ for real-time BR sensing, which is covered in this work for the first time.

2.2 Experimental Section

2.2.1 Materials and methods: BR was procured from Sigma Aldrich. All other chemicals, as well as reagents, were bought from Sigma Aldrich, Merck (India), and Alfa-Aesar. Real human serum is collected from IITG Hospital. Milli-Q water has been used for the preparation of the stock solution for all the experiments. Recordings of ^{1}H NMR (400 MHz, 500 MHz) and ^{13}C

(100 MHz, 125 MHz) NMR spectra were performed on the Varian-AS400 NMR spectrometer (400 MHz and 500 MHz). For recording UV-visible absorption spectra and photoluminescence spectra, Perkin Elmer Lambda-25 and Horiba Fluoromax-4 spectrofluorometers have been used with 1 ml of quartz cuvettes (path length = 1 cm, slit = 3 nm). Time-resolved fluorescence decay profiles were obtained from the Edinburg Life Spec II instrument. Horiba Jobin Vyon, Model LabRam HR, was used to obtain Raman spectra with a 785 nm laser source. FTIR was measured in a Perkin Elmer FT-IR spectrophotometer, and fluorescence absolute quantum yield was obtained from an Edinburgh FLS980 fluorescence spectrometer. FESEM images were obtained from the Zeiss Sigma Field Emission Scanning Electron Microscope (FESEM).

2.2.2 Synthetic Procedure

2.2.2(a). Synthesis of 9,9-bis(6-bromohexyl)-9H-fluorene, (M2): The starting monomer (M2) was synthesized following the reported procedure.[34] A mixture of fluorene (1g, 6.015 mmol), 50 % NaOH (aq), and tetra butyl ammonium iodide (TBAI) (0.582 g, 1.805 mmol) was taken in a clean RB flask and was made inert by applying free-thaw degassing technique (3 times). After that, 1,6-dibromohexane (6.48 mL, 42.12 mmol) was injected cautiously through a syringe, maintaining the inert condition. Finally, the reaction mixture was heated at 80 °C with proper stirring for 5 h. The completion of the reaction was monitored by TLC in hexane and then extracted with chloroform. The extracted organic layer was again washed repeatedly with water (3 times), and then the excess 1,6-dibromohexane was removed by Kugelrohr to get the crude product. Finally, the crude product was further purified by passing over a thick silica gel bed using a column chromatography technique where hexane was selected as eluent to obtain the desired product as a highly viscous colorless liquid. (Yield = 90 %, 2.7 g).

MALDI_TOF: The mass of monomer M2 (M = 492.078, M+2 = 494.127).

^{1}H NMR (400 MHz, $CDCl_3$, δ ppm): 7.71 (d, J = 7.8 Hz, 2H), 7.33 (dd, J = 6.8, 4.3 Hz, 6H), 3.28 (t, J = 6.8 Hz, 4H), 2.02 – 1.92 (m, 4H), 1.66 (dd, J = 14.3, 7.1 Hz, 4H), 1.19 (dt, J = 14.7, 7.4 Hz, 4H), 1.11 – 1.02 (m, 4H), 0.68 – 0.56 (m, 4H).

^{13}C NMR (100 MHz, $CDCl_3$, δ ppm): 151.96, 139.24, 130.42, 126.12, 121.60, 121.18, 55.69, 40.33, 34.02, 32.28, 28.68, 27.98, 23.33**.**

2.2.2(b). Synthesis of poly(9,9-bis(6-bromohexyl)-9H-fluorene), PF: The synthesis of PF was done by following the already reported procedure in our lab.[33] Ferric chloride (1.318 g, 8.125 mmol) was made to dissolve completely in 7 mL of nitrobenzene in a clean two-neck RB fitted with an inert argon inlet. Then 9,9-bis(6-bromohexyl)-9H-fluorene (M2) (1g, 2.031

mmol) dissolved in 8 mL of nitrobenzene was injected gently into the reaction mixture, maintaining the inert condition. Finally, the reaction mixture was continuously stirred for 40 hours at room temperature. Then, the polymer was extracted by precipitation with methanol. The crude precipitates were further purified by extracting chloroform and then precipitated from methanol, centrifuged, filtered (repeated thrice), and finally kept for drying under vacuum for 12 hours to obtain the desired brown powder polymer. (Yield = 49 %, 0.49 g)

^{1}H NMR (500 MHz, $CDCl_3$, δ ppm): 7.84-7.67 (b), 7.56 (b), 56-7.49 (b), 7.36-7.33 (b), 3.28 (b), 2.06-2.14 (b), 0.62-1.53 (b).

GPC in THF, polystyrene standard. M_w= 52601 g mol^{-1}, PDI = 1.99

2.2.2(c). Synthesis of poly1,1'-((2,7-dimethyl-9H-fluorene-9,9-diyl)bis(hexane-6,1-diyl))bis(1H-benzo[d]imidazole) (PFBZ): The synthesis of PFBZ polymer was performed by refluxing PF (29 mg, 0.059 mmol), benzimidazole (69.70 mg, 0.59 mmol) and K_2CO_3 (100 mg) in 2 mL of dry DMF with continuous stirring for 36 h at 110 °C under inert atmosphere. After completion of the reaction, DMF was removed by excess diethyl ether, and the resulting precipitates were dissolved in a minimal amount of chloroform. Then, it was further re-precipitated from methanol to remove the unreacted polymer and benzimidazole. Finally, the precipitate was dried to achieve the desired brownish-yellow polymer (PFBZ). (Yield = 80 %, 23.2 mg)

^{1}HNMR (400 MHz, CDCl3, δ ppm): 7.53-7.69 (b), 7.13-7.18 (b), 3.92 (b), 0.63-1.98 (b),

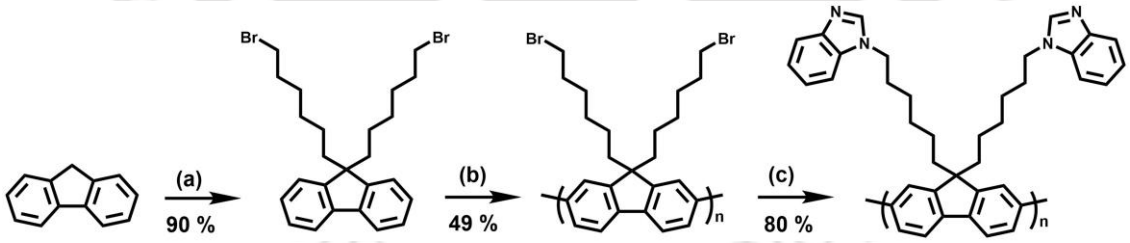

Scheme 2.1 Synthetic pathway of the polymer (PFBZ) (a) aqueous 50 % NaOH, 1,6-dibromohexane, TBAI, 80 °C, 4h. (b) Nitrobenzene, $FeCl_3$, rt, 36 h. (c) benzimidazole, DMF, K_2CO_3 110 °C, 36 h.

2.2.3 Stock Solutions Preparation of PFBZ

The polymer PFBZ stock solution for experiments was prepared in DMF with a concentration of 1 mM. Also, the stock solution of BR with a concentration of 2.5×10^{-2} M was prepared in DMSO and stored in the dark. Similarly, stock solutions of various biologically active metal ions, biomolecules, and amino acids were prepared with the same concentration as the target

analyte, Milli Q water, to check their interference. All the photo physical studies of the developed PFBZ polymer in the absence and presence of various analytes were performed in PBS buffer (10 mM, pH-7.4) containing 6.5 μM of PFBZ in 1 mL quartz cuvette with a path length of 1 cm.

2.2.3 Photoluminescence Quantum Yield

The absolute quantum yield for the developed PFBZ polymer was determined by the use of Horiba Fluoromax-4 spectrometer through the integrated sphere technique.

2.3.4 The overlapped integral value and Förster distance

The magnitude of the spectral overlap integral value determines the amount of energy transfer from PFBZ (donor) towards BR (acceptor), which can be calculated by the formula shown below.[35]

$$J(\lambda) = \int_0^\infty F_D(\lambda)\, \varepsilon_A(\lambda)\lambda^4 d\lambda$$

Where the symbols J(λ) represents the overlapped integral value, F_D (λ) signifies the corrected emission intensity of PFBZ from λ to Δλ normalizing the overall intensity to unity, ε_A represents molar absorptivity (in $M^{-1}cm^{-1}$) of the BR (acceptor) at the wavelength λ. The Förster distance (R_0) between the PFBZ polymer and the BR was determined using the following equation.

$$R_0 = 0.211[(J)\Phi(\eta^{-4})(k^2)]^{1/6}$$

Where J is the amount of spectral overlapping between the emission spectrum of PFBZ (donor) and the absorption spectrum. BR (acceptor), Φ symbolizes the fluorescence quantum yield of PFBZ (donor), η represents the refractive index (RI) of the experimental medium (water =1.33), and k^2 is constant (taken as 0.667) representing the dipole orientation factor.

The overall FRET efficiency (E) has been calculated with the following equation.

$$E = 1 - \frac{\tau_{DA}}{\tau_D}$$

Where the symbols τ_D, τ_{DA} signify the time-resolved photoluminescence lifetimes of the donor, PFBZ, without and with the acceptor, BR, respectively. Then, the appropriate distance (R) for donor-acceptor (D–A), i.e., the PFBZ-BR distance, was determined from the following equation.

$$R = R_0 \sqrt[6]{\frac{1-E}{E}}$$

2.2.5 Inner filter effect (IFE) correction. The suppression effect of IFE in the emission intensity of PFBZ can be determined by means of the following equation (for 1 cm path length cuvette).[36]

$$I_{corr}/I_{obs} = (10)^{(Aex + Aem)/2)}$$

Where I_{obs} and I_{corr} represent the fluorescence emission intensity without and with IFE correction, respectively. A_{em} and A_{ex} represent the values of UV-Vis absorption of the PFBZ (fluorophore) at the wavelengths of emission maxima and excitation with BR (analyte) addition.

2.2.6 Lowest Limit of Detection (LOD)

The calculation of the lowest LOD was done by taking fluorescence spectra of various samples of PFBZ polymer with different concentrations of BR *viz* (0-175ρM) in a PBS solution (10 mM, pH 7.4) containing PFBZ (6.5 µM). From the above calibration plot, the lowest LOD was calculated using the standard formula. LOD=3σ/k, where the symbols σ and k denote the standard deviation (SD) and the slope of the calibration plot, respectively.[37]

2.3 Results and Discussion

2.3.1 Characterization of PFBZ. The PF polymer poly(9,9-bis(6-bromohexyl)-9H-fluorene) was synthesized by using low-cost oxidative coupling reaction and the target yellow color emitting polymer PFBZ poly1,1'-((2,7-dimethyl-9H-fluorene-9,9-diyl) bis(hexane-6,1-diyl))bis(1H ben-zo[d]imidazole) was obtained by post functionalization method as shown in Scheme 1. The synthesized monomer and polymers at each step were well purified and characterized by NMR, mass, and GPC before being used in further studies [Figures. A2.1-A2.6]. The benzimidazole groups incorporated into the alkyl chains of PFBZ acts as a unique site for BR recognition, which amplifies its selectivity and sensing efficiency via multiple non-covalent/H-bonding interactions with the carbonyl groups present in the BR molecule. The PFBZ polymer exhibited high solubility in organic solvents and spontaneously formed nanoparticles in water. The synthesized PFBZ polymer nanoparticles exhibit absorption maxima at 376 nm, excitation maxima at 370 nm, and emission maxima at 526 nm with an absolute fluorescence quantum yield (Φs) of 29 % in aqueous PBS buffer (10 mM pH = 7.4).

2.3.2 Sensing Studies in PBS Buffer Medium

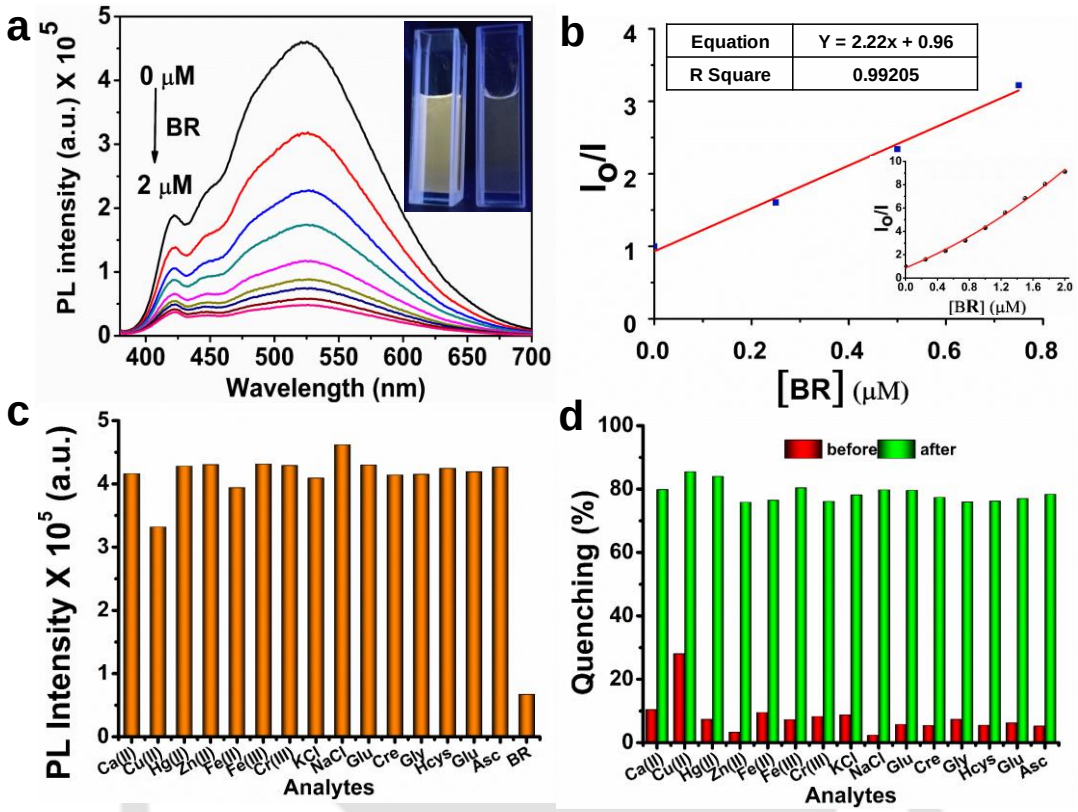

Figure 2.1. (a) PL quenching of PFBZ (6.5 μM) by addition of BR (0-2 μM) in PBS (10 mM pH 7.4) Inset: Photograph of PFBZ (6.5 μM) in PBS buffer (10 mM pH 7.4) before and after BR addition (2 μM). (b) Stern-Volmer plot obtained for PFBZ (6.5 μM) by addition of BR (0-2 μM). (c) Selectivity of PFBZ (6.5 μM) in PBS buffer media (10 mM pH 7.4) towards several analytes present in our body. (d) Percentage interference of several interfering analytes (2 μM) in the detection of BR by PFBZ (6.5 μM) in PBS buffer media (10 mM pH 7.4).

The PFBZ polymer nanoparticle (6.5 μM) emits yellow fluorescence (526 nm) in an aqueous PBS medium (10 mM, pH = 7.4), where the intensity of yellow color diminishes gradually on sequential addition of BR [Figure 2.1a] (**Inset**: Photograph of PFBZ solution in PBS buffer before and after BR addition). Further, it was also observed that the PFBZ polymer nanoparticle is highly sensitive to the BR, with 31 % quenching on its initial (first) addition of only 0.25 μM concentration, and finally becomes saturated at 89 % on further adding up to 2 μM concentration. The fast and drastic quenching on the initial addition of BR (0.25 μM) is due to the combined effect of both the molecular wire effect and the energy transfer process, where the detection process may be enhanced due to multiple non-covalent/H-bonding interactions. The N-atoms of benzimidazole-strapped PFBZ polymer nanoparticles could be expected to undergo multiple H-bonding interactions with the carboxylic moieties present in the BR molecule. The efficiency of PFBZ in response to BR is calculated from the Stern-Volmer (S-

V) relation ($I_0/I = 1 + K_{sv}[Q]$), in which I_o and I represent the emission intensity of PFBZ (fluorophore) before and after the addition of BR (quencher), respectively; Q is the quencher concentration of BR), and K_{sv} represents the Stern-Volmer constant (M^{-1}). The value of K_{sv} obtained from the linear fitting of Stern-Volmer data was found to be 2.22×10^6 $M^{-1,}$ indicating effective sensitivity of PFBZ for BR in PBS buffer (10 mM pH=7.4) [Figure 2.1b]. The K_{sv} plot is fitted linearly at lower concentrations and rises exponentially at higher concentrations [Inset: Figure 2.1b], where this deviation from linearity nature is evidence for amplifying the quenching response of a CP, which might be responsible for the molecular wire effect or multiple mechanisms. Finally, the LOD determined from the relation 3σ/k was found to be 6.9 ρM [Figure A2.7], which is far below the clinical detection range <25 to >50 μmol/L, suggesting the practical applicability of PFBZ for early diagnosis of jaundice and liver malfunctions. Furthermore, such outstanding K_{sv} and LOD are reported for the first time using benzimidazole strapped PFBZ polymer nanoparticles and the highest among all the reported BR probes [Table A2.1].

2.3.3 Selectivity studies in PBS buffer Medium

The selectivity of the PFBZ polymer nanoparticle (6.5 μM) towards BR was analyzed by monitoring the fluorescence change of PFBZ (6.5 μM) in the presence of several competing analytes such as metal ions [Ca(II), Cu(II), Hg(II), Zn(II), Fe(II), Fe(III), Cr(III)], salts (KCl, NaCl), amino acids (homocysteine, glycine, glutamate), and various biomolecules (glucose, ascorbic acid, creatinine) each of concentration 2 μM. The emission intensity of PFBZ (6.5 μM) remained unperturbed by any of these analytes [Figure 2.1c], as seen from the quenching efficiency plots for each analyte, demonstrating excellent selectivity of PFBZ for BR. Furthermore, it was also remarked that all the analytes show negligible interference compared to the sensing of BR (89 % quenching) [Figure 2.1d].

2.3.4 Mechanism of Sensing

The detailed analysis of both theoretical and experimental findings reveals the possibility of more than one mechanism for BR sensing by PFBZ. These can be (a) Förster resonance energy transfer (FRET) or/and inner filter effect (IFE) and (b) ground state complexation. BR has a broad UV-visible absorption spectrum (λ_{max} 434 nm) overlapping with both the excitation spectrum and emission spectrum of PFBZ in PBS buffer (10 mM, pH 7.4), which are the prerequisite conditions for either FRET or IFE or both to occur in the mechanism of sensing

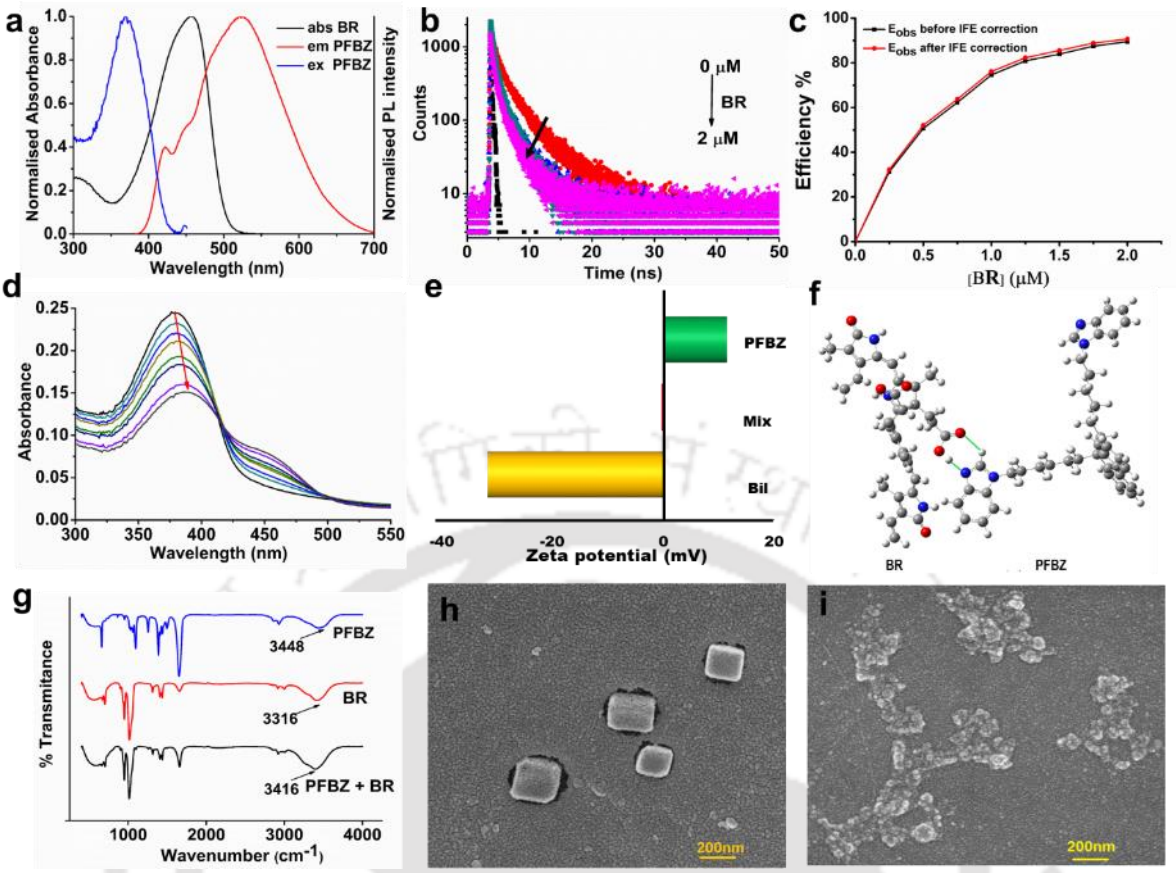

Figure 2.2. (a) Spectral overlap of excitation/emission spectra of PFBZ with the absorption spectra of BR. (b) Lifetime decay of PFBZ before and after the addition of BR. (c) IFE suppression efficiency for PFBZ after the addition of BR. **(d)** UV-visible spectra of PFBZ with BR addition (0-2 μM). (e) Zeta potential spectra of PFBZ and BR and their mixture (f) Structural optimization of PFBZ and BR using the B3LYPP (6-31G*) function in the Gaussian Program. (g) FT-IR spectra of PFBZ, BR, and their mixtures. (h), (i) FESEM images of PFBZ (6.5 μM) in the absence and presence of 2 μM (BR), respectively.

[Figure 2(a)]. In principle, the occurrence of IFE required considerable spectral overlaps of the acceptor (BR) absorption spectrum with excitation and/or emission spectra of the donor (PFBZ). In contrast, FRET occurs only when the spectral overlap occurs exclusively between the emission and absorption spectra of the donor (PFBZ) and accepter (BR), respectively.[38] Hence, to ascertain the dynamic quenching, the time-resolved photoluminescence lifetime of PFBZ (6.5 μM) was studied before and after additions of various concentrations of BR (0.5 μM, 1 μM, 1.5 μM and 2 μM) in PBS buffer (1 mM, pH= 7.4) [Table S2]. Notably, a huge change in the lifetime of PFBZ (3.067 ns) after the final addition of BR (1.542 ns) was observed, confirming the FRET mechanism [Figure 2.2b]. The change in lifetime indicates that FRET is the key cause of sensing rather than IFE in the sensing mechanism. This assumption is also in agreement with the ineffective spectral overlap of the absorption spectrum of BR and the excitation/emission spectra of PFBZ [Figure 2.2a], which consequently gives rise to less

IFE suppression efficiency in the PBS medium (10 mM pH 7.4) [Figure. 2.2c]. From all these observations, it can be concluded that FRET is the pivotal mechanism in sensing, with ~50 % of FRET efficiency [Table A2.3] and no input of IFE [Table A2.4]. Since steady-state quenching efficiency for BR (89 %) is more than FRET efficiency, hence we assume that static quenching also contributes to the sensing mechanism.

To validate the ground state complexation, the UV visible spectra of PFBZ (6.5 µM) were monitored in BR, which shows a 10 nm red shift upon BR addition [Figure 2.2d]. This shift can be attributed to the complexation between the PFBZ and BR, leading to polymer aggregation. Also, the decrement of the PFBZ absorption peak at 380 nm and the corresponding increment of the broad BR peak at 450 with an isobestic point at 415 also support the formation of a non-fluorescent complex between PFBZ and BR.[39] The complexation was well studied by ζ potential measurement, where the positive ζ potential of PFBZ (+11.5 mV) was almost neutralized (0.00963) upon the addition of negatively charged BR (−31.7 mV), indicating effective complexation between PFBZ and BR [Figure 2.2e]. Theoretical and experimental studies were carried out to identify the nature of the interaction between the PFBZ polymer nanoparticle and BR. The complexation was investigated theoretically through Gaussian 03 software using the DFT, B3LYP, and 6-31G* basis sets. It was evident from the resulting structure that there is a possibility of 7-membered ring formation with close proximity between the O-atom of carboxylic moiety (BR) and 'H' of imidazole (PFBZ); 'H' of hydroxy (BR), and N of imine (PFBZ) [Figure 2.2f]. To verify such complexation experimentally, Raman and FTIR spectra of both the PFBZ and BR and their mixtures were recorded. There is a shift in the stretching frequency of the -NH group of benzimidazole in PFBZ from 3448 cm^{-1} to 3416 cm^{-1} in the PFBZ_BR mixture, which confirms multiple H-bonding interactions between the NH of benzimidazole and carboxylic moieties in BR [Figure 2.2g]. This complexation is also evident from Raman spectra, as there is a ~9 nm shift in carbonyl stretching (1600.23 to 1609.08) of BR in the PFBZ_BR complex mixture [Figure. A2.8]. Furthermore. The polymer aggregation by BR was studied using FESEM and TEM analysis. Initially, the PFBZ has a nano cubic structure of diameter ~240 nm [Figure. 2.2h), Figure A9a], which changes into larger aggregate structures [Figure 2.2i, Figure A2.9b] after BR addition. The change in size of the polymer nanoparticles was also supported by DLS measurements. The hydrodynamic diameter of polymer nanoparticles increased from 267 nm to 1043 nm on BR addition [Figure A2.10a, A2.10b]. This interaction brings the combined species close enough with appropriate orientation within a bonding distance and is ideal for enhancing the FRET mechanism.

2.3.5 Detection of BR in blood serum

The outstanding sensitivity and selectivity of PFBZ directed us to examine the practical application of this system in real blood serum samples. Serum samples of 3 individuals, two jaundice patients (J1, J2) and one normal person (N1), were collected from the IITG Hospital and used without further treatment. The BR-containing serum sample was tested by adding it to a cuvette containing PFBZ solution to monitor the change in fluorescence spectra. The amount of BR present in serum was then determined by a calibration plot (Figure A2.11). The results of our standard method were compared with the well-known peroxidase method performed at the Medical laboratory of IIT Guwahati. **Table 2.1** represents the BR concentration determined by our probe and peroxidase method. Hence, the PFBZ detection assay is very reliable, simple, rapid, and cost-effective, as no serum pretreatment is needed. This method is reproducible for the detection of a wide range of BR concentrations and the diagnosis of the onset of jaundice and associated diseases.

Table 2.1. Determination of blood serum BR

Serum samples	BR detected by PFBZ method (10^{-6} M)	BR detected by peroxidase method (10^{-6} M)
J1	49.1±0.1	50
J2	33.1±0.2	33
N1	10.4±0.3	10

Fluorescence Test Kit

After achieving reliable sensing performance through the fluorescence method, a portable, cost-effective paper strip device was fabricated for real-time application. The Whatman filter paper was cut into test strips of the desired dimension of 1 cm by 1 cm and dipped into the PFBZ polymer nanoparticle solution (10^{-3} M), followed by drying on a hot plate at 50 °C. The PFBZ-coated paper strips were then used for real-time onsite detection of BR. Different concentrations of BR stock solution were prepared and drop-cast into fluorescent PFBZ-coated paper strips. The filter papers were then photographed using a 365 nm UV light source (Figure 2.3). Noticeable dark spots of different strengths were observed by the naked eye under 365 nm, which corresponded to the BR concentration drop that was cast. A blank solvent spot was used as a control. The limit of detection was found to be 58.5 ng/cm^{2,} which permits the utility of these paper strips for onsite detection of BR to identify the onset of jaundice and its associated diseases.

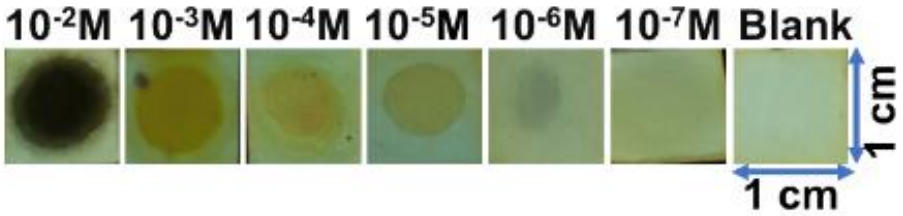

Figure 2.3. Color of paper-based fluorescence test kits under UV-lamp (365 nm) after the addition of 10 μL of various concentrations of BR (10^{-2}M – 10^{-7}M).

2.4 Conclusion

In summary, benzimidazole incorporated yellow emitting conjugated polymer nanoparticle PFBZ was synthesized by means of a low-cost and straightforward oxidative coupling polymerization reaction for sensing BR in a complex biosystem for the first time. The receptor benzimidazole is specific to BR, achieving excellent selectivity in the presence of other interfering analytes, which is the key requirement for an ideal sensing system. PFBZ being a CPN, its sensory signal was amplified to a great extent, improving its sensitivity up to LOD 6.9 ρM, which is far less than the clinically relevant range in aqueous PBS buffer medium at physiological pH and label-free conditions. The sensing mechanism elucidated both experimentally and theoretically was primarily found to be due to FRET and ground state complexation between the PFBZ and BR. It was also found that PFBZ polymer nanoparticles can be successfully utilized in the quantitative study of BR in real blood serum, where the results obtained were in good agreement with the standard clinical routine test results with a very low standard deviation. Further, a paper-based fluorescence test kit was fabricated in a very simple way, giving a quick response time and offering a reliable platform to diagnose the onset of jaundice and liver malfunction for real-time application.

References

1. McDonagh, A. F.; Palma, L. A.; Trull, F. R.; Lightner, D. A. Phototherapy for Neonatal Jaundice. Configurational Isomers of Bilirubin. *J. Am. Chem. Soc.* **1982**, *104*, 6865-6867.

2. Du, Y.; Li, X.; Lv, X.; Jia, Q. Highly Sensitive and Selective Sensing of Free Bilirubin Using Metal–Organic Frameworks-Based Energy Transfer Process. *ACS Appl. Mater. Interfaces* **2017**, *9*, 30925-30932.

3. Chen, Q.; Huggins, M. T.; Lightner, D. A.; Norona, W.; McDonagh, A. F. Synthesis of a 10-Oxo-Bilirubin: Effects of the Oxo Group on Conformation, Transhepatic Transport, and Glucuronidation. *J. Am. Chem. Soc.* **1999**, *121*, 9253-9264.

4. Ahmmed, E.; Mondal, A.; Sarkar, A.; Chakraborty, S.; Lohar, S.; Saha, N. C.; Dhara, K.; Chattopadhyay, P. Bilirubin Quantification in Human Blood Serum by Deoxygenation Reaction Switch-Triggered Fluorescent Probe. *ACS Appl. Bio Mater.* **2020**, *3*, 4074-4080.

5. Senthilkumar, T.; Asha, S. K. Selective and Sensitive Sensing of Free Bilirubin in Human Serum Using Water-Soluble Polyfluorene as Fluorescent Probe. *Macromolecules* **2015**, *48*, 3449-3461.

6. Dal Ben, M.; Bottin, C.; Zanconati, F.; Tiribelli, C.; Gazzin, S. Evaluation of Region Selective Bilirubin-Induced Brain Damage as a Basis for a Pharmacological Treatment. *Sci. Rep*. **2017**, *7*, 1-2.

7. Hansen, T. W. Pioneers in the Scientific Study of Neonatal Jaundice and Kernicterus. *Pediatrics* **2000**, *106*, E15.

8. Willy, T.; Hansen, R.; Ph, D. Bilirubin in the Brain Processes on' I Effects of Bilirubin. *Clinical Pediatrics* **1994**, *33*, 452-459.

9. Wagner, K.-H.; Shiels, R. G.; Lang, C. A.; Seyed Khoei, N.; Bulmer, A. C. Diagnostic Criteria and Contributors to Gilbert's Syndrome. *Crit. Rev. Clin. Lab. Sci.* **2018**, *55*, 129-139.

10. Scheidt, P. C.; Mellits, E. D.; Hardy, J. B.; Drage, J. S.; Boggs, T. R. Toxicity to Bilirubin in Neonates: Infant Development during First Year in Relation to Maximum Neonatal Serum Bilirubin Concentration. *J. Pediatr.* **1977**, *91*, 292-297.

11. Lang, E.; Gatidis, S.; Freise, N. F.; Bock, H.; Kubitz, R.; Lauermann, C.; Orth, H. M.; Klindt, C.; Schuier, M.; Keitel, V.; Reich, M.; Liu, G.; Schmidt, S.; Xu, H. C.; Qadri, S. M.; Herebian, D.; Pandyra, A. A.; Mayatepek, E.; Gulbins, E.; Lang, F.; Häussinger, D.; Lang, K. S.; Föller, M.; Lang, P. A. Conjugated Bilirubin Triggers Anemia by Inducing Erythrocyte Death. *Hepatology* **2015**, *61*, 275-284.

12. Lin, L. Y.; Kuo, H. K.; Hwang, J. J.; Lai, L. P.; Chiang, F. T.; Tseng, C. Den; Lin, J. L. Serum Bilirubin Is Inversely Associated with Insulin Resistance and Metabolic Syndrome among Children and Adolescents. *Atherosclerosis* **2009**, *203*, 563-568.

13. Song, Y. S.; Koo, B. K.; Cho, N. H.; Moon, M. K. Effect of Low Serum Total Bilirubin Levels (≤0.32 Mg/Dl) on Risk of Coronary Artery Disease in Patients with Metabolic Syndrome. *Am. J. Card.* **2014**, *114*, 1695-1700.

14. Fevery, J. Bilirubin in clinical practice: a review. *Liver Int.* **2008**, *28*, 592-605.

15. Jacobsen, J.; Wennberg, R. P. Determination of Unbound Bilirubin in the Serum of Newborns. *Clin. Chem.* **1974**, *20*, 783-789.

16. Ngashangva, L.; Bachu, V.; Goswami, P. Development of New Methods for Determination of Bilirubin. *J. Pharm. Biomed. Anal.* **2019**, *162*, 272-285.

17. Ahlfors, C. E. Measurement of Plasma Unbound Unconjugated Bilirubin. *Anal. Biochem.* **2000**, *279*, 130-135.

18. Brodersen, R.; Bartels, P. Enzymatic Oxidation of Bilirubin. *Eur. J. Biochem.* **1969**, *10*, 468-473.

19. Tenhunen, R.; Marver, HS and Schmid, R. Microsomal heme oxygenase: characterization of the enzyme. *J. Biol. Chem.* **1969**, *244*, 6388-6394.

20. Anjana, R. R.; Anjali Devi, J. S.; Jayasree, M.; Aparna, R. S.; Aswathy, B.; Praveen, G. L.; Lekha, G. M.; Sony, G. S, N-Doped Carbon Dots as a Fluorescent Probe for Bilirubin. *Microchim. Acta* **2018**, *185*, 1–11.

21. Srinivasan, V.; Jhonsi, M. A.; Dhenadhayalan, N.; Lin, K. C.; Ananth, D. A.; Sivasudha, T.; Narayanaswamy, R.; Kathiravan, A. Pyrene-Based Prospective Biomaterial: In Vitro Bioimaging, Protein Binding Studies and Detection of Bilirubin and Fe^{3+}. *Spectrochim. Acta A Mol. Biomol. Spectrosc.* **2019**, *221*, 117150.

22. Yang, W.; Xia, J.; Zhou, G.; Jiang, D.; Li, Q. Sensitive Detection of Free Bilirubin in Blood Serum Using β-Diketone Modified Europium-Doped Yttrium Oxide Nanosheets as a Luminescent Sensor. *RSC Adv.* **2018**, *8*, 17854-17859.

23. Makkad, S. K.; Asha, S. K. Designed Amphiphilic Polystyrene as Surfactant for Oligo(p -Phenylenevinylene)-Incorporated PS Nanobeads and Visual Detection of Bilirubin in Human Blood Serum. *ACS Appl. Polym. Mater.* **2019**, *1*, 1230-1239.

24. Senthilkumar, T.; Asha, S. K. Self-Assembly in Tailor-Made Polyfluorenes: Synergistic Effect of Porous Spherical Morphology and FRET for Visual Sensing of Bilirubin. *Macromolecules* **2013**, *46*, 2159-2171.

25. Malik, A. H.; Hussain, S.; Kalita, A.; Iyer, P. K. Conjugated Polymer Nanoparticles for the Amplified Detection of Nitro-Explosive Picric Acid on Multiple Platforms. ACS Appl. Mater. Interfaces **2015**, *7*, 26968-26976.

26. Conjugated Polymers for Biological and Biomedical Applications, 1st editio.; Prof. Bin Liu, Ed.; Wiley-VCH, Weinheim, Germany, **2018**.

27. Tuncel, D.; Demir, H. V. Conjugated Polymer Nanoparticles. *Nanoscale* **2010**, *2*, 484-494.

28. Zehra, N.; Dutta, D.; Malik, A. H.; Ghosh, S. S.; Iyer, P. K. Fluorescence resonance energy transfer-based wash-free bacterial imaging and antibacterial application using a cationic conjugated polyelectrolyte. *ACS Appl. Mater. Interfaces* **2018**, *10*, 27603-27611.

29. Tian, Z.; Yu, J.; Wu, C.; Szymanski, C.; McNeill, J. Amplified Energy Transfer in Conjugated Polymer Nanoparticle Tags and Sensors. Nanoscale **2010**, *2*, 1999-2011.

30. Zehra, N.; Kalita, A.; Malik, A. H.; Barman, U.; Adil Afroz, M.; Iyer, P. K. Conjugated Polymer-Based Electrical Sensor for Ultratrace Vapor-Phase Detection of Nerve Agent Mimics. *ACS Sens*, **2019**, *5*, 191-198.

31. Malik, A. H.; Hussain, S.; Iyer, P. K. Aggregation-Induced FRET via Polymer–Surfactant Complexation: A New Strategy for the Detection of Spermine. *Anal. Chem.* **2016**, *14*, 7358–7364.

32. Gu, P.-Y.; Wang, Z.; Zhang, Q. Azaacenes as Active Elements for Sensing and Bio Applications. *J. Mater. Chem. B* **2016**, *4*, 7060–7074

33. Mondal, S.; Vashi, Y.; Ghosh, P.; Roy, D.; Barthakur, M.; Kumar, S.; Iyer, P. K. Amyloid Targeting "Artificial Chaperone" Impairs Oligomer Mediated Neuronal Damage and Mitochondrial Dysfunction Associated with Alzheimer's Disease. *ACS Chem. Neurosci.* **2020**, *11*, 3277-3287.

34. Saikia, G.; Iyer, P. K. Facile C−H Alkylation in Water: Enabling Defect-Free Materials for Optoelectronic Devices. *J. Org. Chem.* **2010**, *75*, 2714-2717.

35. Malik, A. H.; Hussain, S.; Iyer, P. K. Aggregation-Induced FRET via Polymer–Surfactant Complexation: A New Strategy for the Detection of Spermine. Anal. Chem. **2016**, *14*, 7358–7364.

36. Lakowicz, J. R. Protein Fluorescence. In Principles of fluorescence spectroscopy; Springer, **1983**, 341–381.

37. Tanwar, A. S.; Patidar, S.; Ahirwar, S.; Dehingia, S.; Iyer, P. K. Receptor Free Inner Filter Effect Based Universal Sensors for Nitroexplosive Picric Acid Using Two Polyfluorene Derivatives in the Solution and the Solid States. *Analyst* **2019**, *144*, 669-676.

38. Tanwar, A. S.; Adil, L. R.; Afroz, M. A.; Iyer, P. K. Inner Filter Effect and Resonance Energy Transfer Based Attogram Level Detection of Nitroexplosive Picric Acid Using Dual Emitting Cationic Conjugated Polyfluorene. *ACS Sens*. **2018**, *3*, 1451-1461.

39. Malik, A. H.; Hussain, S.; Tanwar, A. S.; Layek, S.; Trivedi, V.; Iyer, P. K. An Anionic Conjugated Polymer as a Multi-Action Sensor for the Sensitive Detection of Cu^{2+} and PPi, Real-Time ALP Assaying and Cell Imaging. *Analyst* **2015**, *140*, 4388-4392.

APPENDIX

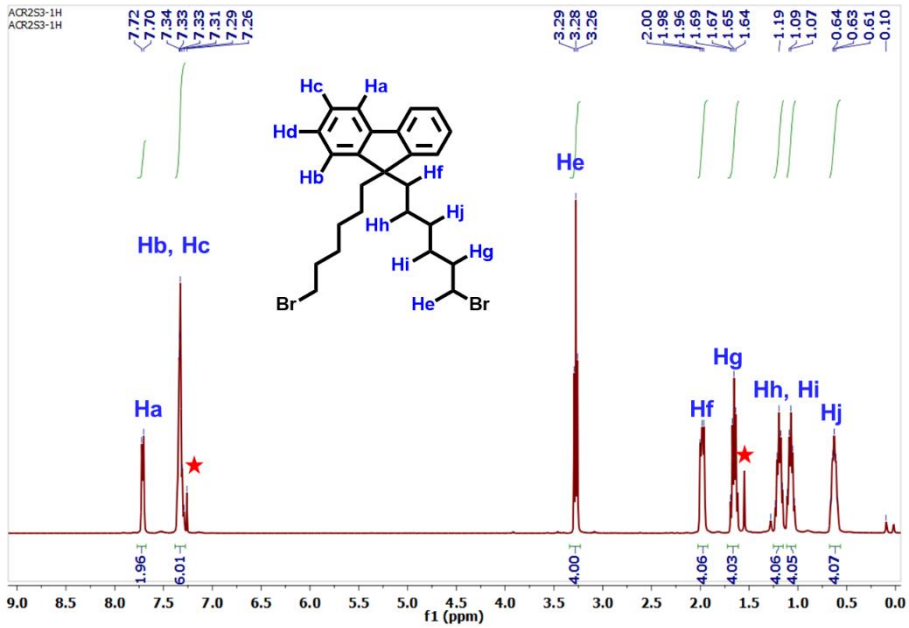

Figure A2.1. ^{1}H NMR spectra of M2 in $CDCl_3$

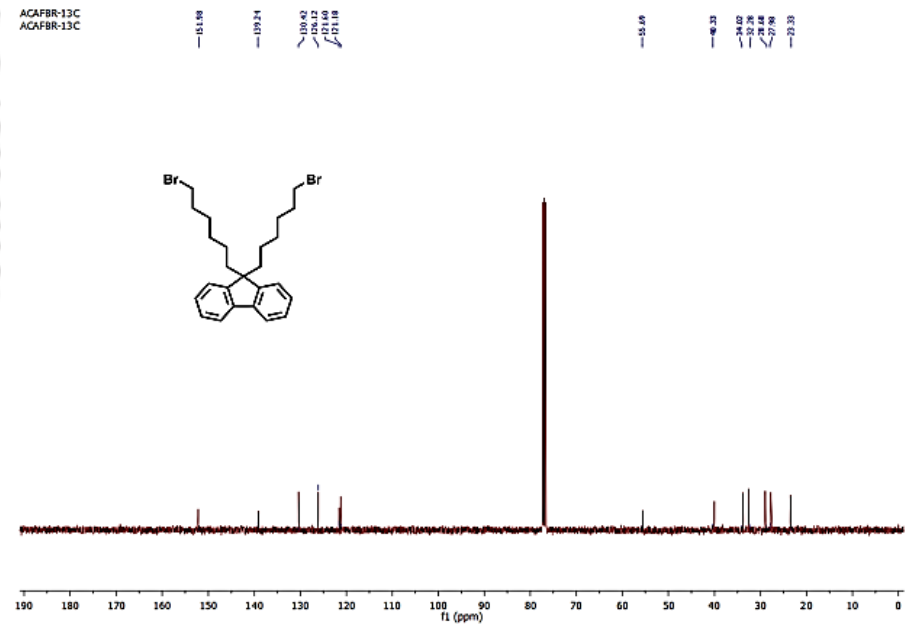

Figure A2.2. ^{13}C NMR spectra of M2 in $CDCl_3$.

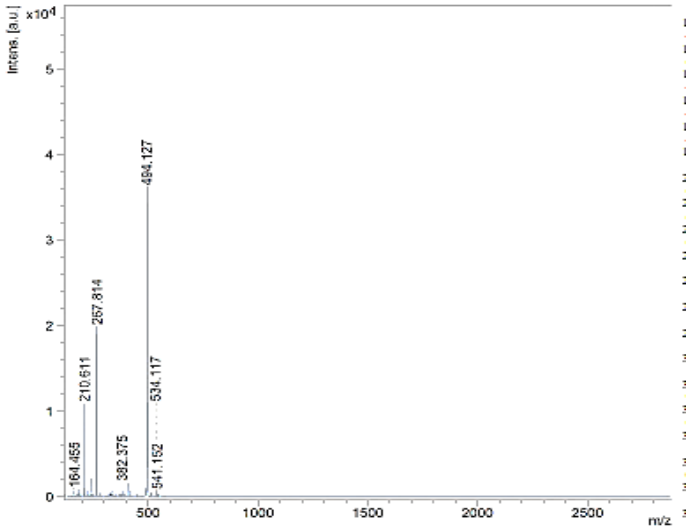

Figure A2.3. Maldi-TOF spectra for monomer M2

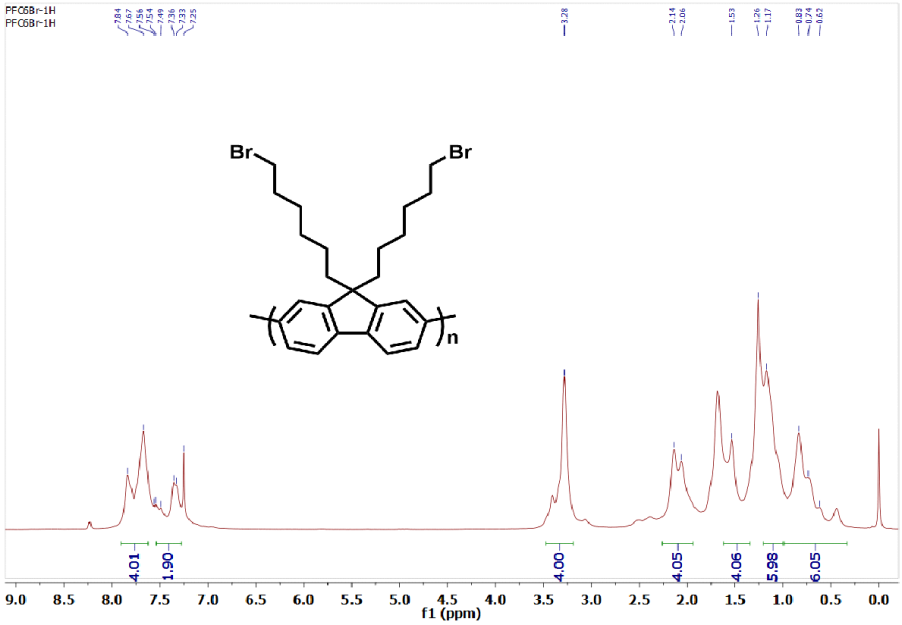

Figure A2.4. ^{1}H NMR spectra of PF in $CDCl_3$.

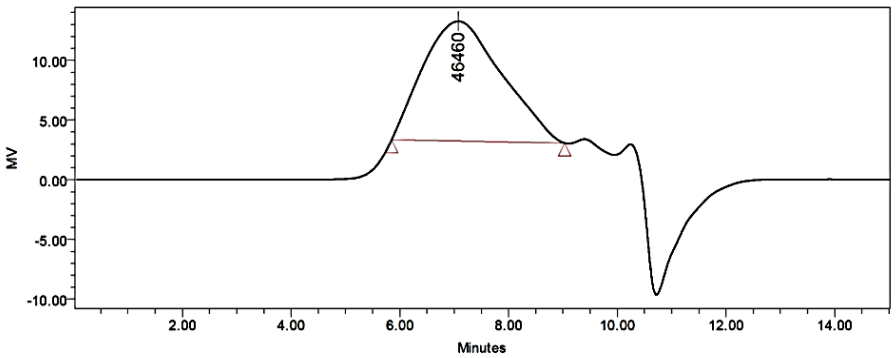

GPC Results

	Retention Time (min)	% Area	Mn	Mw	MP	Mz	Mz+1	Poly dispersity
1	7.077	100.00	26316	52601	46460	85438	114259	1.998798

Figure A2.5 GPC chromatogram of polymer PF

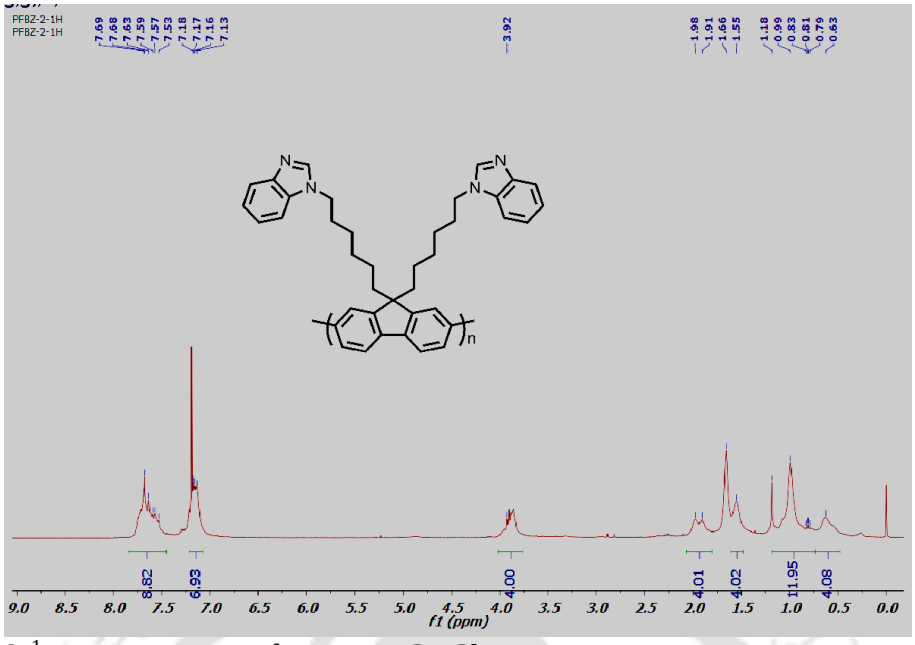

Figure A2.6. ^{1}H NMR spectra of PFBZ in $CDCl_3$.

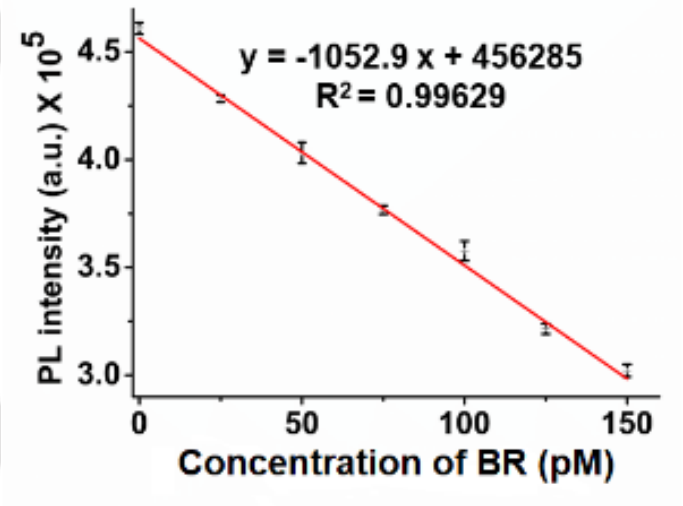

Figure A2.7. Fluorescence intensity of PFBZ (6.5 µM) in PBS buffer (10mM pH 7.4) *vs* BR concentration (0-150ρM).

LOD = 3 × S.D./k= 3 × 2417.21/ (1052.9) = 6.9pM

Table A2.1. A comparative study of some fluorescent probes for bilirubin detection

	Materials used	K_{sv} (M^{-1})	Lod	Medium
Present Manuscript	Conjugated polyfluorene	2.22×10^{6}	6.9 pM	PBS pH = 7.4
ACS Appl. Bio Mater. **2020**, 3, 4074−4080	A coumarin-based small molecule	-	76 nM	HEPES buffer at pH 7.2, 5% DMSO)
ACS Appl. Polym. Mater. **2019**, 1, 1230−1239	Amphiphilic polystyrene	262.008	20 nM,	Ches buffer at pH = 10

Molecular and Biomolecular Spectroscopy. **2019,** 221, 117150	Pyrene Schiff Base AIE nanodots	-	0.3 µg/mlµ M,	DMSO: water (10:90) medium
Anal. Chem. **2018**, 90, 13687-13694	Graphene-isolated-Au-nanocrystals	-	7 µM	CH_2Cl_2
RSC Adv., **2018**, 8, 17854-17859	Europium-Doped Yttrium Oxide Nanosheets	-	41 nM.	-
Macromolecules **2015**, 48, 3449−3461	Conjugated Polyfluorenes	-	150 nm	PBS buffer pH=10
Biosensors and Bioelectronics **2014,** 59 370–376	HSA stabilised gold nanoclusters	-	248 nM	Aliquots (1 mL) containing PBS (pH 7.4)
Macromolecules **2013**, 46, 2159−2171	Conjugated Polyfluorenes	-	-	THF/water

Table A2.2. Fluorescence lifetime decay of each component and their fractions in PBS

Sample	**τ_1 (ns)**	**%**	**τ_2 (ns)**	**%**	**τ_3**	**%**	**τ_{avg} (ns)**
PFBZ	0.361	17.240	1.924	47.250	5.902	35.510	3.067
PFBT-BR (2ul)	0.278	34.913	1.391	44.054	4.337	21.034	1.622
PFBT-BR (4ul)	0.251	34.717	1.293	42.641	4.250	22.642	1.601
PFBT-BR (6ul)	0.229	35.220	1.240	39.540	4.008	25.220	1.582
PFBT-BR (8ul)	0.251	34.787	1.183	39.774	3.856	25.469	1.542

Table A2.3: Förster distance, overlap integral J (λ) values and FRET efficiency, D-A distance is calculated for BR in PBS (1mM, pH=7.4)

Solvent	**Förster distance R_0 (Å)**	**J (λ) values ($M^{-1}cm^{-1}nm^4$)**	**FRET efficiency (%)**	**Donor- Acceptor distance (R) (Å)**
PBS (10mM, pH=7.4)	43.51	5.44×10^{14}	49.72	43.59

Table A2.4. Calculations for IFE corrections for quenching in PBS

BR (µM)	**A_{ex} (370 nm)**	**A_{em} (530 nm)**	**I_{obs}**	**I_{corr}**	**I_{corr} /I_{obs} Correction factor (CF)**	**$I_{corr}/I_{corr,o}$**	**E_{obs}**	**E_{corr}**
0	0.2364	0.0206	460578	619273	1.34455	1	0	0
0.25	0.2229	0.0213	316674	419535	1.32481	0.67746	31.2442	32.2536
0.5	0.2106	0.0211	227170	296659	1.30589	0.47904	50.6772	52.0955
0.75	0.2011	0.0212	173830	224551	1.29178	0.36260	62.2582	63.7395

1	0.1830	0.0201	116988	147827	1.26361	0.23871	74.5996	76.1288
1.25	0.1732	0.0195	87933	109785	1.24850	0.1772	80.9080	82.2719
1.5	0.1477	0.0176	74010	89526	1.20964	0.14456	83.9310	85.5433
1.75	0.1384	0.0167	57719	69008	1.19557	0.11143	87.4680	88.8565
2	0.1384	0.01694	48309	57775	1.19593	0.09329	89.5110	90.6704

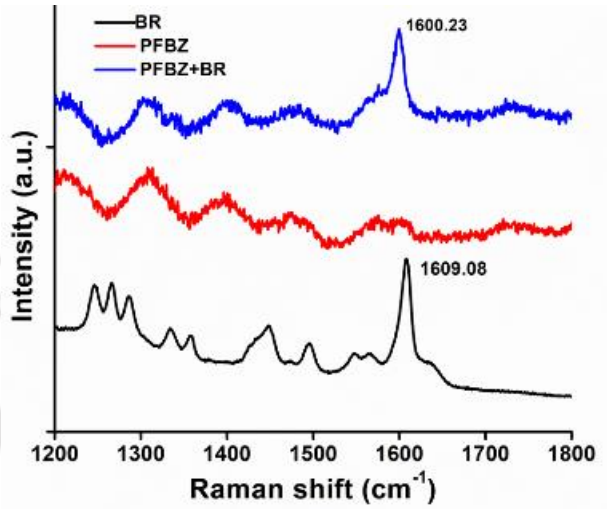

Figure A2.8. Raman spectra of PFBZ, BR and their equimolar mixture (laser 785 nm source).

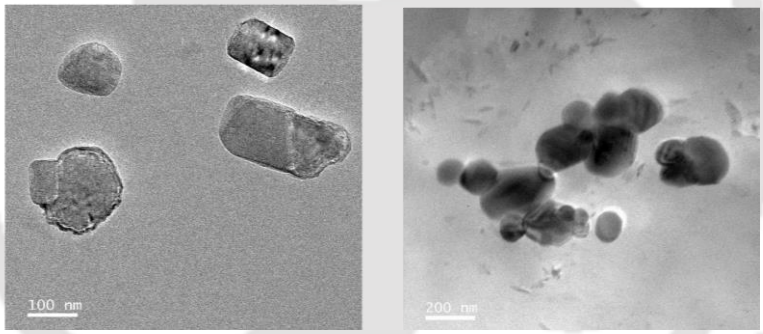

Figure A2.9. TEM images of PFBZ (a), before and (b) after addition of BR.

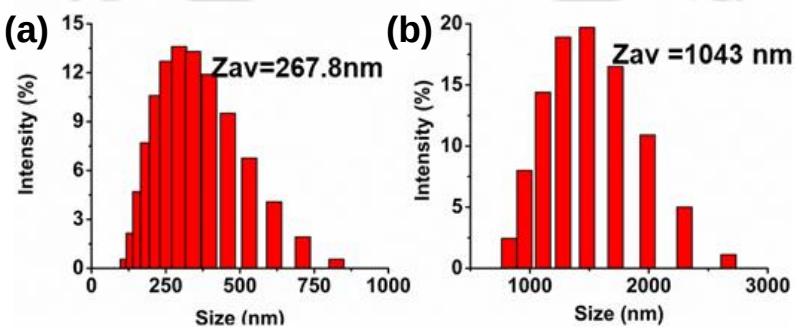

Figure A2.10. DLS spectra of PFBZ (a) before and (b)after addition of BR

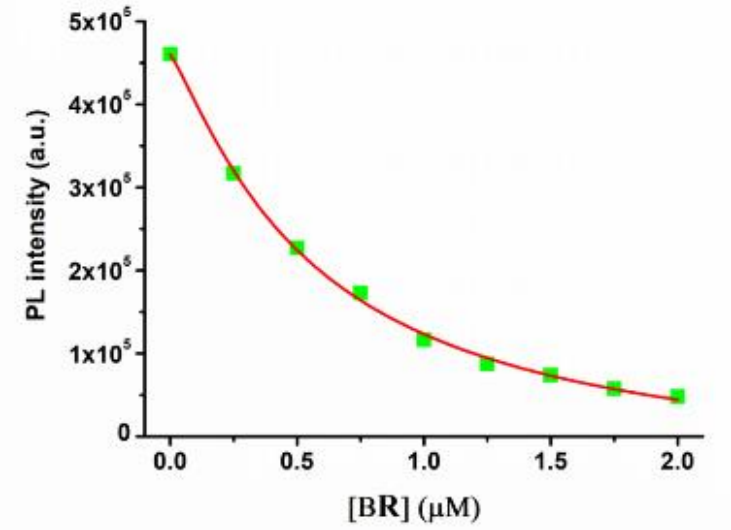

Figure A2.11. Calibration plot of PFBZ (6.5 μM) on the addition of various concentrations of BR (0-2μM).

CHAPTER 3

Receptor Free AIEE Conjugated Polymer Nanoparticle Based PoC Device for Amplified Detection of Pendimethalin

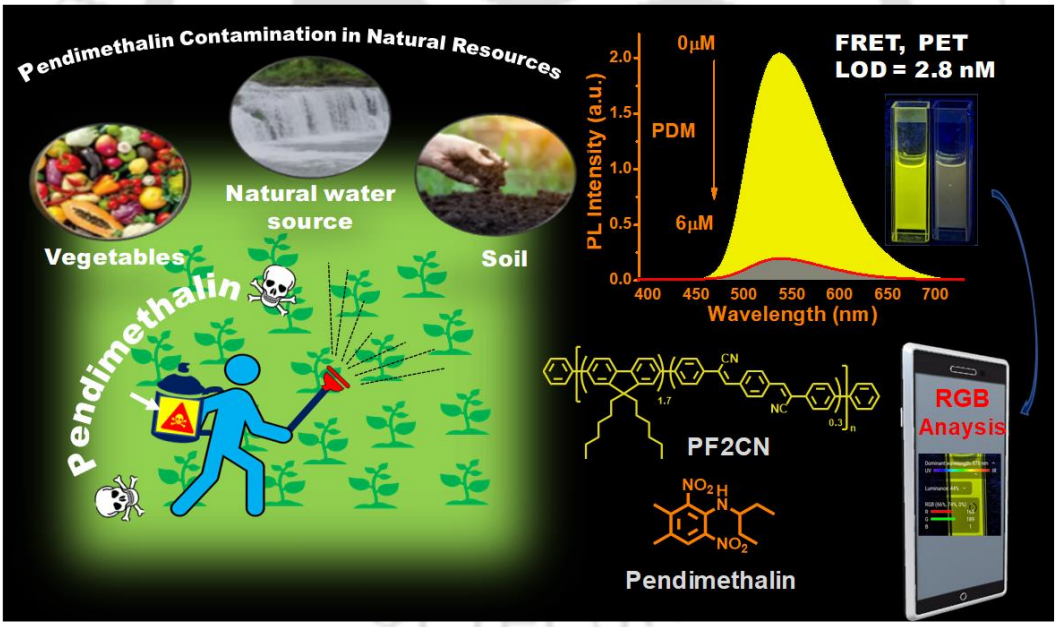

Chanu, M. A.; Adil, L. R.; Iyer, P. K *ACS Appl. Polym. Mater.* **2024**, *6* (12), 6988-6996.

Abstract

Pendimethalin (PDM) is a chemically synthesized herbicide and is primarily employed to control broadleaf weeds and woody plants. It enters our environment from production industries and from human activity in farming. Pendimethalin residues in edible foodstuffs and water sources are a serious worldwide problem as they are linked to various health issues. As such there is an urgent need for the construction of a portable point of care (PoC) testing device for the detection of pendimethalin residues from food and vegetables before being consumed. Considering this challenge, an aggregation induced enhance emission (AIEE) polymer PF2CN is developed by modifying the conjugated backbone of polyfluorene based polymer PFP. The insertion of M2CN monomer into the conjugated backbone of PF2CN plays a key role in tuning the photophysical property of the PF2CN polymer where it shows AIEE activity with red shifted emission. Further the PF2CN polymer shows remarkable sensitivity and selectivity toward PDM with a limit of detection (LOD) of 2.8 nM which is very less than the standard-maximum residual limits for pesticides in food. Notably, the simultaneous occurrence of PET and FRET serves as a "receptor free" selective sensor for PDM. Furthermore, the designed PF2CN conjugated polymer based PDM detection process was miniaturized into a prototype smartphone device, thereby providing a rapid and practical solution for on-site toxic analyte detection thereby providing higher environmental safety and protection.

Key words: Conjugated polymer; Receptor free sensing; Molecular wire effect; ACQ; AIEE**;** Pendimethalin; PoC device; Herbicide.

3.1 Introduction

Herbicide residues in fruits, vegetables, soil, and water are a severe health concern because they accounts for approximately 47.5 % of chronic effects on overall pesticide consumption and multiple organ damage.[1] Herbicides are widely used in the agricultural sector to restrict the growth of unwanted weeds and grasses as a method to increase worldwide food production. These chemicals have a lengthy half-life from 69 days to even 10 months depending on soil types and get leached from the agricultural fields into the water bodies.[2, 3] The persistent accumulation of herbicide residues in natural water bodies and edible foodstuffs causes severe food-chain pollution as well as ecosystem devastation. It can imitate steroid hormones by interacting with estrogen receptors, and can trigger the transcription of estrogen receptor-regulated genes.[4, 5]

Pendimethalin (PDM), a dinitroaniline derivative (N-(1-ethylpropyl)-2,6-dinitro-3,4-xylidine), is a common herbicide of the "K1 group" that is widely used to manage weeds and grasses in cereal crops, peanuts, legumes, peppers, potatoes, soybeans, onions, fruits, vegetables, and other crops.[6] However, the Environmental Protection Agency (EPA) of the United States has designated PDM as a persistent bioaccumulative hazardous substance and a class C carcinogen (possible human carcinogen).[7] Human exposure can occur by ingestion, inhalation, and skin contact.[2] According to China's GB 2763-2019, the national food safety standard residual limits for pesticides in food, the acceptable daily intake (ADI) of PDM is established at 100 g/kg body weight.[8, 9] PDM exposure has been linked to several physiological changes and endocrine effects demonstrated in animal studies, including liver and kidney damage and a number of mutagenic effects, genotoxicity oxidative stress[10] inflammation and the risk of pancreatic cancer in humans.[11] On account of safety concerns, dinitroaniline based herbicide is safe to use and administered strictly according to the labeled guidelines. Furthermore, due to the highly explosive nature of these nitroaniline-based herbicides, they are prohibited from use in regions where sources of ignition, such as smoking and open flames, are present.[12]

Several detection platforms are being developed for herbicide detection, such as gas chromatography (GC),[13] liquid chromatography mass spectrometry (LC-MS),[14] high performance liquid chromatography (HPLC),[15] chemiluminescence,[16] electrochemical,[17] and others.[18, 19] However, such techniques are either expensive or require highly skilled workers, and are time consuming. Further, due to its explosive nature a rapid, simple, and low-cost detection approach is particularly desirable for on-site detection. In this context, fluorescent

probe-based herbicide sensing is gaining much interest because of its quick response, simplicity, high sensitivity, and ability to detect in multiple modes (solution and solid state). Many fluorescence based materials are being developed for the detection of PDM, such as small organic materials,[20] gold nanoparticles,[6] nanowires,[16] quantum dots,[21] supramolecules[24] and silica nanoparticles.[23] However, surprisingly, there are no reports on conjugated polymer (CP) based sensors for PDM. The real challenge in designing sensory materials is the choice of a specific receptor where its incorporation requires multiple steps, time consuming and is difficult to purify. Numerous literatures have proven that CPs have inherent signal amplification property called "molecular wire effect".[24] Therefore, it can display ultrasensitivity and selectivity without any receptor.[25, 26] Thus, a "Receptor-free" strategy that does not need a laborious synthesis and purification technique and less time consuming, but still provides outstanding sensitivity and selectivity is an alternative to address the aforementioned difficulties.

CPs are an ideal class of sensory materials on account of their superquenching ability, high absorption coefficient, better film forming ability, good photostability, less toxicity and many more.[27, 28] However, due to planarity of the backbone in conventional CPs, they are plagued by the notorious aggregation caused quenching (ACQ) effect, in which they are highly emissive in solution but become quenched in the condensed/solid state, limiting their practical utility in film/solid state and constituting a hurdle in materials science. The breakthrough for solving this obstacle was achieved in 2001 since the introduction of the concept "aggregation induced emission/ aggregation induced enhanced emission" (AIE/AIEE).[29] AIE/AIEE molecules utilize the aggregation phenomena to induce/enhance condensed state and solid state emission. The combination of excellent characteristics of CPs along with the AIE property is becoming a smart approach for designing functional luminogens to meet various demands for ultrasensitivity, biocompatibility, practicability and repeatability in sensing applications.[30] However CPs due to the complexity of their molecular arrangement, strategically engineering their backbone to give AIEE property remains very challenging yet highly demanding in the present scenario.

Herein, we have designed an AIEE polymer, PF2CN by Suzuki coupling polymerization reaction (Scheme 1). The monomer (2Z,2'Z)-3,3'-(1,4-phenylene)bis(2-(4-bromophenyl)acrylonitrile) (M2CN) is used to modify the planar backbone of polyfluorene based CP. Hence, planar PFP and a nonplanar PF2CN polymers are developed by the Suzuki

polymerization reaction. PF2CN polymer due to the presence of strong electron withdrawing CN groups, which are slightly above the planar backbone, plays a key role in the AIEE activity and tuning emission wavelength via ICT as compared to PFP. Further, these CPs were utilized for the detection of herbicide PDM. Considering the remarkable sensitivity and selectivity of PF2CN, the polymer is further analyzed for a detailed mechanistic study. The simultaneous occurrence of both electrons transfers and energy transfer is the key cause of ultrasensitivity by PF2CN.

As per our knowledge, these are the first CPs (and AIE platforms) explored for the detection of PDM with reliable sensitivity and point of care (PoC) devices. In order to rapidly address the ever-increasing challenges of PDM use in the agricultural sector and to detect its residue found in edible foodstuffs and natural water sources, a portable smartphone based PoC device was constructed that can be used in a very straightforward way with quick response time for on-site detection.[31]

3.2 Experimental Section

3.2.1 Materials and Methods: PDM and all of the nitroaromatics used in the study were procured from Sigma Aldrich. Milli-Q water has been used for the preparation of the stock solution for all the experiments. Recording of ^{1}H NMR (600 MHz) and ^{13}C NMR (150 MHz) spectra was performed on the Varian-AS400 NMR spectrometer. For recording UV-visible absorption spectra and photoluminescence spectra, PerkinElmer Lambda-35 and Horiba Fluoromax-4 spectrofluorometers have been used with 1 ml quartz cuvettes (path length =1 cm, slit = 3 nm). FESEM images were obtained from a Zeiss Sigma field emission scanning electron microscope (FESEM).

3.2.2 Synthetic Procedure:

3.2.2a (2Z,2'Z)-3,3'-(1,4-phenylene)bis(2-(4-bromophenyl)acrylonitrile) (M2CN): The monomer M2CN was synthesized by Knoevenagel condensation reaction. terephthalaldehyde (0.5 g, 3.73 mmol) and 2-(4-bromophenyl)acetonitrile (1.47 g, 7.46 mmol) were solubilized in 30 ml ethanol at 50 ºC with continuous stirring. 100 mg of potassium tertiary butoxide, (t-BuOK) was solubilized in 5 ml ethanol and then injected into the reaction mixture dropwise. After that, the product gets precipitated as a yellowish precipitate from the reaction mixture. The progress of the reaction was monitored by TLC, and after 4h, the precipitate was filtered

through Whatman filter paper and then wash repeatedly with ethanol to get the pure yellow ppt. (yield=97%, 1.90 g).

MALDI_TOF: The mass of monomer M2CN (mass =490.955) and theoretical mass = 490.20

^{1}H NMR (600MHz, DMSO-d6, δ ppm): 8.18 (s, 2H), 8.09 (s, 4H), 7.75 (s, 8H).

^{13}C NMR (150MHz, DMSO-d6 δ ppm): Due to very low solubility of M2CN in all the organic solvent, we unable to record ^{13}C NMR

3.2.2b 2,7-dibromo-9,9-dihexyl-9H-fluorene (FC6): The monomer (FC6) was synthesized following the reported procedure.[32] A mixture of fluorene (1 g, 3.08 mmol), 50 % NaOH (aq), and tetra butyl ammonium iodide (TBAI) (0.227 g, 0.616 mmol) was taken in a clean RB flask and were made inert by applying free-thaw degassing technique (3 times). After that, 1-bromohexane (3 mL, 21.56 mmol) was injected cautiously through a syringe, maintaining the inert condition. Finally, the reaction mixture was heated at 80 °C with proper stirring for 5 h. The completion of the reaction was monitored by TLC in hexane and then extracted with chloroform. The extracted organic layer was again washed repeatedly with water (3 times), and then the excess1-bromohexane was removed by Kugelrohr to get the crude product. Finally, the crude product was further purified by passing over a thick silica gel bed using a column chromatography technique where hexane was selected as eluent to obtain the desired product as a white crystalline ppt. (Yield = 96 %, 1.6 g)

LC_QTOF_HRMS: The mass of monomer FC6 (m/z +1 = 493.2371)

^{1}H NMR (600MHz, $CDCl_3$, δ ppm): 7.54 (d, J = 8.0 Hz, 2H), 7.46 (s, 4H), 1.95 – 1.91 (m, 4H), 1.15 (dd, J = 13.9, 7.0 Hz, 4H), 1.10 – 1.04 (m, 8H), 0.80 (t, J = 7.3 Hz, 6H), 0.60 (dd, J = 15.9, 7.3 Hz, 4H).

^{13}C NMR (150MHz, $CDCl_3$, δ (ppm): 152.76, 139.40, 130.17, 126.24, 121.45, 121.11, 55.47, 40.18, 31.49, 29.63, 23.63, 22.55, 13.57

3.2.2c Synthesis of Polymer PFP: The polymer PFP was synthesized by the Suzuki Coupling polymerization reaction. A mixture of monomers FC6 (200 mg, 0.406 mmol) and benzene diboronic acid (67 mg, 0.406 mmol) were taken in a clean RB flask fitted with condenser and then made the system inert by degassing followed by purging with argon gas. Thereafter, 5 mg of catalyst Pd $(PPh_3)_4$ was added maintaining the inert condition. A mixture of THF (9 ml) and

2M K_2CO_3 (3 ml) was injected into the reaction mixture and was made inert by applying the free-thaw degassing technique (3 times). The reaction mixture was stirred at reflux conditions under an argon atmosphere. After 48 h., the polymer is end capped by injecting iodobenzene and phenyl boronic acid and continued the reaction for 3 h maintaining the inert condition. The reaction was then cool down and extracted with $CHCl_3$/water. The organic layer was dried under vacuum and further purified by repeated precipitation in methanol. (color, dirty white, Yield = 86%, 220 mg).

^{1}H NMR (600 MHz, $CDCl_3$ δ ppm): 7.77(b), 7.74(b), 7.70(b), 7.61(b), 7.58(b), 7.41(b) 7.31(b) 2.01 (b), 1.03(b), 0.71-0.70(b).

GPC in THF, polystyrene standard. M_w= 37562 g mol^{-1}, PDI = 2.26

3.2.2d Synthesis of Polymer PF2CN: The polymer PF2CN was synthesized by the Suzuki Coupling polymerization reaction. A mixture of monomers M2CN, (52.21 mg, 0.107 m moles) (9,9-dihexyl-9H-fluorene-2,7-diyl) diboronic acid (150 mg, (0.355 mmoles), and FC6 (297.12 mg, 0.604 mmoles) were taken in a clean RB flask fitted with condenser and then made the system inert by degassing followed by purging with argon gas. Thereafter, 5mg of catalyst Pd $(PPh_3)_4$ was added maintaining the inert condition. A mixture of THF (9 ml) and 2M K_2CO_3 (3 ml) was injected into the reaction mixture and was made inert by applying the free-thaw degassing technique (3 times). The reaction mixture was stirred at reflux conditions under an argon atmosphere. After 48 h., the polymer is end capped by injecting iodobenzene and phenyl boronic acid and continued the reaction for 3 h maintaining the inert condition. The reaction was then cool down and extracted with CHCl3/water. The organic layer was dried under vacuum and further purified by repeated precipitation in methanol. (color, yellow, Yield = 80%, 280 mg).

^{1}H NMR (600 MHz, $CDCl_3$ δ ppm): 7.99(b), 7.76(b), 7.73(b), 7.61(b), 7.59(b), 7.57(b) 7.51(b) 7.41-7.40(b) 7.30(b), 2.03(b), 1.06(b) 0.7 (b).

GPC in THF, polystyrene standard. M_w= 49070 g mol^{-1}, PDI = 1.53

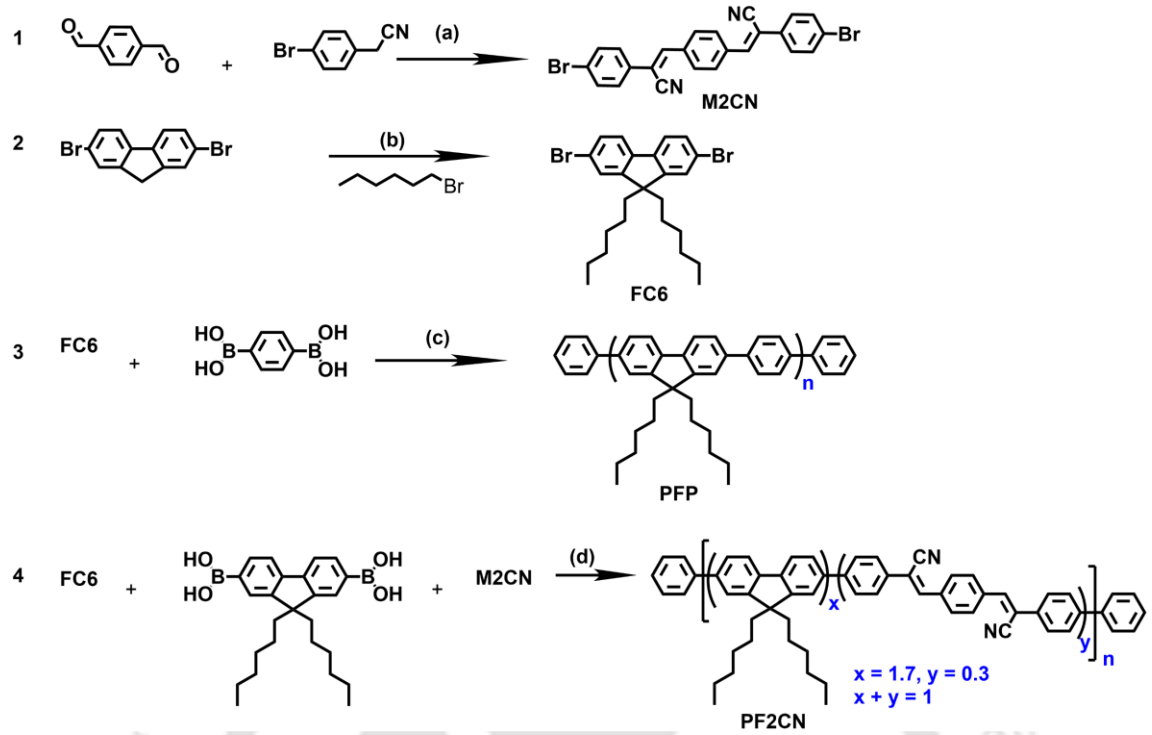

Scheme 3.1. Synthetic pathways of monomers and polymers: (a) t-BuOK, ethanol, rt, 12h.; (b) 50 % (aq) NaOH, TBAI, 70 °C, 4h; (c), (d) tetrakistriphenylphosphine palladium(0), 2 M K_2CO_3 (aq), THF, reflux, 30h.

3.2.3 Stock Solutions Preparation: Polymer PFP and PF2CN stock solutions for experiments were prepared in DMSO with a 1 mg/mL concentration. Also, the stock solution of PDM with a concentration of 1mM was prepared in DMSO. Similarly, stock solutions of all the nitroaromatics used in the interference and selectivity studies were prepared as 1 mM in DMSO. All the photophysical studies of the developed PFP and PF2CN polymers in the absence and presence of various analytes were performed in water medium.

3.2.4 Photoluminescence Quantum Yield (ϕ): The absolute quantum yield for PFP and PF2CN polymers were determined by using Edinburgh FLS 1000 instrument through the integrated sphere technique.

3.2.5 Limit of Detection (LOD): The lowest LOD was determined by analyzing the fluorescence spectra of PFP and PF2CN polymers with varying concentrations of PDM (0-5 µM) and (0-60 nM) in a water medium. Using the standard formula, LOD=3σ/k, the lowest LOD was calculated from the calibration curve, where the symbols σ and k represent the calibration plot's standard deviation (SD) and slope, respectively.[33]

3.2.6 UV- Visible Detection of Pendimethalin (PDM): PDM has has absorption maxima at around 445nm in aqueous medium. To obtained the standard calibration plot from UV-visible

study, different concentrations of PDM (0, 10 nM, 20 nM, 30 nM, 40 nM, 50 nM, 60 nM, 70 nM, 80 nM, 90 nM) were prepared and recorded their absorbance at wavelength of maximum absorption (λ_{445} nm). The calibration plots were linear at a concentration range (0-90 nM) and hence the concentration of unknown PDM was determined from it.

3.2.7 The Overlapping Integral Value: The spectral overlapping integral was determined by the following formula to determine the amount of energy transfer from the donor (PF2CN) to the acceptor (PDM).[34]

$$J(\lambda) = \int_0^\infty F_D(\lambda)\, \varepsilon_A(\lambda)\lambda^4 d\lambda$$

Equation 1

Where the symbols $J(\lambda)$ represents the overlapped integral value, F_D (λ) represents the corrected emission intensity of PF2CN from λ to $\Delta\lambda$ normalizing the overall intensity to unity, ε_A signifies the molar absorptivity (in $M^{-1}cm^{-1}$) of the PDM (acceptor) at the wavelength λ (Equation 1).

3.2.8 Inner Filter Effect (IFE) Correction: The suppression effect of IFE in the emission intensity of PF2CN can be determined by means of the following equation (for 1 cm path length cuvette).[35]

$$I_{corr}/I_{obs} = (10)^{(Aex + Aem)/2)}$$

Equation 2

Where, I_{obs} and I_{corr} represent the fluorescence emission intensity without and with IFE correction, respectively. A_{em} and A_{ex} represent the values of UV-vis absorption of PF2CN (fluorophore) at the wavelengths of emission maxima and excitation with PDM (quencher) addition (Equation 2).

3.2.9 Electrochemical Analysis: The cyclic voltammogram (CV) was performed in inert atmosphere to determine the highest occupied molecular orbital (HOMO) and lowest unoccupied molecular orbital (LUMO) energy levels of PF2CN. Saturated $Ag/AgNO_3$ electrode, glassy carbon electrode and platinum wire, were utilized as reference, working electrodes and counter respectively with $TBAPF_6$ (0.1 M in CH_3CN) as the supporting electrolyte. PF2CN showed a single oxidation peak. The HOMO level (-5.81 eV) was estimated by using the onset technique (Equation 3).

$$\boldsymbol{E_{HOMO} = (E_{(onset,\ ox\ versus\ Fc+/Fc)} + 4.8)\ (eV)}$$

--- ---------Equation 3

The band gap (2.40 eV) of PF2CN were determined from the UV-visible spectrum to compute its LUMO level (-3.41 eV).

3.3 Results and Discussion

The monomers M2CN and FC6 were synthesized by the Knoevenagel condensation reaction and the alkylation reaction respectively (Scheme 1). The polymers PFP and PF2CN were synthesized by the Suzuki cross-coupling polymerization reaction with 80-86 % yield. The synthesized monomers and polymers were well purified at each step and characterized by NMR, mass and GPC before using in further studies (Figure A3.1-A3.9). The M2CN monomer due to the less solubility issue, did not get ^{13}C NMR.

3.3.1 Properties of M2CN:

The monomer M2CN has very low solubility in organic solvents and is insoluble in water due to the presence of large aromatic rings. Theoretical studies were performed by employing the DFT 631G function with the B3LYP basis set in the Gaussian Program.[36] The optimized geometry showed that the planarity of conjugated phenyl rings was disturbed by the -CN group and its HOMO electronic cloud was diffused across the entire molecule. The LUMO electronic clouds are mostly confined across the central benzene ring and the two -CN groups thereby suggesting the possibility of weak intramolecular ICT (Figure 3.1).

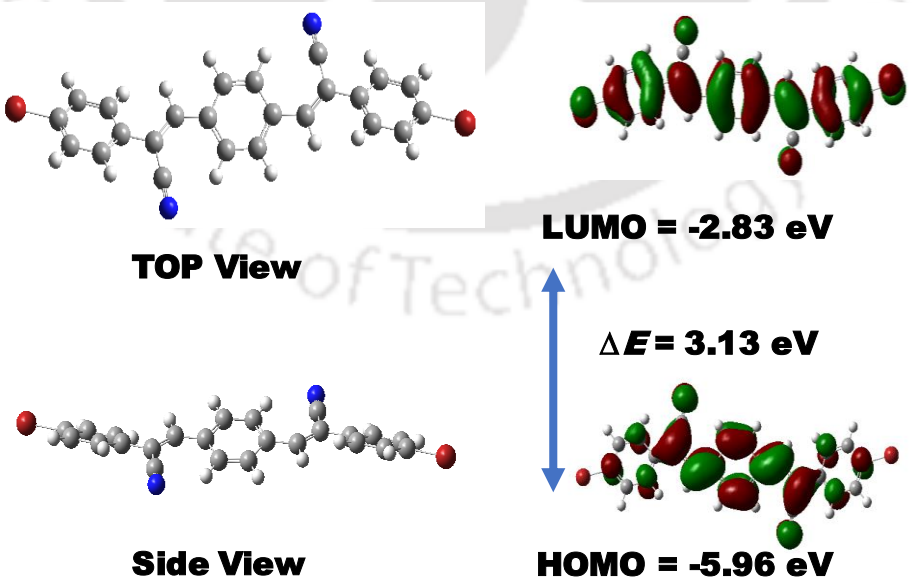

Figure 3.1. DFT optimized structure of M2CN and its HOMO/LUMO electronic distribution calculated using B3LYP/631G of Gaussian 09 program.

3.3.2 Photophysical and Morphological Studies of Polymer PFP and PF2CN.

Because of the strong electron-withdrawing -CN groups, integration of M2CN into the conjugated backbone of polyfluorene is predicted to tune the polymer's photophysical characteristics. The photophysical studies of the CPs were performed in various DMSO-water fractions. The CPs PFP and PF2CN showed corresponding absorption maxima at 360 and 376 nm respectively in DMSO. The absorption peak of PFP in water has ~10 nm shift and the absorption peak of PF2CN in water has a shoulder peak at 430 nm which is attributed to their aggregation (Figure A3.10a, A3.10b). The blue color of the PFP polymer is tuned to the yellow color in PF2CN due to the incorporation of the M2CN monomer via intramolecular charge transfer (ICT). The emission intensity of PFP gradually decreases with the increase of water fraction (f_w) from 0 % to 99 % depicting the ACQ nature (Figure 3.2a, 3.2b). The photophysical data along with corresponding quantum yield are provided in Table A3.1. The self-assembly process of PFP polymer in 99 % f_w was analyzed by FESEM where it formed a large microaggregate assembly with average size as determined from DLS is around 600 nm (Figure 3.2c and Figure A.3.11a). On the other hand, the emission of PF2CN initially decreased with a slight red shift from 0 to 40 % f_w, became non-fluorescence from 50 % to 80 % and then the emission enhanced again at 90 % to 99 % f_w (Figure 3.2d, 3.2e). Further, the self-assembly of PF2CN in 99 % f_w was analyzed by FESEM where the polymer spontaneously formed spherical nanoparticles (Figure 1f) with an average size of 145 nm as determined from DLS (Figure A3.11b).

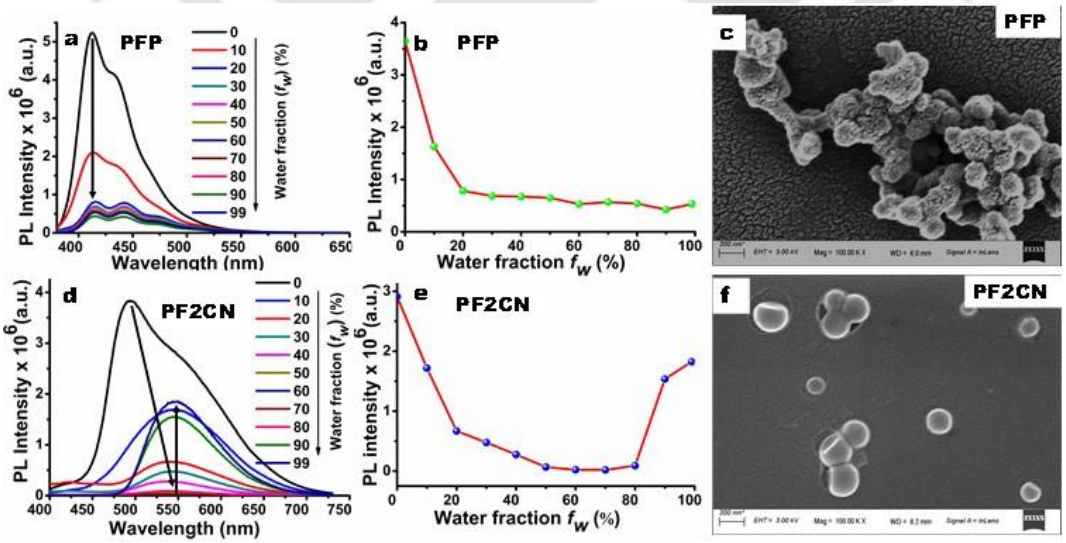

Figure 3.2: (a) Photoluminescence (PL) spectra of PFP in various DMSO-water fractions. (b) Plot of emission intensity vs various f_w in DMSO for PFP (c) FESEM images of PFP (d) PL spectra of PF2CN in various DMSO-water fractions. (e) Plot of emission intensity vs various f_w for PF2CN, (f) FESEM images of PF2CN.

3.3.3 Detection of PDM in an Aqueous Medium:

The optical sensing efficiencies of both PFP and PF2CN polymers were analyzed in an aqueous medium to determine the role of M2CN. The PFP polymer consumed 40 μM PDM to quench its blue emission (Figure 3.3a). In the case of PF2CN, its bright yellow fluorescence was ~92 % quenched by only 6 μM addition of PDM (Figure 3.3b) (inset: the photograph of the fluorescence color change of PF2CN (i) before and (ii) after the addition of PDM). It was observed that initially, the emission intensity of both PFP and PF2CN decreased abruptly due to the inherent molecular wire effect of CP thereby amplifying the sensory signal and then decreased gradually up to ~92 %-95 % with the addition of PDM. The Stern-Volmer (S-V) quenching constant was determined by linear fitting of fluorescence titration and found to be $1.4 \times 10^5\ M^{-1}$ for PFP and $1.6 \times 10^6\ M^{-1}$ for PF2CN (Figure A3.12a, A3.12b) and the lowest limit of detection (LOD) for both the PFP and PF2CN for PDM was 91 nM and 2.8 nM respectively as determined from the relation 3σ/k, which is much below the PDM tolerance limits established by 40 CFR 180.361 reassessed by United States EPA.[37] PF2CN shows higher sensitivity as compared to PFP (Figure A3.13a, A3.13b), suggesting that the incorporation of M2CN improved the sensitivity of polymer to a great extent.

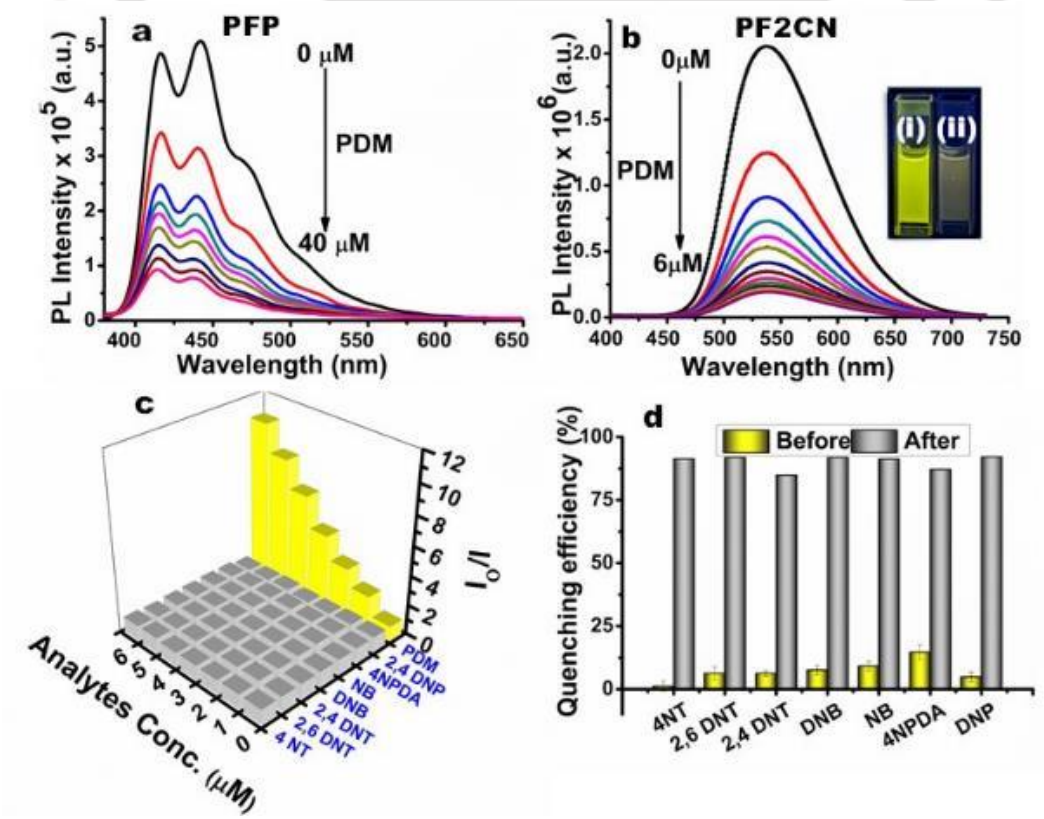

Figure 3.3: Fluorescence spectra of (a) PFP by addition of 40 μM PDM and (b) PF2CN by gradual addition of PDM (inset: photograph of PF2CN (i) before and (ii) after addition of 6 μM PDM. (c) SV plot of PF2CN of various NACs (d) Quenching efficiency spectra of PF2CN before and after 6 μM PDM addition with different NACs.

3.3.4 Selectivity Study:

Selectivity is a major prerequisite for choosing an efficient sensor which remains a very challenging task. The S-V plots for PFP and PF2CN were obtained for all of the interfering nitroaromatic compounds (NACs) i.e. DNP, 4 NPDA, NB, DNB, 2,4 DNT, 2,6 DNT, and 4 NT (structures of these NACs are provided in Figure A3.14). The PFP shows interference of 10-40% quenching efficiency by these NACs (Figure A3.15). however, most interestingly in the case of PF2CN, the NACs have negligible sensitivity as compared to PDM (Figure 3.3c). Further, the percentage interference of various nitroaromatic compounds in the sensing of PDM was studied where they show negligible interference (Figure 3.3d). Hence, considering the remarkable sensitivity and selectivity toward PDM, PF2CN was further investigated for in-depth mechanistic studies in order to implement the real-world on-site detection application platform.

3.3.5 Repeatability Study:

The repeatability of the constructed chemosensor for PDM detection was tested to assess its practical efficiency in sensing. For this we prepared aqueous PF2CN solution with a concentration of 10µM in 5 different vials (M1, M2, M3, M3, M4, M5). The solution was titrated with PDM of concentration (0- 6µM) and compared the quenching performance for every 5 sets of measurements (Figure 3.4a). Similarly, an interday correlation analysis was conducted by preparing 10µM PF2CN in seven different vials (DAY 1, DAY 2, DAY 3, DAY 4, DAY 5, DAY 6, DAY 7). One sample was used each day to detect PDM (0.5 µM, 1 µM, or 1.5 µM) and compared the quenching efficiency for each day (Figure 3.4b). From the above intra and inter day studies, a comparable sensing performance was obtained with a RSD 3.5 % suggesting good repeatability of sensor.

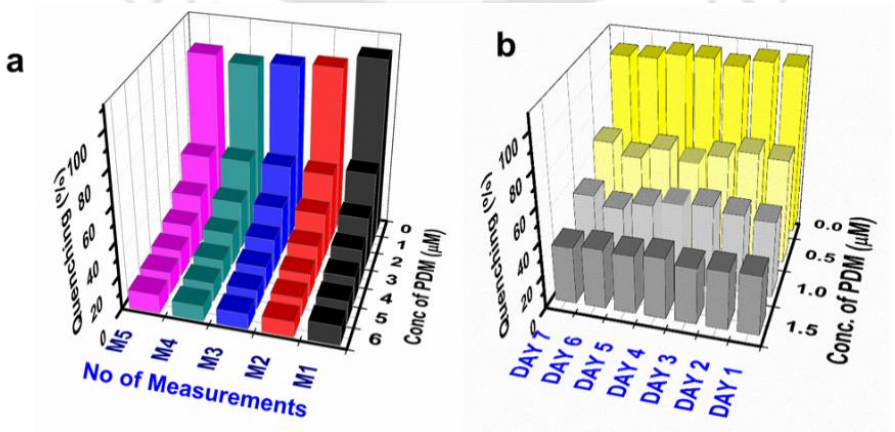

Figure 3.4: (a) Intra- day correlation of sensing performance of PF2CN for 5 different measurements with interval of 5h. (b) Inter day correlation of sensing performance of PF2CN for 7 days.

3.3.6 Mechanism:

Detailed mechanistic studies were performed to investigate the underlying mechanism of sensing PDM by PF2CN. To investigate the potential of electron transfer, the HOMO energy level and lowest energy level of PF2CN were measured by cyclic voltammetry. The LUMO energy level of PF2CN (-3.41 eV) lies above the LUMO energy level of PDM (-3.95 eV) (Figure 3.5a) which strongly suggests the occurrence of the PET process in the sensing mechanism. Other nitro compounds are not quenched in the same manner because their LUMO level is close to or higher than the LUMO level of PF2CN (Figure A.3.16).[20, 38, 39] The remarkable sensitivity of PF2CN and the nonlinear fitting of the S-V plot (Figure A3.17), inspired us to analyse the possibility of other sensing mechanism(s). Apart from PET, the spectral overlap of the absorption spectra of PDM with the excitation and emission spectra of PF2CN suggested the possibility of both IFE and FRET mechanisms in the sensing process (Figure 3.5b). The decrease in the average lifetime of PF2CN from 1.07 ns to 0.73 ns by addition of PDM confirms the presence of FRET mechanism in the sensing process (Figure 3.5c and Table A3.2). However, by calculating the quenching efficiency before and after IFE

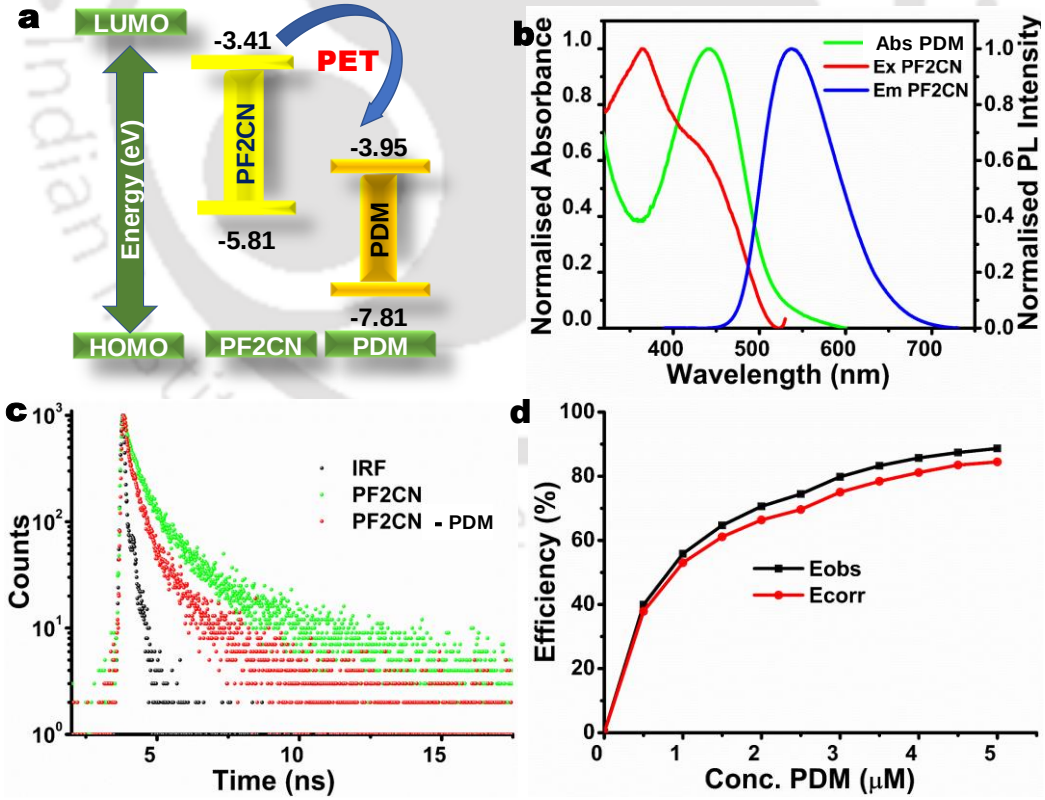

Figure 3.5: (a) HOMO and LUMO energy levels of PF2CN and PDM. (b) Spectral overlapped plot of excitation/ emission of PF2CN with the absorption spectra of PDM. (c) Lifetime decay profile for PF2CN before and after addition of 6 μM PDM. (d) Energy suppression efficiency before and after IFE correction.

correction a negligible change was observed, indicating that IFE has a minor role in the sensing process (Figure 3.5d, Table A3.3). Furthermore, we investigated the probability of ground state complexation by monitoring the UV-visible absorption spectra of PF2CN with and without PDM. There is no generation of new peak or shifting of PF2CN absorption spectra, ruling out the possibility of ground complexation in the sensing process (Figure A3.18).[5]

3.3.7 Real Samples Analysis:

The widespread usage of PDM in various crops, fruits, and vegetables and the lack of appropriate and rapid sensors mandate investigation of various food samples. For this purpose, we have collected two samples each of several vegetables, washed thoroughly and air dried. Each of the vegetables is divided into two groups labeled "A" and "B". The A" group of vegetables was used as a control (without pesticides) and the "B" group was sprayed with pendimethalin solution of 10 mM concentration. After that both "A" and "B" groups of vegetables were sprayed with PF2CN polymer solution of 10 ng/mL concentration. Interestingly, a under 365 nm UV lamp, the "A" groups show bright yellow fluorescence of polymer, though, it gets quenched completely in "B" group samples due to the presence of PDM. However, there is no noticeable change during the daylight (Figure 3.6, Figure A.319).

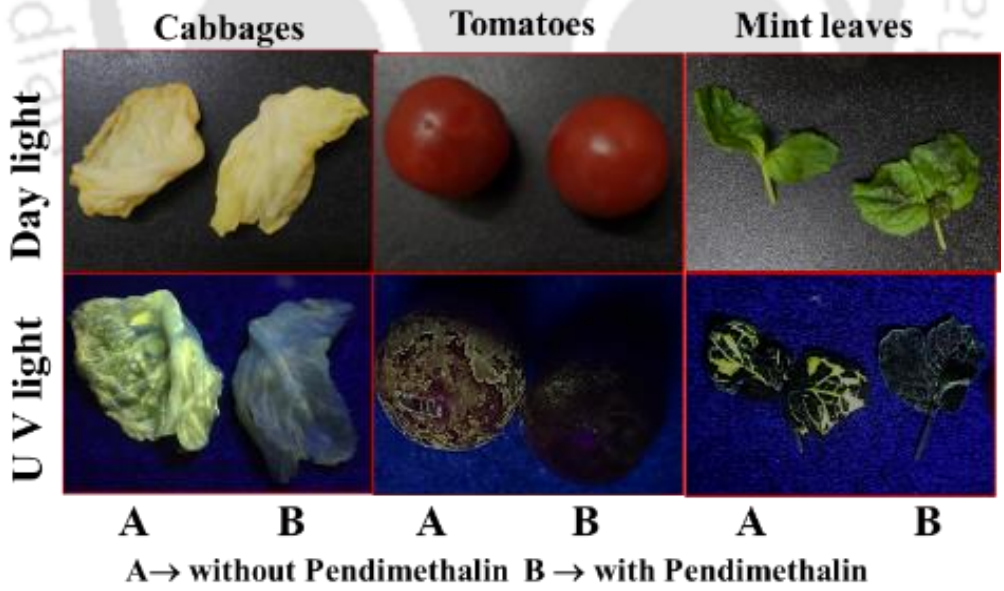

Figure 3.6: Photograph of PF2CN in vegetable samples (A) without and (B) with pendimethalin.

Further a quantitative detection was performed in various water and food samples. For water samples, tap water and natural lake water (Serpentine Lake, IIT Guwahati) and for edible foods

cabbage, tomatoes mint leaves, bitter gourd, brinjal, potatoes, peas, cauliflowers, carrots, chillies, potols, garlics, lady's fingers were chosen to quantify the amount of PDM residues. For the analysis of water samples, the particulates in the water samples were first removed by filtration through a membrane with a pore size of 0.2 μm then spiked with known concentration of PDM. These spiked samples were directly analyzed by PF2CN based fluorescence technique and compared with the calibration plot. However, pretreatment is required in case of food samples following the reported procedure.[20] The food samples were sprayed with a PDM solution of known concentration. After that the samples were finely diced into tiny slices and homogenized uniformly with a clean mortar and pestle. Then, 1 g of these smashed samples were put into a 15 ml centrifuge tube containing 5 ml DMSO. The mixture was vortexed for 5 min, followed by filtration through a membrane with a pore size of 0.2 μm. The filtrate was used for further analysis by the PF2CN based fluorescence technique and compared with the calibration plot. The results show good recoveries of up to 94 % with RSD < 3 (Table A3.4) Futher, the result was again cross-validated with UV-visible detection technique. For this standard parallel calibration plot were obtained which were linear at the concentration range 0-90 nM (Figure 3.8). Both the results are in good agreement (Table 3.1) suggesting the feasibility of this technique for real sample analysis.

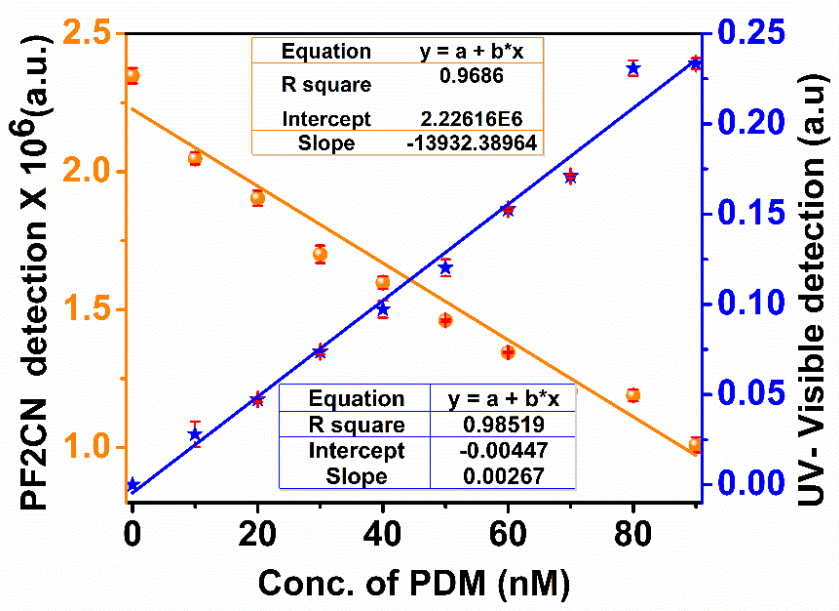

Figure 3.8. Cross validation calibration plot of Pendimethalin detection by UV – Visible detection and PF2CN based flurometric detection methods.

Table 3.1. Table for PDM detection by Standard Recovery Method in various samples and cross validation with UV – Visible detection method

Types of sample	Samples	PDM added (10^{-7} M)	PDM found by UV (10^{-7} M)	Recovery	PDM found by PF2CN based Fluorescence assay (10^{-7} M)	Recovery	RSD (%) (N=3)
Vegetables	Bitter gourds	10	8.91	89 .1	9.02	90.2	1.19
	Brinjals	10	9.42	94.2	9.41	94.1	1.04
	Potatoes	10	9.7	97	9.36	93.6	1.33
	Peas	10	9.69	96.9	10.76	107.6	2.33
	Cauliflowers	10	8.85	88.5	8.675	86.75	3.34
	Carrots	10	9.14	91.4	8.81	88.1	1.12
	Onions	10	9.27	92.7	9.69	96.9	1.70
	Chilies	10	9.91	99.1	10.03	100.3	2.53
	Potols	10	9.50	95	92.58	92.6	1.76
	Garlics	10	9.45	94.5	9.46	94.6	2.65
	Ladies Finger	10	8.65	86.5	86.01	86.01	2.09

3.3.8 Smartphone Based PoC Device:

The entire fluorescence based PDM detection process was miniaturized into a smartphone based prototype, providing the practicability of a quick and simple solution for on-site detection. The prototype contains a dark chamber, hand held UV lamp, a smart phone and its holder. For RGB analysis the PF2CN with various concentrations of PDM (0.5 µM- 2.5 µM) were prepared in a quartz cuvettes and placed inside the dark chamber (Figure 3.7a). The fluorescence photograph of these cuvette was captured through a smartphone and the corresponding RGB values were calculated by a color scanning android application called "Color Picker" (Figure 3.7b, 3.7c). As yellow color is formed by combination of "red" and "green" color in the RGB color model, the changes in fluorescence intensity of the samples was estimated from the plot of "R" value and "G" value (Figure 3.7d, 3.7e). The experiment was repeated three times and a linear calibration plot with linear regression coefficients (R^2) of 0.99658 and 0.991421 were obtained respectively for "G" value and "R" value. These plots

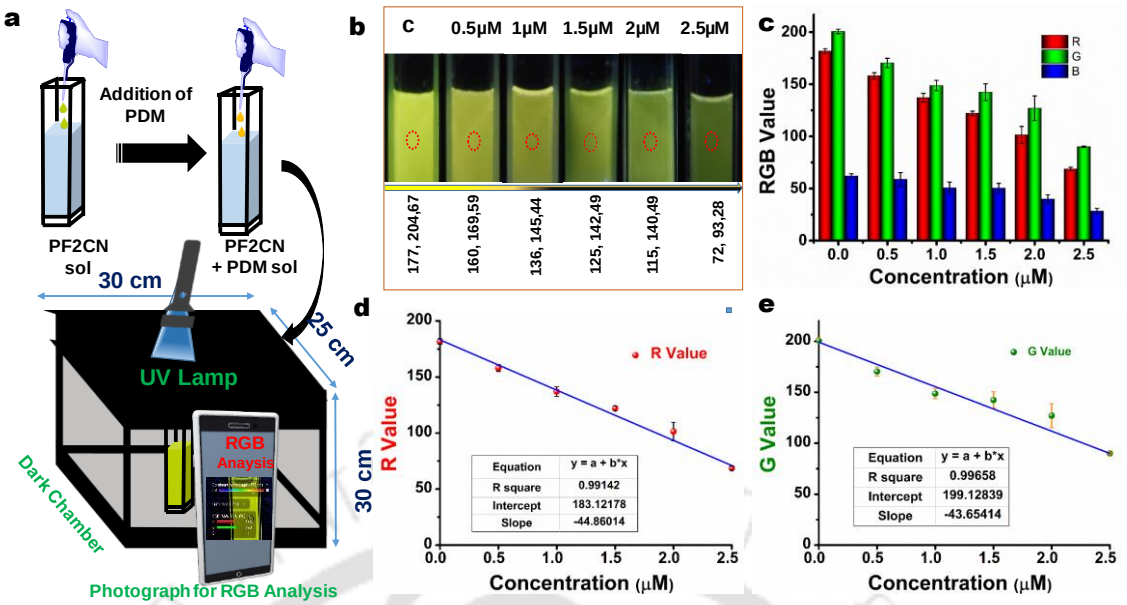

Figure 3.7: (a) Constructed PoC device for direct on-site estimation of PDM (b) Fluorescence photograph for PF2CN in absence and presence of various concentration of PDM, (c) RGB values of the captured photographic images, (d) "R" and (e) "G" values plots for the corresponding red spotted circle of the capture photographic images.

will be helpful in determining the approximate concentration of PDM in unknown samples for easy and rapid on-site detection.

Furthermore, the results obtained from the proposed sensing techniques (fluorescence and smartphone) were compared with those obtained from prior reports (Table A3.5). As per our knowledge this is the first CP design for detection of PDM with remarkable LOD. Further, it also offers rapid on-site detection in a very simple manner with a smartphone based PoC device.

3.4 Conclusion

The consumption of pesticide residues is associated with various health issues. Thus, a portable smartphone PoC device as a preventive measure was constructed based on the fluorescent response of the synthesized AIEE conjugated polymer. This AIEE active polymer PF2CN synthesized by modifying the planar backbone of polyfluorene by the Suzuki coupling polymerization reaction was used as a fluorescent sensor. The insertion of monomer M2CN into the conjugated backbone plays a key role in tuning the photophysical properties of PF2CN. The comparative studies are supported by using the PFP polymer which is devoid of the M2CN monomer and shows blue emission and an ACQ nature. Further PFP and PF2CN were employed for the detection of PDM. The PF2CN polymer shows ultrasensitivity and selectivity

which is due to the simultaneous occurrence of both electrons transfer and energy transfer in the sensing mechanism. Further, the PF2CN based fluorescence assay displayed reliable results in real samples such as water and edible foodstuffs. As such the development of smartphone based PoC testing device for onsite detection of PDM residues in a very simple approach with quick response time could be highly beneficial in modern healthcare preventive services. As per our knowledge this is the first conjugated polymeric probe used for the detection of PDM with high selectivity and sensitivity including its portability and PoC device.

References

1. Qiao, L.; Yuan, N.; Han, G.; Cheng, B.; Zhang, D.; Song, J.; Mu, Y. Determination of Pendimethalin Dynamic Residual Distribution in Crucian Carp Tissues and Associated Risk Assessment. *Int. J. Anal. Chem.* **2021**, 1-9.

2. Lee, H.-S.; Amarakoon, D.; Tamia, G.; Park, Y.; Smolensky, D.; Lee, S.-H. Pendimethalin Induces Apoptotic Cell Death through Activating ER Stress-Mediated Mitochondrial Dysfunction in Human Umbilical Vein Endothelial Cells. *Food Chem. Toxicol.* **2022**, *168*, 113370.

3. Strandberg, M.; Scott-Fordsmand, J. J. Effects of Pendimethalin at Lower Trophic Levels—a Review. *Ecotoxicol. Environ. Saf.* **2004**, *57*, 190-201.

4. Bolger, R.; Wiese, T. E.; Ervin, K.; Nestich, S.; Checovich, W. Rapid Screening of Environmental Chemicals for Estrogen Receptor Binding Capacity. *Environ. Health Perspect.* **1998**, *106* , 551-557.

5. Sarıgöl Kılıç, Z.; Aydın, S.; Ündeğer Bucurgat, Ü.; Başaran, N. In Vitro Genotoxicity Assessment of Dinitroaniline Herbicides Pendimethalin and Trifluralin. *Food Chem. Toxicol.* **2018**, *113*, 90-98.

6. Rohit, J. V.; Kailasa, S. K. Simple and Selective Detection of Pendimethalin Herbicide in Water and Food Samples Based on the Aggregation of Ractopamine-Dithiocarbamate Functionalized Gold Nanoparticles. *Sens. Actuators B Chem.* **2017**, *245*, 541-550.

7. El-Sharkawy, N. I.; Reda, R. M.; El-Araby, I. E. Assessment of Stomp®(Pendimethalin) Toxicity on Oreochromis Niloticus. *Journal of American Science* **2011**, *7*, 568-576.

8. Agriculture, M. O.; Gb, R. A.; O T P S R O, C. J. National Food Safety Standard-Maximum Residue Limits for Veterinary Drugs in Foods. **2019**, *1*, 31650-32019.

9.China, G.-J. *R. o., National Food Safety Standard-Maximum Residue Limits for Pesticides in Food*; 2019.

10. Ansari, S. M.; Saquib, Q.; Attia, S. M.; Abdel-Salam, E. M.; Alwathnani, H. A.; Faisal, M.; Alatar, A. A.; Al-Khedhairy, A. A.; Musarrat, J. Pendimethalin Induces Oxidative Stress, DNA Damage, and Mitochondrial Dysfunction to Trigger Apoptosis in Human Lymphocytes and Rat Bone-Marrow Cells. *Histochem. Cell Biol.* **2018**, *149*, 127-141.

11. Ahmad, M. I.; Zafeer, M. F.; Javed, M.; Ahmad, M. Pendimethalin-Induced Oxidative Stress, DNA Damage and Activation of Anti-Inflammatory and Apoptotic Markers in Male Rats. *Sci. Rep.* **2018**, *8*, 17139.

12. Giglio, A.; Vommaro, M. L. Dinitroaniline Herbicides: A Comprehensive Review of Toxicity and Side Effects on Animal Non-Target Organisms. *Environ. Sci. Pollut. Res. Int.* **2022**, *29*, 76687-76711.

13. Engebretson, J.; Hall, G.; Hengel, M.; Shibamoto, T. Analysis of Pendimethalin Residues in Fruit, Nuts, Vegetables, Grass, and Mint by Gas Chromatography. *J. Agric. Food Chem.* **2001**, *49* (5), 2198-2206

14. Singh, R.; Dhaduk, B.; Dhalani, J. A Rapid Quantification Method for Simultaneous Determination of Pendimethalin and Metribuzin Contents in Suspoemulsion Formulation. *Results Chem.* **2023**, *5*, 100779.

15. Shah, J.; Rasul Jan, M.; Shehzad, F.-U.-N.; Ara, B. Quantification of Pendimethalin in Soil and Garlic Samples by Microwave-Assisted Solvent Extraction and HPLC Method. *Environ. Monit. Assess.* **2011**, *175*, 103-108.

16. Pan, Y.; Liu, X.; Liu, J.; Wang, J.; Liu, J.; Gao, Y.; Ma, N. Chemiluminescence Sensors Based on Molecularly Imprinted Polymers for the Determination of Organophosphorus in Milk. *J. Dairy Sci.* **2022**, *105* (4), 3019-3031.

17. Galli, A.; De Souza, D.; Machado, S. A. S. Pendimethalin Determination in Natural Water, Baby Food and River Sediment Samples Using Electroanalytical Methods. *Microchem. J.* **2011**, *98*, 135-143.

18. Rubira, R. J. G.; Furini, L. N.; Constantino, C. J. L.; Sanchez-Cortes, S. SERS Detection of Prometryn Herbicide Based on Its Optimized Adsorption on Ag Nanoparticles. *Vib. Spectrosc.* **2021**, *114*, 103245.

19. Deng, A.; Tan, W.; He, S.; Liu, W.; Nan, T.; Li, Z.; Wang, B.; Li, Q. X. Monoclonal Antibody-based Enzyme Linked Immunosorbent Assay for the Analysis of Jasmonates in Plants. *J. Integr. Plant Biol.* **2008**, *50* (8), 1046-1052.

20. Pratibha; Kapoor, A.; Rajput, J. K.; Kumar, A. Dualistic Fluorescence as Well as Portable Smartphone-Assisted RGB-Relied Sensing Assay for the Ultra-Sensitive Determination of Pendimethalin in Food and Water Samples by AIEE Active Organic Probes. *Anal. Chem.* **2022**, *94*, 17685-17691.

21. Ghinaiya, N. V.; Park, T. J.; Kailasa, S. K. Synthesis of Bright Blue Fluorescence and Water-Dispersible Cesium Lead Halide Perovskite Quantum Dots for the Selective Detection of Pendimethalin Pesticide. *J. Photochem. Photobiol. A Chem.* **2023**, *444*, 114980.

22 Panchal, M.; Athar, M.; Jha, P. C.; Kongor, A.; Mehta, V.; Bhatt, K.; Jain, V. Turn-off Fluorescence Probe for the Selective Determination of Pendimethalin Using a Mechanistic Docking Model of Novel Oxacalix[4]Arene. *RSC Adv.* **2016**, *6*, 53573-53577.

23. Noor, M.; Iqbal, K. M.; Kanwal, T.; Rehman, K.; Ali, M.; Shah, M. R. Synthesis and Characterization of Modified Silica Nanoparticles Based Molecularly Imprinted Polymers as a Sensor for Selective Detection of Pendimethalin from Drinking Water. *J. Mol. Struct.* **2023**, *1287*, 135635.

24. Swager, T. M. The Molecular Wire Approach to Sensory Signal Amplification. *Acc. Chem. Res.* **1998**, *31*, 201-207.

25. Tanwar, A. S.; Patidar, S.; Ahirwar, S.; Dehingia, S.; Iyer, P. K. "Receptor Free" Inner Filter Effect Based Universal Sensors for Nitroexplosive Picric Acid Using Two Polyfluorene Derivatives in the Solution and Solid States. *Analyst* **2019**, *144*, 669-676.

26. Adil, L. R.; Gopikrishna, P.; Krishnan Iyer, P. Receptor-Free Detection of Picric Acid: A New Structural Approach for Designing Aggregation-Induced Emission Probes. *ACS Appl. Mater. Interfaces* **2018**, *10*, 27260-27268.

27. Wu, W.; Bazan, G. C.; Liu, B. Conjugated-Polymer-Amplified Sensing, Imaging, and Therapy. *Chem* **2017**, *2*, 760-790.

28. Rochat, S.; Swager, T. M. Conjugated Amplifying Polymers for Optical Sensing Applications. *ACS Appl. Mater. Interfaces* **2013**, *5*, 4488-4502.

29. Luo, J.; Xie, Z.; Lam, J. W. Y.; Cheng, L.; Tang, B. Z.; Chen, H.; Qiu, C.; Kwok, H. S.; Zhan, X.; Liu, Y.; Zhu, D. Aggregation-Induced Emission of 1-Methyl-1,2,3,4,5-Pentaphenylsilole. *Chem. Commun.* **2001**,*18*, 1740-1741

30. Hu, R.; Yang, X.; Qin, A.; Tang, B. Z. AIE Polymers in Sensing, Imaging and Theranostic Applications. *Mater. Chem. Front.* **2021**, *5*, 4073-4088.

31. Hussain, S.; Chen, X.; Wang, C.; Hao, Y.; Tian, X.; He, Y.; Li, J.; Shahid, M.; Iyer, P. K.; Gao, R. Aggregation and Binding-Directed FRET Modulation of Conjugated Polymer Materials for Selective and Point-of-Care Monitoring of Serum Albumins. *Anal. Chem.* **2022**, *94*, 10685-10694.

32. Saikia, G.; Iyer, P. K. Facile C−H Alkylation in Water: Enabling Defect-Free Materials for Optoelectronic Devices. *J. Org. Chem.* **2010**, *75*, 2714-2717

33. Chanu, M. A.; Mondal, S.; Zehra, N.; Tanwar, A. S.; Iyer, P. K. Conjugated Polymer Nanoparticles as a Fluorescence Probe for Amplified Detection of Human Serum Bilirubin. *ACS Appl. Polym. Mater*. **2022**, *4*, 3491-3497.

34. Lakowicz, J. R. Quenching of fluorescence. *Springer Boston, MA***. 1983**, 257-301.

35. Tanwar, A. S.; Khatun, M. N.; Chanu, M. A.; Sarmah, T.; Im, Y.-H.; Iyer, P. K. A Water-Soluble Conjugated Polyelectrolyte for Selective and Sensitive Detection of Carcinogenic Chromium(Vi). *Analyst* **2023**, *148* (23), 6011-6019.

36. Gaussian 09, Revision E.01, Frisch, M. J.; Trucks, G. W.; Schlegel, H. B.; Scuseria, G. E.; Robb, M. A.; Cheeseman, J. R.; Scalmani, G.; Barone, V.; Mennucci, B.; Petersson, G. A.; Nakatsuji, H.; Caricato, M.; Li, X.; Hratchian, H. P.; Izmaylov, A. F.; Bloino, J.; Zheng, G.; Sonnenberg, J. L.; Hada, M.; Ehara, M.; Toyota, K.; Fukuda, R.; Hasegawa, J.; Ishida, M.; Nakajima, T.; Honda, Y.; Kitao, O.; Nakai, H.; Vreven, T.; Montgomery, J. A., Jr.; Peralta, J. E.; Ogliaro, F.; Bearpark, M.; Heyd, J. J.; Brothers, E.; Kudin, K. N.; Staroverov, V. N.; Kobayashi, R.; Normand, J.; Raghavachari, K.; Rendell, A.; Burant, J. C.; Iyengar, S. S.; Tomasi, J.; Cossi, M.; Rega, N.; Millam, J. M.; Klene, M.; Knox, J. E.; Cross, J. B.; Bakken, V.; Adamo, C.; Jaramillo, J.; Gomperts, R.; Stratmann, R. E.; Yazyev, O.; Austin, A. J.; Cammi, R.; Pomelli, C.; Ochterski, J. W.; Martin, R. L.; Morokuma, K.; Zakrzewski, V. G.; Voth, G. A.; Salvador, P.; Dannenberg, J. J.; Dapprich, S.; Daniels, A. D.; Farkas, Ö.; Foresman, J. B.; Ortiz, J. V.; Cioslowski, J.; Fox, D. J. Gaussian, Inc., Wallingford CT, **2009.**

37. Trifluralin in Drinking-Water: Background Document for Preparation of WHO Guidelines for Drinking Water Quality. 2nd ed. Vol.2. *Health criteria and other supporting information*. World Health Organization, Geneva, 1996.

38. Bhalla, V.; Gupta, A.; Kumar, M.; Rao, D. S. S.; Prasad, S. K. Self-Assembled Pentacenequinone Derivative for Trace Detection of Picric Acid. *ACS Appl. Mater. Interfaces* **2013**, *5*, 672-679.

39. Jiang, N.; Li, G.; Che, W.; Zhu, D.; Su, Z.; Bryce, M. R. Polyurethane Derivatives for Highly Sensitive and Selective Fluorescence Detection of 2,4,6-Trinitrophenol (TNP). *J. Mater. Chem. C Mater. Opt. Electron. Devices* **2018**, *6*, 11287-11291.

Appendix

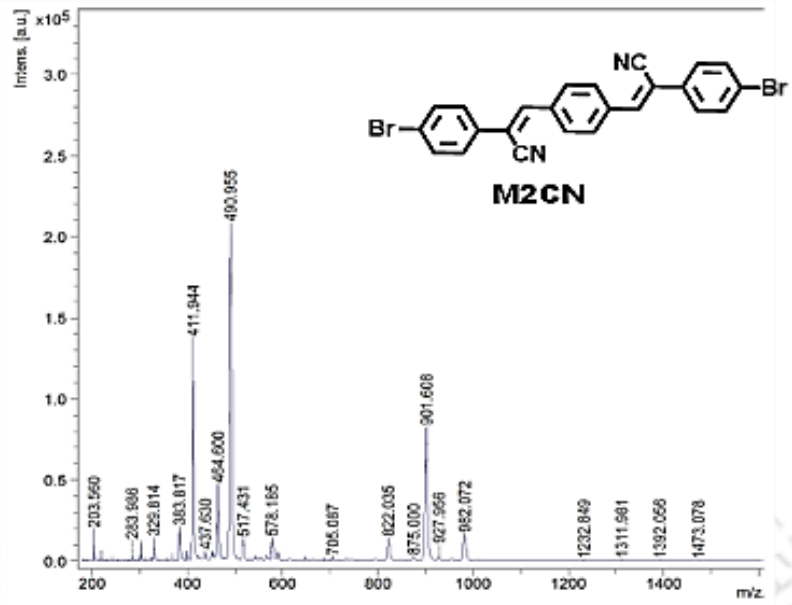

Figure A3.1. MALDI-TOF image of M2CN.

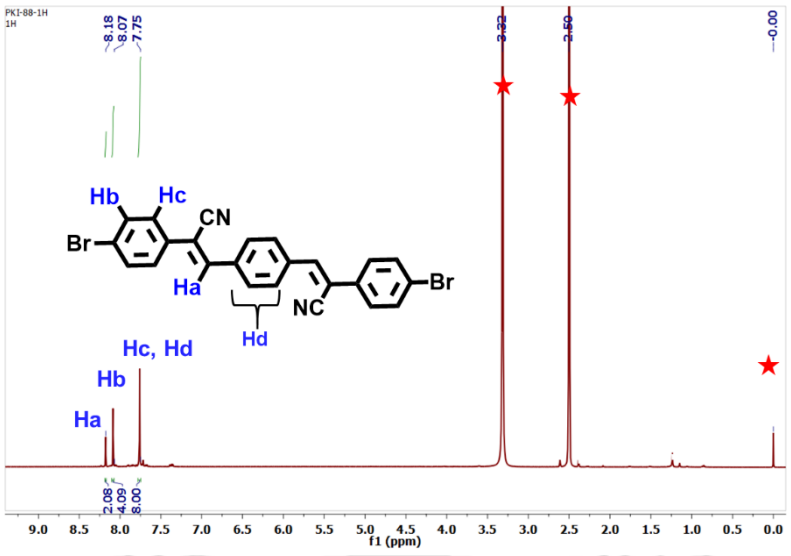

Figure A3.2. ^{1}H NMR spectra of M2CN in DMSO-d6

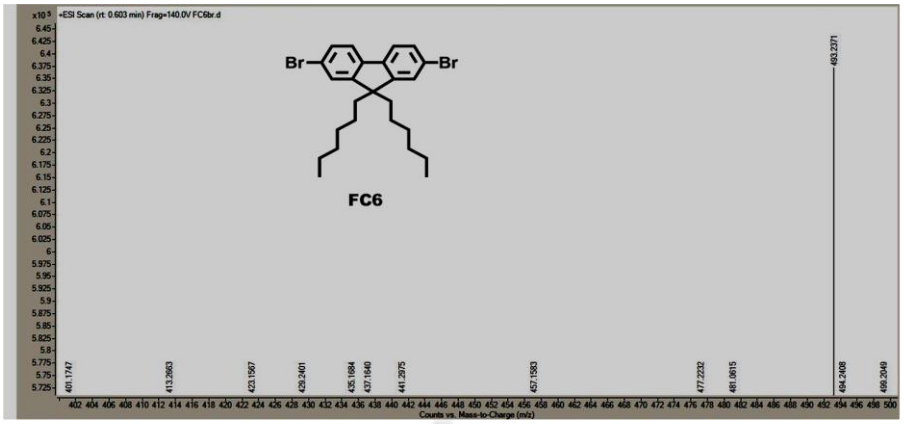

Figure A3.3. LC_QTOF_HRMS spectra of FC6

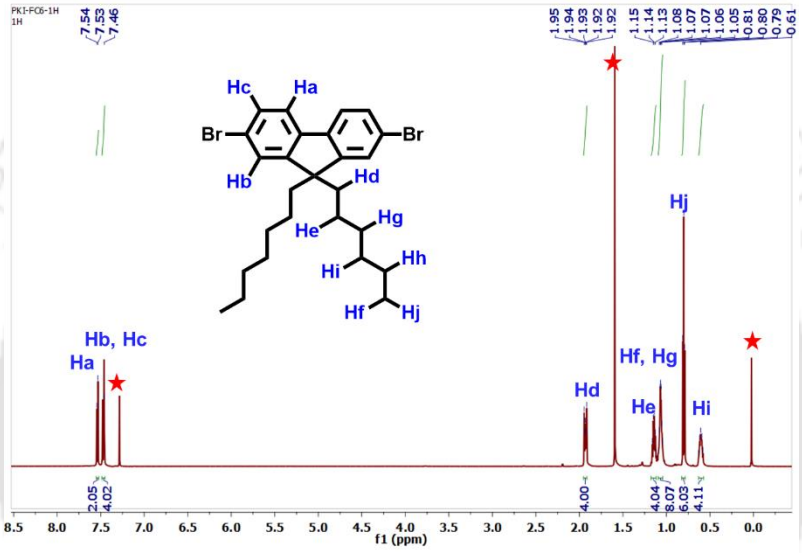

Figure A3.4. ^{1}H NMR spectra of FC6 in $CDCl_3$

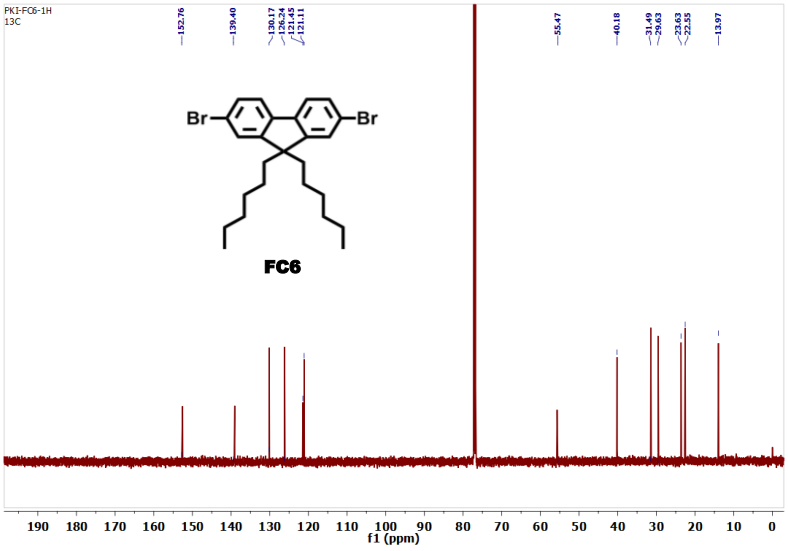

Figure A3.5. ^{13}C NMR spectra of FC6 in $CDCl_3$

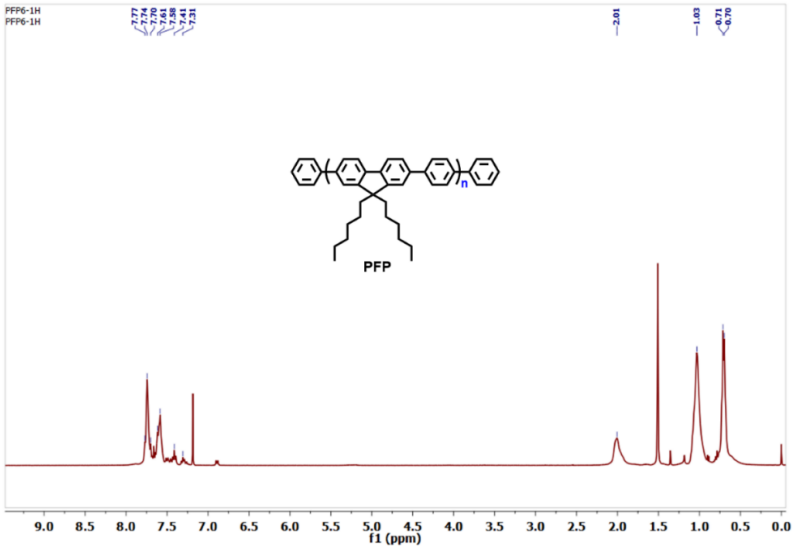

Figure A3.6. ^{1}H NMR spectra of PFP in $CDCl_3$

GPC Results

	Retention Time (min)	% Area	Mn	Mw	MP	Mz	Mz+1	Poly dispersity
1	7.387	100.00	16617	37562	30771	70273	101294	2.260469

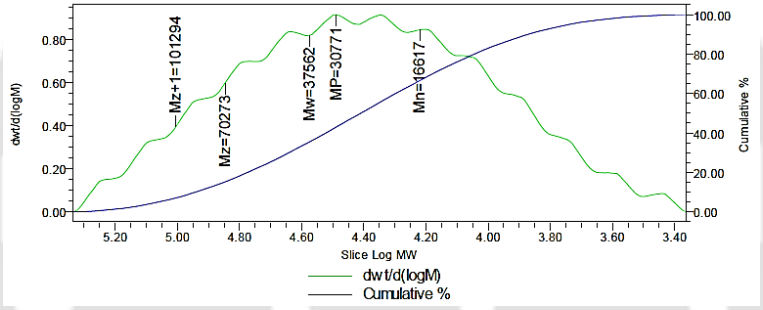

Figure A3.7: GPC chromatogram of polymer PF2CN

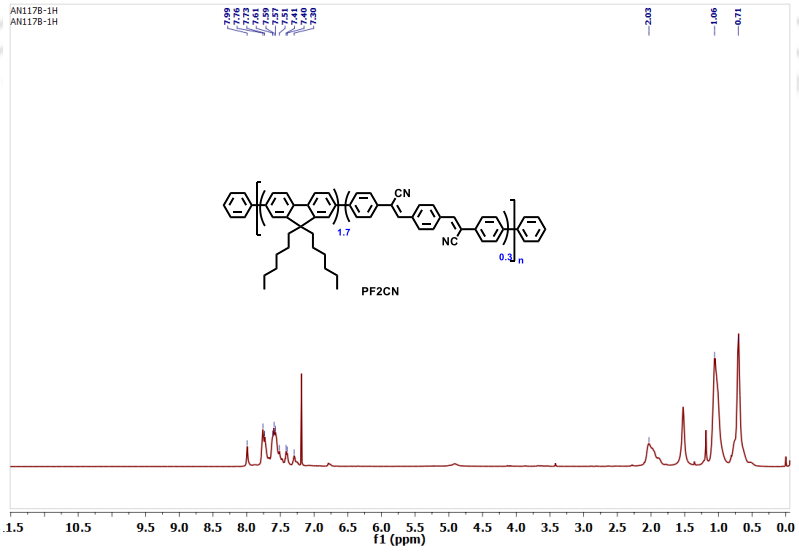

Figure A3.8. ^{1}H NMR spectra of PF2CN in $CDCl_3$

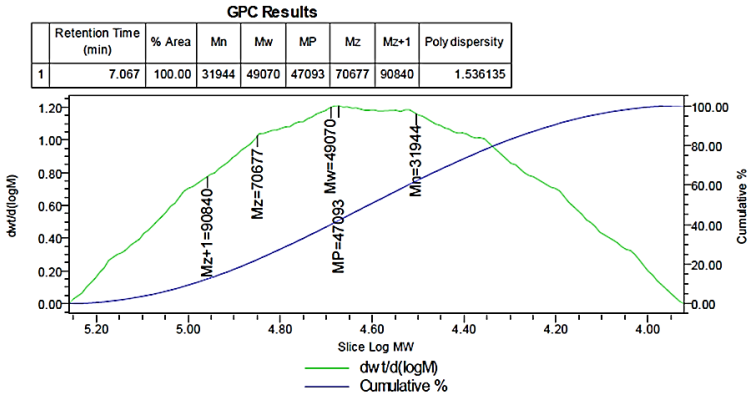

Figure A3.9: GPC chromatogram of polymer PF2CN

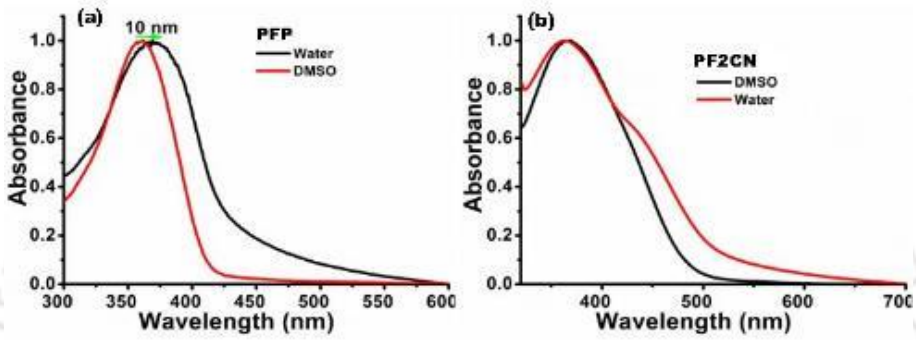

Figure A3.10. UV-Visible absroption spectra of (a) PFP and (b) PF2CN in DMSO and water.

Table A3.1 UV-Visible absroption spectra of (a) PFP and (b) PF2CN in DMSO and water

Sample	λ_{ex} (nm)	λ_{em} (nm)	(ϕ) (%)
PFP- DMSO	360	430	81.61
PFP-Water	370	430	25.21
PF2CN- DMSO	375	510	74.46
PF2CN-Water	375	540	66.23

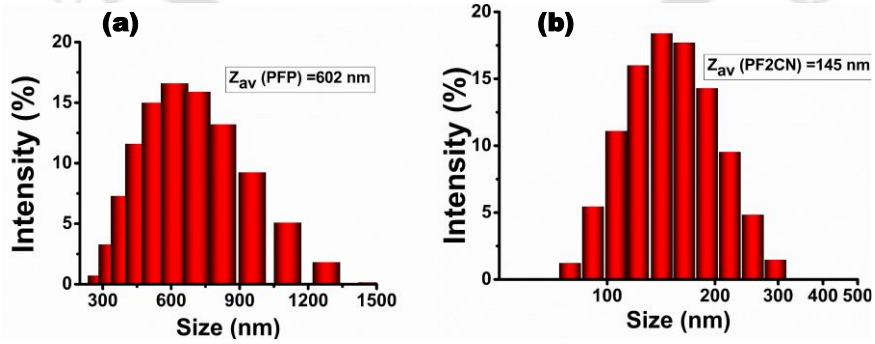

Figure A3.11 DLS plots for PFP and PF2CN in water

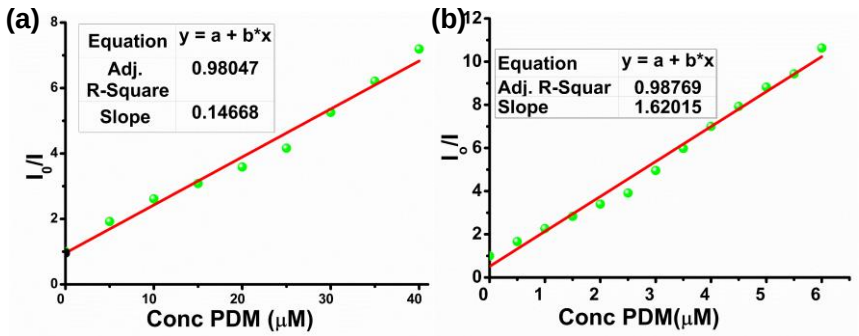

Figure A3.12. Linear fitting of Stern- Volmer plot of (a) PFP and (b) PF2CN for the detection of PD

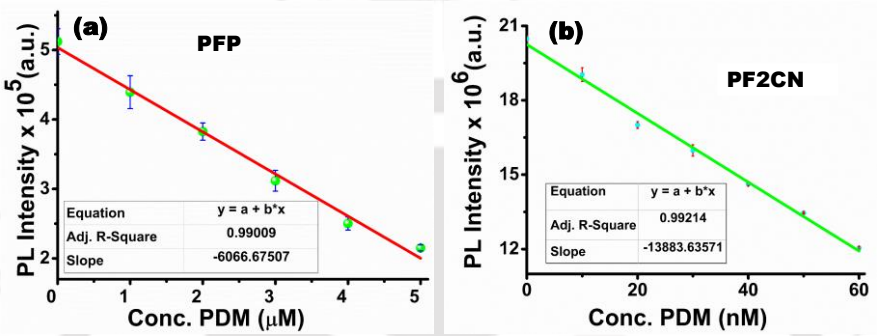

Figure A3.13. Plot of fluorescence emission intensity vs concentration of PDM for LOD determination

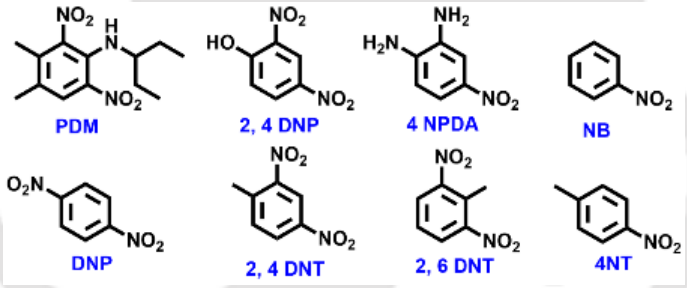

Figure A3.14. Structure of NACs used in the study.

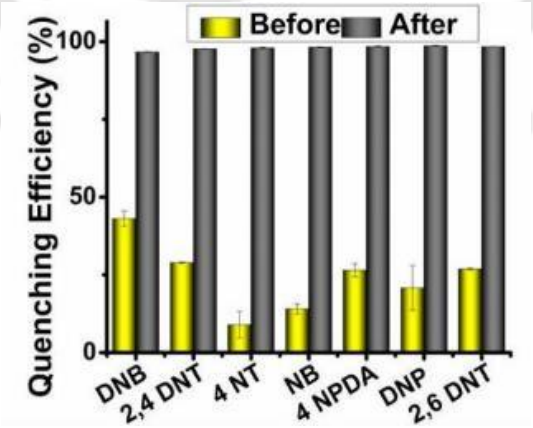

Figure A3.15. Interference study of PFP with different nitroaromatics before and after PDM addition.

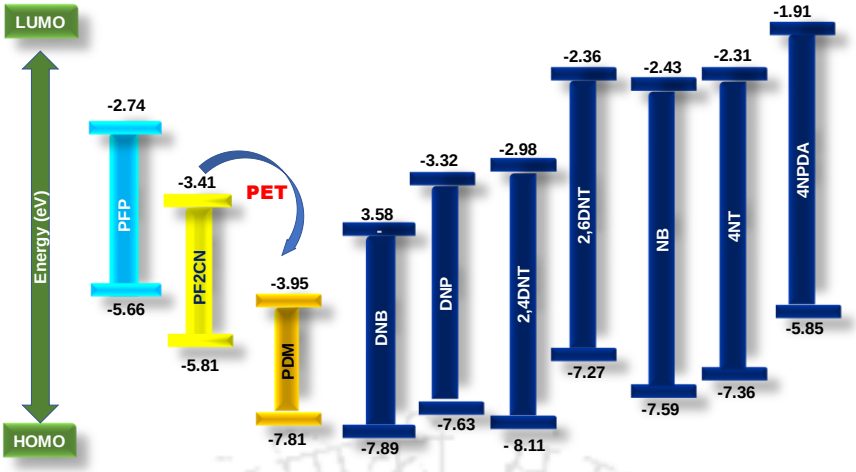

Figure A3.16. HOMO and LUMO energy levels of PFP, P2CN and various NACs.

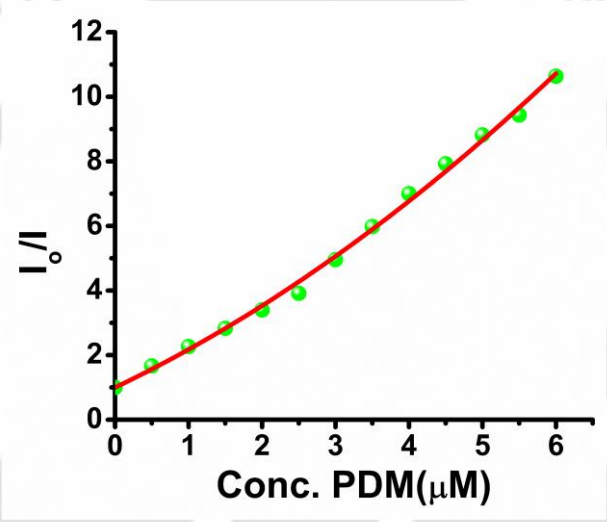

Figure A3.17. Stern – Volmer Plot of PF2CN for the detection of PDM.

Table 3.2. Fluorescence lifetime decay of each component and their fractions in water

Sample	f_i (%)	τ_1 (ns)	f_2 (%)	$\%\tau_2$ (ns)	τ_{avg} (ns)
PF2CN	59.103	0.283	40.897	2.196	1.065
PF2CN-PDM (1ul)	60.082	0.308	39.918	2.096	1.021
PF2CN-PDM (2ul)	59.780	0.286	40.220	1.934	0.948
PF2CN-PDM (3ul)	62.365	0.273	37.635	1.813	0.852
PF2CN-PDM (4ul)	60.344	0.240	39.656	1.645	0.797
PF2CN-PDM (5ul)	61.982	0.257	38.018	1.617	0.774
PF2CN-PDM (6ul)	61.830	0.231	38.170	1.553	0.735

Table 3.3. Calculations for IFE corrections for quenching in water

PDM (μM)	A_{ex} (370 nm)	A_{em} (550 nm)	I_{obs}	I_{corr}	I_{corr}/I_{obs} Correction factor (CF)	I_{corr}/I_{corr} , °	E_{obs}	E_{corr}
1	0.3471	0.0527	1980520	3138436	1.5846	0.9949	0	0.5003
2	0.3671	0.0613	874562.2	1432344	1.6377	0.4541	55.8417	54.5895
3	0.3832	0.0689	582411.4	980295.1	1.6831	0.3107	70.5930	68.9211
4	0.4030	0.0786	399476.1	695515.6	1.7410	0.2205	79.8297	77.9496
5	0.4233	0.0903	282944.5	511157.5	1.8065	0.1620	85.7136	83.7944
6	0.4451	0.10151	224583	421408.7	1.8764	0.1336	88.6604	86.6398

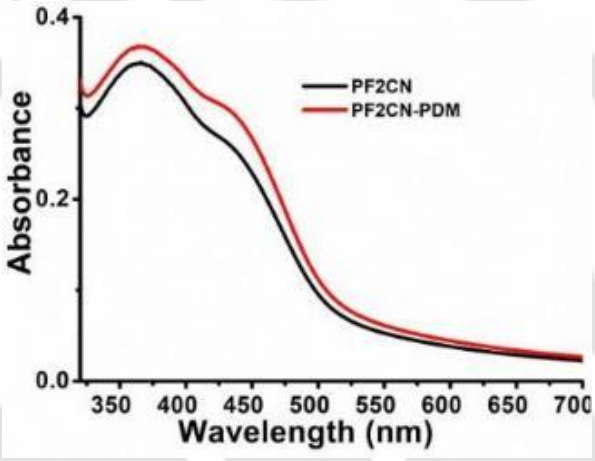

Figure A3.18. UV-Visible absorption spectra of PF2CN before and after PDM addition.

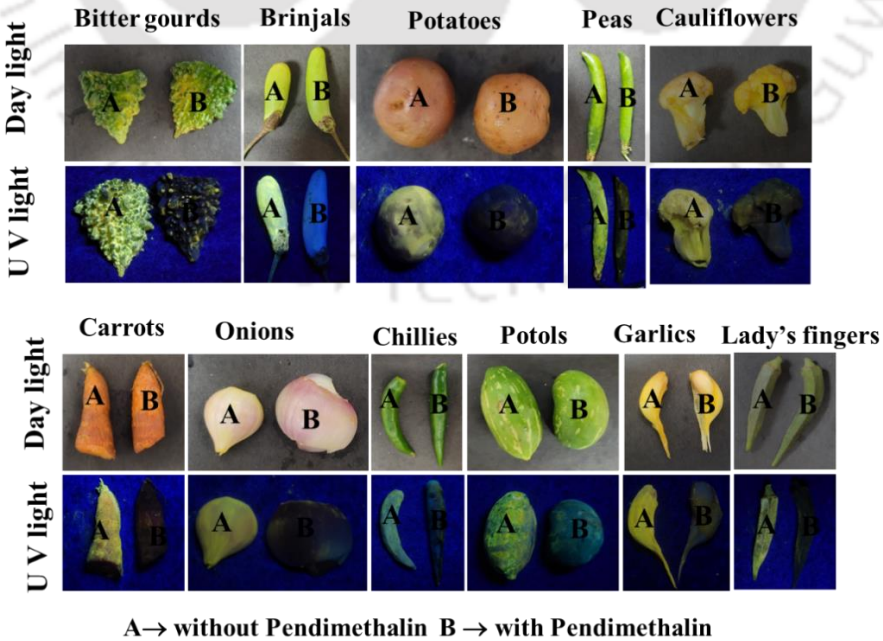

Figure A3.19. Photograph of PF2CN in vegetable samples (A) without and (B) with Pendimethalin

Table 3.4. Table for PDM detection by Standard Recovery Method in various samples

Types of sample	Samples	PDM added (10^{-7} M)	PDM found (10^{-7} M)	Recovery	RSD (%) (N=3)
Water	Tap water	5	5.38	107.6	0.93
		10	9.89	98.9	1.05
		15	14.57	97.13	1.19
	Lake water	5	5.15	102.86	2.16
		10	10.17	101.7	1.87
		15	15.28	101.88	0.66
Food samples	Cabbage	5	4.78	95.76	1.23
		10	9.48	94.86	1.73
		15	15.39	102.6	0.76
	Tomato	5	5.17	103.4	1.00
		10	10.28	102.86	1.90
		15	15.34	102.28	0.82
	Mint leaves	5	4.87	97.53	2.07
		10	9.5	95.46	1.87
		15	14.1	94.55	1.88

Table 3.5. Comparison table for PDM detection with the previous reports

Sl. No.	Material	Sensitivity K_{sv} / K_a (M^{-1})	Lod (M)	Mechanism	Method	Ref
1	Conjugated polymers PFP and PF2CN	K_{sv} = 1.4 x 10^5 K_{sv} = 1.6 x 10^6	91 x 10^{-9} and 2.76 x 10^{-9}	Both FRET and PET	Fluorescence, Smartphone detection	This work
2	BDO[a]	K_a = 1.26 x 10^5	3.8 x 10^{-9}	Either purely static or purely dynamic quenching	Fluorescence	*RSC Adv.* **2016**, *6*, 53573-53577
3	Silver solid amalgam electrode	-	4.0 x 10^{-7}	-	Differential Pulse voltammetry	*Chemicke Listy*, **2006**.*100*, 1105

4	HMDE[b]	-	1.8×10^{-8}	-	Differential Pulse Polarography	*Bull. Chem. Soc. Jpn.* **2000**, *73*, 2477-2480
5	-		1.5×10^{-7}		GC[c]	*J. Agric. Food Chem.* **2001**, *49*, 2198-2206
6	-	-	2.1×10^{-7}		HPLC[d]	*Environ. Monit. Assess.* **2011**, *175*, 103-108
7	Insitu plated BiFE[e]	-	3.7×10^{-8}	Electro-reduction	Voltammetry	*Electrochim. Acta* **2015**, *168*, 379-385
9	Molecular imprinting nanowires	-	1.4×10^{-5}	Recognition	Chemiluminescence	*J. Dairy Sci.* **2022**, *105*, 3019-3031
10	RAC-DTC[f]-Au NPs	-	2.2×10^{-7}	Electrostatic interactions and H-bonding	UV-Vis Spectroscopy	Sens. Actuators B Chem. **2017**, 245, 541-550

BDO[a] = Bidansylated oxacalix[4] arene fluoroionophore, HMDE[c] = Hanging mercury drop electrode, GC[c] = Gas Chromatography, HPLC[d] = High performance liquid chromatography BiFE[e] = Bismuth-film electrode, RAC-DTC[f] = Ractopamine-dithiocarbamate.

CHAPTER 4

Ratiometric Turn-On Detection of HSA using Aggregation Induced Enhanced Emission Conjugated Polyelectrolyte and Prototype Smartphone Device

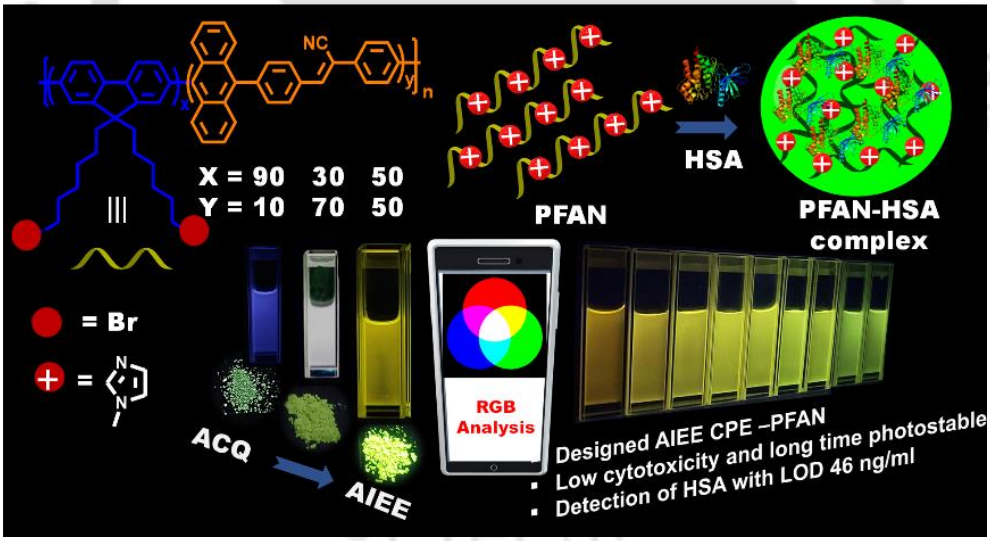

Chanu, M. A.; Adil, L. R.; Ghosh, P.; Khubchandani, D. D.; Iyer P. K. **(Communicated).**

Abstract

Controlling molecular motion and charge transfer of an organic luminogen is the key to deliver various photo-physical properties. Nevertheless, conjugated polymers due to the complexity and diversity of their structures, the studies of structure-motion-property relationship remains a bottleneck. The incorporation of AIE monomer with a twisted donor- acceptor (D-A) architecture is a strategy to tune the photo-physical properties of a conjugated polymer. As such, three sets of polymers P1, P2 and P3 were designed by incorporating various mole percentage of AIE monomer in the polymer backbone to study their photophysical properties in solution and aggregated state. This resulted in significant shift of polyfluorene emission from blue to white and yellow, reflecting the increase of D-A strength from P1 to P3. Further. its condensed state emission property was improved by a unique design strategy thereby converting ACQ polymer (P1) into AIEE polymer (P3). Finally, the PFAN polymer derived from the AIEE-P3 polymer represents an appropriate biosensor for monitoring serum albumins (SAs) that deviate from the normal 35-55 g/L range. Based on the silico study human serum albumin (HSA) has stronger binding energy than bovine serum albumin BSA which agrees with the experimental finding. The mechanism for such remarkable detection with "Ratiometric Turn On" response was due to PFAN-HSA and PFAN-BSA binding induced AIEE mechanism. Furthermore, to benefit the healthcare services especially the elderly or patients with chronic illness, the developed PFAN conjugated polyelectrolyte (CPE)-based HSA detection method was miniaturized into a prototype Smartphone device.

Keywords: AIE, AIEE, ratiometric, turn on sensing, serum albumin, PoC, conjugated polyelectrolyte

4.1 Introduction

The discovery of aggregation-induced emission (AIE) and aggregation-induced enhanced emission revolutionized the material and chemical science, enabling both solution and condensed state applicability in a wide range of fields such as sensing,[1] imaging,[2] theranostics,[3] anticounterfeiting,[4] and optoelectronics devices.[5] This property challenges the phenomenon of aggregation caused quenching (ACQ)[6, 7] shown by conventional luminophore. Integrating AIE/AIEE properties into a conjugated polymer provides a superior material in terms of its efficiency and properties in comparison to a small molecule AIEgen on account of inter and intramolecular synergistic interactions.[8] Moreover, AIE polymers have advantages over conventional fluorescent polymers in various aspects, including improved photo-stability, less toxicity, efficient luminescence efficiency in condensed and solid states, and significant Stokes shifts, making them appealing for practical applications.[9-11]

In recent years, considerable attention has been devoted to designing smart AIE polymers with diverse structures and configurations.[12-14] Controlling molecular motion is the key to convert ACQ to AIE polymer, but studying the structure-motion-property correlation particularly in polymer is quite challenging due to the complicated nature of structural framework and behavior.[15] The incorporation of an AIE monomer into the polymer's backbone or side chain is a well-established approach for developing an AIE/AIEE polymer,[16] nevertheless, the polymer's AIE/AIEE activity depends on the molar ratio of the AIE monomer to be incorporated. Also, as hydrophobicity increases, the solubility of AIE polymers diminishes; hence an optimum molar ratio is required to ensure both AIE activity and good organic solubility. The intense condensed state fluorescence of AIE polymer resulting from structural rigidification by solvent viscosity[17] and/or supramolecular-based interactions[18] is very attractive for designing turn-on sensors with better sensitivity and less background interference.[19-21] Furthermore, AIE polymer having twisted D-A architecture AIE polymer having twisted D-A architecture[22, 23] may detect both molecular motion and changes in solvent polarity, indicating a potential way for constructing a ratiometric sensor for visual detection.[24]

AIE-conjugated polyelectrolytes (AIE-CPEs) have recently received a tremendous interest among the AIE polymers because of their wide range of applications, including fluorescent sensors,[25, 26] optoelectronic devices,[27] bio imaging,[28] photo theranostics,[29] drug delivery,[30] etc. They offer various promising characteristics due to the combined effect of AIE/AIEE, intrinsic property of conjugated polymers, and the capacity of electrolyte charge adjustment. For

instance, the inherent molecular wire effect CPEs gained from CPs greatly boosts their sensitivity as sensors due to the rapid flow of electrons or energy down the conjugated backbones.[29, 31, 32] Meanwhile, the presence of various charges in CPEs allows them to be employed for the selective detection of oppositely charged analytes, such as metal ions, charged small molecules, and biomacromolecules like DNA, proteins etc.[33-35] Additionally, because of their AIE property, such detection can be expanded in solid state.[36, 37] Above all, the main success of AIE-CPEs is the increase in solubility due to presence hydrophilic ionic side groups, which was a barrier in many neutral AIE-polymers for diverse applications.

Herein, by considering the above challenges, we have attempted a stepwise strategy to convert a well-known ACQ polyfluorene backbone into an AIE backbone by copolymerization with an AIE monomer.[23] In the process, the solutions' state and aggregates' state properties of three conjugated polymers (P1, P2, P3) were carefully tuned by simply changing the mole fractions of the monomeric units. Fluorescence emission was greatly tuned from blue to yellow, and a white emission was achieved at a particular mole fraction, which was very challenging. The excellent solid-state emissive property was attained by increasing the mole fraction of the AIE monomer. Further, the polymer's solubility was improved by functionalization with methyl imidazole. The methyl imidazole-functionalized AIE polymer PFAN (Z)-3,3'-((2-(10-(4-(2-cyano-2-(p-tolyl)vinyl)phenyl)anthracen-9-yl)-7-methyl-9H-fluorene-9,9-diyl)bis(hexane-6,1-diyl))bis(1-methyl-1H-imidazol-3-ium) is further utilized for detection of human serum albumins (HSA) and bovine serum albumin (BSA), predominant proteins responsible for numerous physiological and metabolic functions present in human and animal sera.[38] The condition of low HSA (hypoalbuminemia) and high HSA (microalbuminuria) levels from the normal range of 35-55 g/L have been linked to various disorders, including type II diabetes[39], and chronic kidney disease[40], liver cirrhosis,[41] etc.

Among the several reported detection techniques[42, 43] for HSA/BSA, fluorescence is one of the most cost-effective, simple, and quick methods with great sensitivity. Numerous fluorescent molecules have been developed with divergent mechanisms,[44-46] but they still require improvement in sensitivity, visual detection, and portability for real-time application. Conjugated polyelectrolytes undergo quick inter/ intra-chain exciton migration due to π-electron delocalization, amplifying the fluorescence signal and hence increasing sensitivity.[47] The incorporation of M4 monomer into the backbone of conjugated polyelectrolyte allows the recognition of HSA/BSA in a ratiometric turn-on manner, enabling visual detection. The

detailed mechanism for such an efficient turn-on response in a ratiometric manner is electrostatic interaction-induced aggregation, which has been supported by experimental and theoretical findings where M4 plays a pivotal role for turn-on and ratiometric response by making PFAN polymer into AIEE and solvatochromic nature. Furthermore, to ensure a simple portable sensor, a smartphone integrated point of care (PoC) device was developed for monitoring HSA-related diseases easily, and economically for onsite detection, which will benefit in remote areas particularly for the elderly and people with chronic diseases.

4.2 Experimental Section

4.2.1 Materials and Methods: BSA and HSA and all the analytes used in the study were procured from Sigma Aldrich. Milli-Q water has been used for the preparation of the stock solution for all the experiments. Recording of ^{1}H NMR (600 MHz) and ^{13}C NMR (150 MHz) spectra was performed on the Varian-AS400 NMR spectrometer. For recording UV-Visible absorption spectra and photoluminescence spectra, Cary 60 UV-Vis Spectrophotometer and Horiba Fluoromax-4 spectro fluorometers have been used with 1 ml quartz cuvettes (path length =1 cm, slit = 3 nm). FESEM images were obtained from the Zeiss Sigma Field Emission Scanning Electron Microscope (FESEM). Lifetime and quantum measurement were done in Edinburgh FLS1000 Photoluminescence Spectrometer Dynamic light scattering and Zeta potential measurements were done DLS spectrometer Malvern Nano ZS90. DFT study is perform for monomer in Gaussian09 and for polymer Gaussian16[48]. Docking study was done in AutoDock Tools-1.5.7

4.2.2 Synthetic Procedure

4.2.2(a). 4-(10-bromoanthracen-9-yl)benzaldehyde, M3: The monomer (M3) was synthesized by Suzuki Coupling reaction. A mixture of monomers 9,10 dibromoanthracene (M1) (500 mg, 1.49 mmol) and 4 formyl phenyl boronic acid (M2) (268.4 mg, 1.79 mmol) were taken in a clean RB flask fitted with water condenser and then made the system inert by degassing followed by purging with argon gas. Thereafter, 5 mg of catalyst $Pd(PPh_3)_4$ were added maintaining the inert condition. A mixture of THF (9 ml) and 2 M K_2CO_3 (3 ml) were injected into the reaction mixture and were made inert by applying free-thaw degassing technique (3 times). The reaction mixture was stirred at reflux condition under an argon atmosphere and the progress of reaction were monitored by TLC. After 24h., the reaction was stopped and extracted with $CHCl_3$/water. The organic layer was dried under vacuum and it was

purified by column chromatography by 30 % $CHCl_3$/hexane solvent fraction. (yellow color solid, Yield = 84 %, 450 mg).

MALDI_TOF: The mass of monomer M3 (m/z =360.988)

^{1}H NMR (600 MHz, $CDCl_3$, δ ppm): 10.20 (s, 1H), 8.63-8.65 (d, 2H), 8.11-8.13 (d, 2H), 7.60-7.63 (m, 4H), 7.54-7.56 (d, 2H), 7.39-7.42 (t, 2H),

^{13}C NMR (150 MHz, $CDCl_3$, δ ppm): 191.95, 145.29, 135.95, 135.86, 132.02, 130.02, 130.57, 130.19, 129.85, 128.09, 127.10, 126.72, 126.08, 123.64.

4.2.2(b). (Z)-3-(4-(10-bromoanthracen-9-yl)phenyl)-2-(4-bromophenyl)acrylonitrile, (M4): The monomer M4 was synthesized by Knoevenagel Condensation reaction. The monomer M3 (50mg, 0.138 mmol) and 4 bromophenyl acetonitrile were solubilized in 20 ml ethanol at 50 ^{0}C with continuous stirring. 23 mg of Potassium tertiary butoxide (t-BuOK) was solubilized in 2ml ethanol and then injected into the reaction mixture dropwise. After the product gets precipitated as yellowish precipitate from the reaction mixture. The progress of the reaction was monitored by TLC and after 4h the precipitate was filtered through Whatman filter paper and then wash repeatedly by ethanol to get the pure amorphous yellow ppt. (yield=96 %, 72 mg).

MALDI_TOF: The mass of monomer M4 (m/z =538.909)

^{1}H NMR (600 MHz, CDCl3, δ ppm): 8.63 (s, 2H), 8.12 (d, J = 8.0 Hz, 2H), 7.69 (s, 1H), 7.64 (d, J = 8.4 Hz, 6H), 7.61 (d, J = 7.9 Hz, 2H), 7.54 (d, J = 8.1 Hz, 2H), 7.43 – 7.40 (m, 2H).

^{13}C NMR (150 MHz, CDCl3, δ ppm): 142.24, 141.39, 132.98, 130.22, 129.44, 128.08, 127.56, 127.07, 126.94, 125.95, 123.66, 117.68, 111.04.

4.2.2(c). 2,7-dibromo-9,9-bis(6-bromohexyl)-9H-fluorene (M5): The synthesis of the monomers M5 was done by following the already reported procedures.[49] The starting material 2, 7 dibromo fluorene (1 g, 3.106 mmol), and tetra butyl ammonium iodide (TBAI) (0.229 g, 0.621 mmol) were taken in a clean RB flask and made inert condition by applying free-thaw and degassing technique (3 times). After that, 1,6-dibromohexane (2.82 ml, 18.636 mmol) followed by 50 % NaOH were injected cautiously through a syringe, maintaining the inert condition. Finally, the reaction was performed at 80 °C with proper stirring for 5h. TLC in hexane was used to monitor reaction completion, then separated the organic part from water in a separating funnel with water/chloroform mixture. The excess 1,6-dibromohexane from the recovered organic layer dried by Kugelrohr and further purification was done by column chromatography with hexane as eluent to obtain the final product as white crystalline solid. (Yield = 95 %, 1.92 g)

^{1}H NMR (600 MHz, $CDCl_3$, δ ppm): 7.52 (d, J = 8.0 Hz, 1H), 7.46 (d, J = 8.1 Hz, 1H), 7.43 (s, 1H), 3.29 (t, J = 6.8 Hz, 2H), 1.96 – 1.91 (m, 2H), 1.71 – 1.64 (m, 2H), 1.20 (dt, J = 15.2, 7.7 Hz, 2H), 1.11 – 1.06 (m, 2H), 0.62 – 0.56 (m, 2H).

^{13}C NMR (150 MHz, $CDCl_3$, δ (ppm): 152.19, 139.09, 130.05, 126.12, 121.58, 121.53, 55.57, 40.03, 32.79, 32.61, 28.95, 27.75, 23.47.

2.2.2(d). 2,2'-(9,9-bis(6-bromohexyl)-9H-fluorene-2,7-diyl)bis(4,4,5,5-tetramethyl-1,3,2-dioxaborolane), (M6): The mixture monomer M5 (1g, 1.5 mmol), bis-(pinacolato)diborane (0.95 g, 3.75 mmol) and KOAc (1 g, 10 mmol were taken in a clean 250 ml RB flask. The mixture is degassed and then 5 mg of [Pd(dppf)Cl2] (dppf-1,1'-bis(diphenylphosphanyl)ferrocene) was added cautiously followed by 12 ml 1, 4 dioxane (dry). The reaction stirred properly at w 85 ^oC for 24h. Then the mixture was dried at high vacuum and then extracted the organic soluble part by using ethyl acetate/ water mixture. Further purification was done by flash chromatography using 5 % ethyl acetate hexane mixture as eluent to get. M6 as white crystals (0.63 g, 66 %)

^{1}H NMR (600 MHz, $CDCl_3$, δ ppm): 7.81 (d, J = 7.5 Hz, 2H), 7.72 (d, J = 9.7 Hz, 4H), 3.25 (t, J = 6.8 Hz, 4H), 2.05 – 1.98 (m, 4H), 1.67 – 1.57 (m, 4H), 1.39 (s, 24H), 1.14 – 1.11 (m, 4H), 1.09 – 0.98 (m, 4H), 0.57 – 0.50 (m, 4H).

^{13}C NMR (150 MHz, $CDCl_3$, δ ppm): 150.17, 143.50, 133.90, 129.12, 119.94, 83.56, 55.13, 40.17, 34.06, 32.49, 29.32, 27.38, 24.50, 23.57.

4.2.2(e). Synthesis of P1, P2 and P3 polymers: They were synthesized by Suzuki Coupling reaction by taking the required molar ratio of monomers M4, M5 and M6 as given in Table 4.1. A mixture of monomers M4, M5 and M6 were taken in a clean RB flask fitted with a condenser and then made the system inert by degassing followed by purging with argon gas. Thereafter, 5 mg of catalyst $Pd(PPh_3)_4$ were added maintaining the inert condition. A mixture of THF (9 ml) and 2 M K_2CO_3 (3 ml) were injected into the reaction mixture and were made inert by applying free-thaw degassing technique (3 times). The reaction mixture was stirred at reflux condition under an argon atmosphere. After 30h., the reaction the reaction was cool down and extracted with $CHCl_3$/water. The organic layer was dried under vacuum and purified repeated precipitation in methanol and acetone. The molecular weight (MW) of polymers were determined by GPC using polystyrene as a standard.

For P1:
^{1}H NMR (600 MHz, $CDCl_3$, δ ppm): 7.87 (b), 7.73-7.69 (b), 7.60-7.51 (b), 7.12-6.91 (b) 3.0 (b), 2.19 (b)1.28-1.19 (b), 1.70 (b) 0.84 (b).

For P2:
^{1}H NMR (600 MHz, $CDCl_3$, δ(ppm): 8.11-7.95 (b), 7.75-7.57 (b), 7.37-7.31 (b), 7.06 (b), 7.84 (b), 3.22 (b), 2.05 (b)1.62 (b), 1.09 (b) 0.76 (b).

For P3:
^{1}H NMR (600 MHz, $CDCl_3$, δ ppm): 8.17-8.01 (b), 7.82-7.77 (b), 7.62 (b), 7.49 (b), 7.36 (b), 3.25 (b), 1.98 (b)1.67 (b), 1.09 (b) 0.82-0.67 (b).

TAble 4.1: The molar ratio of monomers used in polymerization of P1, P2 and P3 along with their yield (MW)

Polymer	Mole fractions of monomers taken			Yield (%)	MW (gmole^{-1})	PDI
	M4 (MW 539.27 gmole^{-1})	M5 (MW 650.13 gmole^{-1})	M6 (MW 744.26 gmole^{-1})			
P1	43.47 mg (0.08 mmole)	210 mg (0.322 mmole)	300 mg (0.403 mmole)	470 mg (85 %)	16688	1.60
P2	130.39 mg (0.242 mmole)	104.8 mg (0.161 mmole)	300 mg (0.403 mmole)	430 mg (80 %)	14391	1.54
P3	217.37 mg (0.403 mmole)	0	300 mg (0.403 mmole)	450 mg (87 %)	15324	1.78

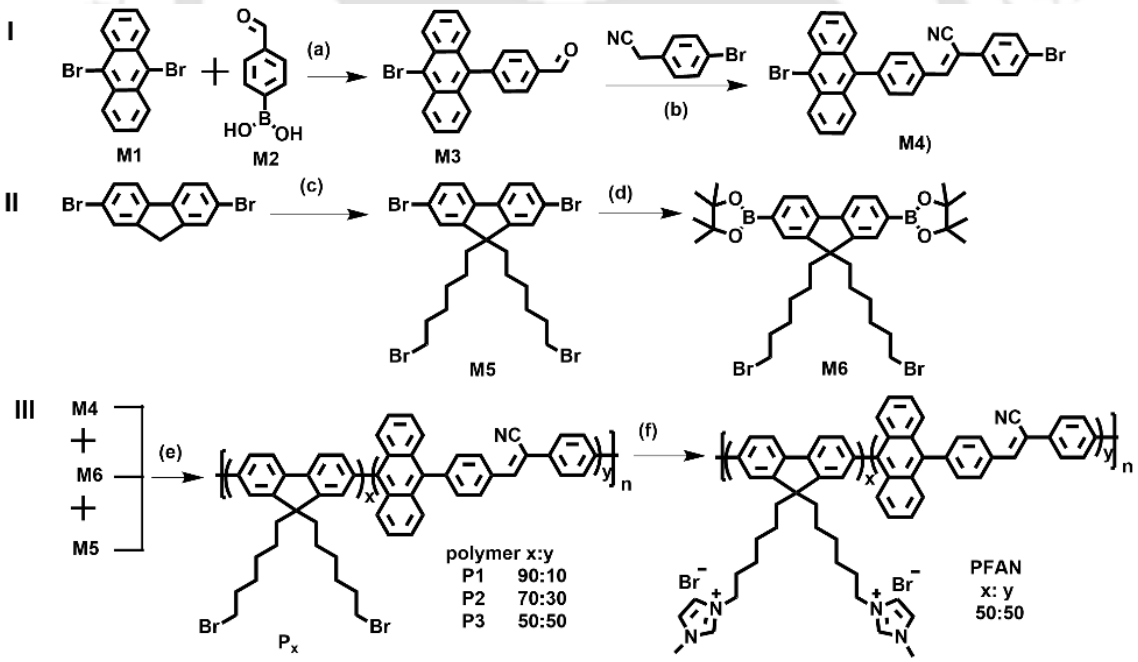

Scheme 4.1: Synthetic pathways for monomers and polymers: (a) tetrakistriphenylphosphine palladium(0), 2 M, K_2CO_3 (aq.), THF, reflux, 24h.; (b) t-BuOK, ethanol, rt, 12h.; (c) 1,6-Dibromohexane, 50 % (aq.) NaOH, TBAI, 70 °C, 4h; (d) bis(pinacolato)diboron, [Pd(dppf)Cl_2], KOAc, dioxane, 85 °C, 12h; (e) tetrakistriphenylphosphine palladium(0), 2M K_2CO_3 (aq), THF, reflux, 30h.; (f) 1-methylimidazole, DMF, 110 ^{0}C, 24h.

4.2.3 Photoluminescence quantum yield (ϕ). The absolute quantum yield for P1, P2, P3 and PFAN polymers were determined by using Edinburgh FLS 1000 instrument through integrated sphere technique.

4.2.4 Limit of detection (LOD). The lowest LOD was determined by analyzing the fluorescence spectra of PFAN with varying concentrations of HSA (0-70 µg/ml) and BSA (0-90 µg/ml) in water medium. Using the standard formula, LOD=3σ/k, the lowest LOD was calculated from the calibration curve, where the symbols σ and k represent the calibration plot's standard deviation (SD) and slope, respectively.

4.2.5 Cell Viability Assay. MTT assay was performed to evaluate the cytotoxicity of the polymer PFAN using HEK 293 cell. Both cells were seeded into a 96-well plate at the density of 10,000 cells/well and incubated for 24 h. Cells were washed with 1X PBS and followed by the treatment of series of different concentration of polymer PFAN at 0, 10, 20, 30, 40, 50, 60, 50, 60, 70, 80, 90 and 100 µg/mL for 24 h at 37 °C in incubator. Cells were washed with 1X PBS on incubation of 24 h. 10 µL of MTT of stock concentration 5 mg/mL and 90 µL DMEM medium was added to each well and incubated for 4 hours at 37 °C in incubator. After incubation of 4 h, 75 µL of medium was removed and 50 µL of DMSO was added to each well followed by further incubation of 10 minutes. The multimode microplate reader (Thermofisher Varioskan LUX) was used to record absorbance at wavelength of 490 nm. All the experiments were carried out in triplicate.

4.2.6 Molecular Docking. The purpose of molecular docking was to analyze the stable conformation of the probe while it is attached to a protein, focusing on its geometric and energetic properties. The software AutoDockTools-1.5.7 was utilized to produce a docked arrangement of PFAN monomer with HSA and BSA. This process involves the application of a genetic algorithm (GA) and a Lamarckian genetic algorithm to generate several conformations. The program was utilized to examine the binding free energies and binding locations of PFAN monomer within the active site of HSA/BSA. The crystal structure of HSA and BSA was obtained from RCSB PDB (4K2C and 3V03) and underwent energy refinement, hydrogen additions, and solvent removal using AutoDockTools-1.5.7 to ensure that all residues achieved a proper and stable conformation. The Lamarckian GA (pdb file) was chosen as the output and utilized in AutoDockTools-1.5.7 to conduct docking simulations. The process of minimizing and optimizing the energy of PFAN monomer was also carried out. Ultimately, the analysis of the docking result of the PFAN monomer was conducted using Discovery Studio Visualizer programmes.[50] The docking structure with the lowest binding energy, as determined by AutoDockTools-1.5.7, was selected as the optimal binding conformation.

4.2.7 Serum Sample Analysis. Fresh serum samples were collected from the Indian Institute of Technology, Guwahati (IIT G) Hospital and diluted 100 times with Milli Q water to estimate HSA using the standard recovery method. The serum samples were then spiked with 0 mg mL^{-1}, 0.5 mg mL^{-1}, 1.5 mg mL^{-1}, and 3 mg mL^{-1} of HSA to make four distinct analytical samples. To record fluorescence spectra, 10 µl of each sample was introduced in a 1 ml cuvette containing PFAN (5 µg mL^{-1}) polymer. Each measurement was taken three times, and the amount of HSA was calculated using the Standard Recovery Technique.

4.3 Results and Discussion

The AIEE monomer (Z)-3-(4-(10-bromoanthracen-9-yl)phenyl)-2-(4-bromophenyl)acrylonitrile (M4), is synthesized by the Knoevenagel Condensation reaction between M3 and 4-Bromobenzyl cyanide. 2,7-dibromo-9,9-bis(6-bromohexyl)-9H-fluorene (M5) was prepared by alkylation reaction, which was further undergoing Miyaura borylation reaction to obtain monomer 2,7-bis[9,9′-bis(6″-bromohexyl)fluorenyl]-4,4,5,5-tetramethyl[1,3,2]dioxaborolane (M6). The polymers P1, P2 and P3 were synthesized by Suzuki cross-coupling polymerization reaction with 70-80 % yield. PFCN was synthesized by post-functionalizing P3 polymer with 1- methylimidazole. The synthesized monomers were well characterized by NMR and mass spectrometry, and the polymers were characterized by NMR and GPC before being used in further studies (Scheme 4.1 and Figure A4.1-A4.17). The monomer M4 is AIEE in nature. We could convert the well-known ACQ polyfluorene backbone into an AIEE copolymer by increasing the mole fraction of M4, along with tuning of the solid state and solution state properties of the resulting copolymers.

4.3.1 Characterization of Monomer M4:

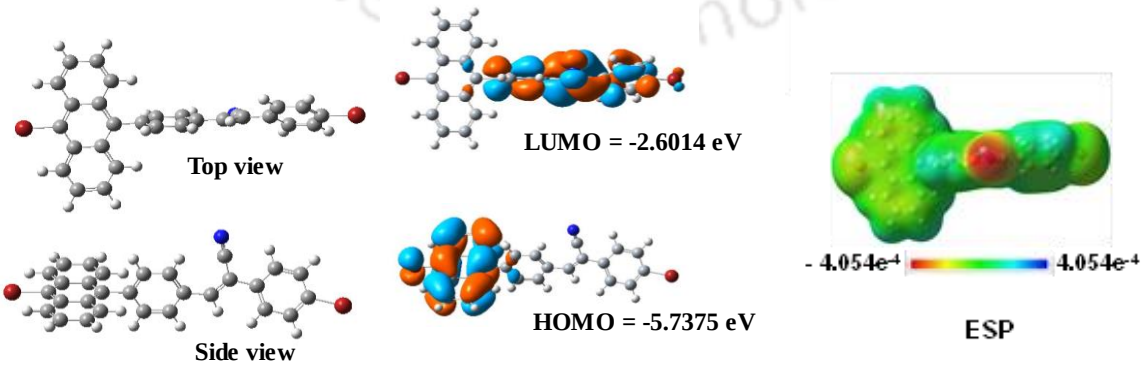

Figure 4.1. Optimized structure of M4 monomer using B3LYP and 631G (d.p) of Gaussian software.

DFT studies were employed to study the monomer M4 behavior by applying the 631G function with the B3LYP basis set in the Gaussian Program. The optimized geometry shows that M4 has a nonplanar skeleton, which is necessary for a molecule's AIE activity, and had the well separated HOMO-LUMO electronic clouds responsible for color tuning. The HOMO electronic clouds are restricted in the anthracene moiety, and the LUMO electronic clouds were diffuse over the phenyl acetonitrile ring due to the presence of a strong electron-withdrawing CN group, where the electron density is minimal as clearly visible in the electronic charge distribution shown by ESP mapping, suggesting a possibility of intramolecular charge transfer (ICT) (Figure 4.1).

The monomer M4 is soluble in polar organic solvents, and its 1 mM stock solution was prepared in DMSO. The photo-physical studies were performed in various DMSO/water fractions due to the good miscibility of DMSO and water. The monomer displayed absorption maxima at around 362 nm, 382 nm, and 403 nm, which matches the characteristic anthracene backbone (Figure 4.2a). The peaks are slightly red-shifted in water and can be attributed to aggregation. Further, its fluorescence property was recorded by increasing the water fraction (f_w) in DMSO (λ_{ex} 400 nm) (Figure 4.2b). Initially, the monomer M4 had an emission at 453 nm and with the increase of f_w percentage, the emission at 453 nm gradually decreased, and a new peak slowly increased at 500 nm with the highest emission maxima at 99 % f_w, suggesting the AIEE property of the monomer (Figure 4.2c). The naked-eye visualization of fluorescence

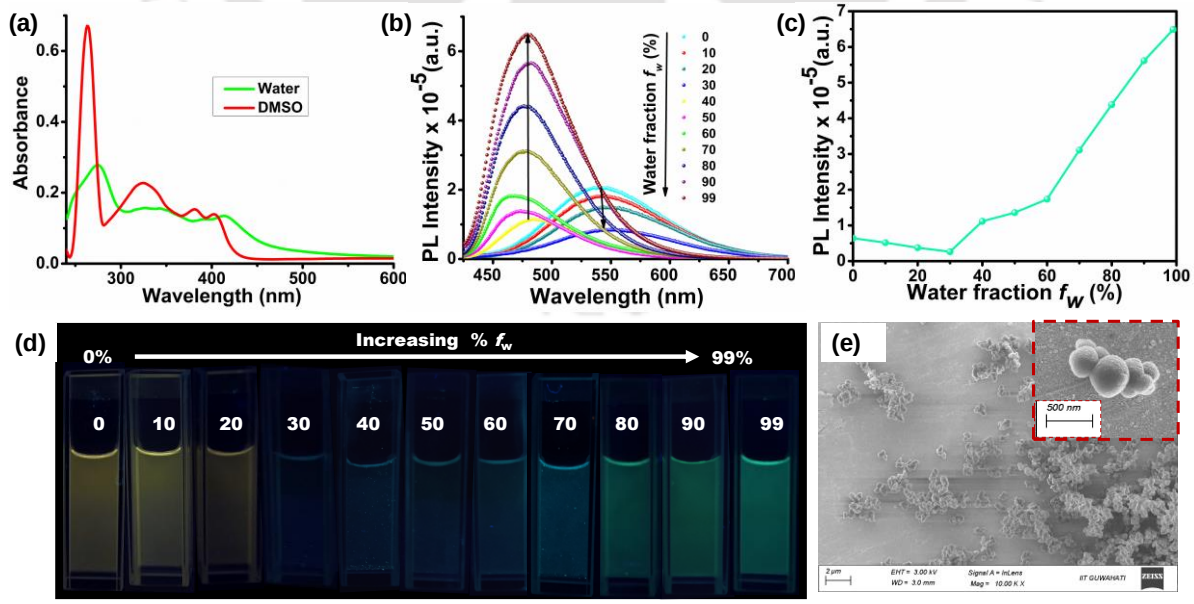

Figure 4.2: (a) UV-visible spectra of monomer M4 in % f_w in DMSO. (b) Fluorescence spectra of M4 in various % f_w in DMSO. (c) PL intensity vs. % f_w in DMSO. (d) Photograph of M4 with different % f_w under 350nm UV lamp. (e) FESEM images of M4 at 99 % f_w.

change under a UV lamp in various DMSO/water fractions is shown in Figure 4.2d. The emission is blue shifted due to the aggregation restricting molecular motion and disturbing the ICT process. Finally, FESEM and FETEM were used to analyze the morphology of M4 at 99 % f_w, where it self-assembled into a spherical nanoparticle (Figure 4.2e and Figure A4.18a). These spherical nanoparticles had an average hydrodynamic size of around 140 nm, according to DLS measurements (Figure A.4.18b).

4.3.2 Photophysical Studies of Synthesized Polymers P1, P2 and P3:

Polymers P1, P2, and P3 were synthesized by copolymerizing fluorene-based monomers (M5, M6) with various mole fractions of M4 monomer (10:90, 30:70, 50:50) via Suzuki coupling polymerization. Due to the incorporation of a non-planar monomer M4, with an electron-accepting tendency in the conjugated system, their photo-physical characteristics are effectively tuned both in solution and condensed state. The absorption spectra of these polyfluorene-based polymers show λ_{max} at 370 nm with a hump at around 400 nm (Figure 4.3a). The hump at 400 nm is because of M4, which becomes prominent at P3. The emissive properties of these polyfluorene-based polymers are clearly influenced by the molar ratio of various monomeric units present in copolymerization; P1 shows blue, P2 white, and P3 yellow color in a particular organic solvent (DMSO) reflecting the increased D-A strength. The photographs (image) of the fluorescence color and their corresponding CIE coordinates are also shown in inset (Figure 4.3b, 4.3c and 4.3d). Further, P2 being white emissive, its absorption

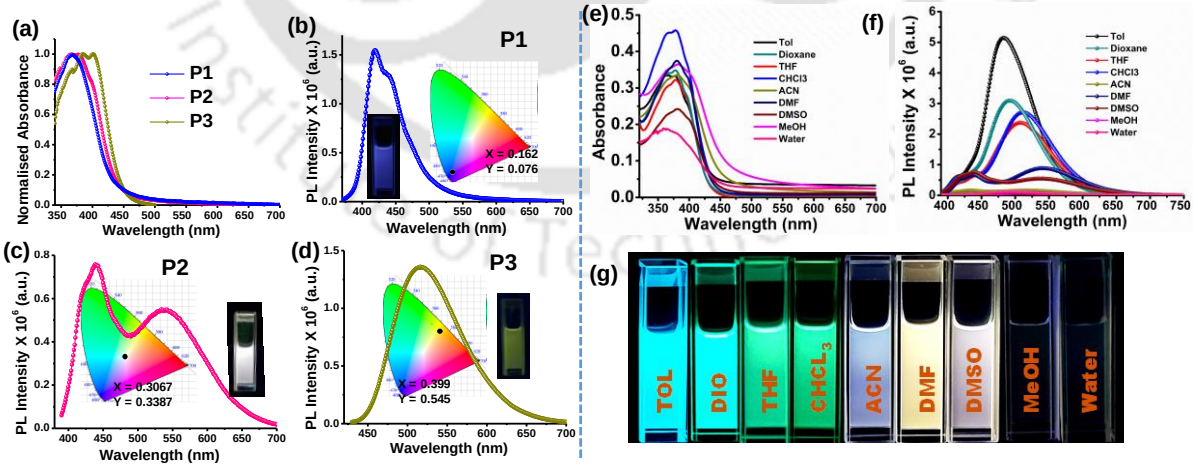

Figure 4.3. (a) UV-visible spectra of P1, P2 and P3 in DMSO; PL spectra of (b) P1, (c) P2 and (d) P3 in DMSO with their corresponding CIE coordinates and photographs under UV lamp; (e) UV-visible spectra of P2 in various organic solvents; (f) PL spectra P2 in various organic solvents; (g) Photographic image of P2 in various organic solvents under UV lamp.

and emissive properties were monitored in various organic solvents. The absorption spectra of P2 in various organic solvents show only change in the absorbance without much impact on λ_{max} value (Figure 4.3e). But it emits nearly white emission in ACN, DMF and DMSO due to the coverage of whole vision region of spectrum (Figure 4.3f, 4.3 g) where solvent polarity plays a key role in controlling the molecular motion and the D-A charge transfer process from fluorene to M4 in copolymer.

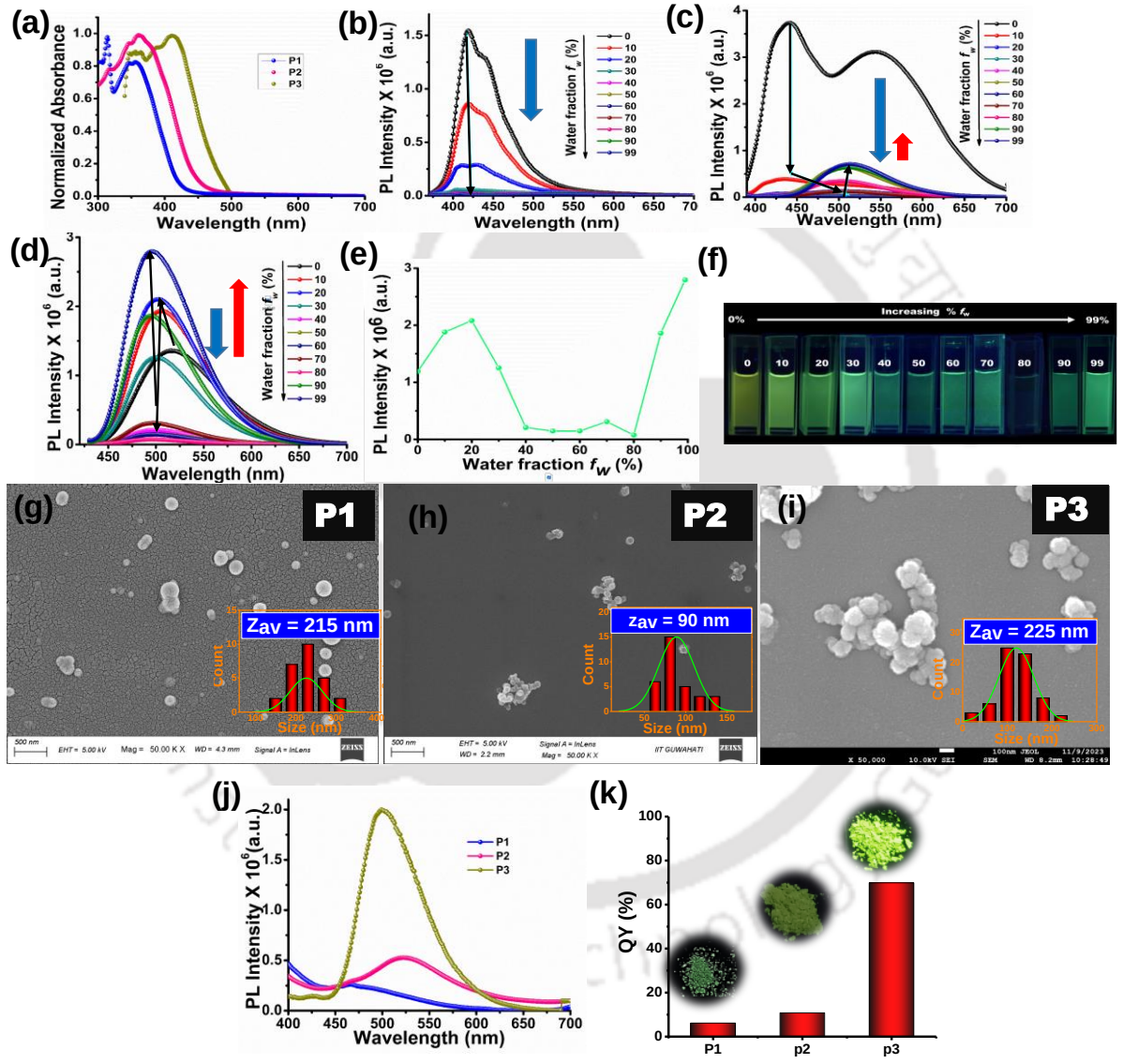

Figure 4.4. (a) UV-visible spectra of P1, P2 and P3 in water; AIE study of polymer of (b) P1, (c) P2 (d) P3 in various DMSO/water fraction; (e) PL intensity vs. water fraction (f_w) of P3; (f) photographic image of P3 in various % f_w under UV lamp; FESEM images of (g) P1, (h) P2, (i) P3 in 99 % f_w; (j) solid state emission and their corresponding (k) quantum yield and photograph under UV lamp (365 nm).

The effect of the molar ratio variation of the monomers is also checked in the condensed state. The aggregated state absorption spectra of P1, P2, and P3 in water show a peak at 370 nm in P1, a broader spectrum at around 410 nm in P2, which becomes red-shifted and more prominent in P3 due to the presence of M4 (Figure 4.4a). The AIE studies in various DMSO/water fractions show that only P3 is AIEE in nature but P1 is ACQ and P2 has weak emission (Figure 4.4b, 4.4c and 4.4d). Polymer P3 has an emission maximum at 99 % f_w with a shift of visual emission color from yellow to green (Figure 4.4e and 4.4f). The morphological study shows that all the polymers self-assemble into a spherical nanoparticle in 99 % f_w with average size of 214 nm for P1, 96 nm for P2 and 225 nm for P3 (Figure 4.4g, 4.4h and 4.4i). The solid-state photo-physical properties agree with the aggregated state, where P1and P2 has weak solid-state emission but P3 has intense solid-state emission (Figure 4.4j). The comparison of the solid-state photo-physical properties and quantum yield of these polymers is shown in (Figures 4.4k, and Table A4.1).

4.3.3 Characterization of polymer PFAN:

The AIEE-P3 polymer is functionalized with 1 methyl imidazole to obtain PFAN polymer, where the polymer solubility improves drastically and acts as a sensory material for serum albumins. The PFAN polymer shows absorption spectra at around 410 nm in DMSO, which becomes 10 nm red-shifted in toluene due to aggregation (Figure 4.5a). Also, PFAN retains the AIEE activity of P3 even after functionalization with 1-methyl imidazole, where maximum emission is obtained at 90 % toluene fraction (% f_{tol}) (Figure 4.5b, 4.5c). The solid-state quantum yield of PFAN at emission 560 nm (ex. 410 nm) is ~85.22 % which one of the best among the AIEE conjugated polyelectrolytes and is very challenging to achieve. The emissive property of PFAN was also analyzed in various solvents, which shows a 30 nm red shift with an increase of solvent polarity because of solvent sensitive emission effect (Figure A4.19). Interestingly, PFAN shows yellow emission in water (λ_{ex} ~410 nm, λ_{em} ~560 nm) with a quantum yield ~67.63 % which is suitable for biosensing application thereby avoiding the use of dangerous UV source for excitation and toxic solvents. Moreover, the emission is highly photostable (Figure 4.5d), broad range of pH stability (Figure 4.5e) and has less cytotoxicity where the cell viability in the mammalian HEK 293 (normal) cell lines is more than 80 % (Figure 4.5f). All the above properties make PFAN an ideal material for biosensing applications.

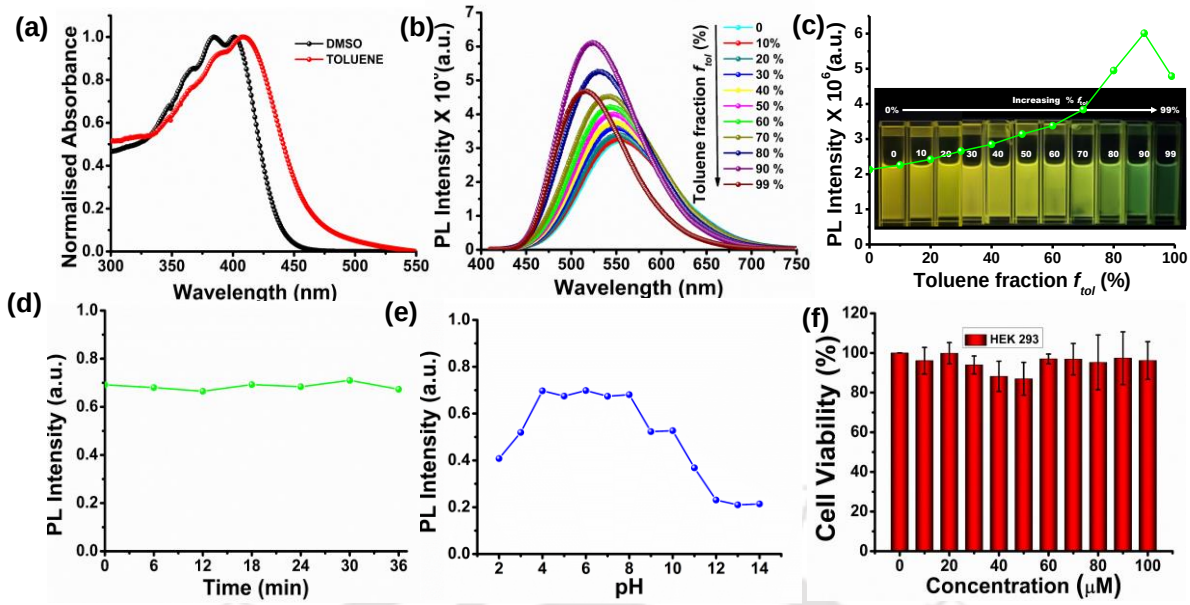

Figure 4.5. (a) UV-visible spectra of PFAN in DMSO and toluene; (b) AIE study in various DMSO/ toluene fractions (% f_{tol}); (c) Photographic image in various DMSO/toluene (% f_{tol}) fractions under UV lamp: inset PL intensity vs. f_{tol}; (d) Photostability of PFAN under UV irradiation; (e) pH stability of PFAN (f) Cell viability of PFAN in HEK 293 (normal) cell line.

4.3.4 Sensing of Serum Albumin:

The AIEE property of PFAN is demonstrated as a superior sensor for serum albumins (SAs) with ratiometric turn-on response in the pure aqueous medium due to their huge significance of SAs in disease diagnosis such as hyperalbuminemia, microalbuminuria, and several physiological disorders. Figure 5.6a and 4.6b show that the PFAN polymer gradually shifts its emission maxima (λ_{em}) from 560 nm (yellow fluorescence) to 500 nm (green fluorescence) by the addition of SAs (i.e., HSA/BSA) with a turn-on response. The limit of detection as obtained from the linear plot calculated by using the formula $3\sigma/k$ is 46 ng/ml for HSA and 97 ng/ml for BSA (Figure 4.6c). The sensing ability is also analyzed in various amino acids, proteins, biomolecules, and enzymes where it shows less sensitivity towards them (Figure 4.6d and 4.6e), and the reason for this will be discussed in the mechanism section.

4.3.5 Mechanisms of Serum Albumin:

A molecular docking analysis was performed to identify the likely location where the PFAN monomer binds to HSA and BSA. The structure of PFAN monomer was optimized by applying the 631G (d, p, charge = +2) function with the B3LYP basis set in the Gaussian16 Program (Figure A4.20). Figure 4.7a, 4.7b and 4.7c, illustrates the optimal binding configuration of probe the PFAN monomer with HSA (PDB ID: 3V03),[51] characterized by the lowest binding

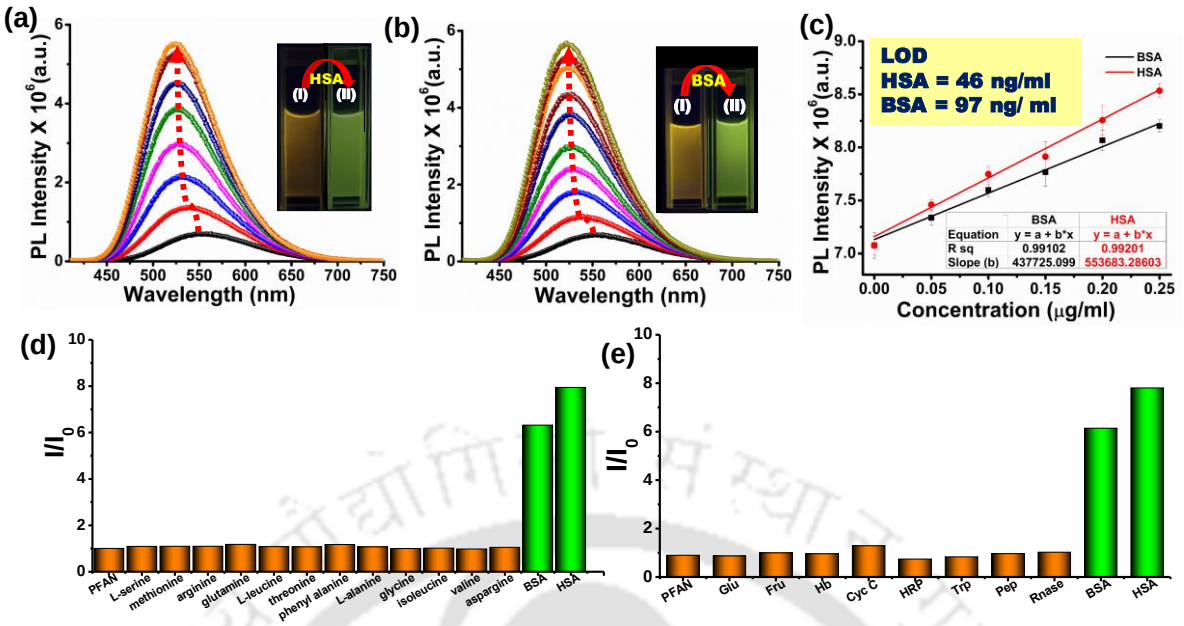

Figure 4.6: PL ratiometric turn-on spectra of PFAN by gradual addition of (a) HSA (0-70μg/ml) and (b) BSA (0-90 μg/ml); (c) calibration plot for LOD calculation for PFAN detection of HSA and BSA; (d) selectivity study of PFAN with various amino acids, (e) biomolecules, enzymes and proteins.

energy of -11.79 kcal/mol. In Figure 4.7d, 4.7e and 4.7f, it has been seen that the best critical configuration of the probe is with the PFAN monomer with BSA (PDB ID: 4K2C)[52]. This configuration has the lowest binding energy of -9.7 kcal/mol, which is a negative value indicating that binding to BSA is likely to happen spontaneously and is energetically favorable. Both proteins interact with the PFAN monomer through various types of non-bonding interactions, including carbon-hydrogen, π-cation, π-anion, π-alkyl, π-π T-shaped, and hydrogen bond interactions. Table 4.1, highlights the primary interactions between the involved amino acids and the bond distances. Molecular docking analysis confirms that the probe binds with both HSA and BSA proteins. However, the free binding energy of the HSA-Probe complex is observed to be lower than that of the BSA-Probe complex.

The results obtained from the docking study was again validated by performing various experimental studies. UV-visible spectra of PFAN was recorded with sequential addition of HSA (0 – 70 μg/ml) and BSA (0- 90 μg/ml). Remarkably there is an increment of absorption peak at around at around 255 nm which corresponds to π – π* transition of anthracene moiety along with the lifting of tail at 290 nm (Figure 4.8a and Figure A4.21a). These findings support the docking results of binding between PFAN and SAs (HSA/BSA). Furthermore, the DLS measurements show the average particle size distribution of the polymer PFAN (Z_{av} =141 nm), which increased upon the addition of SAs (36.2 nm for HSA and 24.5 nm for BSA), leading

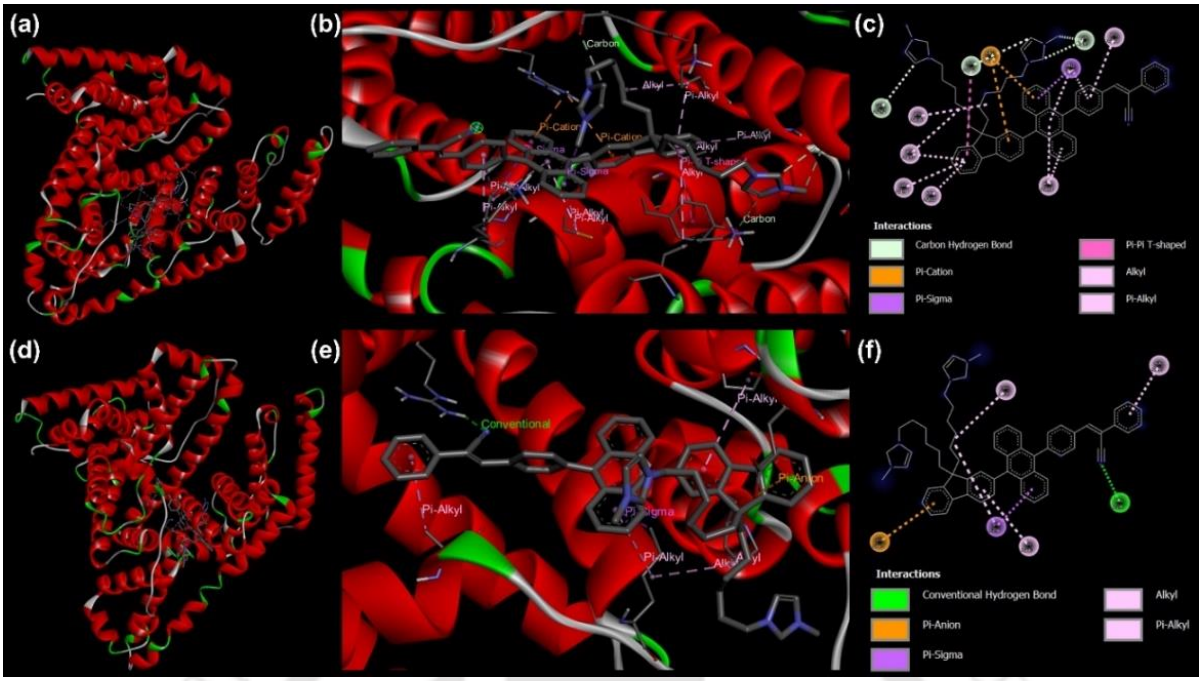

Figure 4.7: Molecular Docking analysis of PFAN monomer with HSA (PDB ID: 3V03), and BSA (PDB ID: 4K2C). (a) PFAN monomer fitting with HSA protein binding site, (b) different types of interaction with the interacting amino acids, (c) 2D image of the probe with interacting amino acids, (d) BSA protein with the PFAN monomer, (e) Probe is interacting with different major interactions (f) 2D diagram of the probe with interacting amino acids.

Table 4.1: Summary of the Molecular Interactions of HSA and BSA with PFAN monomer

Proteins	Major interactions	Interacting amino acids	Bond distance	Binding energy
	Carbon-hydrogen	TYR 452A	3.72 Å	-11.79 kcal/mol
HSA	π-cation	ARG 218A	3.66 Å	
(PDB ID:	π -sigma	PRO 447A	3.06 Å	
3V03)	Carbon-hydrogen	ASP 187A	3.43 Å	
	π -alkyl	CYS 448A	3.59 Å	
BSA	H-bond	ARG 198A	2.47 Å	-9.70 kcal/mol
(PDB ID:	π -Sigma	LYS 294A	3.54 Å	
4K2C)	π -Anion	GLU 443A	4.99 Å	

to the formation of PFAN- HSA complex (Z_{av} =1596 nm) and PFAN-BSA complex (Z_{av} =1003 nm) (Figure 4.8b and Figure A4.21b). These results provide more evidence for complexation and are in close agreement with the changes in the absorption spectra. Additionally, a favorable pathway for the complexation process was revealed by the ζ potential measurements (Figure 4.8c and Figure A4.21c), where the net charge of PFAN (+17.2 mV) becomes almost neutral, i.e., +0.85 mV (HSA) and -0.87 (BSA) due to a strong binding affinity towards the negatively

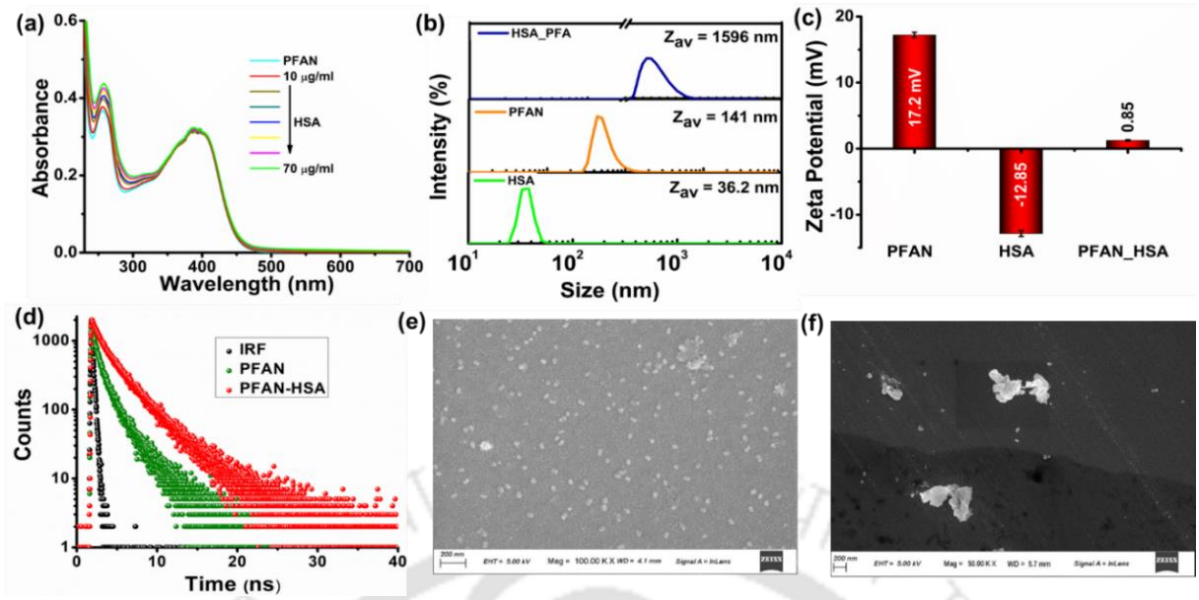

Figure 4.8: (a) UV spectra of PFAN by addition of HSA; (b) DLS profile of PFAN, HSA and PFAN_HSA; (c) Zeta potential and (d) Lifetime decay profile of PFAN before and after addition of HSA; FESEM images of PFAN (e) before and (f) after addition of HSA.

charged HSA and BSA (-12.85 mV and -11.35 mV). The resulting neutral charges for the PFAN-HSA/ BSA complex evidence that serum albumins had successfully bonded to the surface of PFAN assemblies. So, from the above findings, we can infer that PFAN electrostatic interaction with SAs induced aggregation of PFAN-HSA and PFAN-BSA complexes, which resulted in significant color change with a turn-on response due to aggregation inhibiting the ICT processes. This change is not observed in the case of P3 polymer, confirming the importance of 1-methyl imidazole in the sensing mechanism (Figure A4.22a, A4.22b). The increment in the average lifetime of PFAN-HSA (2.65 ns) and PFAN-BSA (2.58 ns) complexes from PFAN (1.38 ns) further supported the proposed mechanism (Figure 4.8d, Figure A4.21d and Table A4.2). Here, the molecular movements are constrained by complexation and aggregation in PFAN-HSA and BSA complexes, resulting in a decrease in the rate of non-radiative decay, which contributes to an increase in lifetime. Finally, the morphological changes of PFAN after the addition of SAs were analyzed by FESEM study where the PFAN self-assembled into aspherical nanoparticle in water which agglomerated into massive ensembles via hydrophobic and electrostatic interactions on addition of SAs illustrating the aforementioned mechanism (Figure 4.8e, 4.8f and Figure A4.21e, A4.21f). The less sensitive nature of PFAN to other enzymes and proteins is due to the involvement of other factors in the sensing mechanism. The isoelectric point (PI)[53, 54] of proteins and enzymes is a key parameter for determining net charge responsible for binding PFAN. As HSA (PI = 5.2) and BSA (4.8) have a net negative charge at neutral conditions (pH =7), they are more likely to bind to PFAN,

triggering the aggregation processes thereby restricting the molecular motion and ICT process (Table A4.3). Pepsin (PI = 2.5, pH =7) and hemoglobin (PI = 6.8) also have a net negative charge, but tryptophan (Trp) emissions are self-quenched by denaturation.[55] and intramolecular Trp-heme electron and energy transfer mechanisms[56]. The current strategy highlights the exploration of AIEE conjugated polyelectrolytes to directly detect HAS/BSA with a 'ratiometric turn-on' response.

4.3.6 Real sample Analysis:

The excellent specific sensitivity of PFAN directed us to examine the practical application of this system in real blood serum samples. A serum sample was collected from the IIT Guwahati Hospital, and the quantitative analysis of HSA was done using a calibration curve and a standard recovery method. The PFAN can successfully recover SAs up to 96% of the spiked HSA from with RSD < 3 % (Table 4.2). Considering the good recovery and low RSD, it could be beneficial for clinical diagnosis of HSA-related health problems.

Table 4.2: **Real sample Analysis data**

Samples	Amount HSA spiked (µg/ml)	Amount HSA found (µg/ml)	Recovery (%)	RSD (%)
S_0	0.00	5.35 ± 0.14	-	2.6
S_1	5	9.98 ± 0.28	96	2.8
S_2	15	20.07 ± 0.46	98	2.2
S_3	30	36.46 ± 0.97	103	2.6

Furthermore, estimating HSA in a point-of-care (PoC) approach is extremely desirable in rural areas and for elderly individuals. As such the fluorescence detection method is miniature into a smartphone-integrated portable device comprising of a dark chamber and a UV lamp (Figure 4.9a). Various samples of PFAN with HSA (0-70 µg/ml) and BSA (0-90 µg/ml) were prepared, and their corresponding fluorescence images were captured under UV- lamp via a smartphone (Figure 4.9b and 4.9d). The RGB values of the captured images were determined by using a color scanning android application (app) called "Color Picker "and a calibration curve with correlation coefficient was obtained from G/R values against the concentration of HSA and BSA (Figure 4.9c and 4.9e). This calibration curve will help find the concentration of HSA and BSA for the rapid diagnosis of SA-associated disorders such as hypoalbuminemia at desired sites.

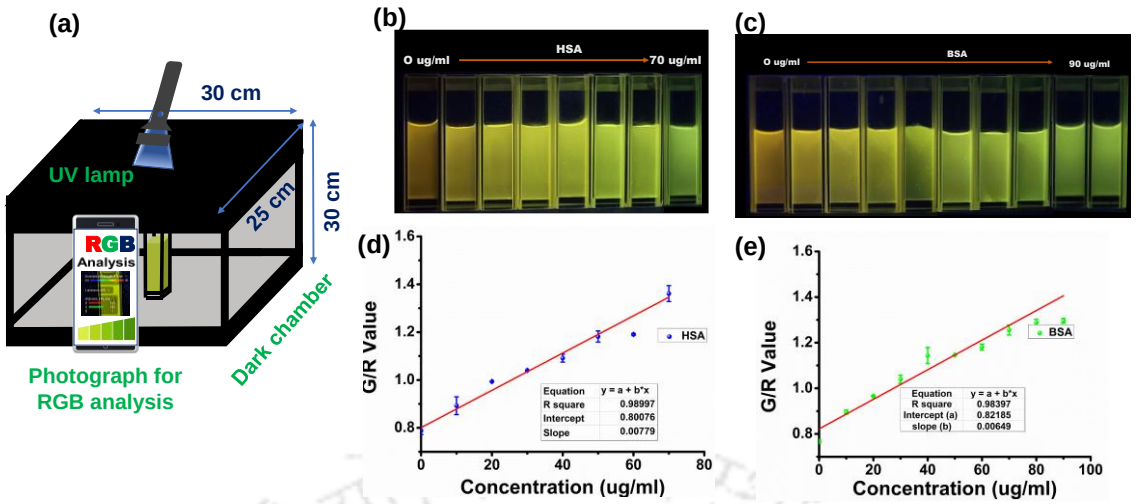

Figure 4.9: (a) Constructed PoC device for onsite HSA and BSA detection; photograph under UV lamp for (b) HSA (0-70 µg/ ml) detection by PFAN (c) G/R value for HSA detection by PFAN (d) BSA (0- 90 µg/ ml) detection by PFAN; (e) G/R value for BSA detection by PFAN.

Furthermore, the sensing performance of PFAN against HSA and BSA was compared with the prior reports (Table A4.4). As per our knowledge this is the first AIEE-CP design for detection of HSA and BSA with excellent LOD. Further, the detection mechanism which leads to "Ratiometric- Turn ON' signal is PFAN-HSA and PFAN_BSA interaction induced aggregation thereby disturbing the D-A charge transfer process and it was supported by theoretical and experimental studies. It also offers rapid onsite detection in a very simple manner with smartphone based PoC device.

4.4 Conclusion

To explore the structure-motion-property relationship of a conjugated molecular, three sets of polymers P1, P2, and P3 were developed by incorporating varying mole fractions of AIE monomer (M4) with electron accepting tendency, thereby controlling molecular motion and charge transfer in solution and aggregated states. The change in molar ratio of M4 in P1, P2, and P3 resulted in a shift in polyfluorene emission from blue to white and yellow, representing the increase in D-A strength from P1 to P3. Furthermore, this developed designed strategy improved the condensed state emission property by transforming ACQ polymer (P1) into AIEE polymer (P3). Finally, the PFAN polymer was derived from the AIEE-P3 by functionalization with 1-methy imidazole as a receptor for monitoring serum albumins (HSA and BSA) that deviate from the healthy range i.e. 35-55g/L. Further, based on the docking and experimental findings, we can conclude that the remarkable sensitivity for human serum albumin (HSA) and bovine serum albumin (BSA) was due to PFAN-HSA and PFAN-BSA binding induced AIEE

mechanism providing a "Ratiometric Turn On" response. The selectivity of PFAN against complex bio environments (such amino acids, biomolecules, enzymes, and proteins), photo-stability and less cytotoxicity offer a good biosensor for quantification of HSA levels in real serum samples with an RSD of less than 3%. As such to benefit the healthcare services, this fluorescence-based detection is miniature into a smartphone-based prototypes testing device for detecting HSA onsite, easily and rapidly. Notably this is the first AIEE conjugated polymeric probe capable of detecting HSA with great selectivity and sensitivity with the proposed mechanism.

References

1. Meher, N.; Iyer, P. K., Spontaneously Self-Assembled Naphthalimide Nanosheets: Aggregation-Induced Emission and Unveiling a-PET for Sensitive Detection of Organic Volatile Contaminants in Water. *Angew. Chem. Int. Ed.* **2018,** *57* (28), 8488-8492.

2. Yuan, Y.; Xu, S.; Cheng, X.; Cai, X.; Liu, B., Bioorthogonal Turn-On Probe Based on Aggregation-Induced Emission Characteristics for Cancer Cell Imaging and Ablation. *Angew. Chem. Int. Ed. Eng.l* **2016,** *55* (22), 6457-61.

3. Ghosh, P.; Shokeen, K.; Mondal, S.; Kandasamy, T.; Kumar, S.; Ghosh, S. S.; Iyer, P. K., Amyloid Targeting Red Emitting AIE Dots for Diagnostic and Therapeutic Application against Alzheimer's Disease. *ACS Chem. Neurosci.* **2024,** *15* (2), 268-277.

4. Li, X.-f.; Zhou, W.; Liu, Y.-c.; Hou, M.; Feng, G.-l.; Ji, Y.-m.; Zhang, Y.; Xing, G.-w., Design and assembly of AIE-active fluorescent organic nanoparticles for anti-counterfeiting fluorescent hydrogels and inks. *Chem. Commun.* **2022,** *58* (82), 11547-11550.

5. Hwang, J.; Nagaraju, P.; Cho, M. J.; Choi, D. H., Aggregation-induced emission luminogens for organic light-emitting diodes with a single-component emitting layer. *Aggregate* **2023,** *4* (1), e199.

6. Luo, J.; Xie, Z.; Lam, J. W. Y.; Cheng, L.; Chen, H.; Qiu, C.; Kwok, H. S.; Zhan, X.; Liu, Y.; Zhu, D.; Tang, B. Z., Aggregation-induced emission of 1-methyl-1,2,3,4,5-pentaphenylsilole. *Chem. Commun.* **2001,** *18*, 1740-1741.

7. An, B.-K.; Kwon, S.-K.; Jung, S.-D.; Park, S. Y., Enhanced Emission and Its Switching in Fluorescent Organic Nanoparticles. *J. Am. Chem. Soc.* **2002,** *124* (48), 14410-14415.

8. Hu, R.; Yang, X.; Qin, A.; Tang, B. Z., AIE polymers in sensing, imaging and theranostic applications. *Mater. Chem. Front.* **2021,** *5* (11), 4073-4088.

9. Wang, K.; Zhang, X.; Zhang, X.; Yang, B.; Li, Z.; Zhang, Q.; Huang, Z.; Wei, Y., Fabrication of cross-linked fluorescent polymer nanoparticles and their cell imaging applications. *J. Mater. Chem. C* **2015,** *3* (8), 1854-1860.

10. Lu, L.; Wang, K.; Wu, H.; Qin, A.; Tang, B. Z., Simultaneously achieving high capacity storage and multilevel anti-counterfeiting using electrochromic and electrofluorochromic dual-functional AIE polymers. *Chem. Sci.* **2021,** *12* (20), 7058-7065.

11. Ban, X.; Zhou, T.; Cao, Q.; Zhang, K.; Tong, Z.; Xu, H.; Zhu, A.; Jiang, W., Combining molecular encapsulation and an AIE strategy to construct an efficient blue TADF polymer for solution-processed multilayer white OLEDs. *J. Mater. Chem. C* **2022,** *10* (40), 15114-15125.

12. Zhan, R.; Pan, Y.; Manghnani, P. N.; Liu, B., AIE Polymers: Synthesis, Properties, and Biological Applications. *Macromol. Biosci.* **2017,** *17* (5), 1600433.

13. Zhang, J.; Xue, F.; Wang, Z., AIE-Active Fluorescent Porous Polymers for Recognizable Detection of Imidacloprid and Structure–Property Relationship. *Chem. Mater.* **2022,** *34* (23), 10701-10710.

14. Zhou, T.; Zhang, K.; Cao, Q.; Xu, H.; Ban, X.; Zhu, P.; Li, Q.; Shi, L.; Ge, F.; Jiang, W., Benzonitrile-based AIE polymer host with a simple synthesis process for high-efficiency solution-processable green and blue TADF organic light emitting diodes. *J. Mater. Chem. C* **2022,** *10* (6), 2109-2120.

15. Tu, D.; Zhang, J.; Zhang, Y.; Sung, H. H. Y.; Liu, L.; Kwok, R. T. K.; Lam, J. W. Y.; Williams, I. D.; Yan, H.; Tang, B. Z., How do molecular motions affect structures and properties at molecule and aggregate levels? *J. Am. Chem. Soc.* **2021,** *143* (30), 11820-11827.

16. Hu, R.; Leung, N. L. C.; Tang, B. Z., AIE macromolecules: syntheses, structures and functionalities. *Chem. Soc. Rev.* **2014,** *43* (13), 4494-4562.

17. Liu, S.; Cheng, Y.; Zhang, H.; Qiu, Z.; Kwok, R. T. K.; Lam, J. W. Y.; Tang, B. Z., In Situ Monitoring of RAFT Polymerization by Tetraphenylethylene-Containing Agents with Aggregation-Induced Emission Characteristics. *Angew. Chem. Int. Ed.* **2018,** *57* (21), 6274-6278.

18. Ravindran, E.; Ananthakrishnan, S. J.; Varathan, E.; Subramanian, V.; Somanathan, N., White light emitting single polymer from aggregation enhanced emission: a strategy through supramolecular assembly. *J. Mater. Chem. C* **2015,** *3* (17), 4359-4371.

19. Gui, S.; Huang, Y.; Hu, F.; Jin, Y.; Zhang, G.; Yan, L.; Zhang, D.; Zhao, R., Fluorescence Turn-On Chemosensor for Highly Selective and Sensitive Detection and Bioimaging of Al3+ in Living Cells Based on Ion-Induced Aggregation. *Anal. Chem.* **2015,** *87* (3), 1470-1474.

20. He, Z.; Liu, P.; Zhang, S.; Yan, J.; Wang, M.; Cai, Z.; Wang, J.; Dong, Y., A Freezing-Induced Turn-On Imaging Modality for Real-Time Monitoring of Cancer Cells in Cryosurgery. *Angew. Chem. Int. Ed.* **2019,** *58* (12), 3834-3837.

21. Yuan, Y.; Zhang, C.-J.; Kwok, R. T. K.; Mao, D.; Tang, B. Z.; Liu, B., Light-up probe based on AIEgens: dual signal turn-on for caspase cascade activation monitoring. *Chem. Sci.* **2017,** *8* (4), 2723-2728.

22. Adil, L. R.; Gopikrishna, P.; Krishnan Iyer, P., Receptor-Free Detection of Picric Acid: A New Structural Approach for Designing Aggregation-Induced Emission Probes. *ACS Appl. Mater. Interfaces* **2018,** *10* (32), 27260-27268.

23. Malik, A. H.; Kalita, A.; Iyer, P. K., Development of Well-Preserved, Substrate-Versatile Latent Fingerprints by Aggregation-Induced Enhanced Emission-Active Conjugated Polyelectrolyte. *ACS Applied Materials & Interfaces* **2017,** *9* (42), 37501-37508.

24. Li, Y.; Liu, S.; Han, T.; Zhang, H.; Chuah, C.; Kwok, R. T. K.; Lam, J. W. Y.; Tang, B. Z., Sparks fly when AIE meets with polymers. *Mater. Chem. Front.* **2019,** *3* (11), 2207-2220.

25. Pu, K.-Y.; Liu, B., Conjugated Polyelectrolytes as Light-Up Macromolecular Probes for Heparin Sensing. *Adv. Funct. Mater.* **2009,** *19* (2), 277-284.

26. Liang, J.; Li, K.; Liu, B., Visual sensing with conjugated polyelectrolytes. *Chem. Sci.* **2013,** *4* (4), 1377-1394.

27. Wan, Y.; Ramirez, F.; Zhang, X.; Nguyen, T.-Q.; Bazan, G. C.; Lu, G., Data driven discovery of conjugated polyelectrolytes for optoelectronic and photocatalytic applications. *npj Comput. Mater.* **2021,** *7* (1), 69.

28. Huang, B.; Wang, K.; Zhang, J.; Yan, H.; Zhao, H.; Han, L.; Han, T.; Tang, B. Z., Targeted and Long-Term Fluorescence Imaging of Plant Cytomembranes Using Main-Chain Charged Polyelectrolytes with Aggregation-Induced Emission. *ACS Appl. Mater. Interfaces* **2024,** *16* (16), 20011-20022.

29. Ghosh, P.; Iyer, P. K., Conjugated Polyelectrolytes: Illuminating the Path to Neurodegenerative Disorders Detection and Treatment. *ACS Appl. Mater. Interfaces* **2024,** *16* (16), 20034-20054.

30. Kahveci, Z.; Vázquez-Guilló, R.; Martínez-Tomé, M. J.; Mallavia, R.; Mateo, C. R., New Red-Emitting Conjugated Polyelectrolyte: Stabilization by Interaction with Biomolecules and Potential Use as Drug Carriers and Bioimaging Probes. *ACS Appl. Mater. Interfaces* **2016,** *8* (3), 1958-1969.

31. Tanwar, A. S.; Chanu, M. A.; Parui, R.; Barman, D.; Im, Y.-H.; Krishnan Iyer, P., Dynamic quenching mechanism based optical detection of carcinogenic Cr(vi) in water and on economical paper test strips via a conjugated polymer. *RSC Appl. Polym.* **2024,** *2* (2), 196-204.

32. Chanu, M. A.; Mondal, S.; Zehra, N.; Tanwar, A. S.; Iyer, P. K., Conjugated Polymer Nanoparticles as a Fluorescence Probe for Amplified Detection of Human Serum Bilirubin. *ACS Appl. Polym. Mater.* **2022,** *4* (5), 3491-3497.

33. Tanwar, A. S.; Khatun, M. N.; Chanu, M. A.; Sarmah, T.; Im, Y.-H.; Iyer, P. K., A water-soluble conjugated polyelectrolyte for selective and sensitive detection of carcinogenic chromium(vi). *Analyst* **2023,** *148* (23), 6011-6019.

34. You, J.; Park, T.; Kim, J.; Heo, J. S.; Kim, H.-S.; Kim, H. O.; Kim, E., Highly Fluorescent Conjugated Polyelectrolyte for Protein Sensing and Cell-Compatible Chemosensing Applications. *ACS Appl. Mater. Interfaces* **2014,** *6* (5), 3305-3311.

35. Tanwar, A. S.; Parui, R.; Garai, R.; Chanu, M. A.; Iyer, P. K., Dual "Static and Dynamic" Fluorescence Quenching Mechanisms Based Detection of TNT via a Cationic Conjugated Polymer. *ACS Meas. Sci. Au* **2022,** *2* (1), 23-30.

36. Wang, Y.; Yao, H.; Zhuang, Z.; Yao, J.; Zhou, J.; Zhao, Z., Photostable and biocompatible AIE-active conjugated polyelectrolytes for efficient heparin detection and specific lysosome labelling. *J. Mater. Chem. B* **2018,** *6* (40), 6360-6364.

37. Hu, R.; Ye, R.; Lam, J. W. Y.; Li, M.; Leung, C. W. T.; Zhong Tang, B., Conjugated Polyelectrolytes with Aggregation-Enhanced Emission Characteristics: Synthesis and their Biological Applications. *Chem. Asian J.* **2013,** *8* (10), 2436-2445.

38. Nicoletti, F. P.; Howes, B. D.; Fittipaldi, M.; Fanali, G.; Fasano, M.; Ascenzi, P.; Smulevich, G., Ibuprofen Induces an Allosteric Conformational Transition in the Heme Complex of Human Serum Albumin with Significant Effects on Heme Ligation. *J. Am. Chem. Soc.* **2008,** *130* (35), 11677-11688.

39. Folsom, A. R.; Ma, J.; Eckfeldt, J. H.; Nieto, F. J.; Metcalf, P. A.; Barnes, R. W.; The Atherosclerosis Risk in Communities Study, I., Low serum albumin: Association with diabetes mellitus and other cardiovascular risk factors but not with prevalent cardiovascular disease or carotid artery intima-media thickness. *Annals of Epidemiology* **1995,** *5* (3), 186-191.

40. Levey, A. S.; Becker, C.; Inker, L. A., Glomerular filtration rate and albuminuria for detection and staging of acute and chronic kidney disease in adults: a systematic review. *Jama* **2015,** *313* (8), 837-846.

41. Bernardi, M.; Maggioli, C.; Zaccherini, G., Human albumin in the management of complications of liver cirrhosis. *Crit. Care* **2012,** *16* (2), 211.

42. Lin, Z.-H.; Chen, I. C.; Chang, H.-T., Detection of human serum albumin through surface-enhanced Raman scattering using gold "pearl necklace" nanomaterials as substrates. *Chem. Commun.* **2011,** *47* (25), 7116-7118.

43. Wang, H.; Wu, Y.; Song, J.-F., Interface potential sensing from adsorption of human serum albumin (HSA) on carbon nanotube (CNT) monitored by zero current potentiometry for HSA determination. *Biosens. Bioelectron.* **2015,** *72*, 225-229.

44. Liang, Z.; Sun, Y.; Zeng, H.; Sun, K.; Yang, R.; Li, Z.; Zhang, K.; Chen, X.; Qu, L., Simultaneous Detection of Human Serum Albumin and Sulfur Dioxide in Living Cells Based on a Catalyzed Michael Addition Reaction. *Anal. Chem.* **2020,** *92* (24), 16130-16137.

45. Huang, Y.; Lv, T.; Qin, T.; Xu, Z.; Wang, L.; Liu, B., A DS2-specific flavonoid-based probe with a unique dual-emissive response to human serum albumin. *Chem. Commun.* **2020,** *56* (75), 11094-11097.

46. Mucha, S. G.; Piksa, M.; Firlej, L.; Krystyniak, A.; Różycka, M. O.; Kazana, W.; Pawlik, K. J.; Samoć, M.; Matczyszyn, K., Non-toxic Polymeric Dots with the Strong Protein-Driven Enhancement of One- and Two-Photon Excited Emission for Sensitive and Non-destructive Albumin Sensing. *ACS Appl. Mater. Interfaces* **2022,** *14* (35), 40200-40213.

47. Chen, J.; Fan, Z.; Zhang, C.; Duan, H.; Fan, L.-J., Amphiphilic Conjugated Polyelectrolyte-Based Sensing System for Visually Observable Detection of Neomycin with High Sensitivity. *ACS Appl. Polym. Mater.* **2021,** *3* (4), 2088-2097.

48. Frisch, M.J.; Trucks, G.W.; Schlegel, H.B.; Scuseria, G.E.; Robb, M.A.; Cheeseman, J.R., Scalmani, G., Barone, V., Mennucci, B., Petersson, G.A., Nakatsuji, H., Caricato, M.; Li, X., Hratchian, H.P.; Izmaylov, A.F.; Bloino, J.; Zheng, G.; Sonnenberg, J.L.; Hada, M., Ehara, M.; Toyota, K.; Fukuda, R.; Hasegawa, J.; Ishida, M., Nakajima, T.; Honda, Y.; Kitao, O.; Nakai, H., Vreven, T.; Montgomery Jr.; J.A.; Peralta, J.E.; Ogliaro, F.; Bearpark, M.; Heyd, J.J.; Brothers, E.; Kudin, K.N.; Staroverov, V.N.; Kobayashi, R.; Normand, J.; Raghavachari, K.; Rendell, A.; Burant, J.C.; Iyengar, S.S.; Tomasi, J.; Cossi, M.; Rega, N.; Millam, J.M.; Klene, M.; Knox, J.E.; Cross, J.B.; Bakken, V.; Adamo, C.; Jaramillo, J.; Gomperts, R.; Stratmann, R.E.; Yazyev, O.; Austin, A.J.; Cammi, R.; Pomelli, C.; Ochterski, J.W.; Martin, R.L.; Morokuma, K.; Zakrzewski, V.G.; Voth, G.A.; Salvador, P.; Dannenberg, J.J.; Dapprich, S., Daniels, A.D.; Farkas, O.; Foresman, J.B.; Ortiz, J.V.; Cioslowski, J. and Fox, D.J. (2010) Gaussian 09, Revision B.01. Gaussian Inc., Wallingford

49. Saikia, G.; Iyer, P. K. Facile C−H Alkylation in Water: Enabling Defect-Free Materials for Optoelectronic Devices. *J. Org. Chem.* **2010**, *75*, 2714-2717.

50. Sanner, M. F., Python: a programming language for software integration and development. *J Mol Graph Model* **1999,** *17* (1), 57-61.

51. Wang, Y.; Yu, H.; Shi, X.; Luo, Z.; Lin, D.; Huang, M., Structural mechanism of ring-opening reaction of glucose by human serum albumin. *J. Biol. Chem.* **2013,** *288* (22), 15980-15987.

52. Majorek, K. A.; Porebski, P. J.; Dayal, A.; Zimmerman, M. D.; Jablonska, K.; Stewart, A. J.; Chruszcz, M.; Minor, W., Structural and immunologic characterization of bovine, horse, and rabbit serum albumins. *Mol. Immunol.* **2012,** *52* (3-4), 174-182.

53. Hussain, S.; Chen, X.; Wang, C.; Hao, Y.; Tian, X.; He, Y.; Li, J.; Shahid, M.; Iyer, P. K.; Gao, R., Aggregation and Binding-Directed FRET Modulation of Conjugated Polymer

Materials for Selective and Point-of-Care Monitoring of Serum Albumins. *Anal. Chem.* **2022,** *94* (30), 10685-10694.

54. Sun, P.; Lu, X.; Fan, Q.; Zhang, Z.; Song, W.; Li, B.; Huang, L.; Peng, J.; Huang, W., Water-soluble iridium (III)-containing conjugated polyelectrolytes with weakened energy transfer properties for multicolor protein sensing applications. *Macromolecules* **2011,** *44* (22), 8763-8770.

53. Campos, L. A.; Sancho, J., The active site of pepsin is formed in the intermediate conformation dominant at mildly acidic pH. *FEBS Lett.* **2003,** *538* (1-3), 89-95.

55. Monni, R.; Al Haddad, A.; van Mourik, F.; Auböck, G.; Chergui, M., Tryptophan-to-heme electron transfer in ferrous myoglobins. *Proc. Natl. Acad. Sci.* **2015,** *112* (18), 5602-5606.

Appendix

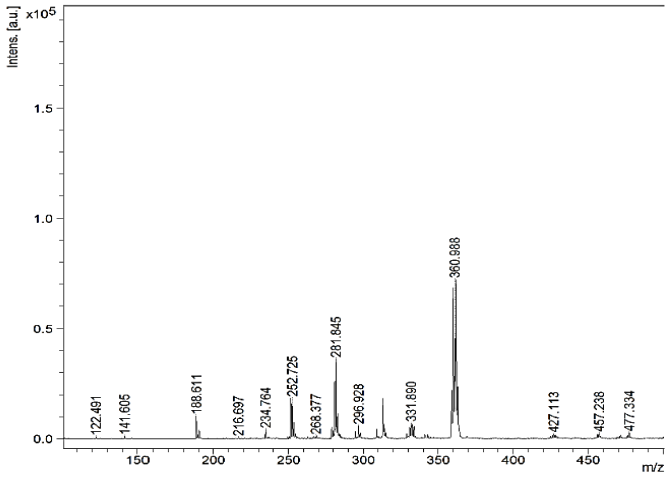

Figure A4.1: Maldi-TOF spectra for monomer M3

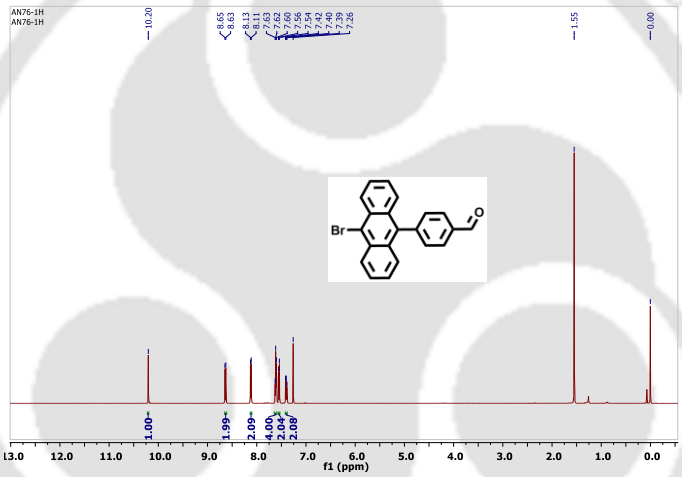

Figure A4.2: ^{1}H NMR spectra of M3 in $CDCl_3$.

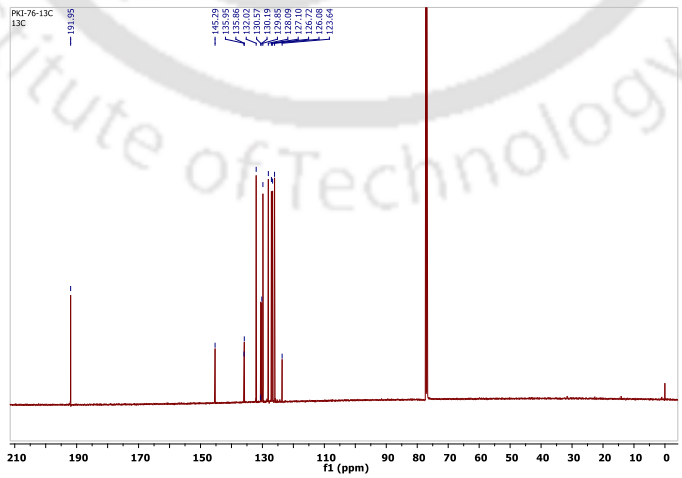

Figure A4.3: ^{13}C NMR spectra of M3 in $CDCl_3$.

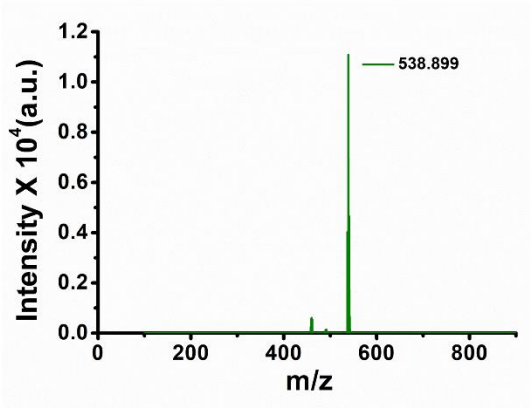

Figure A4.4: Maldi-TOF spectra for monomer M4.

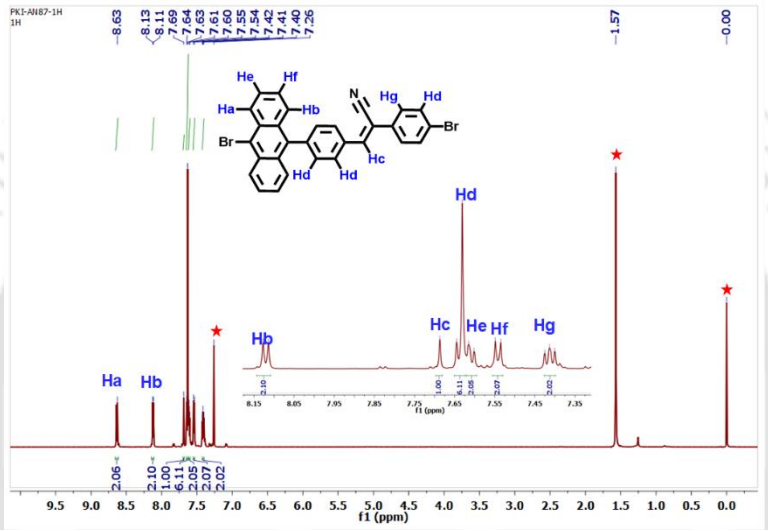

Figure A4.5: ^{1}H NMR spectra of M4 in $CDCl_3$.

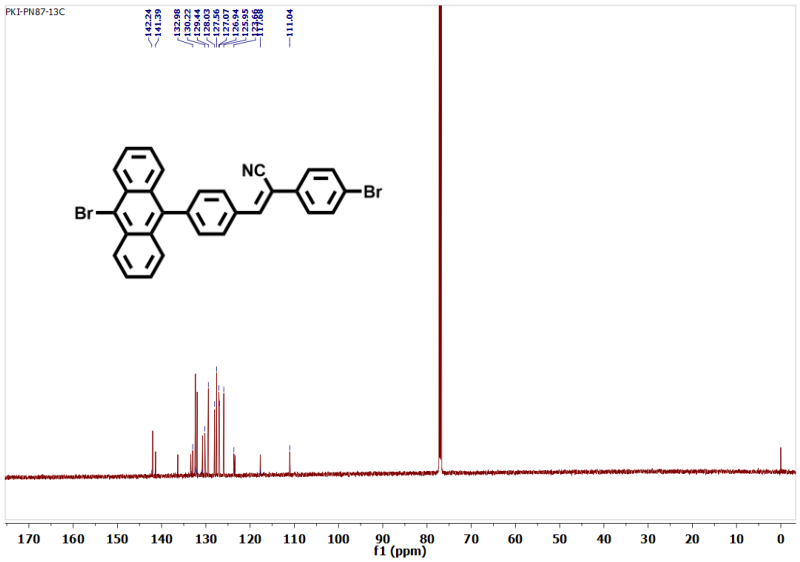

Figure A4.6: ^{13}C NMR spectra of M4 in $CDCl_3$.

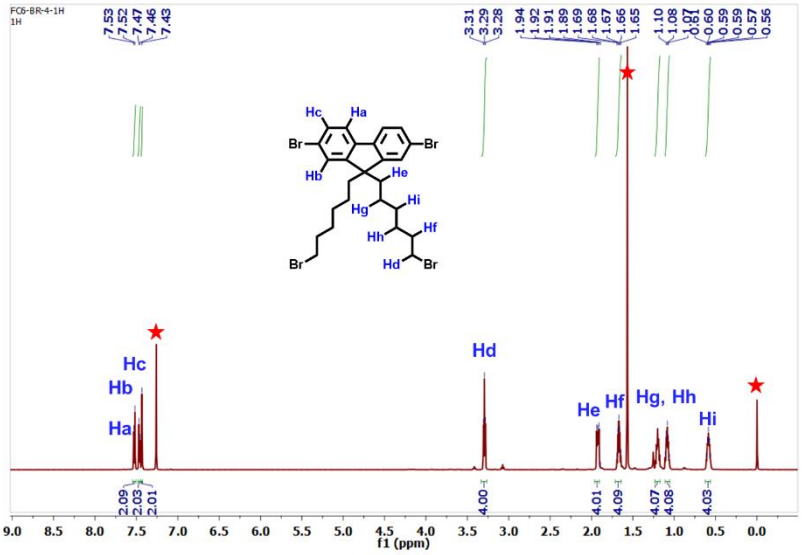

Figure A4.7: ^{1}H NMR spectra of M5 in $CDCl_3$.

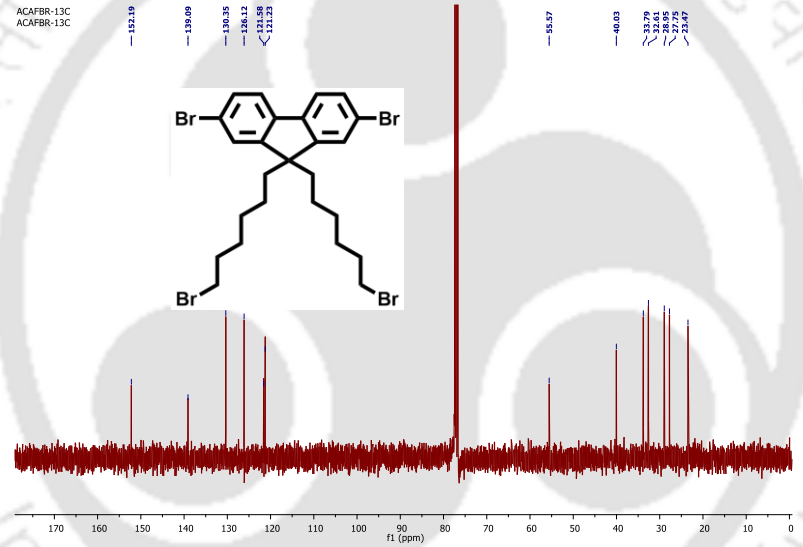

Figure A4.8: ^{13}C NMR spectra of M5 in $CDCl_3$.

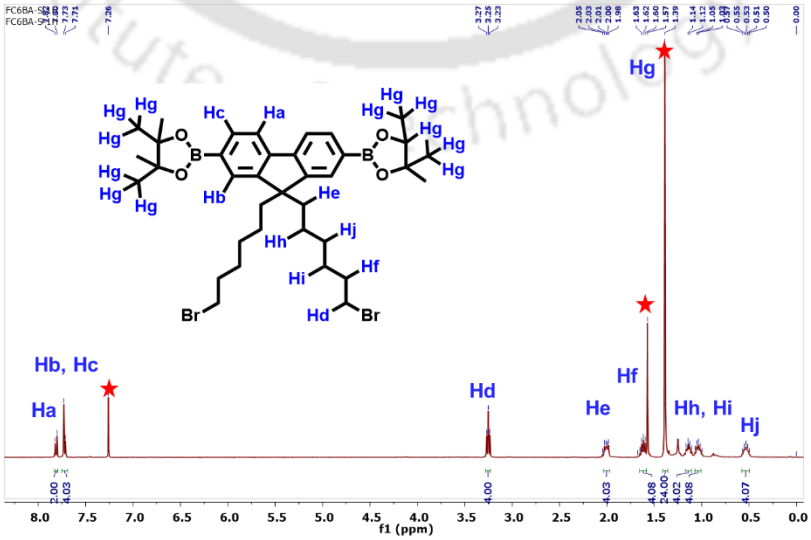

Figure A4.9: ^{1}H NMR spectra of M6 in $CDCl_3$.

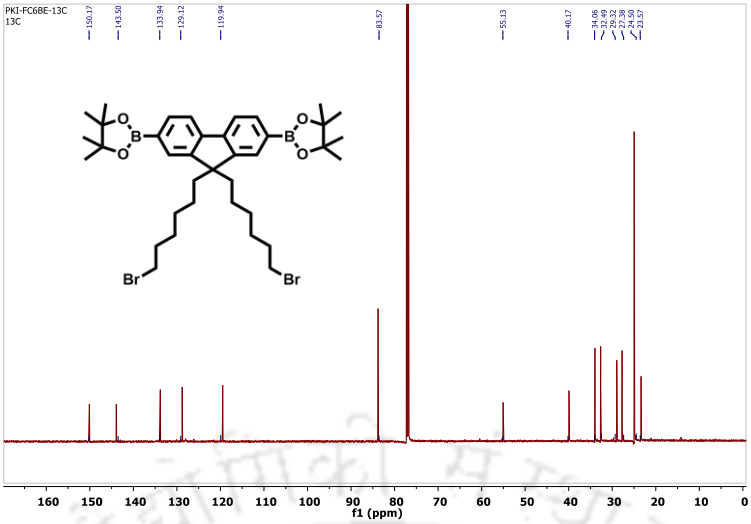

Figure A4.10: ^{13}C NMR spectra of M6 in $CDCl_3$.

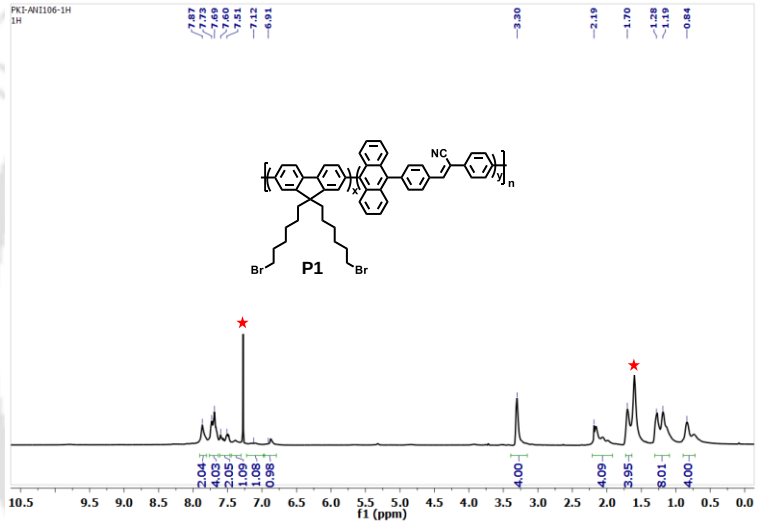

Figure A4.11: ^{1}H NMR spectra of P1 in $CDCl_3$.

GPC Results

	Retention Time (min)	% Area	Mn	Mw	MP	Mz	Mz+1	Poly dispersity
1	8.017	100.00	10422	16688	13313	26099	36791	1.601272

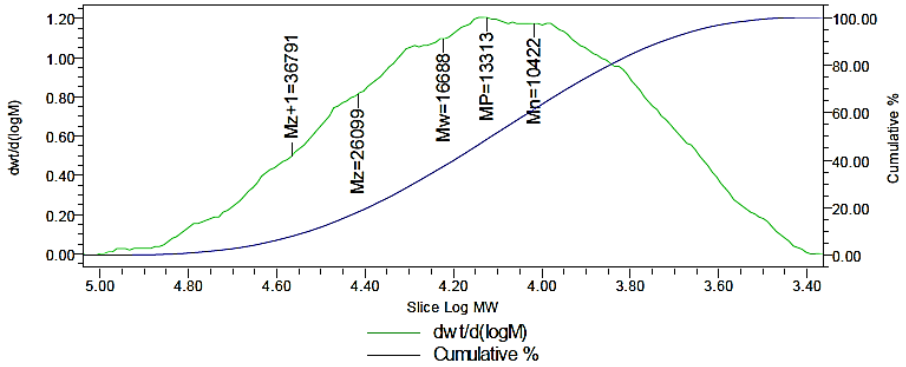

Figure A4.12: GPC chromatogram of polymer P1.

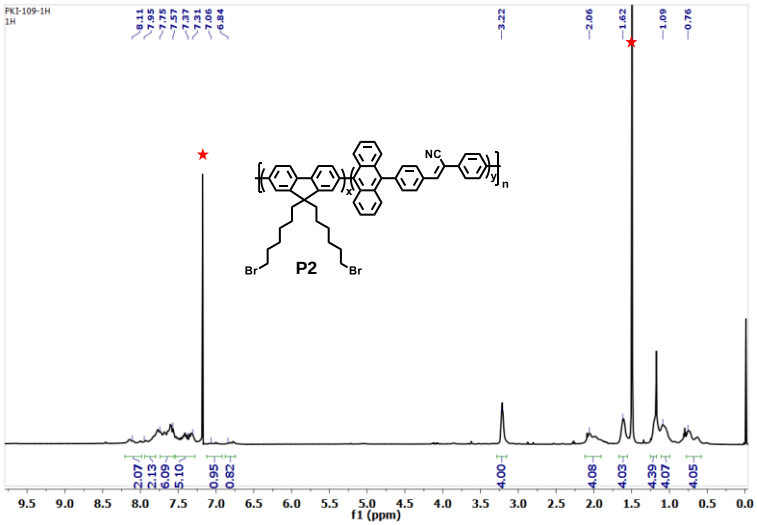

Figure A4.13: ^{1}H NMR spectra of P2 in $CDCl_3$.

GPC Results

	Retention Time (min)	% Area	Mn	Mw	MP	Mz	Mz+1	Polydispersity
1	8.233	100.00	9301	14391	9980	21616	29108	1.547316

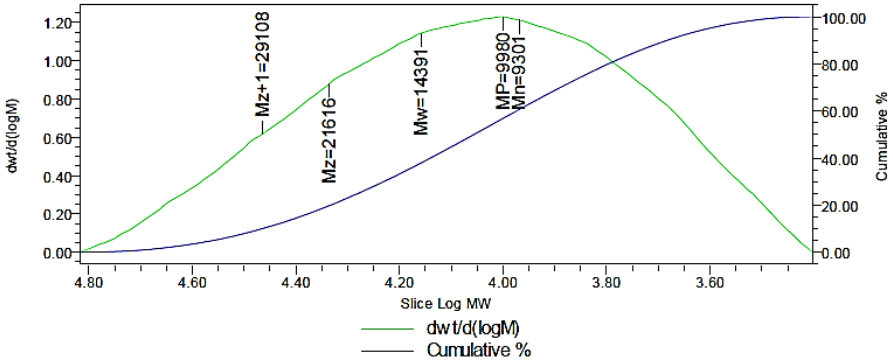

Figure A4.14: GPC chromatogram of polymer P1.

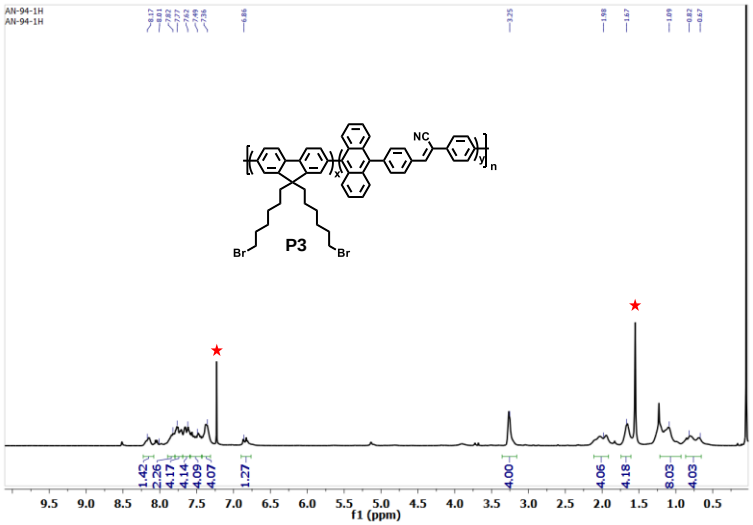

Figure A4.15: ^{1}H NMR spectra of P3 in $CDCl_3$.

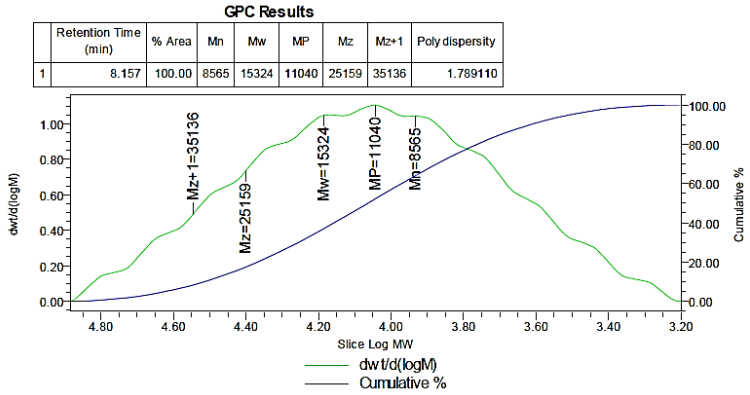

Figure A4.16: GPC chromatogram of polymer P1.

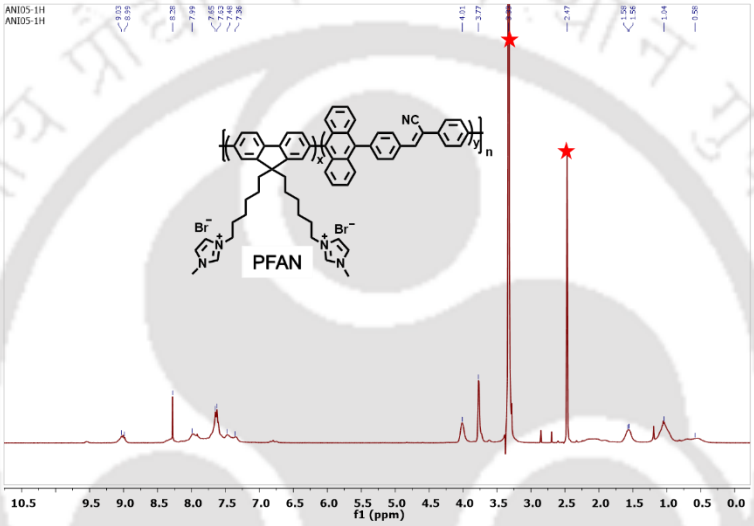

Figure A4.17: ^{1}H NMR spectra of PFAN in DMSO-d6.

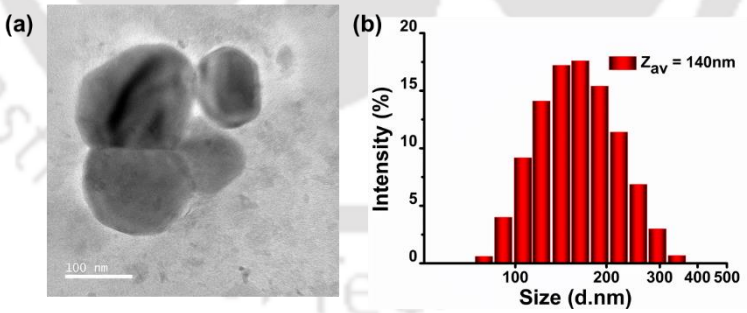

Figure A4.18: TEM images and DLS measurement of M4 monomer.

Table A4.1: The comparison of the solid-state photo-physical properties and quantum yield.

Sample	λ_{ex} (nm)	λ_{em} (nm)	PLQY (%)
P1 (solid)	370	465	6.14
P2 (solid)	370	520	10.75
P3 (solid)	370	500	69.88

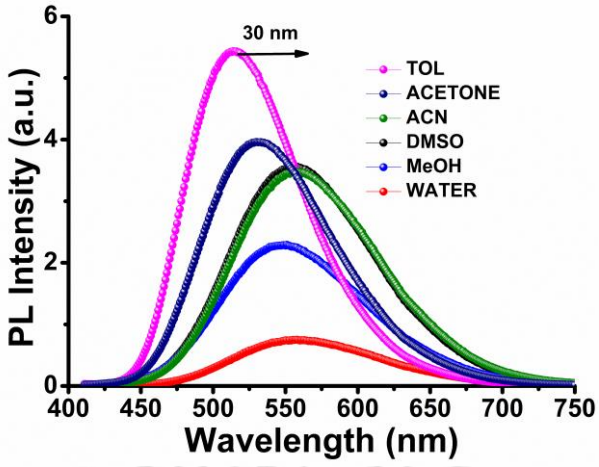

Figure A4.19: Solvent dependent study of PFAN.

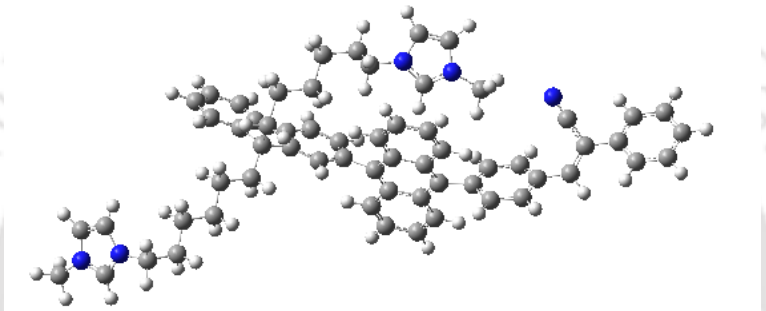

Figure A4.20: Optimized structure of PFAN monomer using B3LYP function 631G (d, p, charge = +2) basis set of Gaussian Program 16.

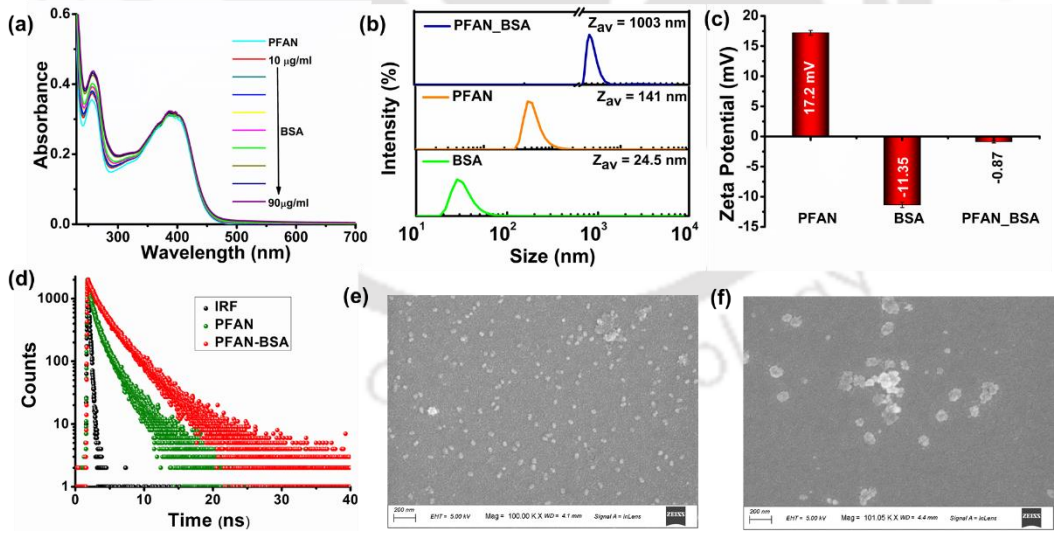

Figure A4.21: Mechanism of BSA detection: (a) UV-Vis spectra of PFAN by addition of BSA; (b) DLS profile of PFAN, BSA and PFAN-BSA; (c) Zeta potential and (d) Lifetime decay profile of PFAN before and after addition of BSA; FESEM images of PFAN (e) before and (f) after addition of BSA.

Table A4.2: Lifetime decay data for PFAN in absence and presence of HSA and BSA with an excitation pulse of 405 nm laser.

Sample	a_1 (%)	τ_1 (ns)	a_2 (%)	τ_2 (ns)	χ^2	τ_{av} (ns)
PFAN	58.714	0.591	41.286	2.504	1.047	1.38
PFAN-HSA	45.331	1.260	54.669	3.799	1.046	2.65
PFAN-BSA	43.991	1.177	56.009	3.691	1.030	2.58

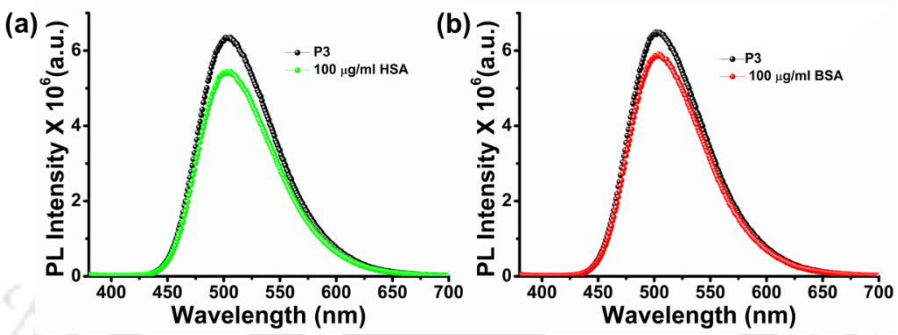

Figure A4.22: PL spectra of P3 in absence and presence of 100 µg/ ml HSA and BSA.

Table A4.3: Isoelectric point (IP) of various proteins and enzymes at pH 7

Proteins	IP (net charge at pH 7)
Cytc	10.5(+)
HRP	9.0(+)
trypsin	10.5(+)
RNase	9.6(+)
pepsin	2.5(−)
Hb	6.8(−)
BSA	4.8(−)
HSA	5.2(−)

Table A4.4: Comparison table of HAS and BSA detection with the reported literature

Publications	Material uesd	Limit of detection (LOD)	Selectivity	Mechanism	PoC Testing
Present work	AIEE conjugated polyelectrolytes	BSA-97ng/mL HSA-46ng/mL	Selective	Molecular binding induced AIEE	Yes
*Anal.Chem.***2022**,*94*,10685−10694	Conjugated polymer surfactant ensembles	BSA 0.50 µg/mL HSA 0.81µg/mL	Selective	Intermolecular Reverse FRET	Yes

ACS Appl. Mater. Interfaces **2017**, *9*, 33461	Conjugated polyelectrolyte-Pt(II) complex	Not Reported	Not Selective	Metal Displacement	No
ACS Appl. Mater. Interfaces **2014**, *6*, 3305	Conjugated polyelectrolyte	Not Reported	Not Selective	De-aggregation	No
Macromolecules **2009**, *42*, 5933	Conjugated polyelectrolytes	Not Reported	Not Selective	Charge Transfer	No
Macromolecules **2008**, *41*, 4003	Conjugated polyelectrolyte	Not Reported	Selective	Interchain FRET	No
Langmuir, **2005,** *21*, 7985	Conjugated polyelectrolyte	Not Reported	Not Selective	Aggregation	No
Angew. Chem. Int. Ed. **2020**, *59*, 3131	Ed. 2020, 59, 3131 2'-hydroxychalcone derivative	HSA 1.08 µg/ml	Selective	De-aggregation	Yes
Anal. Chem. **2017**, *89*, 10085	Small organic nanoprobe	HSA 0.14 µM (9.3 mg L^{-1})	Selective	Disassembly Induced Emission	No
Chem. Commun. **2019**, *55*, 13983	Flavanoid derivative	HSA 2.13 µg/mL	Selective	AIE	No
Chem. Commun. **2018**, *54*, 8383	Styryl derivative	BSA 3.19 µg/mL	Selective	TICT Inhibition	No
Chem. Commun. **2016**, *52*, 6064	2 Dicyanomethylene-3 cyano-4,5,5-trimethyl-2,5-dihydrofuran derivative	SA 2.5 µg/mL	Selective	AIE	No
Sens. Actuators B. **2018**, *255*, 854	Pentaphenylpyrrole derivative	BSA 2.18µg/mL HAS 1.68 µg/mL	Not Reported	AIE	NO
ACS Appl. Mater. Interfaces **2015**, *7*, 26094	Pentaaryl substituted pyrrole	BSA 2.18 µg/mL HAS 1.68 µg/mL	Selective	AIE	No

CHAPTER 5

Switching from Cationic Side Chain into Cationic Backbone in Polyfluorene Polyelectrolytes to Effectively Combat Antibiotic Resistance and Biocompatible Antibacterial Coating

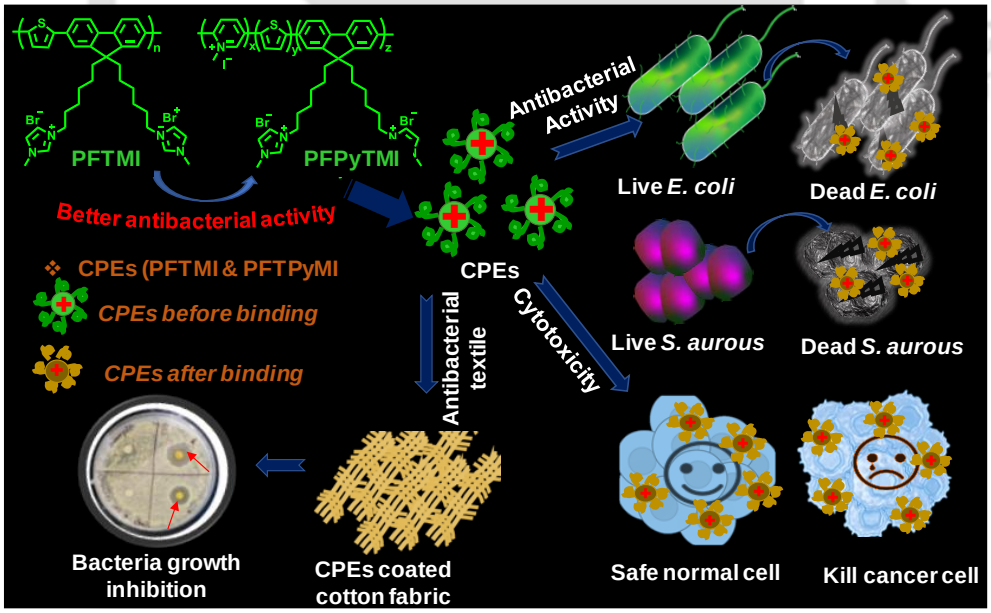

Chanu, M. A.; Kumari, K.; Adil, L. R.; Ramakrishnan, V.; Iyer P. K **(Manuscript Prepared)**

Abstract

The rapid rise of antibiotic resistance poses a severe threat to human health and civilization. To combat this antibiotic-resistant developed by pathogenic bacterial strains, a new and effective bactericidal material is urgently demanded. Here, new cationic conjugated polyelectrolytes (CPEs) PFTMI and PFTPyMI were synthesized, one with exclusively cationic side chain and the other with cationic backbone and cationic side chain respectively. This cationic charge is responsible for effective binding with the bacterial membrane and hence killing by disrupting the membrane without the need of light or energy. PFTPyMI outperforms PFTMI in antibacterial activity, with minimum inhibitory concentrations (MIC) of 1 µg/ml for *Escherichia coli* (*E. coli)* and 4 µg/ml for *Staphylococcus aureus* (*S. aureus)* due to its cationic backbone enhancing the electrostatic attraction and hence killing efficiency. Further the presence of bacteria in aqueous media can be easily detected from the fluorescence color change by using 365 nm portable UV lamp. Remarkably, both CPEs are low cytotoxic to normal HEK293 cell lines and toxic to HeLa cell which open up a new avenue for exploration in real-time biomedical applications. Further CPEs are employed as an anti-coating agent over a cotton pad, and the results were extremely promising and are far better than commercially available antibiotics, such as kanamycin.

Keywords: Antibiotic resistance, antibacterial, conjugated polyelectrolyte, MIC, cytotoxicity, anti-coating, biomedical

5.1 Introduction:

The rapid emergence of antibiotic-resistant bacteria in recent years, posing a significant global concern due to failure of antibiotics treatment in various infections caused by different bacterial strains.[1, 2] The results of a recent study showed that 70 % of normal strains of *E. Coli* which is responsible for pneumonia, bacteremia, and abdominal infections are almost become antibiotics resistant within just three hours of exposure to antibiotics.[3] As per the most recent survey conducted by the Centers for Disease Control and Prevention (CDCP), antibiotic resistance has led to millions of hospitalizations and death globally every year.[4] By 2050, it is expected that the number of deaths would surpass that of cancer by 10 million yearly.[5] The World Health Organization (WHO) states that antibiotic resistance poses a threat to the environment, food and nutrition security and safety, human and animal health and welfare, economic and social development.[6] To solve the alarming situation of antibiotic resistance, it is urgent to develop simple, cost-effective and efficient antibacterial materials for identifying and killing the pathogenic bacteria. Researchers worldwide have been striving to develop new efficient antibacterial materials based on peptides, polyelectrolytes, hydrogels, organic and inorganic nanomaterials to tackle bacterial infections and epidemic diseases.[4, 6-12] Considerable attention has been given on development of cationic materials capable of detecting and disrupting the bacterial membrane, resulting in bacterial ablation.[8, 13]

Fluorescence conjugated polyelectrolytes (CPEs) on account of is biocompatibility, high fluorescence quantum yield and cost effectiveness represents a promising material in various multidisciplinary research such as material, biomedical and optoelectronics.[14, 15] The inherent signal amplification property of conjugated polyelectrolytes makes a superior candidate for sensing, imaging and therapeutic applications.[16-18] Recently, they have been reported to be an attractive antibacterial agent that function in both dark and light activated conditions.[19, 20] Considering the importance of positive charge, various CPEs are developed by integrating imidazolium ion, pyridinium ion or quaternary ammonium salts at their side chains or by making co-assembly with the cationic surfactants.[19, 21, 22] The role of various chain lengths was also explored in poly(phenylene ethynylene)-based CPEs, where the polymer with the shortest chain (n = 7) killed bacteria most effectively due to its most efficient membrane disruption capabilities.[18] However, less attention has been paid in developing the cationic backbone in conjugated polyelectrolytes, especially the pyridinium ion at the backbone of CPEs and its comparative study with the cationic side group for the antibacterial activity. The conjugated

backbone of polymers is the direct signaling unit, which is expected to boost the electrostatic interaction with the negatively charge bacterial membrane and hence the antibacterial activity. Cationic CPEs target and disintegrate bacterial cell membranes through electrostatic attraction and penetrates into the lipid membrane. This causes physical damage to the bacterial cell membrane and makes it difficult to repair, inhibiting the development of bacterial resistance. Besides killing, supramolecular approach on CPEs has achieved astonishing results such as bacterial detection and discrimination.[23] However recognition of bacteria based on emission intensity at a single wavelength might be affected by autofluorescence, instrument variation, and environmental manipulations. In this regard, the development of CPEs that changes ratiometrically on interaction with bacteria opens up a new possibility for real-time detection of bacteria in aqueous conditions with high sensitivity and minimal background signal.

Antibacterial coating on fabrics or surfaces becomes vital because aerosols containing bacteria produced by regular human actions such as speaking, sneezing and coughing, can transmit respiratory infectious diseases. The pathogenic aerosols spread randomly, infecting vulnerable populations.[24] As such the used of anti-bacterial coating on fabric will ensure personal protection. The important condition required for the antibacterial coating material is that it must be biocompatible and water-insoluble for reusability. Many such materials such as organic and inorganic small molecules, in hydrogels, polymers are proven successful for this application recently.[6, 8, 25] However, there is still a need for enhancement in terms of efficacy without light activation, biocompatibility, and real-time usability. There is also a need to assess their action in comparison to commercially available antibiotics.

Herein, to address the above challenges, two polyfluorene based conjugated polyelectrolytes, one with exclusively cationic side groups (PFTMI) and the other with both backbone and cationic side groups (PFTPyMI), were synthesized. Furthermore, the antibacterial activities of both CPEs were examined, where the cationic charge successfully binds with the negatively charged bacteria, disintegrating its membrane, and relatively more significant in PFTPyMI-CPE. The small nanoparticle size of both CPEs enables easy penetration into the bacterial membrane and hence increased their activity. The photophysical properties of CPEs which are susceptible to change in solvent microenvironment helps to identify bacteria in aqueous media with a fluorescence color change, which quite significant. Remarkably, both CPEs shows low cytotoxicity in normal cells while toxic to cancer cells, making them ideal for use in real-time biomedical applications. Considering the necessity for antibacterial fabric in the present day, a

preliminary study using petri dish method was conducted on cotton pad, the most often used fabric. The results were highly positive and are more promising than commercially available antibiotics like kanamycin.

5.2 Experimental Section

5.2.1 Materials and Methods: All the reagents and chemical used in the study were procured from Sigma Aldrich. Human Embryonic Kidney (HEK) 293 cell line and HeLa cell line was purchased from NCCS Pune. Milli-Q water has been used for the preparation of the stock solution for all the experiments. Recording of ^{1}H NMR (600 MHz) and ^{13}C NMR (150 MHz) spectra was performed on the Varian-AS400 NMR spectrometer. For recording UV-Visible absorption spectra and photoluminescence spectra, Cary 60 UV-Vis Spectrophotometer and Horiba Fluoromax-4 spectrofluorometers have been used with 1 ml quartz cuvettes (path length =1 cm, slit = 3 nm). FESEM images were obtained from the Zeiss Sigma Field Emission Scanning Electron Microscope (FESEM). Lifetime and quantum measurement were done in Edinburgh FLS1000 Photoluminescence Spectrometer Dynamic light scattering and Zeta potential measurements were done DLS spectrometer Malvern Nano ZS90. DFT study is perform for polymer was done in Gaussian16.

5.2.2 Synthetic procedure

5.2.2(a). 2,5-dibromo-1-methylpyridin-1-ium (C1Py): 2,5-dibromopyridine (500 mg) in 10 ml acetonitrile were taken in 50 ml round bottom (RB) flask fitted with water condenser. The mixture was stirred continuously at 60 ^{o}C. Then injection of 100 µL methyl iodide solution into the reaction mixture resulted into the precipitation of product. The injection of methyl iodide was continued for 6 h until all the 2,5-dibromopyridine gets converted into the product which was monitored by TLC. Finally, the precipitate was washed repeatedly with diethyl ether until a pure product dirty white ppt. (C1Py) is obtained.

LC_QTOF_HRMS: The mass of monomer C1Py (m/z = 251.8841)

^{1}HNMR (500 MHz DMSO, δ ppm): 9.63 (s, 1H), 8.54 (d, *J* = 8.6 Hz, 1H), 8.39 (d, *J* = 8.5 Hz, 1H), 4.33 (s, 3H).

^{13}C NMR (125 MHz, DMSO-d6, δ ppm): 149.81, 146.26, 141.03, 121.59, 121.26, 55.30

5.2.2(b). 2,7-dibromo-9,9-bis(6-bromohexyl)-9H-fluorene (FC6Br4): The starting material 2,7 dibromo fluorene (1g, 3.106 mmol), and tetra butyl ammonium iodide (TBAI) (0.229 g, 0.621 mmol) were taken in a clean RB flask and made inert condition by applying free-thaw

and degassing technique (3 times). After that, 1,6-dibromohexane (2.82 ml, 18.636 mmol) followed by 50 % NaOH were injected cautiously through a syringe, maintaining the inert condition. Finally, the reaction was performed at 80 °C with proper stirring for 5h. TLC in hexane was used to monitor reaction completion, then separated the organic part from water in a separating funnel with water/chloroform mixture. The excess 1,6-dibromohexane from the recovered organic layer dried by Kugelrohr and further purification was done by column chromatography with hexane as eluent to obtain the final product as white crystalline solid. (Yield = 95 %, 1.92 g)

^{1}H NMR (600 MHz, $CDCl_3$, δ ppm): 7.52 (d, J = 8.0 Hz, 1H), 7.46 (d, J = 8.1 Hz, 1H), 7.43 (s, 1H), 3.29 (t, J = 6.8 Hz, 2H), 1.96 – 1.91 (m, 2H), 1.71 – 1.64 (m, 2H), 1.20 (dt, J = 15.2, 7.7 Hz, 2H), 1.11 – 1.06 (m, 2H), 0.62 – 0.56 (m, 2H).

^{13}C NMR (150 MHz, $CDCl_3$, δ (ppm): 152.20, 139.16, 130.48, 125.82, 121.57, 121.47, 55.73, 40.26, 34.01, 32.36, 28.81, 27.46, 23.43.

5.4.2.2(c). 3,3'-((2,7-dibromo-9H-fluorene-9,9-diyl)bis(hexane-6,1-diyl))bis(1-methyl-1H-imidazol-3-ium) (FMI): 1 g of FC6Br4 was mixed with 1ml DMF and 1ml of methyl iodide solution in a clean round bottom flask. The reaction mixture was heated at 80 ^{o}C with continuous stirring for 24 h. After that, the solvent was dried and precipitated in diethyl ether to produce a white amorphous powder as final product (FMI). (1.2g, 97 %)

LC_QTOF_HRMS: The mass of monomer FMI (m/z = 327.082)

^{1}HNMR (600MHzDMSO, δ ppm): 9.01 (s, 2H), 7.80 (d, J = 8.1 Hz, 2H), 7.66 (ddd, J = 9.4, 8.4, 1.7 Hz, 6H), 7.53 (dd, J = 8.1, 1.8 Hz, 2H), 4.05 (t, J = 7.1 Hz, 4H), 3.80 (s, 6H), 1.99 (m, 4H), 1.53 (dt, J = 14.6, 7.2 Hz, 4H), 1.02 – 0.95 (m, 8H), 0.41(m, 4H).

^{13}C NMR (100MHz, CDCl3, δ ppm): 152.52, 139.19, 136.79, 130.97, 126.60, 124.21, 123.01, 121.33, 55.84, 49.31, 35.98, 29.71, 29.02, 25.64, 23.68

5.2.2(d). Synthesis of polymer PFTMI CPEs: PFTMI was synthesised by Stille coupling polymerization reaction. The precursor monomers 2,5-bis(trimethylstannyl)thiophene (100 mg, 0.244 mmoles) and FMI (160 mg, 0.244 mmoles) were taken in a were taken in a Schlenk tube fitted with a condenser along with argon inlet. Then the mixture is made inert by degassing and purging with Argon. Thereafter, 5 mg of catalyst $Pd(PPh_3)_4$ was added in inert condition. A mixture of DMF/Toluene (1:3) were added into the reaction mixture and stirred at 110 °C for 30 h maintaining the inert condition. After 30 h, the reaction is cool down and solvent was dried under vacuum. The crude CPE was further purified by repeated precipitation in ether and acetone. (color reddish brown, 135 mg, Yield 85 %).

5.2.2(e). Synthesis of polymer PFTPyMI CPEs: PFTPyMI was also synthesised by Stille coupling polymerization reaction. The precursor monomers 2,5-

bis(trimethylstannyl)thiophene (100 mg, 0.244 mmoles), FMI (80 mg, 0.122 mmoles) and C1Py (30 mg, 0.122 mmoles) were taken in a were taken in a Schlenk tube fitted with a condenser along with argon inlet. Then the mixture is made inert by degassing and purging with Argon. Thereafter, 5 mg of catalyst $Pd(PPh_3)_4$ was added in inert condition. A mixture of DMF/Toluene (1:3) were added into the reaction mixture and stirred at 110 °C for 30 h maintaining the inert condition. After 30 h, the reaction is cool down and solvent was dried under vacuum. The crude CPE was further purified by repeated precipitation in ether and acetone. (color reddish brown, 173 mg, Yield 82 %).

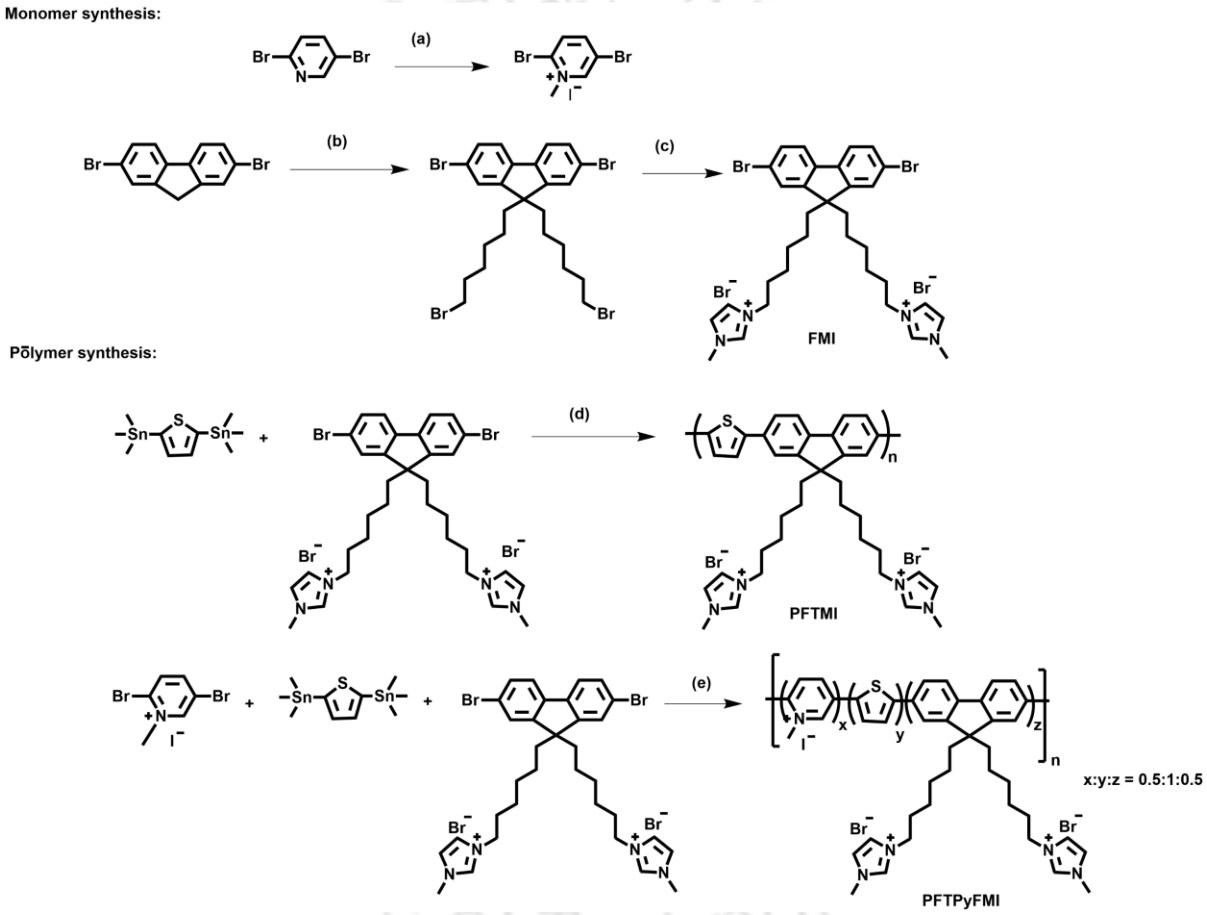

Scheme 5.1: Synthetic pathways of monomers and polymers: (a) Iodomethane, reflux; 6h (b) dibromohexane, 50 % NaOH, TBAI; (c) 1-methyl imidazole, DMF, reflux, 24h.; (d), (f) tetrakistriphenylphosphine palladium (0), 2 M K_2CO_3 (aq), toluene/ DMF, 110 ^oC, 30h.

5.2.3. Photoluminescence Quantum Yield (ϕ): The absolute quantum yield for PFTMI and PFTPyMI were determined by using Edinburgh FLS 1000 instrument through integrated sphere technique.

5.2.4. Antibacterial Activity: The antibacterial activity of polymeric compounds was evaluated with Gram-positive (*Staphylococcus aureus*, strain MTCC 96) and Gram-negative

(*Escherichia coli*, strain K12) bacteria. The stock of bacterial solution was streaked on an agar plate and incubated at 37 °C overnight. A single colony was added to fresh Nutrient Broth media (N.B. media) and incubated at 37 °C overnight. 10 µL of the grown culture was added to the working solution of bacterial cells so that it could be used for the assay in its log phase. The optical density of the culture was diluted to 0.1 a.u. Hence, the bacterial stock solution contained 10^8 CFU/mL. 100 µL of this bacterial solution was added to the 96-well plate, and serial dilutions of the polymer were prepared (range: 1-128 µg/mL) as reported earlier and incubated at 37 °C for 24 hours. Readings were recorded at 600 nm by using a microplate reader (i-Mark BIO-RAD).

5.2.4. Membrane Disruption Analysis by FESEM and FETEM: The bacterial culture of both *Staphylococcus aureus* and *Escherichia coli* bacteria of mid-log phase cells (10^8 CFU/mL) were treated with the polymers and incubated at 37 °C. After incubation, cells were centrifuged at 5000×g for 5 minutes. The pellets were treated with 2.5 % glutaraldehyde and incubated at 4°C for 3 hours. Further, bacterial suspension was centrifuged again at 5000×g for minutes. Bacterial cells were washed twice with phosphate buffer (pH 7.4) and loaded on a glass coverslip and carbon-coated 200-mesh copper grids. The loaded samples were washed with deionized water and ethanol (30–100%). The samples on glass coverslip were air-dried, sputter-coated with gold, and analyzed using FESEM (Zeiss, Sigma 300) at an accelerating voltage of 3 kV. The sample dried on a Cu grid was analyzed by performing imaging with FETEM (Joel, JSM-2100 LaB6).

5.2.6. Cell Culture: Human Embryonic Kidney (HEK) 293 cell line and HeLa cell line was purchased from NCCS Pune and was maintained in Dulbecco's Modified Eagle Media (DMEM) supplemented with 10 % fetal bovine serum (FBS), 1 % antibiotic cocktail (10,000 units/mL penicillin and 10 mg/mL streptomycin and 25 µg/mL Amphotericin B) at 37 °C in a humidified incubator with 5 % CO_2.

5.2.7. Cell Viability Assay: MTT assay was performed to evaluate the cytotoxicity of the polymer PFTMI and PFTPyMI using HEK 293 cell. Both cells were seeded into a 96-well plate at the density of 10,000 cells/well and incubated for 24 h. Cells were washed with 1X PBS and followed by the treatment of series of different concentration of polymer PFAN at 0, 10, 20, 30, 40, 50, 60, 50, 60, 70, 80, 90 and 100 µg/ml for 24 h at 37 °C in incubator. Cells were washed with 1X PBS on incubation of 24 h. 10 µL of MTT of stock concentration and 90 µL DMEM medium was added to each well and incubated for 4 hours at 37 °C in incubator. After

incubation of 4 h, 75 µL of medium was removed and 50 µL of DMSO was added to each well followed by further incubation of 10 minutes. The multimode microplate reader (Thermofisher Varioskan LUX) was used to record absorbance at wavelength of 490 nm. All the experiments were carried out in triplicate.

5.2.8. Calcien Assay: To perform calcein assay, both HEK 293 and HeLa cells were seeded into well at the density of 10,000 /well and incubated for 24 h. Cells were washed with 1X PBS and followed by the treatment with 100 µg/mL of polymer PFTMI and PFTPyMI and incubated for 24 h. The working solution of calcein dye (1 µM) was prepared in serum free DMEM medium by using the stock solution (1 mM). 100 µL of calcein dye was added to the cells on incubation of 24 h, and further incubated for half an hour. Cells were then washed with 1X PBS and imaging was done by inverted fluorescence microscope (Nikon TS2R-FL).

5.2.8. Disc Diffusion Assay: The bacterial culture of both *Staphylococcus aureus* and *Escherichia coli* bacteria of mid-log phase cells (10^8 CFU/mL) were spread on the agar plate. This experiment was performed in duplicate. Four sterile cotton pads were used for each plate. 100 µg/mL of polymer PFTMI and PFTPyMI were added to the cotton pads over the disc. A standard commercial antibiotic, Kanamycin (100 µM), was used as a positive control, and only NB media was used as a negative control. These plates were incubated at 37 °C for 24 hours and examined for the inhibition zone. This test was repeated three times.

5.3. Results and Discussion:

The monomers C1Py was synthesized by simple methylation reaction of precursor molecules 2,5-dibromopyridine and FMI was synthesized by functionalization of FC6BR4 with 1-methyl imidazole respectively (Scheme 5.1). Then the conjugated polyelectrolytes (CPEs) PFTMI and PFTPyMI were synthesized by Stille coupling polymerization reaction with 80-85 % yield. The synthesized monomers were well purified at each step and characterized by NMR and mass before using in further studies and also the polymers were well characterized by NMR and FTIR (Figures A5.1-A5.11). Also, both PFTMI and PFTPyMI are quite thermostable up to 300 ^{o}C (Figure A5.12).

5.3.1. Photophysical and Morphological Studies of Synthesized Polymers:

The photophysical properties of both PFTMI and PFTPyMI were performed in aqueous medium. Both the CPEs show absorption maxima (λ_{max}) at 400 nm with emission at 505 nm

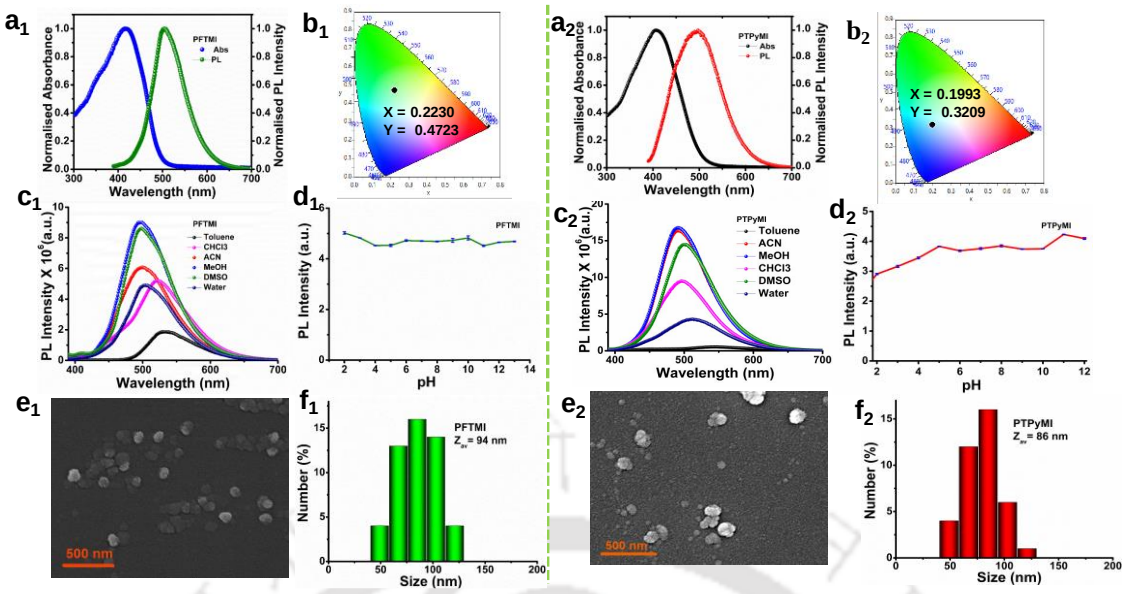

Figure 5.1: (a_1), (a_2) Normalised absorption and emission spectra of PFTMI and PFTPyMI; (b_1), (b_2) CIE co-ordiates of emission spectra of PFTMI and PFTPyMI; (c_1), (c_2) Lifetime decay spectra of PFTMI and PFTPyMI; (d_1), (d_2) pH stability (pH 2-14) for PFTMI and PFTPyMI; (e_1), (e_2) FETEM images PFTMI and PFTPyMI; and (f_1), (f_2) DLS profile of PFTMI and PFTPyMI respectively.

for PFTMI and 496 nm for PFTPyMI (Figure 5.1a_1, 5.1a_2). The CIE- co-ordinates for their respective emission are provided in Figure 5.1b_1, 5.1b_2. PFTPyMI being more hydrophllic, it has better quantum yield (78.31 %) than PFTMI (60.91 %) in aqueous medium. The lifetime of the excited state was also recorded, the polymer PFTMI has an average lifetime of 0.94 ns and PFTPyMI has 1.24 ns (Figure 5.1c_1, 5.1c_2 and Table A5.1). The complete photophysical data are provided in Table A5.2. The CPEs aqueous state emission is stable at wide pH range (pH5-pH10) (Figure 5.1d_1, 5.1d_2). FESEM analysis reveals that both CPEs self-assemble into a spherical nanoaggregate with average size 96 nm for PFTMI and 94 nm for PFTPyMI (Figure 5.1e_1, 5.1e_2). The self-assembly process of CPEs were also analyzed in several environments such as various organic solvent and concentration dependence studies. In polar solvents (DMSO, water, MeOH), the PFTMI emit at 510 nm and PFTPyMI at 496 nm but in non-polar solvents (toluene, chloroform), CPEs show redshifted emission (Figure 5.2a. 5.2b). The red shifted emission is because of aggregation and is validated by concentration dependent emission spectra and solid-state emission spectra. The concentration dependent emission spectra of PFTMI and PFTPyMI are interesting because, PFTPyMI exhibits a significant redshift shift (76 nm) in emission with decreased intensity while PFTMI exhibits fluorescence enhancement with a 30 nm redshift with an increase in concentration from 2 µg/mL to 20 µg/mL (Figure 5.2c, 5.2d). Such an unusual phenomenon can be attributed due to different charge density in the backbone of PFTMI and PFTPyMI thereby differing them inter/intra

molecular interaction and self-assembly process. This leads to change in emissive property of CPEs and PFTPyMI is more susceptible to such changes which may be attributed due to its cationic backbone. The aggregation leads to red shifted emission was also supported by solid state emission spectra and its corresponding CIE co-ordinates (Figure A5.13a, A5.13b). Remarkably such an interesting emissive property of CPEs in response to minor change in solvent environment will be beneficial for designing biosensor with ratiometric signals enabling visual detection.

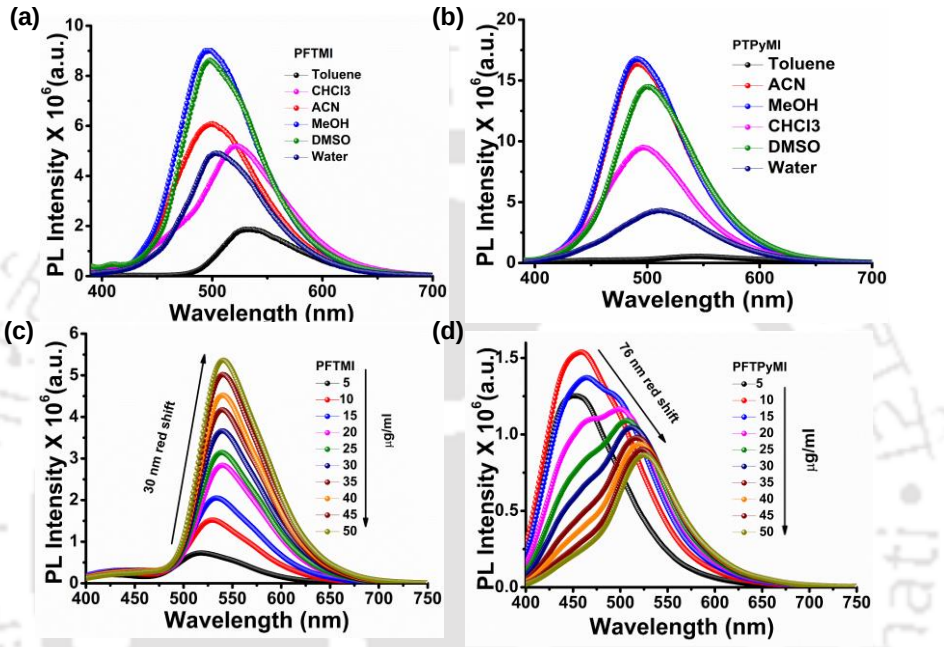

Figure 5.2: (a),(b) Emission spectra of PFTMI and PFTPyMI in various solvents; (c),(d) Concentration dependent spectra of PFTMI and PFTPyMI in dioxane respectively.

Further, theoretical DFT study was also performed to optimize the geometry in a single monomeric unit of CPEs using B3LYP function and 631G (d, p, charge =2/3 for PFTMI/ PFTPyMI) in the Gaussian 16 Program[26] (Figure A5.14). Both the polymer has a planar backbone responsible for good light harvesting property and the side chains are arranged in such a way to restrict π-π restriction thereby giving solid state emission.

4.3.1. Antibacterial Property:

Antibacterial property of PFTMI and PFTPyMI were examined in *Staphylococcus aureus* (S. aureus) and *Escherichia coli* (*E. coli*) to represent Gram positive and Gram-negative bacteria respectively and compared their killing efficacies. Incubation of CPEs (0-128 µg/mL) reduced bacterial live cells by less than 20 % with minimum inhibitory concentration (MIC) of 1µg/mLfor PFTPyMI and 16 µg/mL for PFTMI for *E. coli* (Figure 5.3a). However, in case of

S. aureus, the minimum inhibitory concentration is 4 µg/mL for PFTPyMI and 64 µg/mL for PFTMI (Figure 5. 3b). Since *E. coli* and *S. aureus* have different cellular membrane structures, the CPEs have different binding affinities with their bacterial membrane. Gram-negative bacteria have an extra lipopolysaccharide (LPS) outer membrane in addition to a thin peptidoglycan layer, while Gram-positive bacteria have a thick protective layer of peptidoglycan networks in their cell walls. Gram-negative *E. coli* binds more efficiently to CPEs and has better antibacterial activity due to presence of an extra lipopolysaccharide layer that is negatively charged due to phosphates and carboxylate groups. Further, PFTPyMI due to their cationic backbone may binds even more effective than PFTMI resulting in more killing efficiency.[27]

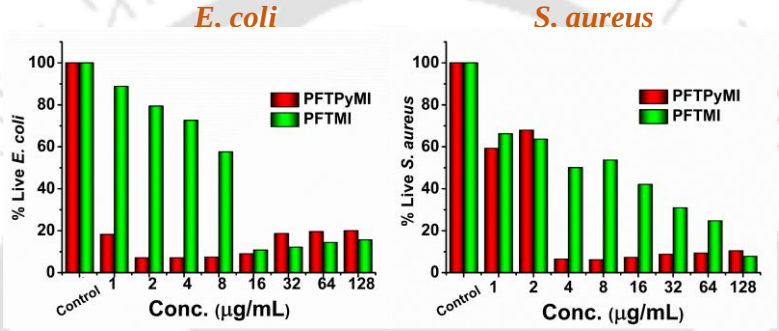

Figure 5.3: Antibacterial assay for both PFTMI and PFTPyMI in (a) E. coli (gram negative) and (b) S. aureus (gram positive) bacteria.

5.3.3. Antibacterial Mechanism:

To understand the antibacterial mechanism, FESEM and FETEM studies were performed for bacteria before and after treatment of CPEs. The control bacteria (*E. coli, S. aureus)* had intact membrane morphology with smooth and obvious regular edges indicating that the bacteria were still alive. However, the treated bacteria showed effective bacterial membrane disruption, which led to the death of the bacteria (Figures 5.4a and 5.4b). Antibacterial activity of imidazolium and pyridinium containing polymers against both Gram (+) and Gram (-) bacteria has been reported earlier.[28-30] Zeta potential measurements were utilized to investigate the binding between CPEs and the bacterial membrane. The average negative zeta potential (ζ_{av}) of *E. coli* (ζ_{av} = -41.5mV) and *S. aureus* (ζ_{av} = -35.3mV) are significantly shifted towards positive zeta potential with the addition of positively charge PFTMI (ζ_{av} = +20.3 mV) and PFTPyMI (ζ_{av} = +24.7mV (Figure 5.4c). *E. coli* binds stronger to CPEs than *S. aureus* due to its higher phosphate group content and more negative ζ-potential and more positive PFTPyMI binds stronger than PFTMI. This binding lead to the disintegration of bacterial membrane

results into death of bacteria. Furthermore, the small nanoparticle size of CPEs allows for easy penetration into the lipid membrane, which facilitates disruption. Interestingly, the CPEs emissive property changes on treatment with bacteria. PFTPyMI (5µg/ml) and PFTMI (5µg/ml) emit cyan and green colors, respectively, but bacteria-treated PFTPyMI and PFTMI emit yellow and orange colors with reduced emission (Figure 5.4d, 5.4e). Notably this visual color change will help to detect bacteria in contaminated water. Further, the reduced emission intensity suggests the utilization of excited energy of CPEs for killing of bacteria through binding. The proposed mechanism is provided in Figure 5.4f. So, PFTPyMI and PFTMI can act as ratiometric bacteria sensor with antibacterial activity from a particular concentration depending on the bacterial strains.

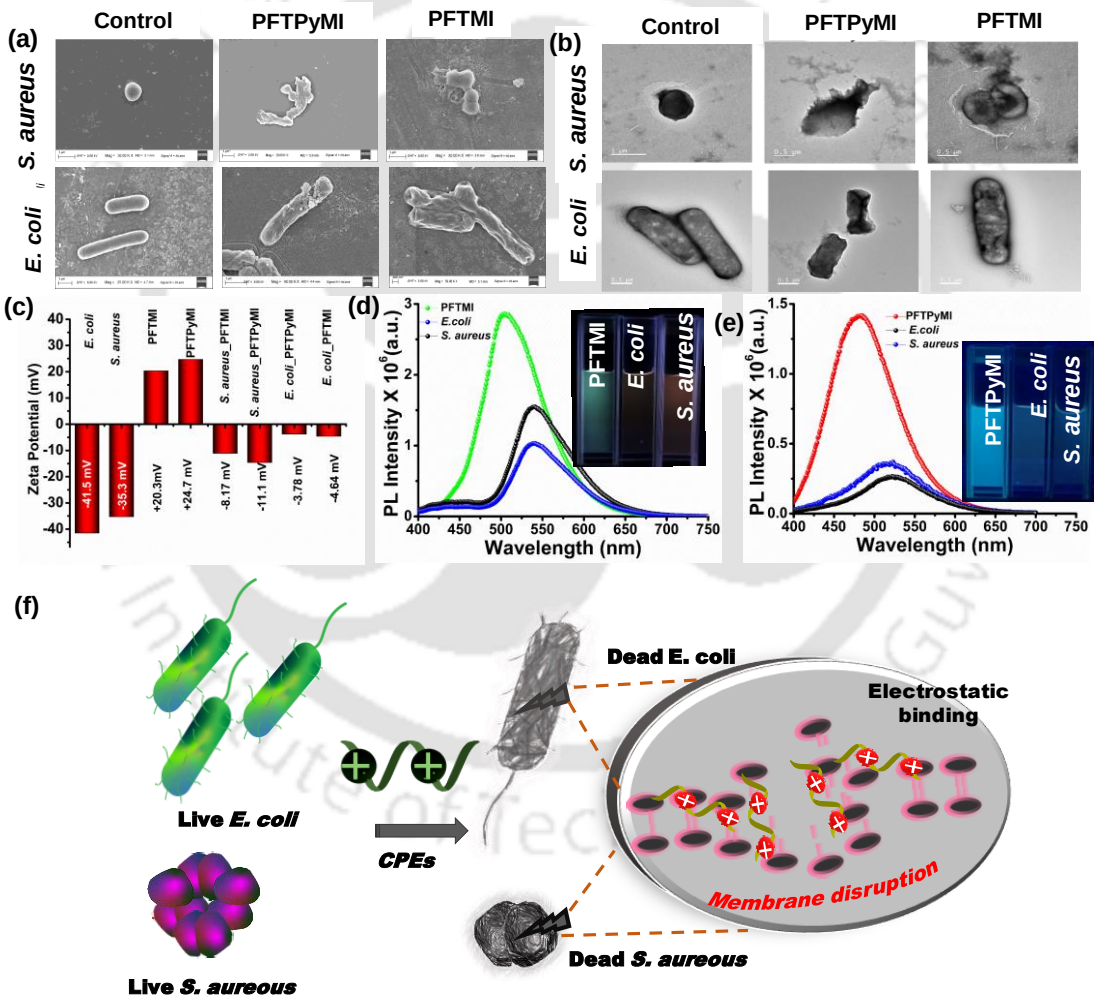

Figure 5.4: (a) FESEM and (b) FETEM images of control bacteria (S. aureus, E. coli), PFTPyMI and PFTMI treated S. aureus and E. coli; (c) Zeta potential plot of E. coli, S. aureus, PFTMI, PFTPyMI CPEs and PFTMI and PFTPyMI treated bacteia; (d) Fluorescence spectra photograph of polymers in absence and presence of bacteria, inset the corresponsing fluorescence image under 365 nm UV lamp; (e) The proposed mechanism for antibacterial action of PFTMI and PFTMI CPEs.

5.3.4. Cytotoxicity Study:

A good antibacterial material should be less cytotoxic towards mammalian cells for practical applicability into biomedical field. The selective killing of bacteria over mammalian cells is gaining attention for use as an antibacterial coating over fabrics or as an additive in paints to make bactericidal surface. As such MTT assay was performed to examine cytotoxicity of both PFTMI and PFTPyMI over HEK 293 (normal) cell and HeLa (cancer) cell. Cell viability for PFTMI and PFTPyMI was above 80 % and 70 % at concentrations up to 100 µg/mL respectively in HEK 293 cell (Figure 5.5a, 5.5b). Notably highly selective killing of bacteria is observed over HEK 293 cells due to differences in surface composition and structure between them. Another attractive result is that PFTMI and PFTPyMI exhibit considerable cytotoxicity towards cancer cell line, Hela cells, showed only 20 % and 10 % viability after treatment (Figure 5.5d, 5.5e). The MTT cytotoxicity results PFTMI and PFTPyMI was also validated by fluorescence live cell imaging with calcein assay. Calcein is a green fluorescence cell permeant dye, used to stain the viable cells. It usually permeates into viable cells through its cell membrane and gets converted into green fluorescent of calcein by the presence of cytosolic esterase enzyme. The viability of cells was determined by the green fluorescence, where more intense green signal represents more viable cells. For this HEK 293 cell and Hela cells were treated with 100 µg/mL PFTMI and PFTPyMI and incubated for 24 hour and fluorescence imaging of the respective cells were performed. In the case of HEK 293 cells, PFTMI and

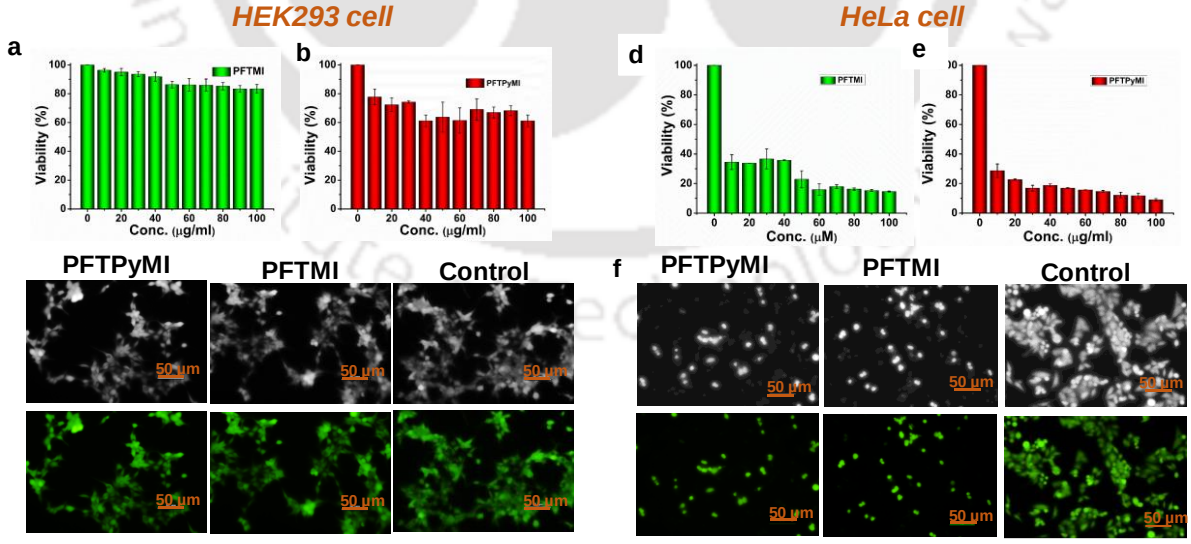

Figure 5.5 (a). (b) Cell viability assay of PFTMI and PFTPyMI in HEK293 cell line (normal cell); (c) Fluorecence Calcien live cell imaging for control HEK293, PFTMI and PFTPyMI treated cell lines; (d). (e) Cell viability assay of PFTMI and PFTPyMI in HeLa cell line(normal cell);(f) Fluorecence Calcien asaay for control Hela cell PFTMI and PFTPyMI treated cell lines.

PFTPyMI treated cells have a comparable amount of fluorescent stain live cells to that of control, indicating that the majority of cells are viable (Figure 5.5c). However, in the case of Hela cells, the number of live cells were significantly reduced, as seen by a decrease in green fluorescence (Figure 5.5f). The stronger cytotoxicity in cancer cells over normal is due to the difference in their membrane potential i.e. cancer cells are negatively-charged and normal cells are either charge-neutral or slightly positive.[31]

5.3.5. Application as an Anti-Coating Material:

The strong antibacterial activity and less cytotoxicity for normal human cell lines of PFTMI and PFTPyMI offer a glimpse of utility to combat pathogenic bacterial infection. As a result, we explored one possible application by coating CPEs to provide antibacterial fabric. For this circular cotton pads were coated with PFTMI (100 µg/mL) and PFTPyMI (100µg/mL) and because the polymers are water insoluble, the coated cotton pad cannot be washed away with water. For the comparative analysis of antibacterial activity, we also coated with commercially available antibiotics i.e. Kanamycin (100 µM) that are used to treat severe bacterial infection. The antibacterial activity of these coated cotton pads against *E. coli* and *S. aureus* were tested using a zone of inhibition dish assay, and to obtain duplicate results, the CPEs coated cotton pads were placed in two locations. Figure 5.6 shows that PFTMI and PFTPyMI have a significant radial area of inhibition around the cotton pads for both *E. coli* and *S. aureus*, but commercially available antibiotics either failed or had very little antibacterial action. The cationic backbone with higher binding affinity of PFTPyMI towards bacteria was the obvious cause of its superior antibacterial activity as compared to PFTMI. For several years, commercial antibiotics such as Kanamycin was once considered a life-saving medication until reports of antibiotic resistance emerged. This observation implies that the antimicrobial

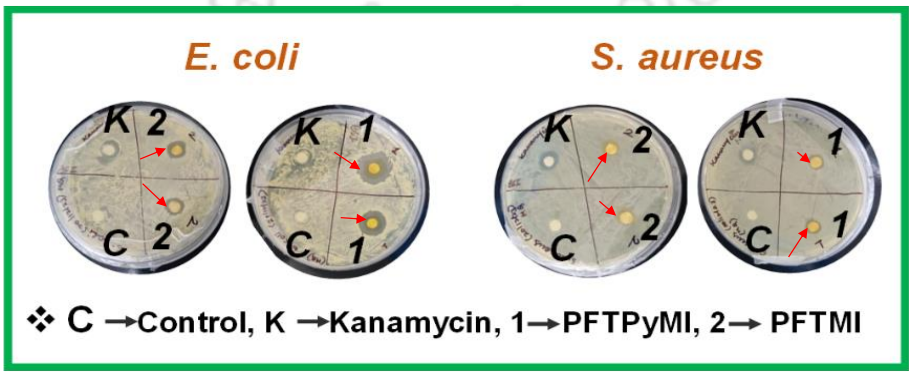

Figure 5.6: Petri dish method bacterial growth inhibition assay for both PFTMI and PFTPyMI in E. coli (gram negative) and S. aureus (gram positive) bacteria.

resistance challenge cannot be solved by using antibiotics alone. In the meantime, recent attention of designing membrane targeting conjugated polyelectrolytes addressed both inherited or non-inherited antibacterial resistance.

5.4. Conclusion:

In we have developed two polyfluorene based conjugated polyelectrolytes PFTMI with only cationic side group and PFTPyMI with cationic backbone and side group. Both CPEs have antibacterial activity, with the positive charge binding to the negatively charged bacterial membrane, causing membrane rupture and hence killing. The disruption of bacterial membrane was clearly visible in FESEM and FETEM images. Comparatively, PFTPyMI shows higher antibacterial activity with MIC 1µg/ml for *E. coli* and 4µg/ml for *S. aureus* which is quite remarkable due to the active participation of both backbone and side groups. Further the presence of bacteria in aqueous media can be detected easy from the fluorescence color change. The less cytotoxic nature in HEK 293 normal cell lines, and toxic towards Hela cell lines offers a new hope for future biomedical applications to combat antibiotic resistance. One such application, it is utilized as an antibacterial coating over a cotton pad to mimic antibacterial fabric and achieved promising results which was less effective or failed by commercially available antibiotics.

References

1. El Haddad, L.; Harb, C. P.; Gebara, M. A.; Stibich, M. A.; Chemaly, R. F., A systematic and critical review of bacteriophage therapy against multidrug-resistant ESKAPE organisms in humans. *Clin. Infec.t Dis.* **2019,** *69* (1), 167-178.

2. Harms, A.; Maisonneuve, E.; Gerdes, K., Mechanisms of bacterial persistence during stress and antibiotic exposure. *Science* **2016,** *354* (6318), aaf4268.

3. Nolivos, S.; Cayron, J.; Dedieu, A.; Page, A.; Delolme, F.; Lesterlin, C., Role of AcrAB-TolC multidrug efflux pump in drug-resistance acquisition by plasmid transfer. *Science* **2019,** *364* (6442), 778-782.

4. Li, X.; Bai, H.; Yang, Y.; Yoon, J.; Wang, S.; Zhang, X., Supramolecular antibacterial materials for combatting antibiotic resistance. *Adv. Mater.* **2019,** *31* (5), 1805092.

5. de Kraker, M. E. A.; Stewardson, A. J.; Harbarth, S., Will 10 million people die a year due to antimicrobial resistance by 2050? *PLoS medicine* **2016,** *13* (11), e1002184.

6. Patel, A.; Goswami, S.; Hazarika, G.; Sivaprakasam, S.; Bhattacharjee, S.; Manna, D., Sulfonium-Cross-Linked Hyaluronic Acid-Based Self-Healing Hydrogel: Stimuli-Responsive Drug Carrier with Inherent Antibacterial Activity to Counteract Antibiotic-Resistant Bacteria. *Adv. Healthcare Mater.* **2024,** *13* (6), 2302790.

7. Li, Q.; Wu, Y.; Lu, H.; Wu, X.; Chen, S.; Song, N.; Yang, Y.-W.; Gao, H., Construction of Supramolecular Nanoassembly for Responsive Bacterial Elimination and Effective Bacterial Detection. *ACS Appl. Mater. Interfaces* **2017,** *9* (11), 10180-10189.

8. Wang, Y.; Yuan, Q.; Li, M.; Tang, Y., Cationic Conjugated Microporous Polymers Coating for Dual-Modal Antimicrobial Inactivation with Self-Sterilization and Reusability Functions. *Adv. Funct. Mater.* **2023,** *33* (19), 2213440.

9. Guilhelmelli, F.; Vilela, N.; Albuquerque, P.; Derengowski, L.; Silva-Pereira, I.; Kyaw, C., Antibiotic development challenges: the various mechanisms of action of antimicrobial peptides and of bacterial resistance. **2013,** *4*. 353.

10. Saidin, S.; Jumat, M. A.; Mohd Amin, N. A. A.; Saleh Al-Hammadi, A. S., Organic and inorganic antibacterial approaches in combating bacterial infection for biomedical application. *Materials Science and Engineering: C* **2021,** *118*, 111382.

11. Kulshrestha, S.; Khan, A. U., Nanomedicine for anticancer and antimicrobial treatment: an overview. *IET Nanobiotechnology* **2018,** *12* (8), 1009-1017.

12. Yuan, H.; Wang, B.; Lv, F.; Liu, L.; Wang, S., Conjugated-Polymer-Based Energy-Transfer Systems for Antimicrobial and Anticancer Applications. *Adv. Mater.* **2014,** *26* (40), 6978-6982.

13. Liu, S.; Wang, B.; Yu, Y.; Liu, Y.; Zhuang, Z.; Zhao, Z.; Feng, G.; Qin, A.; Tang, B. Z., Cationization-Enhanced Type I and Type II ROS Generation for Photodynamic Treatment of Drug-Resistant Bacteria. *ACS Nano* **2022,** *16* (6), 9130-9141.

14. Feng, L.; Zhu, C.; Yuan, H.; Liu, L.; Lv, F.; Wang, S., Conjugated polymer nanoparticles: preparation, properties, functionalization and biological applications. *Chem. Soc. Rev.* **2013,** *42* (16), 6620-6633.

15. Wu, W.; Bazan, G. C.; Liu, B., Conjugated-Polymer-Amplified Sensing, Imaging, and Therapy. *Chem* **2017,** *2* (6), 760-790.

16. Liang, J.; Li, K.; Liu, B., Visual sensing with conjugated polyelectrolytes. *Chem. Sci.* **2013,** *4* (4), 1377-1394.

17. Pu, K.-Y.; Liu, B., Fluorescent Conjugated Polyelectrolytes for Bioimaging. *Adv. Funct. Mater.* **2011,** *21* (18), 3408-3423.

18. Ji, E.; Parthasarathy, A.; Corbitt, T. S.; Schanze, K. S.; Whitten, D. G., Antibacterial Activity of Conjugated Polyelectrolytes with Variable Chain Lengths. *Langmuir* **2011,** *27* (17), 10763-10769.

19. Yuan, H.; Liu, Z.; Liu, L.; Lv, F.; Wang, Y.; Wang, S., Cationic Conjugated Polymers for Discrimination of Microbial Pathogens. *Adv. Mater.* **2014,** *26* (25), 4333-4338.

20. Zhu, S.; Wang, X.; Yang, Y.; Bai, H.; Cui, Q.; Sun, H.; Li, L.; Wang, S., Conjugated Polymer with Aggregation-Directed Intramolecular Förster Resonance Energy Transfer Enabling Efficient Discrimination and Killing of Microbial Pathogens. *Chem. Mater.* **2018,** *30* (10), 3244-3253.

21. Lu, L.; Rininsland, F. H.; Wittenburg, S. K.; Achyuthan, K. E.; McBranch, D. W.; Whitten, D. G., Biocidal Activity of a Light-Absorbing Fluorescent Conjugated Polyelectrolyte. *Langmuir* **2005,** *21* (22), 10154-10159.

22. Wang, L.; Zhao, Q.; Zhang, Z.; Lu, Z.; Zhao, Y.; Tang, Y., Fluorescent Conjugated Polymer/Quarternary Ammonium Salt Co-Assembly Nanoparticles: Applications in Highly Effective Antibacteria and Bioimaging. *ACS Applied Bio Materials* **2018,** *1* (5), 1478-1486.

23. Bai, H.; Chen, H.; Hu, R.; Li, M.; Lv, F.; Liu, L.; Wang, S., Supramolecular Conjugated Polymer Materials for in Situ Pathogen Detection. *ACS Appl. Mater. Interfaces* **2016,** *8* (46), 31550-31557.

24. Cox, C. S., Airborne bacteria and viruses. *Science Progress (1933-)* **1989**, 469-499.

25. Gao, D.; Li, X.; Li, Y.; Lyu, B.; Ren, J.; Ma, J., Long-acting antibacterial activity on the cotton fabric. *Cellulose* **2021,** *28* (3), 1221-1240.

26. Gaussian 16, Revision B.01, Frisch, M.J.; Trucks, G.W.; Schlegel, H.B.; Scuseria, G.E.; Robb, M.A.; Cheeseman, J.R.; Scalmani, G.; Barone, V.; Petersson, G.A.; Nakatsuji, H.; Li, X.; Caricato, M.; Marenich, A.V.; Bloino, J., Janesko, B.G., Gomperts, R., Mennucci, B., Hratchian, H.P., Ortiz, J.V., Izmaylov, A.F., Sonnenberg, J.L., Williams-Young, D., Ding, F., Lipparini, F., Egidi, F., Goings, J., Peng, B., Petrone, A., Henderson, T., Ranasinghe, D., Zakrzewski, V.G., Gao, J., Rega, N., Zheng, G., Liang, W., Hada, M., Ehara, M., Toyota, K., Fukuda, R., Hasegawa, J., Ishida, M., Nakajima, T., Honda, Y., Kitao, O., Nakai, H., Vreven, T., Throssell, K., Montgomery Jr., J.A., Peralta, J.E., Ogliaro, F., Bearpark, M.J., Heyd, J.J., Brothers, E.N., Kudin, K.N., Staroverov, V.N., Keith, T.A., Kobayashi, R., Normand, J., Raghavachari, K., Rendell, A.P., Burant, J.C., Iyengar, S.S., Tomasi, J., Cossi, M., Millam, J.M., Klene, M., Adamo, C., Cammi, R., Ochterski, J.W., Martin, R.L., Morokuma, K., Farkas, O., Foresman, J.B., Fox, D.J. Gaussian, Inc., Wallingford CT: **2016** GaussView 5.0. Wallingford, E.U.A

27. Xu, Q.; He, P.; Wang, J.; Chen, H.; Lv, F.; Liu, L.; Wang, S.; Yoon, J., Antimicrobial activity of a conjugated polymer with cationic backbone. *Dyes and Pigments* **2019,** *160*, 519-523.

28. Riduan, S. N.; Zhang, Y., Imidazolium salts and their polymeric materials for biological applications. *Chem. Soc. Rev.* **2013,** *42* (23), 9055-9070.

29. Zehra, N.; Dutta, D.; Malik, A. H.; Ghosh, S. S.; Iyer, P. K., Fluorescence Resonance Energy Transfer-Based Wash-Free Bacterial Imaging and Antibacterial Application Using a Cationic Conjugated Polyelectrolyte. *ACS Appl. Mater. Interfaces* **2018,** *10* (33), 27603-27611.

30. Sambhy, V.; Peterson, B. R.; Sen, A., Antibacterial and hemolytic activities of pyridinium polymers as a function of the spatial relationship between the positive charge and the pendant alkyl tail. *Angew. Chem.* **2008,** *120* (7), 1270-1274.

31. Le, W.; Chen, B.; Cui, Z.; Liu, Z.; Shi, D., Detection of cancer cells based on glycolytic-regulated surface electrical charges. *Biophys. Rep.* **2019,** *5*, 10-18.

Appendix

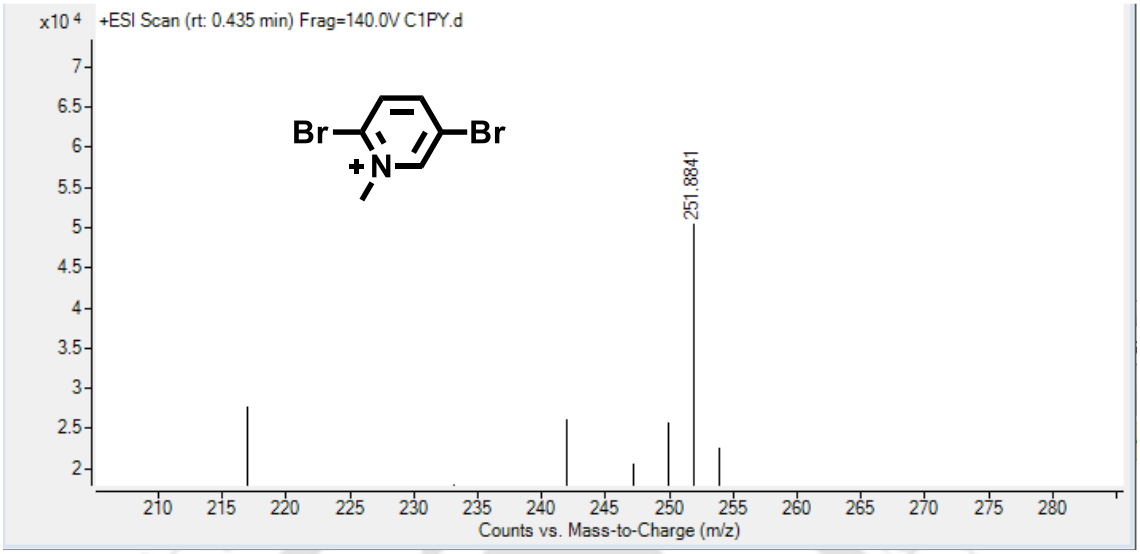

Figure A5.1: _LC_QTOF_HRMS_spectra_of_C1Py

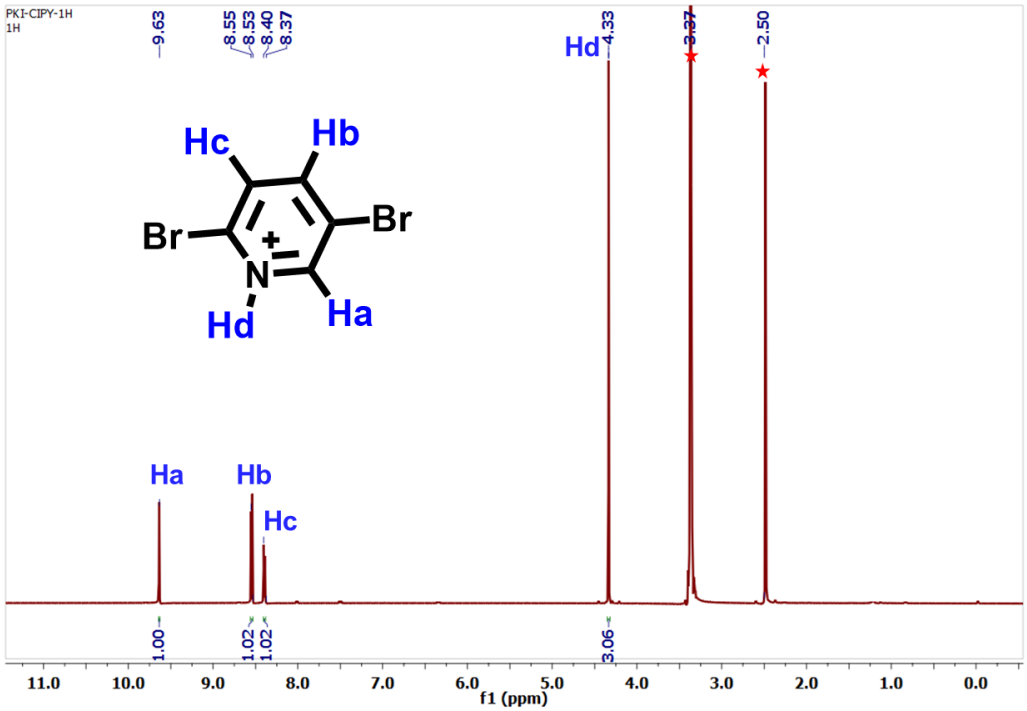

Figure A5.2: ^{1}H NMR spectra of C1Py in DMSO-d6.

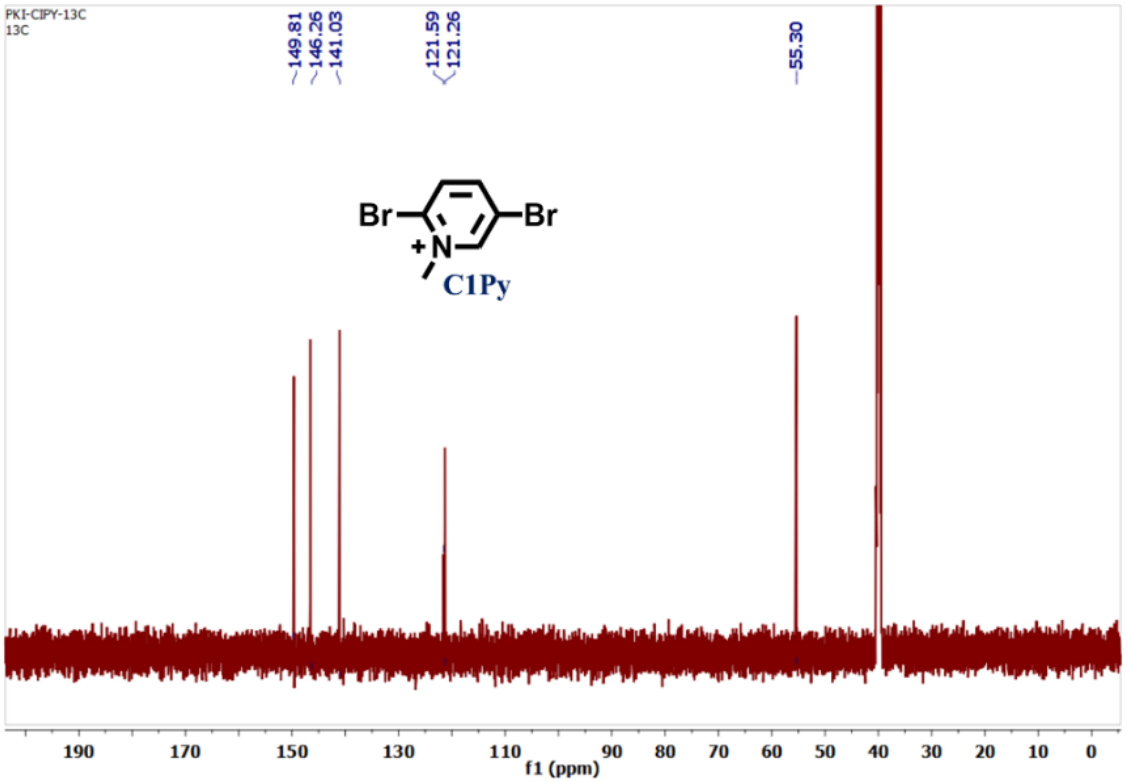

Figure A5.3: ^{13}C NMR spectra of C1Py in DMSO-d6.

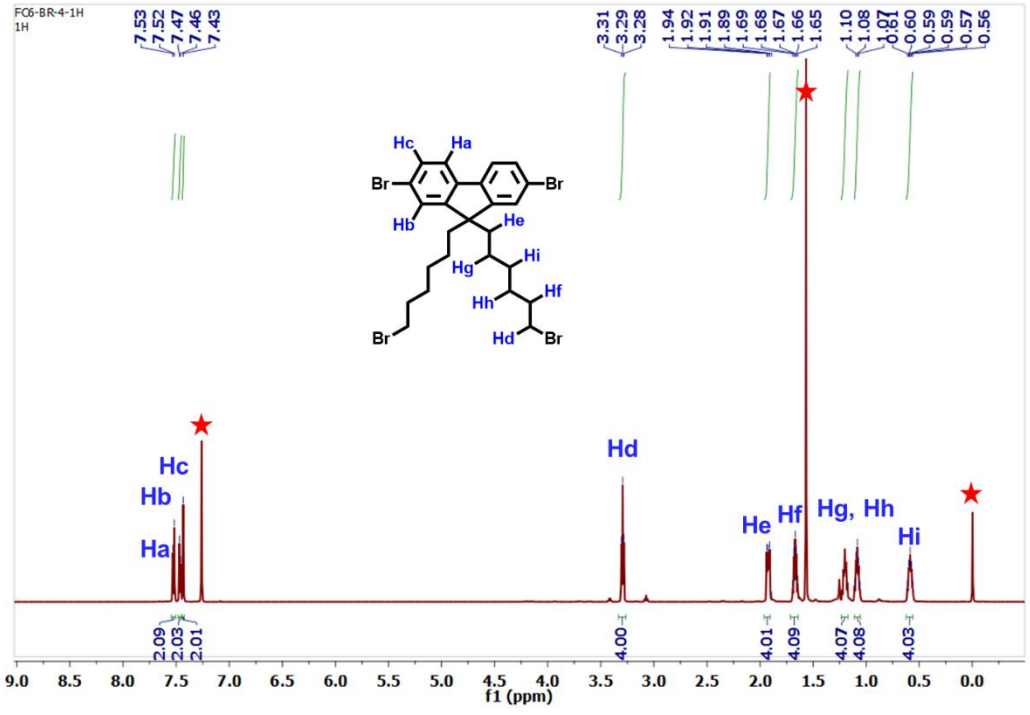

Figure A5.4: ^{1}H NMR spectra of Fc6BR4 in $CDCl_3$

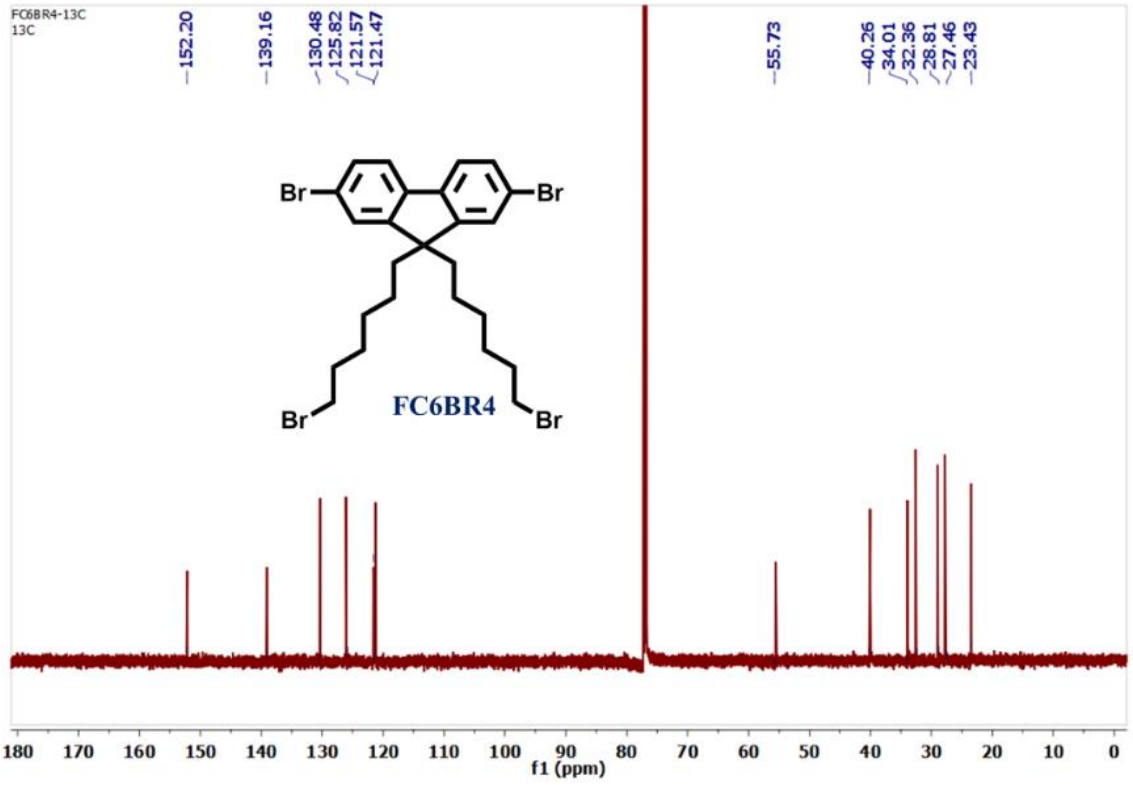

Figure A5.5: ^{13}C NMR spectra of FC6BR4 in $CDCl_3$

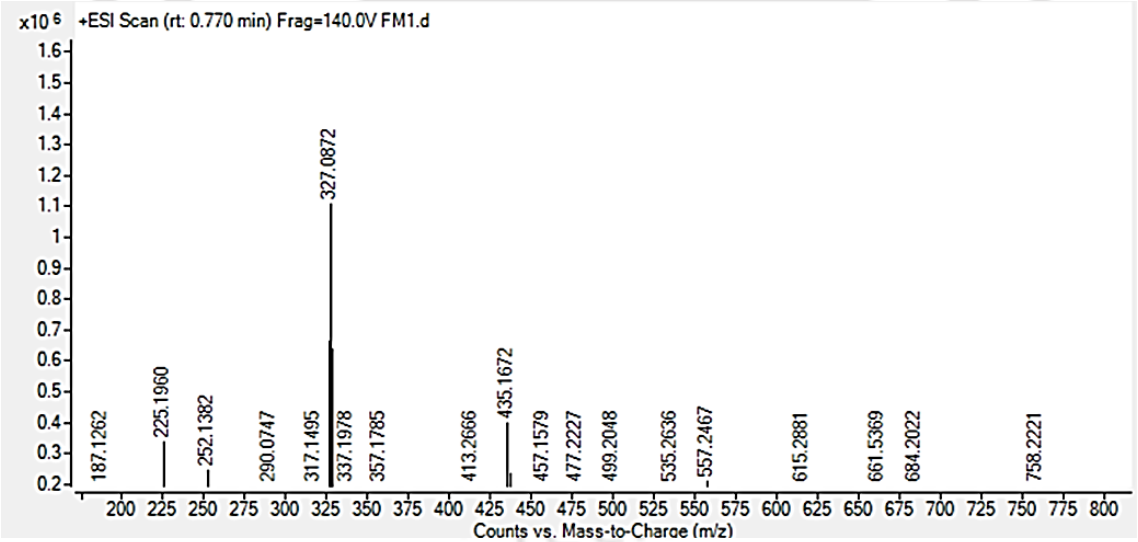

Figure A5.6: LC_QTOF_HRMS spectra of FMI

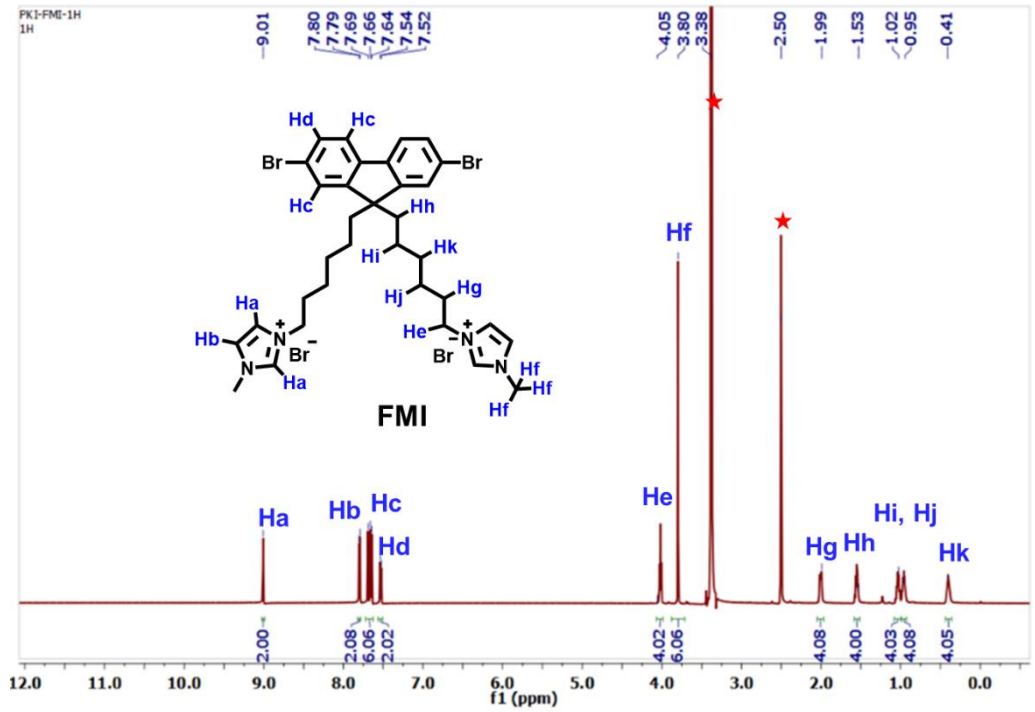

Figure A5.7: ^{1}H NMR spectra of FMI in DMSO-d6.

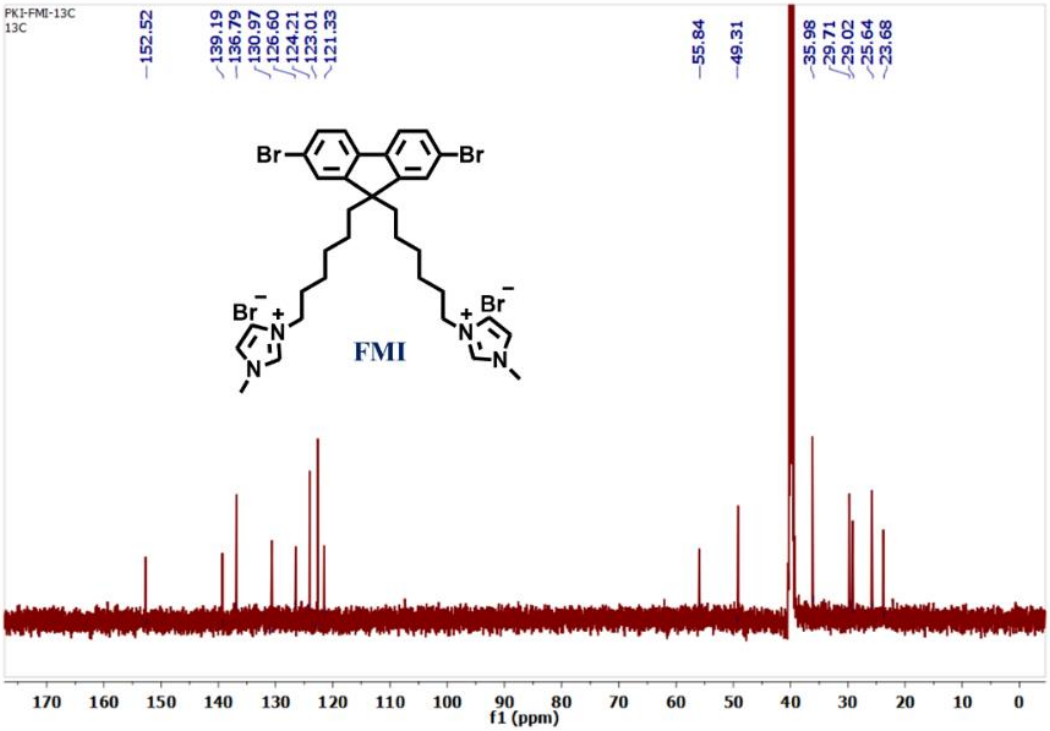

Figure A5.8: ^{13}C NMR spectra of FMI in DMSO-d6.

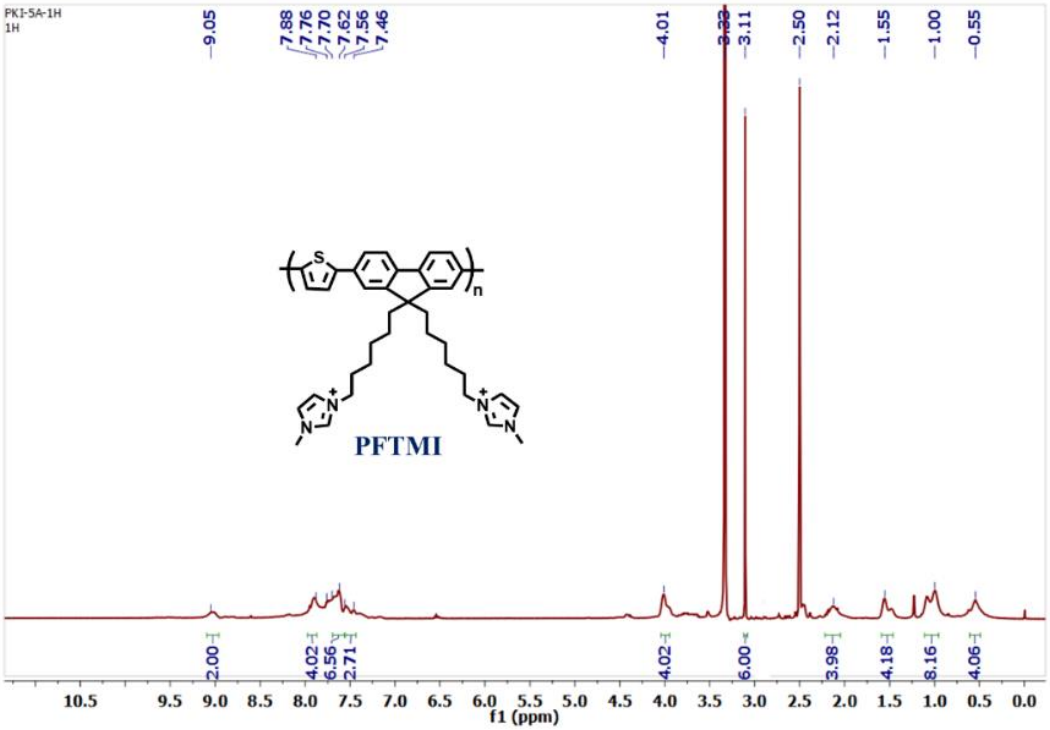

Figure A5.9: ^{1}H NMR spectra of PFTMI in DMSO-d6.

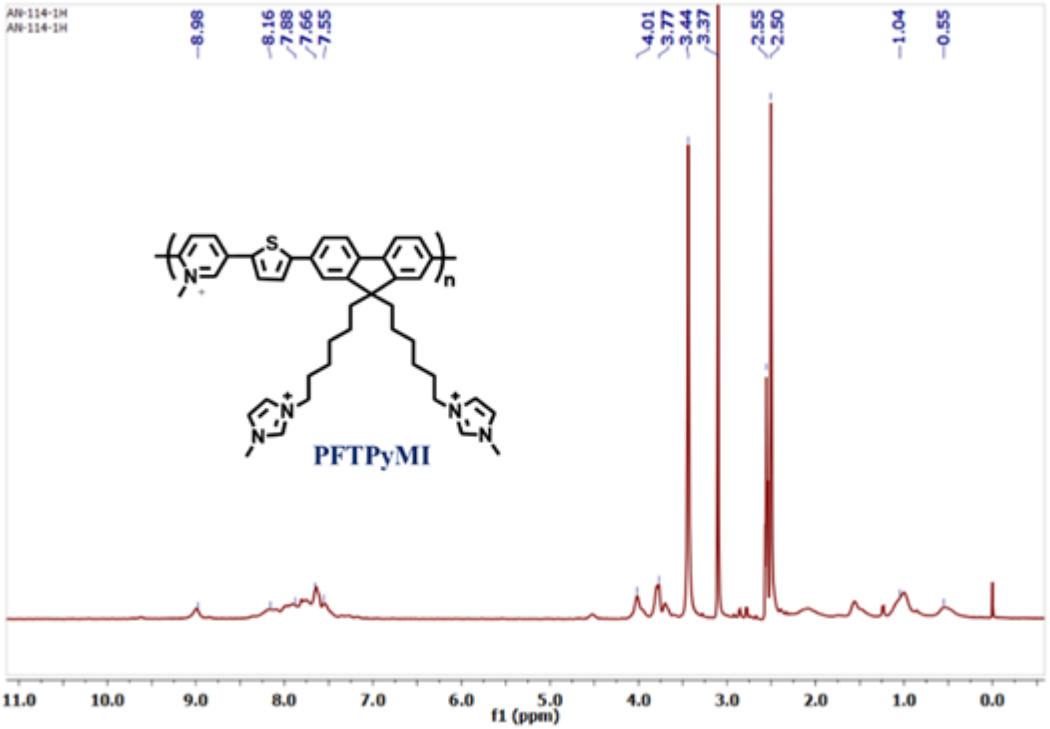

Figure A5.10: ^{1}H NMR spectra of PFTPyMI in DMSO-d6.

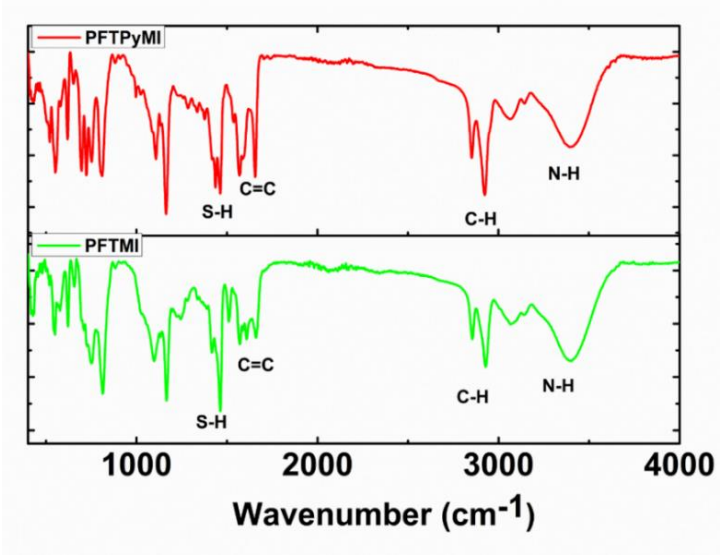

Figure A5.11: FTIR spectra of PFTMI and PFTPyMI

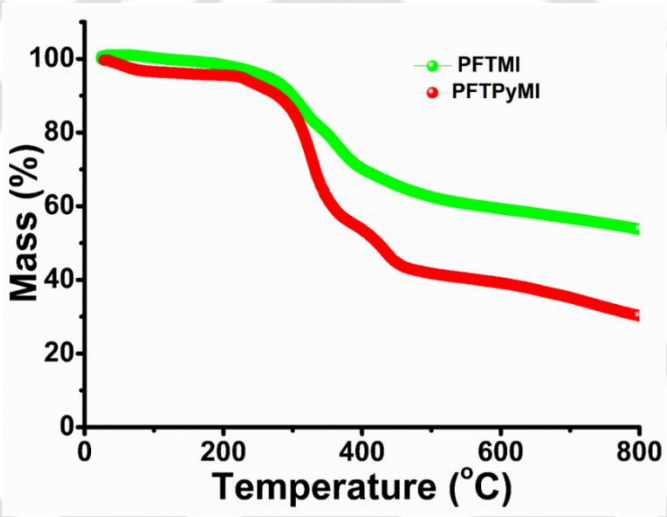

Figure A5.12: Thermal degradation of PFTMI and PFTPyMI

Table A5.1: Fluorescence lifetime decay data for PFTMI and PFTPyMI

CPEs	τ_1 (ns)	τ_2(ns)	χ^2	τ_{av}(ns)
PFTMI	0.88	1.271	0.97	0.94
PFTPyMI	0.97	2.37	0.97	1.24

Table A5.2: Photophysical data for PFTMI and PFTPyMI

CPEs	λ_{abs}(nm)	λ_{em}(ns)	ϕ (%)	τ_{av}(ns)
PFTMI	400	505	78.31	0.94
PFTPyMI	400	496	60.91	1.24

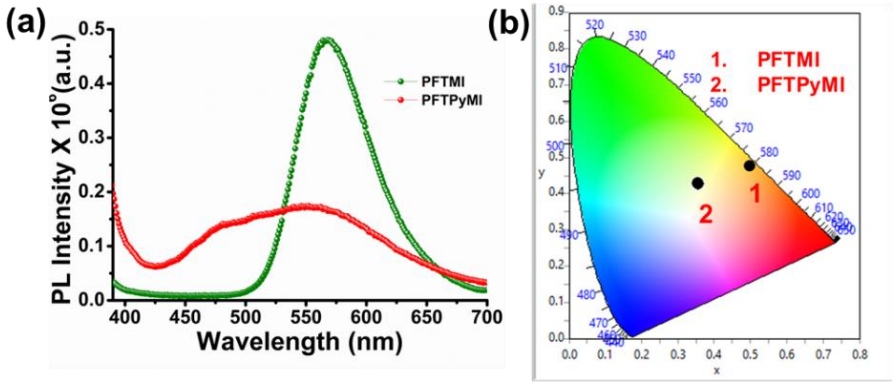

Figure A5.13: (a) Solid state emssion spectra of PFTMI and PFTPyMI; (b) CIE co-ordinates for solid state emission spectra of PFTMI and PFTPyMI

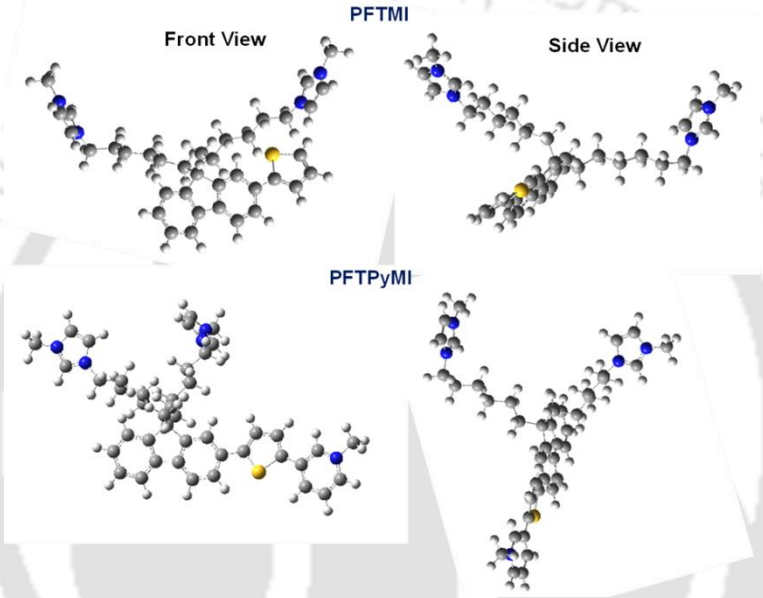

Figure A5.14: Optimsed structure of M4 monomer using B3LYP and 631G(d.p) charge =2 for PFTMI and Charge =3 for PFTPyMI of Gaussian 16 Program. *S*

Thesis Overview and Future Perspective

Conjugated polymers (CPs) are semiconducting materials that draw attention from material science and engineering. They have unique optical and electrical properties, making them active substrate for various kinds of applications such as sensing, biomedical and. optoelectronic devices. Among the various applications, sensing has gained tremendous research attraction on account of its remarkable sensitivity, strong light-harvesting and good conducting abilities, high photo/thermal stability, and biocompatibility. The signal amplification property of CPs compared to other molecules due to their efficient intra- and intermolecular charge or energy transfer eventually make them as an innovative technological material. Furthermore, the conjugated polymer framework can be easily adjusted to desired optical or electrical band gaps and water solubility, by designing D-A CPs and conjugated polyelectrolytes. Moreover, modern optoelectronic devices, sensing, and theranostic applications demand CPs with high solid-state emissions or practical applicability in aqueous media, which can be attainable through the smart design of AIE/AIEE-CPs. To develop a stable and highly efficient sensing platform, several molecular design criteria, such as the choice specific receptor, orientation, and packing of polymeric chains, should be considered when designing conjugated polymers as transducers. In consideration of rising demand for personal health monitoring sensor and reliable methods for chemical danger assessments, this thesis entitled "**Rational engineering of Polyfluorene based Conjugated Polymers for Sensing and Antibacterial Applications"** has as its main goal solving the issues and difficulties related to current sensing systems. It primarily focuses on the design and development of effective, quick, and portable systems based on conjugated polymers for on-site detection of several biologically and environmentally important analytes. In order to achieve the best possible fluorescence signal, chemical processing, excellent sensitivity, and selectivity towards particular analytes of interest, various polyfluorene derivatives such as homopolymer, D-A polymer, AIEE polymer, conjugated polyelectrolytes that have appended functional groups have been designed and synthesized. Then, the designed CPs are successfully are effectively integrated into the cost-effective, portable user friendly device for real-time tracking of disease biomarkers, herbicides, biologically important proteins, pathogens etc.

To verify the potential self-signal amplifying biosensors, a benzimidazole incorporated conjugated homopolymer (PFBZ) was synthesized by oxidative coupling polymerization

reaction in good yield for the specific detection of bilirubin (jaundice biomarker) (***Chapter 2***). The excellent sensitivity of PFBZ towards bilirubin selectively was due to complexation and FRET mechanisms which were confirmed from both theoretical and experimental findings. Furthermore, the detection is quick, simple, and extremely reliable, even in real serum samples, where the results were close agreement to the clinical method of bilirubin detection. Finally, a fluorescent paper-based test kits were developed for on-site detection.

To achieve solid state emission and adjust the optical band gap, PF2CN polymer was synthesized by Suzuki coupling polymerization reaction in good yield for the detection of pendimethalin (mutagenic and carcinogenic herbicide) (***Chapter 3***). The detection mechanism was FRET and PET making it a highly sensitive and selective pendimetalin sensor that can be extended in real vegetables and natural water samples where the results was cross validated with conventional technique. Finally, a smartphone integrated point of care testing device was developed via quantifying the fluorescence color change (RGB value variation) of PF2CN under UV light by color-scanning android application for rapid onsite detection in a very straightforward manner.

To explore the structure-motion-property relationship of a conjugated molecular, three sets of polymers P1, P2, and P3 were created by incorporating varying mole fractions of AIE monomer (M4) with electron accepting tendency, thereby controlling molecular motion and charge transfer in solution and aggregated states (***Chapter 4***). The change in molar ratio of monomer M4 in P1, P2, and P3 resulted in a shift in polyfluorene emission from blue to white and yellow, representing the increase in D-A strength from P1 to P3. Furthermore, this developed designed strategy improved the condensed state emission property by transforming ACQ polymer (P1) into AIEE polymer (P3), which is important for bio sensing applications that can work in aqueous medium. Finally, AIEE conjugated polyelectrolyte PFAN polymer was derived from the AIEE-P3 polymer for monitoring of serum albumins achieving a "Ratiometric Turn On" response because of complexation induced AIEE mechanism. Finally, this fluorescence-based detection is miniature into a smartphone-based prototypes testing device for detecting HSA on-site, easily and rapidly to benefit the healthcare usage.

To explore the role of positive charge for antibacterial application conjugated polyelectrolytes PFTMI and PFTPyMI by Stile coupling polymerization (***Chapter 5***). PFTPyMI with cationic backbone and side group are showing more antibacterial activity

than PFTMI with only cationic side group because of more efficient binding toward bacterial membrane resulting in membrane disruption. Further the presence of bacteria in aqueous media can be detected easy from the fluorescence color change. The less cytotoxic nature in HEK 293 normal cell lines, and toxic towards Hela cell lines offers a new hope for future biomedical applications to combat antibiotic resistance. One such application, it is utilized as an antibacterial coating over a cotton pad to mimic antibacterial fabric and achieved promising results which was less effective or failed by commercially available antibiotics.

Thesis Overview

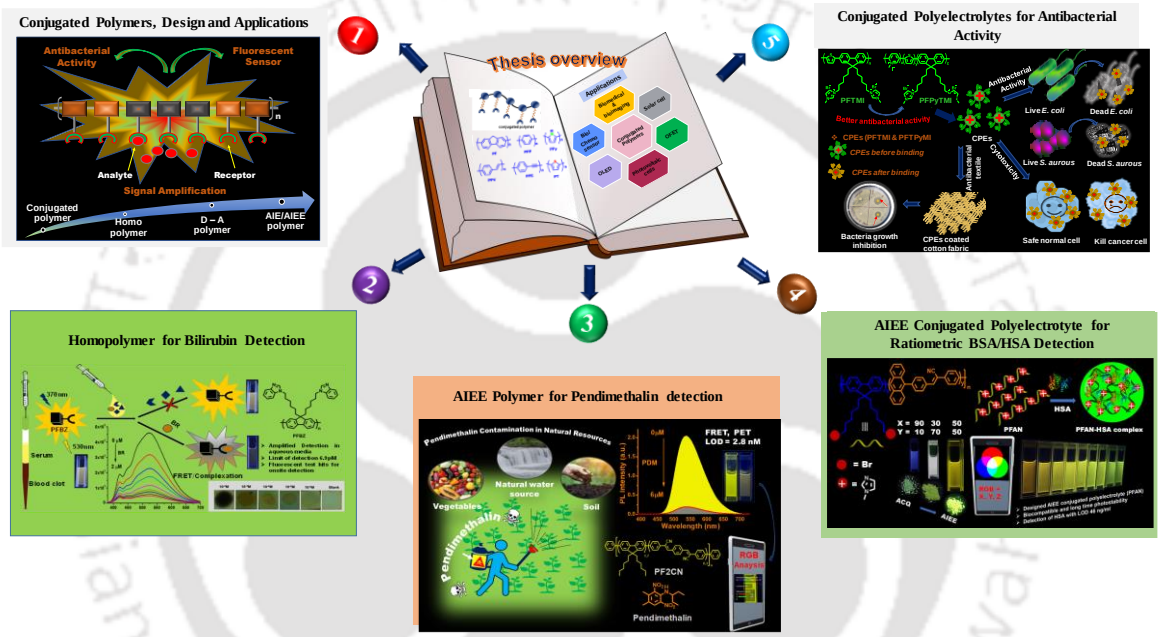

Future Directions

The present thesis discusses the development and characterization of various conjugated polymers and utilization as signal transducers based on fluorescence “turn-off”, “receptor free” “ratiometric turn on” sensing. Nonetheless, there is scope for further studies on a few topics covered in this thesis. For instance, bacterial detection and killing utilizing PFTMI and PFTPyMI might be expanded to in-vivo and mixed bacterial cultures. Similarly, PFBZ-based bilirubin detection could be more innovative and user-friendly via smartphone-integrated platform or wireless sensing tags with real-time monitoring abilities. Overall, the future direction of developing CP-based sensors could be focused on colorimetric, array-based sensing, and establishing technologically advanced receptors. Furthermore, future CP-designed strategies should be broadened for various kinds of applications such as biomedical, energy storage, photocalytic applications, and so on.

Publications

1. **Chanu, M. A**.; Adil, L. R.; Iyer, P. K. Receptor Free AIEE Conjugated Polymer Nanoparticle based PoC device for Amplified Detection of Pendimethalin. *ACS Appl. Polym. Mater*. **2024**, *6,* 6988-6996

2. Tanwar, A. S.; **Chanu, M. A**.; Parui, R; Barman, D.; Im, Y.; Iyer, P. K. Dynamic Quenching Mechanism Based Optical Detection of Carcinogenic Cr (VI) In Water and On Economical Paper Test Strips via A Conjugated Polymer. *RSC Appl. Polym.* **2024***, 2,* 196-204.

3. Banoo, F.; **Chanu, M. A**.; Iyer, P. K.; Khijwania, S. K. Novel Optical Fiber Sensor for Explosive (Trinitrophenol) Detection. *J. Lightwave Technol.* **2024**, 1-9

4. Khatun, M. N.; **Chanu, M. A**.; Barman, D.; Ghosh, P.; Sarmah, T.; Adil, L. R.; Iyer, P. K. Sensors Based on Polymer Nanomaterials. In *Sensory Polymers*; Elsevier, **2024**, 391-428

5. Tanwar, A. S.; Khatun, M. N.; **Chanu, M. A**.; Sarmah, T.; Im, Y.-H.; Iyer, P. K. A Water-Soluble Conjugated Polyelectrolyte for Selective and Sensitive Detection of Carcinogenic Chromium (Vl). *Analyst* **2023,** *148*, 6011-6019.

6. **Chanu, M.A**.; Mondal, S.; Zehra**,** N.; Tanwar, A.S.; Iyer, P. K. Conjugated Polymer Nanoparticles as a Fluorescence Probe for Amplified Detection of Human Serum Bilirubin *ACS Appl. Polym. Mater*. **2022**, *4*, 3491-3497.

7. Adil, L. R.; Parui R., Khatun, M. N.; **Chanu, M.A**. Li, L.; Wang, S.; Iyer, P. K. Nanomaterials for Sensors: Synthesis and Applications. *Elsevier*, **2022**, 121-168.

8. Tanwar, A. S.; Parui, R.; Garai, R.; **Chanu, M. A.**; Iyer, P. K. Dual "Static and Dynamic" Fluorescence Quenching Mechanisms Based Detection of TNT via a Cationic Conjugated Polymer. *ACS Meas. Sci. Au,* **2021***, 2*, 23-30.

9. **Chanu, M. A**.; Adil, L. R.; Ghosh, P.; Khubchandani, D. D.; Iyer P. K. Ratiometric Turn-On Detection of HSA using Aggregation Induced Enhanced Emission Conjugated Polyelectrolyte and Prototype Smartphone based Sensor. (**Manuscript communicated**)

10. **Chanu, M. A**.; Kumari, K.; Adil, L. R.; Ramakrishnan, V.; Iyer P. K. Switching from Cationic Side Chain into Cationic Backbone in Polyfluorene Polyelectrolytes to Effectively Combat Antibiotic Resistance and Antibacterial Coating. (**Manuscript Prepared**)

Conferences and Workshop Attended

1. Presented a poster in the ***6th International Conference on Advanced Nanomaterials and Nanotechnology*** held during Dec 18- 21, 2019, organized by Centre for Nanotechnology, IIT Guwahati

2. Presented an oral in the ***International E- Conference on New Frontiers in Science and Technology*** held during July, 9-11, 2020 organized by Research Institute of Science and Technology Manipur, India.

3. Presented a poster in the ***North East Research Conclave 2022*** held during May 20-22, 2022 organised by Indian Institute of Technology Guwahati, India, Science, Technology and Climate Change Dept. & Dept. of Education, Govt. of Assam.

4. Presented a poster in the ***International Conference on Frontiers in Chemical Sciences*** held during Dec, 2-4, 2022 organised by the Department of Chemistry, IIT Guwahati.

5. Presented a poster in the ***Research Conclave'23*** held during May 14-16, 2023 organized by Student Academic Board (SAB), IIT Guwahati.

6. Presented a poster in the ***17th International Conference on Polymer Science and Technology SPSI-Macro 2023*** held during Dec 10-13, 2023 organized by IIT Guwahati.

7. Attended ***5th National Workshop on NEMS/MEMS and Theragnostic Devices***, *February, 21-23,* 2019, IIT Guwahati.

8. Attended Seminar on ***Basics of small Angles X-ray Scatterings***, February 26, 2020, IIT Guwahati.

9. Successfully completed ***Wiley Author Webinar Series "Learn to Publish*** held during June-July 2020

10. Attended online training workshop on ***Computational Density Functional Theory*** held during July, 4-5, 2020, organized by Thanthai Periyar Government Polytechnic College Vellore-632002, Tamil Nadu, India

11. Attended ***the full agenda of ACS on Campus Virtual Event****, on August 10,* 2020.

12. Successfully completed ***Online Course ACS Reviewer Lab*** on August 22, 2020

13. Attended the live session on ***Patent Protection for Innovation Driven Educational Institutions*** August 29, 2020, organized by Turnip Innovations in association with the Frontiers Legal

Donor-σ-Acceptor Dyad-Based Polymers for Portable Sensors: Controlling Photoinduced Electron Transfer via Tuning the Frontier Molecular Orbital Energies of Acceptors

Author: Na Yeon Kwon, Youngseo Kim, Meenal Kataria, et al
Publication: Macromolecules
Publisher: American Chemical Society
Date: Mar 1, 2022

PERMISSION/LICENSE IS GRANTED FOR YOUR ORDER AT NO CHARGE

This type of permission/license, instead of the standard Terms and Conditions, is sent to you because no fee is being charged for your order. Please note the following:

- Permission is granted for your request in both print and electronic formats, and translations.
- If figures and/or tables were requested, they may be adapted or used in part.
- Please print this page for your records and send a copy of it to your publisher/graduate school.
- Appropriate credit for the requested material should be given as follows: "Reprinted (adapted) with permission from {COMPLETE REFERENCE CITATION}. Copyright {YEAR} American Chemical Society." Insert appropriate information in place of the capitalized words.
- One-time permission is granted only for the use specified in your RightsLink request. No additional uses are granted (such as derivative works or other editions). For any uses, please submit a new request.

If credit is given to another source for the material you requested from RightsLink, permission must be obtained from that source.

BACK CLOSE WINDOW

Fluorescent Conjugated Polymer/Quarternary Ammonium Salt Co-assembly Nanoparticles: Applications in Highly Effective Antibacteria and Bioimaging

Author: Lianqi Wang, Qi Zhao, Ziqi Zhang, et al
Publication: ACS Applied Bio Materials
Publisher: American Chemical Society
Date: Nov 1, 2018

PERMISSION/LICENSE IS GRANTED FOR YOUR ORDER AT NO CHARGE

This type of permission/license, instead of the standard Terms and Conditions, is sent to you because no fee is being charged for your order. Please note the following:

- Permission is granted for your request in both print and electronic formats, and translations.
- If figures and/or tables were requested, they may be adapted or used in part.
- Please print this page for your records and send a copy of it to your publisher/graduate school.
- Appropriate credit for the requested material should be given as follows: "Reprinted (adapted) with permission from {COMPLETE REFERENCE CITATION}. Copyright {YEAR} American Chemical Society." Insert appropriate information in place of the capitalized words.
- One-time permission is granted only for the use specified in your RightsLink request. No additional uses are granted (such as derivative works or other editions). For any uses, please submit a new request.

If credit is given to another source for the material you requested from RightsLink, permission must be obtained from that source.

BACK CLOSE WINDOW

Luminescent Chemodosimeters for Bioimaging

Author: Yuming Yang, Qiang Zhao, Wei Feng, et al
Publication: Chemical Reviews
Publisher: American Chemical Society
Date: Jan 1, 2013

PERMISSION/LICENSE IS GRANTED FOR YOUR ORDER AT NO CHARGE

This type of permission/license, instead of the standard Terms and Conditions, is sent to you because no fee is being charged for your order. Please note the following:

- Permission is granted for your request in both print and electronic formats, and translations.
- If figures and/or tables were requested, they may be adapted or used in part.
- Please print this page for your records and send a copy of it to your publisher/graduate school.
- Appropriate credit for the requested material should be given as follows: "Reprinted (adapted) with permission from {COMPLETE REFERENCE CITATION}. Copyright {YEAR} American Chemical Society." Insert appropriate information in place of the capitalized words.
- One-time permission is granted only for the use specified in your RightsLink request. No additional uses are granted (such as derivative works or other editions). For any uses, please submit a new request.

If credit is given to another source for the material you requested from RightsLink, permission must be obtained from that source.

BACK CLOSE WINDOW

A Supramolecular Cross-Linked Conjugated Polymer Network for Multiple Fluorescent Sensing

Author: Xiaofan Ji, Yong Yao, Jinying Li, et al
Publication: Journal of the American Chemical Society
Publisher: American Chemical Society
Date: Jan 1, 2013

PERMISSION/LICENSE IS GRANTED FOR YOUR ORDER AT NO CHARGE

This type of permission/license, instead of the standard Terms and Conditions, is sent to you because no fee is being charged for your order. Please note the following:

- Permission is granted for your request in both print and electronic formats, and translations.
- If figures and/or tables were requested, they may be adapted or used in part.
- Please print this page for your records and send a copy of it to your publisher/graduate school.
- Appropriate credit for the requested material should be given as follows: "Reprinted (adapted) with permission from {COMPLETE REFERENCE CITATION}. Copyright {YEAR} American Chemical Society." Insert appropriate information in place of the capitalized words.
- One-time permission is granted only for the use specified in your RightsLink request. No additional uses are granted (such as derivative works or other editions). For any uses, please submit a new request.

If credit is given to another source for the material you requested from RightsLink, permission must be obtained from that source.

BACK CLOSE WINDOW